

OXIDATIVE METABOLISM AND MITOCHONDRIAL CALCIUM HANDLING IN MOUSE  
MODELS OF HUNTINGTON'S DISEASE

James M. Hamilton

Submitted to the faculty of the University Graduate School  
in partial fulfillment of the requirements  
for the degree  
Doctor of Philosophy  
in the Department of Pharmacology and Toxicology,  
Indiana University

November 2017

Accepted by the Graduate Faculty of Indiana University, in partial fulfillment of the requirements for the degree of Doctor of Philosophy.

Doctoral Committee

---

Nickolay Brustovetsky, Ph.D., Chair

---

Theodore R. Cummins, Ph.D.

August 23, 2017

---

Andy Hudmon, Ph.D.

---

Alexander G. Robling, Ph.D.

---

William J. Sullivan, Ph.D.

## ACKNOWLEDGEMENTS

First, and above all else, I would like to thank my mentor, Dr. Nickolay Brustovetsky, for generously offering his knowledge, advice, and support. I am endlessly grateful for his guidance and mentorship. Words cannot adequately express the appreciation I have for the time and effort he devoted to making me a better researcher, writer, presenter, and thinker. He was always willing to discuss any questions, concerns, ideas, or experiments that I brought to him. I would also like to thank Tatiana Brustovetsky for selflessly offering her experience and assistance to improve my research. Her willingness to patiently share her expertise made me a better researcher and helped me acquire and refine invaluable skills. I would also like to thank former lab mate Dr. Jessica Pellman for her support and friendship in the lab. She was always available to provide candid advice regarding both scientific and non-scientific matters. I am particularly thankful for her assistance with calcium imaging experiments.

I would like to thank our collaborators, who contributed to this work by generously providing training, technical guidance, discussions, and access to resources and equipment. Most saliently I would like to thank Dr. Robert Harris and members of his lab, particularly Praveen Kusumanchi, and Pengfei Wu, for gracefully accommodating the, at times, torrent of experiments we performed by allowing us unfettered use of the Seahorse XF24 Analyzer in their lab. Additionally, Harris Lab member Oun Kheav was instrumental in providing training so that we could perform metabolic cage experiments. I would also like to give a special thanks to Dr. Alexander Robling for kindly allowing us to use the x-ray densitometer in his lab for our DEXA scanning experiments. We are also very grateful to Caroline Miller in the Electron Microscopy Center at Indiana University School of Medicine for help with electron microscopy and George Eckert in the Department of Biostatistics for help with power analysis.

My sincerest thanks to my committee members, Drs. Ted Cummins, Andy Hudmon, Alex Robling, and Bill Sullivan for the time they have taken to meet with me and for all the thoughts, suggestions, and support they have provided regarding this project and my professional growth. I would also like to thank the current and former members of the administrative staff in the Department of Pharmacology and Toxicology, particularly Amy Lawson, Rob Lawson, Lisa King, and Joanna Plew, for generally keeping everything running smoothly.

Lastly, I would like to thank the funding sources that permitted me to carry out this work. This research project was made possible by funding provided through an NIH grant R01 NS078008 awarded to Dr. Brustovetsky. I would also like to thank the funding sources that allowed me to travel to several conferences where I presented my work, had the opportunity to meet other researchers in the field, and learned more than I could have imagined. Thank you to the Department of Pharmacology and Toxicology RR Paradise Travel Award Committee for providing me with the means to travel to the Society for Neuroscience Meetings in 2014 and 2016. Thank you to the Graduate and Professional Education Grant Committee, administered by the Graduate and Professional Student Government and to the Graduate Student Travel Award Committee at the Indiana University School of Medicine for providing me with additional funds to travel to the Society for Neuroscience Conference in 2016. Finally, thanks to the Indiana University Graduate Division for affording me the opportunity to travel to the Society for Neuroscience Conference in 2014 via the IUPUI University Fellowship.

## OXIDATIVE METABOLISM AND CALCIUM HANDLING IN HUNTINGTON'S DISEASE

Huntington's disease (HD) is an autosomal dominantly inherited, fatal neurodegenerative disorder for which there is no cure. HD is clinically characterized by progressively worsening motor, cognitive, and psychiatric disturbances. Currently available therapeutics for HD only treat symptoms, but do not address underlying disease pathology. HD pathogenesis is linked to a mutation in the huntingtin gene, which encodes a protein called huntingtin (Htt) that is normally involved in a variety of cellular processes. In healthy individuals, the N-terminus of huntingtin possesses a polyglutamine stretch containing less than 35 glutamines, however, the mutated huntingtin protein (mHtt) has an elongated polyglutamine tract that correlates with the development of HD. The mechanism of deleterious action by mHtt is unknown, but a major hypothesis postulates that mHtt may cause mitochondrial dysfunction. However, the data regarding involvement of mitochondrial impairment in HD pathology are contradictory. Some investigators previously reported, for example, that mHtt suppresses mitochondrial respiratory activity and decreases mitochondrial  $\text{Ca}^{2+}$  uptake capacity. However, other investigators found increased respiratory activity and augmented mitochondrial  $\text{Ca}^{2+}$  uptake capacity.

We used transgenic mouse models of HD to investigate the effect of full-length and fragments of mHtt on oxidative metabolism and  $\text{Ca}^{2+}$  handling using a combination of isolated mitochondria, primary neurons, and whole-animal metabolic measurements. We evaluated the effect of full-length mHtt on isolated mitochondria and primary neurons from YAC128 mice. We found no alteration in respiratory activity or  $\text{Ca}^{2+}$  uptake capacity, indicative of mitochondrial damage, between mitochondria or neurons from

YAC128 mice compared to wild-type (WT) mice. Furthermore, we measured whole-animal oxidative metabolism and physical activity level and found that YAC128 mice do not display any decline in metabolic and physical activity. Although full-length mHtt-expressing YAC128 mice may be a more faithful genetic recapitulation of HD, data suggests mHtt fragments may be more toxic. To assess the effect of mHtt fragments, we used isolated brain mitochondria and primary striatal neurons from the R6/2 mouse model and found no significant impairment in respiration or Ca<sup>2+</sup> handling. Thus, our data strongly support the hypothesis that mHtt does not alter mitochondrial functions assessed either with isolated mitochondria, primary neurons, or whole animals.

Nickolay Brustovetsky, Ph.D., Chair

## TABLE OF CONTENTS

List of Tables.....	xi
List of Figures.....	xii
List of Abbreviations.....	xvii
I. Introduction.....	1
A. Huntington's Disease .....	1
a. Huntingtin Protein Function .....	5
b. Models of HD.....	7
c. Proposed Mechanisms of Neurodegeneration in HD .....	14
B. Mitochondrial Dysfunction in HD .....	18
a. Defects in Oxidative Metabolism .....	23
i. Evidence Supporting Oxidative Metabolism Defects in HD.....	23
ii. Evidence Against Oxidative Metabolism Defects in HD .....	27
b. Defects in Mitochondrial Calcium Handling and Calcium Uptake.....	31
i. Evidence Supporting Mitochondrial Ca <sup>2+</sup> Handling Defects in HD.....	31
ii. Evidence Against Mitochondrial Ca <sup>2+</sup> Handling Defects in HD .....	34
C. Hypothesis and Goals .....	36
II. Materials and Methods .....	39
A. Materials .....	39
B. Animals .....	39
C. Isolation and Purification of Mitochondria .....	41
D. Western Blotting .....	47

E. Mitochondrial Respiration .....	48
F. Mitochondrial Ca <sup>2+</sup> Uptake .....	48
G. Mitochondrial Membrane Potential and Swelling.....	49
H. Transmission Electron Microscopy.....	49
I. ATP and ADP Measurements .....	50
J. Blue Native-PAGE and Western Blotting.....	51
K. Cell Culture.....	51
L. Cell Respirometry .....	52
M. Calcium Imaging.....	53
N. Neuronal Transfection .....	54
O. Live-cell Laser Spinning-disk Confocal Microscopy .....	55
P. Calorimetric Analysis .....	55
Q. Mouse Body Composition .....	56
R. Statistics .....	56
III. Results .....	60
A. Oxidative Metabolism and Ca <sup>2+</sup> Handling in the YAC128 Mouse Model of HD... 60	
a. Claspings phenotype of YAC128 mice and genotyping .....	60
b. Expression of mHtt and morphological characterization of brain mitochondria isolated from YAC128 mice .....	63
c. Respiration of purified brain nonsynaptic and synaptic mitochondria from 2- and 10-month-old YAC128 mice as well as unpurified brain,	



liver, and heart mitochondria from YAC128 mice .....	68
d. Protein expression in mitochondria from WT and YAC128 mice.....	78
e. Membrane potential measurements in nonsynaptic and synaptic mitochondria from YAC128 mice.....	82
f. Cellular respiration and extracellular acidification of neurons and ATP/ADP measurements in isolated mitochondria and primary neurons from YAC128 mice .....	85
g. Whole-animal metabolic activity of YAC128 mice .....	91
h. Ca <sup>2+</sup> uptake capacity of nonsynaptic and synaptic mitochondria from YAC128 mice.....	94
<b>B. Respiration and Ca<sup>2+</sup> Uptake Capacity in Striatal Nonsynaptic and Synaptic     Mitochondria Isolated from YAC128 Mice .....</b>	<b>99</b>
a. Clasp phenotype of early symptomatic YAC128 mice.....	99
b. Expression of mHtt in striatal mitochondria and purity of mitochondrial preparations.....	100
c. Respiration of nonsynaptic and synaptic striatal mitochondria from YAC128 mice.....	102
d. Expression of nuclear-encoded proteins in mitochondria from YAC128 and WT mice .....	106
e. Ca <sup>2+</sup> uptake capacity of striatal nonsynaptic and synaptic mitochondria from YAC128 and WT mice.....	108
<b>C. Oxidative Metabolism and Ca<sup>2+</sup> Handling in the R6/2 Mouse Model of HD.....</b>	<b>112</b>

a. Clasp phenotype of R6/2 mice and respiration of nonsynaptic and synaptic mitochondria derived from R6/2 and WT mice .....	113
b. Expression of nuclear-encoded proteins in mitochondria from R6/2 mice ..	118
c. Cellular respiration and extracellular acidification of striatal neurons from R6/2 mice .....	120
d. Ca <sup>2+</sup> uptake capacity of nonsynaptic and synaptic mitochondria from R6/2 mice .....	123
e. Mitochondrial Ca <sup>2+</sup> accumulation in striatal neurons from R6/2 mice .....	126
f. Morphological characterization of mitochondria in striatal neurons from R6/2 mice .....	128
IV. Discussion and Future Directions .....	131
A. Oxidative metabolism and mitochondrial Ca <sup>2+</sup> handling in the YAC128 mouse model .....	131
B. Oxidative metabolism and Ca <sup>2+</sup> handling in striatal mitochondria from YAC128 mice .....	135
C. Oxidative metabolism and mitochondrial Ca <sup>2+</sup> handling in the R6/2 mouse model .....	141
D. Future Directions .....	148
V. Reference List .....	165
Curriculum Vitae	

## LIST OF TABLES

Table 1: Genetic Rodent HD Models .....	12
Table 2: Calculation of a sample size using Power Analysis Method for YAC128.....	58
Table 3: Calculation of a sample size using Power Analysis Method for R6/2.....	59
Table 4: Body composition of YAC128 and WT mice .....	93

## LIST OF FIGURES

Figure 1: Electron Transport Chain (ETC), ATP synthase, and Mitochondrial Calcium Uniporter .....	21
Figure 2: Representative measurements of respiration and mitochondrial membrane potential in isolated synaptic mitochondria .....	22
Figure 3: Isolation and purification of brain nonsynaptic and synaptic mitochondria .....	45
Figure 4: Separation of nonsynaptic mitochondria and synaptosomes on discontinuous Percoll gradient .....	46
Figure 5: Behavioral phenotype of 2-month-old YAC128 mice and a representative genotyping .....	62
Figure 6: Detection of wild-type mouse huntingtin (Htt) and mutant human huntingtin (mHtt) in homogenates, and cytosolic and synaptic mitochondrial fractions from 2-month-old YAC128 and WT mice .....	66
Figure 7: Representative electron micrographs of nonsynaptic and synaptic brain mitochondria isolated from YAC128 and WT mice .....	67
Figure 8: Respiratory activity of brain nonsynaptic mitochondria isolated from 2-month-old WT and YAC128 mice .....	70
Figure 9: Respiratory activity of brain synaptic mitochondria isolated from 2-month-old WT and YAC128 mice .....	71
Figure 10: Respiratory activity of nonsynaptic mitochondria isolated from 10-month-old WT and YAC128 mice .....	72
Figure 11: Respiratory activity of synaptic mitochondria isolated from 10-month-old WT and YAC128 mice .....	73

Figure 12: KCN completely inhibits respiration of isolated brain mitochondria .....	74
Figure 13: Respiratory activity of unpurified brain mitochondria isolated from 2-month-old WT and YAC128 mice .....	75
Figure 14: Respiratory activity of liver mitochondria isolated from 2-month-old WT and YAC128 mice .....	76
Figure 15: Respiratory activity of heart mitochondria isolated from 2-month-old WT and YAC128 mice .....	77
Figure 16: Expression of nuclear encoded mitochondrial proteins in nonsynaptic and synaptic mitochondria isolated from 2- and 10-month-old WT and YAC128 mice .....	80
Figure 17: Blue Native gel electrophoresis and western blotting with brain mitochondria lysates .....	81
Figure 18: Mitochondrial membrane potential in nonsynaptic and synaptic mitochondria isolated from 2-month-old WT and YAC128 mice .....	83
Figure 19: The effect of bovine serum albumin (BSA) on mitochondrial membrane potential in nonsynaptic and synaptic mitochondria isolated from 2-month-old WT and YAC128 mice .....	84
Figure 20: OCR and ECAR of cultured neurons from YAC128 and WT mice: 'high glucose conditions' .....	88
Figure 21: OCR and ECAR of cultured neurons from YAC128 and WT mice: 'low glucose conditions' .....	89
Figure 22: ADP and ATP content in brain mitochondria and cultured striatal neurons derived from YAC128 and WT mice .....	90

Figure 23: Oxygen consumption, CO <sub>2</sub> release, energy expenditure, and total physical activity of 10-month-old YAC128 and WT mice .....	92
Figure 24: Ca <sup>2+</sup> uptake capacity of brain nonsynaptic mitochondria isolated from YAC128 and wild-type FVB/NJ mice .....	96
Figure 25: Ca <sup>2+</sup> uptake capacity of brain synaptic mitochondria isolated from YAC128 and wild-type FVB/NJ mice .....	97
Figure 26: Ca <sup>2+</sup> -induced mitochondrial swelling and depolarization in synaptic mitochondria from WT and YAC128 mice.....	98
Figure 27: Purity of striatal nonsynaptic and synaptic mitochondria isolated from FVB/NJ and YAC128 mice and detection of mHtt in mitochondrial fractions.....	101
Figure 28: Respiratory activity of striatal nonsynaptic mitochondria isolated from 2-month-old FVB/NJ and YAC128 mice .....	104
Figure 29: Respiratory activity of striatal nonsynaptic and synaptic mitochondria isolated from 2-month-old FVB/NJ and YAC128 mice .....	105
Figure 30: Expression of nuclear encoded mitochondrial proteins in nonsynaptic and synaptic striatal mitochondria derived from FVB/NJ and YAC128 mice .....	107
Figure 31: Ca <sup>2+</sup> uptake capacity of brain nonsynaptic mitochondria isolated from the striatum of FVB/NJ and YAC128 mice.....	110
Figure 32: Ca <sup>2+</sup> uptake capacity of brain synaptic mitochondria isolated from the striatum of FVB/NJ and YAC128 mice.....	111
Figure 33: Comparison of motor phenotype of 6-week-old R6/2 and WT mice and representative genotyping.....	115

Figure 34: Respiratory activity of brain nonsynaptic mitochondria isolated from 6- to 8-week-old WT and R6/2 mice .....	116
Figure 35: Respiratory activity of brain synaptic mitochondria isolated from 6- to 8-week-old WT and R6/2 mice.....	117
Figure 36: Expression of nuclear encoded mitochondrial proteins in nonsynaptic and synaptic mitochondria isolated from 8-week-old WT and R6/2 mice .....	119
Figure 37: OCR and ECAR of cultured striatal neurons from WT and R6/2 mice in 'high' and 'low' glucose medium conditions .....	122
Figure 38: Ca <sup>2+</sup> uptake capacity of brain nonsynaptic mitochondria isolated from 6-to 8-week-old WT and R6/2 mice .....	124
Figure 39: Ca <sup>2+</sup> uptake capacity of brain synaptic mitochondria isolated from 6- to 8-week-old WT and R6/2 mice.....	125
Figure 40: Mitochondrial Ca <sup>2+</sup> accumulation following transient glutamate-induced elevations in cytosolic Ca <sup>2+</sup> in striatal neurons derived from WT and R6/2 mice .....	127
Figure 41: Representative 3D reconstructions of mitochondrial networks and electron micrographs of cultured striatal neurons from WT and R6/2 mice .....	130
Figure 42: Characterization of undifferentiated WT and HD hiPSCs .....	152
Figure 43: Characterization of hiPSCs induced to a neural progenitor fate .....	153
Figure 44: Characterization of cortical progenitors derived from WT and HD hiPSCs..	155
Figure 45: Characterization of neurons derived from cortical progenitors from WT and HD hiPSCs.....	156
Figure 46: Characterization of striatal progenitors derived from WT and HD hiPSCs...	158

Figure 47: Characterization of neurons derived from striatal progenitors from WT and HD hiPSCs.....	159
Figure 48: Genotypic analysis of CAG repeat expansion and expression of mHtt in progenitors derived from human HD iPSCs.....	161
Figure 49: Ca <sup>2+</sup> dynamics in response to NMDA in striatal neurons derived from WT and HD human iPSCs .....	163



## LIST OF ABBREVIATIONS

2,4-DNP	2,4-dinitrophenol
3-NPA	3-nitropropionic acid
ADP	adenosine-5'-diphosphate
AFP	$\alpha$ -Fetoprotein
Ant	antimycin A
ATP	adenosine-5'-triphosphate
a.u.	arbitrary units
AUC	area under the curve
B6CBA	background mouse strain for R6/2
BACHD	transgenic rodent model of HD expressing HTT on bacterial artificial chromosome
BDNF	brain derived neurotrophic factor
BRACH	BRACHURY
BSA	bovine serum albumin
[Ca <sup>2+</sup> ] <sub>c</sub>	cytosolic calcium concentration
CNS	central nervous system
COX IV	cytochrome oxidase subunit IV
CREB	cyclic adenosine monophosphate-responsive element binding protein
CsA	cyclosporin A
CyD	cyclophilin D
DAPI	2-(4-amindinophenyl-1H-indole-6-carboxamide)
DARPP-32	dopamine and cyclic AMP-regulated phosphoprotein relative molecular mass 32,000
DEXA	dual-energy X-ray absorptiometry
DIV	days <i>in vitro</i>
DKK1	Dickkopf WNT Signaling Pathway Inhibitor 1
DMSO	dimethyl sulfoxide
ECAR	extracellular acidification rate
EGTA	ethylene glycol tetraacetic acid
ETC	electron transport chain
FCCP	carbonyl cyanide-p-trifluoromethoxyphenylhydrazone
FGF	fibroblast growth factor
FVB/NJ	background mouse strain for YAC128
GABA	gamma-aminobutyric acid
GAPDH	glyceraldehyde 3-phosphate dehydrogenase
glu/glut	glutamate
GST	glutathione S-transferase
HD	Huntington's disease
HEAT	huntingtin, elongation factor 3, protein phosphatase 2A, and TOR1
HEPES	4-(2-hydroxyethyl)-1-piperazineethanesulfonic acid
HTT	huntingtin gene
Htt	huntingtin protein
iPSCs	induced pluripotent stem cells
IT15	interesting transcript 15
K <sub>d</sub>	dissociation constant
mAb	monoclonal antibody
mal	malate
MAP-2	microtubule associated protein-2

MEK1/2	mitogen-activated protein kinase kinase 1/2
mHtt	mutant huntingtin protein
MK-801	(+)-5-methyl-10,11-dihydro-5H-dibenzo[a,d]cyclohepten-5, 10-imine maleate
Mn-SOD	manganese superoxide dismutase
MRI	magnetic resonance imaging
MSN	medium spiny neuron
Mtc	mitochondria
NMDA	N-methyl-D-aspartate
NMDAR	N-methyl-D-aspartate receptor
NMDG	N-methyl-D-glucamine
OCR	oxygen consumption rate
Oligo	oligomycin
PAGE	polyacrylamide gel electrophoresis
PBS	phosphate-buffered saline
PCR	polymerase chain reaction
PGC-1 $\alpha$	peroxisome proliferator-activated receptor gamma coactivator 1-alpha
polyQ	poly-glutamine
PTP	permeability transition pore
pyr	pyruvate
RER	respiratory exchange ratio
ROS	reactive oxygen species
Rot	rotenone
SD	standard deviation
SDS	sodium dodecyl sulfate
SEM	standard error of the mean
Shh	Sonic hedgehog protein
succ	succinate
TBZ	tetrabenazine
TPP <sup>+</sup>	tetraphenylphosphonium
V <sub>2</sub>	mitochondrial respiration in the presence of substrates
V <sub>3</sub>	mitochondrial respiration in the presence of substrates and ADP
V <sub>4</sub>	mitochondrial respiration in the presence of substrates following consumption of ADP
V <sub>DNP</sub>	mitochondrial respiration in the presence of 2,4-dinitrophenol
VO <sub>2</sub>	oxygen consumption rate (in the context of whole animal respiration)
VCO <sub>2</sub>	carbon dioxide release rate
VDAC1	voltage-dependent anion channel isoform 1
VMAT2	vesicular monoamine transferase 2
WT	wild-type
YAC	yeast artificial chromosome
YFP	yellow fluorescent protein

## **I. Introduction**

### **A. Huntington's Disease**

Huntington's disease (HD) was first described in detail by George Huntington in 1872, lending his name to the eponymous disease. Huntington, a 22-year-old physician living in Long Island, NY at the time of publication of his seminal report, "On Chorea", had aggregated not only his own clinical observations but those of his father and grandfather, also physicians, to generate the most concise and clinically accurate account of the disease to that point. Although written descriptions of the disease predate Huntington's account, his was the first to describe the hereditary nature and comprehensively discuss symptoms of HD (Huntington 1872;Roos 2010). Indeed, the most discerning symptom of HD is the abrupt, irregular, spontaneous, and uncontrolled movements described as chorea. In addition to motor symptoms, psychiatric disturbances and cognitive abnormalities are the two other components of a classically evoked triad of symptoms which are commonly used to describe the overt presentation of the disease (Bates *et al.* 2015). Specific psychiatric aberrations associated with HD include personality changes, anxiety, and depression and cognitive impairments are most commonly marked by a decline in abstract thinking and loss of executive function. Recent evidence suggests that alterations in mental state and cognition may precede onset of motor symptoms, leading to the designation of the so-called prodromal stage of HD. The stage of HD that is typically referred to as symptomatic HD is characterized by the initiation of motor symptoms. Memory loss also manifests as the disease advances (Govert and Schneider 2013). By virtue of the progressive nature of HD, patients will gradually lose the ability to perform the most basic of tasks, including walking, talking, swallowing, and ultimately the ability to take care of themselves. Complications from some of these diminished capabilities are life-threatening. The most common cause of death for HD patients is complications from aspiration pneumonia, due to difficulty or

inability to swallow food, drink, and sputum (Haines and Conneally 1986; Bates *et al.* 2002; Heemskerk and Roos 2012).

Huntington's disease is an autosomal dominantly inherited neurodegenerative disorder affecting approximately 1 in 10,000 people, with variable incidence among different ethnic groups (Shoulson and Young 2011; Pringsheim *et al.* 2012). Among individuals of European ancestry the prevalence rate is estimated to be 11-14 per 100,000 people, whereas some east Asian populations have a prevalence rate of only 1 per 100,000 (Roos 2010; Bates *et al.* 2015). In the United States, it is estimated that 30,000 individuals have manifest HD (Shoulson and Young 2011). Approximations of HD prevalence are generally considered to be underestimates due to the late onset of the disease and resultant inaccurately low rate of diagnosis among young, asymptomatic individuals (Bates *et al.* 2015). Commencement of motor symptoms typically occurs at midlife, with an average age of onset of 38 years (Govert and Schneider 2013). However, the age of motor symptom onset varies widely, with symptom onset recorded to have occurred as early as 2 years and as late as 80 years of age (Myers 2004). Historically, the term "manifest HD" was used to indicate the period of HD at which motor symptoms become apparent, and it was believed that the onset of chorea represented the earliest symptoms of HD. Although not solely confined to the context of Huntington's disease, "chorea" is the term frequently used to describe the irregular, abrupt, spontaneous, and involuntary movements associated with HD. More recently, however, it has been shown that measurable but only slightly perceptible cognitive, motor, and psychiatric changes precede the onset of overt motor symptoms (Biglan *et al.* 2009; Biglan 2010). This finding led to a change in the naming convention to describe HD symptom progression. Currently, "prodromal HD" is considered the stage of the disease at which subtle changes in cognition or psychiatric state can be measured before the onset of manifest motor symptoms (Reilmann *et al.* 2014).

Since HD can be definitively diagnosed with a genetic test and symptom progression is delayed, the potential exists for pre-symptomatic therapy. However, the treatments currently in use only act to mitigate symptoms, but do not address underlying causes of neuropathology. The dearth of disease-modifying therapeutics may be partially due to an incomplete understanding of the mechanisms of neuronal dysfunction and death in HD. Currently, the only FDA-approved treatment for HD is tetrabenazine (TBZ), which is indicated for the treatment of chorea associated with HD (Kaur *et al.* 2016). TBZ is an inhibitor of vesicular monoamine transferase 2 (VMAT2), preventing the reuptake of monoamines into intracellular vesicles and effectively hindering the release of dopamine (Zheng *et al.* 2006). Unfortunately, the adverse effects of TBZ administration can be severe with side effects including insomnia, fatigue, akathisia, anxiety, and increased suicidal ideation (Chen *et al.* 2012). Moreover, the beneficial effect of TBZ may decline over time (Fasano and Bentivoglio 2009). Thus, the development of new therapies for treating and curing HD borne from a deeper understanding of the molecular mechanisms of disease is critical for individuals suffering with HD.

Degeneration associated with HD is localized to the brain. The brain region that is most vulnerable to the effects of the disease is the striatum, and the most salient symptoms of HD have been correlated with and are consistent with striatal loss (Vonsattel and DiFiglia 1998; Bates *et al.* 2002; Walker and Raymond 2004). At more advanced stages of the disease, cortical loss has also been observed, but cortical pathology occurs to a lesser extent than striatal loss (Rosas *et al.* 2003). Diminution of striatal volume has been detected before symptom onset via magnetic resonance imaging, and in some cases striatal volume loss has been observed up to 10 years before the onset of motor symptoms (Rosas *et al.* 2003; Aylward *et al.* 2013). The mechanism by which striatal neurons are differentially vulnerable is unclear. Comprising

about 95% of all neurons in the striatum are the gamma-aminobutyric acid (GABA)ergic medium spiny neurons (MSNs) (Vonsattel and DiFiglia 1998; Han *et al.* 2010). MSNs, the major inhibitory neurons of the striatum, are the most vulnerable and earliest affected cell type in HD (Reiner *et al.* 1988; Walker and Raymond 2004; Ehrlich 2012). The mechanism of increased vulnerability of MSNs in HD is not clear, but may include an inherently lower metabolic activity of MSNs. (Nishino *et al.* 2000).

In 1993, a consortium called the Huntington's Disease Collaborative Research Group found that HD is linked to a gene that had previously only been known as IT15 ("interesting transcript 15") (MacDonald *et al.* 1993). Prior to this discovery, researchers had merely managed to identify the chromosome upon which the gene resided using genetic linkage (Bird *et al.* 1986). Following the study by MacDonald *et al.*, the gene was renamed huntingtin (*HTT*) and found to be located on the p arm of chromosome 4 at position 16.3 (MacDonald *et al.* 1993). In most healthy individuals *HTT* contains a stretch of 16-20 CAG repeats encoding a poly-glutamine (polyQ) stretch near the NH<sub>2</sub> terminus of the huntingtin protein (Htt). However, a lower percentage of healthy individuals may have slightly longer CAG repeat tracts of 21-26 repeats. An expansion mutation in *HTT* leading to the elongation of the CAG repeat tract to more than 35 repeats will result in HD with 100% penetrance. Individuals who possess a CAG stretch in the *HTT* gene of 27-34 repeats have a possibility of developing HD, but the likelihood is less than 100% (Myers 2004; Paulson and Albin 2011). Such individuals, even if they do not develop symptoms of HD, are still at risk of passing HD to their offspring, especially if the expansion is being passed from the father (Ridley *et al.* 1988; Ashizawa *et al.* 1994). The mechanism for this increased likelihood of a father passing an expansion that could lead to HD remains unresolved, but may be related to instability of the CAG repeat during spermatogenesis (Wheeler *et al.* 2007). If the *HTT* gene is expanded to possess greater than 35 repeats, the resultant pathogenic protein product is dubbed mutant huntingtin

(mHtt) (MacDonald *et al.* 1993). Genetic anticipation has been observed in HD, possibly due to increased genetic instability during replication as the expanded CAG tract becomes longer (Bates *et al.* 2002). Greater number of repeats has been correlated with earlier age of onset of motor symptoms and more severe symptom progression (Roze *et al.* 2010).

#### **a. Huntingtin Protein Function**

*HTT* encodes a 350 kDa protein, called huntingtin (Htt), that is ubiquitously expressed throughout all tissues (MacDonald *et al.* 1993). Wild-type (WT) Htt is localized to the cytoplasm and loosely associated with the outer mitochondrial membrane since the protein can be removed from the membrane just by washing mitochondria with NaCl (Sharp *et al.* 1995). The protein possesses a polyQ stretch of varying length near the N-terminus (Zuccato *et al.* 2010). The wild-type Htt protein has a polyQ stretch that is not more than 35 glutamines, but is typically only 16-20 glutamines in most humans (MacDonald *et al.* 1993). Although wild-type Htt is known to be expressed ubiquitously, it is most highly expressed in neurons of the central nervous systems (CNS) (Sharp *et al.* 1995). However, the level of expression of wild-type Htt does not differ between various regions of the brain nor is Htt more highly expressed in MSNs, the most vulnerable cell type in HD (Sharp *et al.* 1995; Schilling *et al.* 1995). Moreover, the level of wild-type Htt expression is not correlated with vulnerability to HD (Trottier *et al.* 1995; Fusco *et al.* 1999).

Htt expression is essential for development and lack of Htt results in embryonic lethality (DiFiglia *et al.* 1995). Without Htt expression, the developing embryo cannot undergo proper gastrulation (Woda *et al.* 2005). A later study indicated that the mutated form of Htt, mHtt, is alone sufficient to mediate proper embryonic development. Leavitt *et al.* demonstrated that introducing mHtt to an endogenous Htt knock-out precludes

embryonic lethality, indicating that at least some of the normal functions of Htt are retained by mHtt (Leavitt *et al.* 2001). Another study using Cre/loxP excision strategy to conditionally inactivate Htt in adult mice resulted in the acquisition of motor deficits similar to those seen in HD mice as well as cerebral atrophy in these mice (Reddy *et al.* 1999; Dragatsis *et al.* 2000). These studies not only indicate that Htt is critical for embryonic development and maintenance of neuronal viability, but also suggest that the expanded polyQ mutation in mHtt does not necessarily eliminate normal protein functions inherent to wild-type Htt.

Since Htt is a large protein of 350 kDa with several functional domains, it has the capacity to be involved in numerous processes and functions. The best-described functions of Htt include regulation of brain derived neurotrophic factor (BDNF) production (Zuccato *et al.* 2001; Gauthier *et al.* 2004), vesicle transport (Brandstaetter *et al.* 2014), endocytosis (Velier *et al.* 1998), transcriptional regulation (Li and Li 2004), and anti-apoptotic function (Rigamonti *et al.* 2000).

Wild-type Htt is known to interact with over 100 proteins, primarily facilitated by the presence of 36 HEAT (huntingtin, elongation factor 3, protein phosphatase 2A, and TOR1) consensus sequences, each about 40 amino acids in length, within Htt (Neuwald and Hirano 2000). These domains mediate interactions with proteins that are involved in various processes including pre- and post-synaptic signaling, cytoskeletal organization, calcium signaling, and mitochondrial functions (Shirasaki *et al.* 2012). The strength of interaction of Htt with some proteins has been observed to be dependent on polyQ length. Indeed, certain proteins interact more strongly with either Htt or mHtt (Harjes and Wanker 2003; Li and Li 2004). Among the many hypotheses regarding the effect of the expanded polyQ in mHtt is the proposition that the expansion mutation may promote interaction with a different suite of binding partners thus leading to either the loss of



certain functions, the gaining of new functions, or both. Some groups have reported that both gain- and loss-of-function are involved in HD pathology (Zuccato *et al.* 2010).

Although Htt does not have a DNA binding domain that would allow direct binding to nucleic acids, it does interact with proteins that are known to bind to DNA. Thus wild-type Htt has the capacity to influence transcription (Cha 2007). Mutant Htt was found to bind p53 and increase its expression and transcriptional activity, leading to the upregulation of certain nuclear-encoded mitochondrial proteins and altered membrane potential (Bae *et al.* 2005). Additionally, mHtt has been shown to repress transcription of PGC-1 $\alpha$ , a gene encoding a transcriptional co-activator that regulates expression for genes involved in mitochondrial respiration and mitochondrial biogenesis (Cui *et al.* 2006). Moreover, the knock-out of PGC-1 $\alpha$  in mice results in mitochondrial defects, altered motor functions, and striatal degeneration (Cui *et al.* 2006). These findings suggest that Htt and mHtt are involved in the regulation of mitochondrial functions.

## **b. Models of HD**

Prior to the discovery of the genetic mutation linked to HD, researchers relied on chemical models to study HD. Use of such models was justified by the observation that certain neurotoxins recapitulated the striatal degeneration that is the hallmark of HD pathology (McGeer and McGeer 1976). Compounds used in these early studies could be categorized into one of two categories: excitotoxic chemicals and mitochondrial toxins. Quinolinic acid and kainic acid, compounds responsible for inducing excitotoxicity, when injected into the brains of mice caused striatal lesions that were reminiscent of the atrophy observed in HD patients (Beal *et al.* 1986). Inhibitors of Complex II of the mitochondrial electron transport chain such as malonic acid and 3-nitropropionic acid were likewise used to generate chemical models of HD because, when administered to mice, these toxins produced striatal lesions and motor disturbances similar to HD

patients (Borlongan *et al.* 1995;Brouillet *et al.* 1999). Although these chemicals produced HD-like motor disturbances and striatal degeneration, they only served as an approximation of disease pathology because they neglected to account for the genetic underpinnings of the disease. However, these models provide some insight into potential deleterious mechanisms in HD because they served as some of the first pieces of evidence to indicate that HD pathology may be linked to either abnormal cytosolic Ca<sup>2+</sup> dynamics or mitochondrial dysfunction (McGeer and McGeer 1976;Borlongan *et al.* 1995). However, such extrapolations should be made with caution because the mechanisms that underlie chemically induced motor abnormalities and striatal loss could be distinct from the mechanisms involved in HD pathology.

Following the identification of the mutation linked to HD, the first rodent models of HD were developed based on genetic manipulation of the *HTT* gene (Ramaswamy *et al.* 2007;Pouladi *et al.* 2013). The genetic rodent models of HD that express an elongated polyQ stretch can be broadly classified into three categories with respect to the characteristics of the protein expression in each: (i) N-terminal (polyQ-containing) truncated fragment of human mutant Htt; (ii) full-length human mutant Htt protein; and (iii) full-length mouse mutant Htt protein. Table 1 summarizes the three types of HD rodent models, citing specific examples, and provides detail about relevant findings from each model.

One of the first genetic mouse models of HD to be generated was the R6/2 mouse, which expresses an N-terminal fragment of human mHtt with an expanded polyQ region (Mangiarini *et al.* 1996). The R6/2 mice are notable for their accelerated symptom progression, which results in a more severe phenotype that afflicts mice at a younger age compared to full-length mHtt models (Ramaswamy *et al.* 2007). Though not the most genetically accurate models, N-terminal fragment-expressing mice are used by researchers to study HD symptom progression or the potential mechanisms of fragment-

induced HD pathology. Mice such as the YAC128 model express full-length human mHtt and are considered a more accurate genetic representation of the human disease due to the presence of a motor and cognitive phenotype. YAC128 mice exhibit neuronal degeneration and motor deficits similar to fragment HD models albeit on a more protracted time course (Slow *et al.* 2003). A shared caveat for all transgenic mouse models, whether expressing full-length or fragment of human mHtt, is that they possess more than two alleles of Htt or mHtt. In addition to endogenous mouse Htt gene, the human mHtt transgene (which in some cases has integrated multiple times into the genome) is expressed. Obviously, this is a departure from the genetics of human HD patients who typically have one normal copy of *HTT* and one mutant copy.

Models of HD that have an expanded CAG repeat introduced into normal endogenous mouse HTT (so-called “knock-in models”) are considered the most genetically faithful representation of the genetics of human disease. The mutant protein is expressed in every tissue and has been observed in both the cytosolic and nuclear compartments (Menalled 2005). However, these models possess a very mild disease phenotype, typically live the full lifespan of a normal mouse, and, in some cases, striatal atrophy never occurs (Wheeler *et al.* 1999; Wheeler *et al.* 2000). For these reasons, knock-in models have received only tepid attention from many researchers because these models may not closely recapitulate the symptoms and pathology of the disease. The selection of a rodent model for the study of disease mechanisms in HD requires pensive consideration to choose the best model based on which aspects of the disease are to be investigated.

In the initial studies described herein, the YAC128 mouse model was used to assess various aspects of mitochondrial function and Ca<sup>2+</sup> handling in neurons. As the name suggests, this model takes advantage of a yeast artificial chromosome (YAC) to allow for expression of the relatively large human mutant *HTT* gene in its entirety. The

full-length human mutant *HTT* gene expressed by this mouse possesses a 128 CAG repeat expansion with the gene under control of human *HTT* promoter as well as upstream and downstream *cis*-regulatory elements (Slow *et al.* 2003). Mutant Htt is expressed in all tissues of the mouse where full-length protein is localized to the cytosol, and fragments of mHtt reside in both the cytosol and nucleus (Slow *et al.* 2003). Full-length mHtt transgenic models typically display delayed symptom onset, allowing for the study of HD mechanisms in pre-symptomatic animals. This advantage provides researchers with the opportunity to investigate the primary causes of disease without the potentially confounding impediment of studying animals that already display an HD phenotype (Fan and Raymond 2007). The YAC128 mouse was developed as an improvement upon previous YAC models that had shorter polyQ stretches (Hodgson *et al.* 1999). The longer glutamine expansion leads to a decrease in the age at which motor phenotypes are first observed, making these animals more convenient for use in some studies. The correlation between increased polyQ length and decreased age of symptom development is also a characteristic of the human disease (Roze *et al.* 2010). In YAC128 mice, motor symptoms are visible by 12 weeks and significant striatal atrophy can be observed by 9 months (Bates *et al.* 2002; Slow *et al.* 2003; Ramaswamy *et al.* 2007). These findings indicate that striatal loss may not be necessary for the onset of motor symptoms, and may suggest that neuronal dysfunction occurs well before striatal atrophy. The YAC128 model was initially chosen for use in this study because, although it is not the most genetically faithful model, it does express full-length human mHtt and it displays motor symptoms and striatal atrophy, unlike many knock-in models. Additionally, the slowed progression of symptom onset in YAC128 mice compared to R6/2 mice, a mHtt fragment model, allows for the pre-symptomatic study of adult animals.

The R6/2 mouse model is one of the first-developed and the most well-studied mHtt fragment transgenic mouse model of HD (Mangiarini *et al.* 1996). In contrast to full-length mHtt models, such as YAC128, these mice express the N-terminal fragment of human mHtt with a 144-glutamine stretch. The fragment contains only exon 1 of the human HTT gene in addition to the human HTT promoter (Mangiarini *et al.* 1996). In this model, mHtt is expressed in all tissues and the protein has been observed in the cytoplasm as well as the nucleus (Sathasivam *et al.* 2010). R6/2 mice display overt and severe behavioral abnormalities by 6 weeks and significant striatal atrophy can be observed by 11 weeks (Stack *et al.* 2005). Whereas full-length transgenic mouse models can live for more than one year, the average lifespan of R6/2 mice is only about 13 weeks (Mangiarini *et al.* 1996; Van Raamsdonk *et al.* 2006). The large number of repeats in the R6/2 model corresponds to juvenile onset HD, which only occurs in about 10% of human cases, but this model provides an opportunity for researchers to assess the potential deleterious effect of mHtt fragments (Mangiarini *et al.* 1996; Nance and Myers 2001). In our study, symptomatic 6- to 8-week-old R6/2 mice were utilized to probe the effect of mHtt fragments on the pathogenesis of HD.

In addition to mouse models, other animals have been used as HD models, including rats, song birds, pigs, sheep, and non-human primates (Yang *et al.* 2008; Jacobsen *et al.* 2010; Yang *et al.* 2010; Yu-Taeger *et al.* 2012). Cell lines that model HD have also been generated. One of the most commonly used cell lines is derived from knock-in mice that possess a 111 glutamine stretch (Trettel *et al.* 2000). These aptly named STHdh<sup>Q111/Q111</sup>, conditionally immortalized, striatal progenitor cells have been used to study oxidative metabolism and Ca<sup>2+</sup> handling and display phenotypes reminiscent of primary striatal neurons from knock-in mice, including increased propensity to cell death (Trettel *et al.* 2000; Gines *et al.* 2003; Milakovic *et al.* 2006).

Table 1: Genetic Rodent HD Models

<b>Rodent Model</b>	<b>Construct</b>	<b>Notable Features</b>
<b><i>Transgenic truncated N-terminal fragment models</i></b>		
Transgenic R6/2 mice (Mangiarini <i>et al.</i> , 1996)	N-terminal fragment (67 aa) of human <i>HTT</i> with 115-150 or 195 CAG repeats	Neuronal atrophy by 3 months (Stack <i>et al.</i> , 2005) Death at 10-13 weeks (Mangiarini <i>et al.</i> , 1996) Decreased respiratory rates in striatal homogenate (Aidt <i>et al.</i> , 2013) Augmented Ca <sup>2+</sup> uptake capacity in brain nonsynaptic mitochondria (Oliveira <i>et al.</i> , 2007)
Transgenic N171-82Q mice (Schilling <i>et al.</i> , 1999)	N-terminal fragment (171, 118, or 586 aa) of human <i>HTT</i> with 82 CAG repeats	Neuronal atrophy by 16 weeks (McBride <i>et al.</i> , 2006)
Transgenic D9-N171-98Q mice, also known as DE5 mice (Brown <i>et al.</i> , 2008)	N-terminal fragment of human <i>HTT</i> with 98 CAG repeats expressed only in medium spiny neurons of the striatum	No striatal atrophy (Kim <i>et al.</i> , 2011) Mild motor abnormalities (Brown <i>et al.</i> , 2008)
Transgenic Short Stop mice (Slow <i>et al.</i> , 2005)	N-terminal fragment (171 aa) of human <i>HTT</i> with 128 CAG repeats	Presence of mHtt aggregates; No behavioral dysfunction or neuronal loss (Slow <i>et al.</i> , 2005)
Transgenic HD rats (von Horsten <i>et al.</i> , 2003)	Express 727 amino acids of the <i>HTT</i> <sub>51Q</sub> gene, corresponding to 22% of the full-length gene	Reduced mitochondrial membrane potential stability in response to Ca <sup>2+</sup> , decreased Ca <sup>2+</sup> uptake capacity, increased propensity to PTP induction (Gellerich <i>et al.</i> , 2008)
<b><i>Transgenic full-length models</i></b>		
Transgenic BACHD mice (Gray <i>et al.</i> , 2008)	Full-length human <i>HTT</i> gene with 97 mixed CAA-CAG repeats	Striatal atrophy by 12 months Symptoms by 6 months (Gray <i>et al.</i> , 2008) Decrease in maximal respiratory capacity of primary neurons (Gouarne <i>et al.</i> , 2013)
Transgenic YAC46 or YAC72 mice (Hodgson <i>et al.</i> , 1999)	Full-length human <i>HTT</i> gene with 46 or 72 CAG repeats	Decreased Ca <sup>2+</sup> uptake capacity (Panov <i>et al.</i> , 2002)

Table 1: Genetic Rodent HD Models (continued)

<b>Rodent Model</b>	<b>Construct</b>	<b>Notable Features</b>
Transgenic YAC128 mice (Slow <i>et al.</i> , 2003)	Full-length human <i>HTT</i> gene with 128 CAG repeats	Neuronal atrophy by 9 months (Slow <i>et al.</i> , 2003) Augmented mitochondrial depolarization in spiny neurons (Fernandes <i>et al.</i> , 2007) Augmented Ca <sup>2+</sup> uptake capacity in brain nonsynaptic mitochondria (Oliveira <i>et al.</i> , 2007)
Transgenic BACHD rats (Yu-Taeger <i>et al.</i> , 2012)	Full-length human <i>HTT</i> gene with 97 mixed CAA-CAG repeats	Early onset motor deficits mHtt aggregates (Yu-Taeger <i>et al.</i> , 2012)
<b>Knock-in full-length models</b>		
Knock-in HdhQ50, Q92, and Q111 mice (Wheeler <i>et al.</i> , 1999)	Mouse <i>HTT</i> gene with inserted 50, 92, or 111 CAG repeats in exon 1	No striatal degeneration (Wheeler <i>et al.</i> , 1999) No cognitive phenotypes (Wheeler <i>et al.</i> , 2000) Gait abnormalities at 24 months in Q111 (Wheeler <i>et al.</i> , 2000) No change in the activities of mitochondrial complexes I-IV (Milakovic and Johnson, 2005)
Knock-in Hdh150Q and Hdhq200 mice (Lin <i>et al.</i> , 2001; Yu <i>et al.</i> , 2003)	Mouse <i>HTT</i> gene with inserted 150 and 200 CAG repeats in exon 1 in a single allele (Hdh <sup>150/+</sup> ) or both alleles (Hdh <sup>150/150</sup> )	No cognitive symptoms Respiratory activity of striatal neurons from Hdh150Q is similar to WT (Oliveira <i>et al.</i> , 2007) No change in Ca <sup>2+</sup> uptake capacity in brain nonsynaptic mitochondria (Oliveira <i>et al.</i> , 2007)

### **c. Proposed Mechanisms of Neurodegeneration in HD**

Huntingtin is a protein composed of over 3100 amino acids and has a molecular weight of 350 kDa (MacDonald *et al.* 1993). It has been observed to interact with a large number of proteins, potentially interfering with a wide array of cellular functions. For this reason, the mutation of huntingtin could potentially affect different processes by either causing loss of certain normal Htt functions or leading to the acquisition of new functions by mHtt. These dichotomic components, gain-of-function and loss-of-function alterations, are not necessarily mutually exclusive, but form the foundation by which hypotheses are generated regarding the mechanisms of mHtt effects in HD. Therefore, the overall pathology of HD may be the result of a convergence of many deleteriously altered cellular mechanisms. Although this dissertation focuses on the possible effects of mHtt on mitochondrial functions, other hypotheses provide alternative explanations for HD pathogenesis. Some of these alternative hypotheses will be briefly described below.

Although mHtt does not possess a DNA binding domain, it has been shown to interact with transcription factors and indirectly influence transcription (Zuccato *et al.*, 2010). Reports indicate that both WT and mHtt are cleaved into N-terminal fragments by caspases, and fragments of mHtt have been found in the nucleus (Warby *et al.* 2008). Initial studies suggesting that mHtt may interfere with transcriptional regulation showed the direct binding of mHtt with transcription factors cAMP-responsive element (CRE) binding protein (CREB) and with TATA box-binding protein (TBP)-associated factor TAF4/TAFII130, thereby altering transcription (Steffan *et al.* 2000; Dunah *et al.* 2002; Shimohata *et al.* 2005). Additionally, evidence suggests that mHtt interacts with the peroxisome proliferator-activated receptor  $\gamma$  (PPAR $\gamma$ ) coactivator-1 $\alpha$  (PGC-1 $\alpha$ ), which is involved in regulation of mitochondrial functions such as mitochondrial biogenesis, respiration, energy metabolism, and thermogenesis (Houten and Auwerx 2004). Data show that PGC-1 $\alpha$  expression is reduced in various models of HD (Cui *et al.* 2006).



Moreover, exogenous expression of PGC-1 $\alpha$  protects primary striatal neurons derived from HD models and direct delivery of PGC-1 $\alpha$  into the striatum of HD mice decreases striatal atrophy (Cui *et al.* 2006). The modes by which the polyQ stretch of mHtt may precipitate transcriptional dysregulation may include binding to transcription factors or other coactivators and preventing their normal function (Cha 2007). Indeed, altered localization of mHtt may mediate this process since mHtt has shown increased nuclear localization compared to WT Htt, which is primarily a cytosolic protein (Kegel *et al.* 2002; Sugars and Rubinsztein 2003).

Another potential consequence of alterations in transcription induced by mHtt could be a decrease of brain-derived neurotrophic factor (BDNF) expression in the brains of HD patients. Medium spiny neurons (MSNs) of the striatum depend on the production and release of BDNF by the cerebral cortex for survival (Baquet *et al.* 2004). Previous studies have established that cortical BDNF is decreased about 50% in brains from HD patients and it has been proposed that the loss of BDNF at MSNs may be a contributor to striatal degeneration in HD (Zuccato and Cattaneo 2007; Zuccato and Cattaneo 2009). Additional quantitative studies using brains from postmortem HD patients have indicated that not only BDNF protein, but also BDNF mRNA levels are decreased in the cortex of patients (Zuccato *et al.* 2008). Likewise, a decrease in BDNF levels has been reported in the brains of various mouse models of HD and the overexpression of BDNF is neuroprotective in a model of HD (Zuccato and Cattaneo 2009; Kells *et al.* 2004). The mechanism leading to decreased BDNF production may involve changes in the localization of a protein complex, REST/NRSF, when mHtt is expressed. Wild-type Htt interacts with REST/NRSF as part of a cytosolic complex; however, mHtt is unable to form this complex, allowing for translocation of REST/NRSF, a silencing factor, to the nucleus (Zuccato *et al.* 2007). Once in the nucleus,

REST/NRSF interacts with a silencer element in the promoter of the gene encoding BDNF, leading to a decrease in transcription (Zuccato *et al.* 2003).

Alterations in autophagy have been proposed to contribute to HD pathogenesis. The purpose of autophagy is to promote cell survival by recycling cell components. During this process, the components of the cytosol are degraded in bulk by being first engulfed by a double membrane bound structure called an autophagosome, then degraded through fusion of the autophagosomes with lysosomes (Menzies *et al.* 2017). Impairment of autophagy could lead to potentially harmful buildup of free mHtt and mHtt aggregates, possibly contributing to cell death (Ventruti and Cuervo 2007). Administration of chemicals to induce autophagy or overexpression of genes involved in autophagy enhances mHtt clearance and improves HD behavior phenotype (Ravikumar *et al.* 2004; Jia *et al.* 2007). Conversely, inhibition of the autophagosome/lysosomal pathway increases mHtt levels in cells and increases cellular toxicity (Ravikumar *et al.* 2002). Early studies using the postmortem brains of HD patients showed an increase in autophagosome-like structures in neurons of patients compared to neurons from the brains of controls, suggesting that autophagy may actually be enhanced in HD (Petersen *et al.* 2001; Qin *et al.* 2003). However, more recent findings suggest that the increased generation of autophagosomes may be due to an inability of autophagosomes to properly recognize and load cytosolic cargo in HD cells (Martinez-Vicente *et al.* 2010).

Both Htt and mHtt are subject to proteolytic cleavage by caspases, including caspases-2, 3, 6, and 7 (Goldberg *et al.* 1996). This discovery led to the development of the toxic fragment hypothesis, which suggests that cleavage of mHtt produces polyQ containing N-terminal fragments of the protein that may be more toxic than full-length mHtt (Wellington *et al.* 2000; Wellington *et al.* 2002). Evidence to support this assertion is derived from experiments showing that inhibition of caspase-mediated mHtt cleavage can ameliorate symptoms of HD in mouse models and the observation that mHtt

fragment models of HD have an accelerated and more severe symptom progression (Mangiarini *et al.* 1996;Chen *et al.* 2000;Graham *et al.* 2006). Mutant Htt fragments exert deleterious effect by having a higher propensity for aggregation compared to Htt. The extent of mHtt aggregation is dependent on the length of the fragment and the length of the polyQ tract (Chen *et al.* 2002). Additionally, accumulation of these polyQ-containing fragments may drive further caspase activity, ultimately leading to cell death (Goldberg *et al.* 1996).

Aggregates of mHtt have been found in both human brains from postmortem HD patients and brains from mouse models of HD (DiFiglia *et al.* 1997;Davies *et al.* 1997). In humans, aggregates have been found in neurons of the striatum and have been observed to occur more frequently in neurons from juvenile patients, suggesting that the increased number of aggregates correlates with an accelerated disease progression (DiFiglia *et al.* 1997). Aggregates have been found both in the nucleus and in the cytosol, with the aggregates within the nucleus containing most the NH<sub>2</sub> terminus fragment of mHtt, whereas cytosolic aggregates contain both full-length and truncated mHtt as well as Htt (Cooper *et al.* 1998). The harmful effects of mHtt aggregation may stem from either the ability of aggregates to bind to and prevent the normal function of other nearby proteins or the difficulty they present to cellular machinery responsible for the degradation and clearance of the aggregates from the cell (Tydlacka *et al.* 2008;Bates *et al.* 2015). An alternative hypothesis suggests that aggregates may actually be beneficial to mHtt-expressing cells by reducing the levels of free mHtt, thus decreasing neuronal death (Arrasate *et al.* 2004). Additional research is required to more fully explore the effect of mHtt aggregation in HD pathology and the role of fragments in this process.

## **B. Mitochondrial Dysfunction in HD**

In addition to the putative detrimental mechanisms described above, there are numerous reports suggesting that mitochondrial bioenergetic deficiency and mitochondrial  $\text{Ca}^{2+}$  handling defects may be important contributors to neuronal dysfunction in HD. However, there is also growing body of evidence indicating the lack of direct detrimental effect of mHtt on mitochondrial functions. Thus, despite numerous studies, the effect of mHtt on oxidative metabolism and mitochondrial  $\text{Ca}^{2+}$  handling remains controversial. Indeed, a previous study using electron microscopy to view immunolabeled mHtt demonstrated the presence of mHtt at the outer membrane, but not inside of mitochondria (Orr *et al.* 2008). Additionally, immunoblotting studies with isolated mitochondria probed for mHtt and Htt show that both mutant and WT protein are lost from the mitochondrial fraction following treatment with trypsin or alkaline conditions (Pellman *et al.* 2015). Despite the loss of mHtt and Htt in these experiments, treated mitochondria show no loss of matrix, IMM, or intermembrane space proteins (Pellman *et al.* 2015). Therefore, since mHtt cannot access the inner compartments of mitochondria the mechanism by which mHtt may induce mitochondrial dysfunction, if it exists, remains unclear. In the following sections is a description of the current experimental data regarding the role of mHtt in oxidative metabolism and mitochondrial  $\text{Ca}^{2+}$  handling.

In many previous studies, assessment of mitochondrial dysfunction has involved the use of isolated brain mitochondria to evaluate respiration, membrane potential,  $\text{Ca}^{2+}$  uptake, and combinations thereof (Oliveira 2010a;Oliveira 2010b). Major mitochondrial functions include generation of ATP through oxidative phosphorylation, of elevated cytosolic  $\text{Ca}^{2+}$  due to  $\text{Ca}^{2+}$  influx into mitochondria mediated by mitochondrial calcium uniporter (MCU), generation of reactive oxygen species (ROS), and regulation of apoptosis (Lehninger *et al.* 1993;Wang and Youle 2009). Figure 1 highlights the basic molecular components of oxidative phosphorylation and mitochondrial  $\text{Ca}^{2+}$  uptake.

Through the oxidation of pyruvate and malate, the Complex I substrates, or succinate, the Complex II substrate, electrons are donated to the electron transport chain (ETC). Transport of electrons is coupled to the transfer of protons from the mitochondrial matrix to the intermembrane space, generating electrical membrane potential (negative inside) and a chemical gradient of protons (more alkaline inside) across the inner mitochondrial membrane. Protons may then return to the mitochondrial matrix through ATP synthase, generating ATP at the expense of membrane potential and proton gradient (Mitchell 1961). Additionally,  $\text{Ca}^{2+}$  is taken into the mitochondrial matrix through the MCU in a process that is driven by membrane potential (Pan *et al.* 2013). Accumulation of  $\text{Ca}^{2+}$  by mitochondria is limited by induction of the permeability transition pore (PTP), a nonspecific pore of still debatable molecular composition whose induction leads to mitochondrial depolarization,  $\text{Ca}^{2+}$  release from mitochondria, and swelling of the organelles (Bernardi *et al.* 1999).

In isolated mitochondria, these processes can be evaluated by measuring mitochondrial respiration,  $\text{Ca}^{2+}$  uptake capacity, and membrane potential. In our study, we routinely measured mitochondrial respiration, mitochondrial membrane potential, and  $\text{Ca}^{2+}$  uptake capacity of mitochondria from HD and WT mice. Measurements of respiration and membrane potential can be done simultaneously or separately using tightly closed, thermostated chamber equipped with Clark-type oxygen electrode and tetraphenylphosphonium ( $\text{TPP}^+$ )-sensitive electrode.  $\text{TPP}^+$  is a hydrophobic cation that easily crosses mitochondrial inner membrane according to membrane potential. Measurements of  $\text{TPP}^+$  concentration outside of mitochondria ( $[\text{TPP}^+]_{\text{ext}}$ ) allow for assessment of the amount of  $\text{TPP}^+$  accumulated in mitochondria, which is indicative of membrane potential: the more  $\text{TPP}^+$  that is accumulated, the higher the membrane potential. A typical experiment with isolated mitochondria (Fig. 2) includes the measurements of respiration in the presence of only oxidative substrates (e.g. pyruvate

plus malate), called State 2 respiration, which is accompanied by generation of high membrane potential and denoted " $V_2$ " (Brand and Nicholls 2011; Brustovetsky and Brustovetsky 2017). Adding ADP to mitochondria leads to transient depolarization and an increased respiratory rate as ADP is converted to ATP in the process of oxidative phosphorylation (State 3,  $V_3$ ). This ADP-stimulated respiratory rate allows for assessment of the activity of the oxidative phosphorylation system. After all added ADP is consumed, respiration spontaneously reverts to a slower rate called State 4 ( $V_4$ ) and simultaneously high membrane potential is restored. The rate of respiration under these conditions is determined predominately by proton leaks across the inner mitochondrial membrane, which could be used to evaluate mitochondrial damage. The addition of 2,4-dinitrophenol (2,4-DNP), a molecule that increases proton permeability of the inner membrane and uncouples oxidative phosphorylation, strongly depolarizes mitochondria and induces the maximal respiratory rate, which is denoted " $V_{DNP}$ ". The maximal respiratory rate allows assessment of ETC activity.

Analysis of  $Ca^{2+}$  uptake capacity is achieved by administering  $Ca^{2+}$  pulses to mitochondria while tracking the  $Ca^{2+}$  concentration in the external medium ( $[Ca^{2+}]_{ext}$ ) outside of mitochondria. Eventually, the permeability transition pore will be induced, mitochondrial will be depolarized and unable to accumulate additional  $Ca^{2+}$ , and previously accumulated  $Ca^{2+}$  will be released from mitochondria (Bernardi *et al.* 1999).

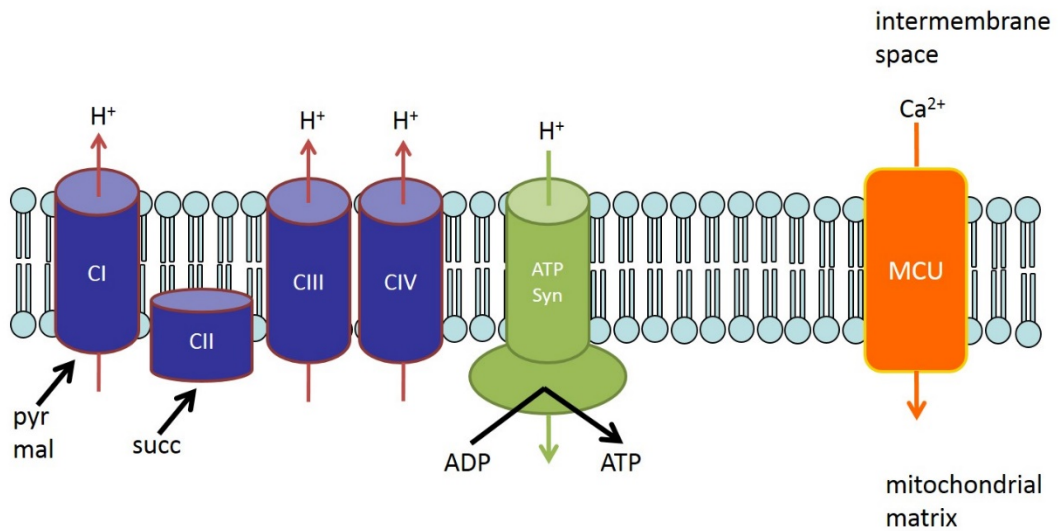


**Figure 1. Electron Transport Chain (ETC), ATP Synthase, and Mitochondrial Calcium Uniporter.** Electrons from the substrates pyruvate and malate (pyr, mal, respectively) enter the ETC through Complex I (CI), whereas the substrate succinate (succ) provides electrons through Complex II (CII). Electrons are then transferred through Complexes III and IV (CIII, CIV, respectively). Transport of electrons is coupled to proton extrusion, generating an electrochemical proton gradient across the inner mitochondrial membrane. Protons passing through ATP Synthase (ATP Syn) drive ATP generation. Ca<sup>2+</sup> is transported into the mitochondrial matrix through the mitochondrial calcium uniporter (MCU) at the expense of membrane potential.

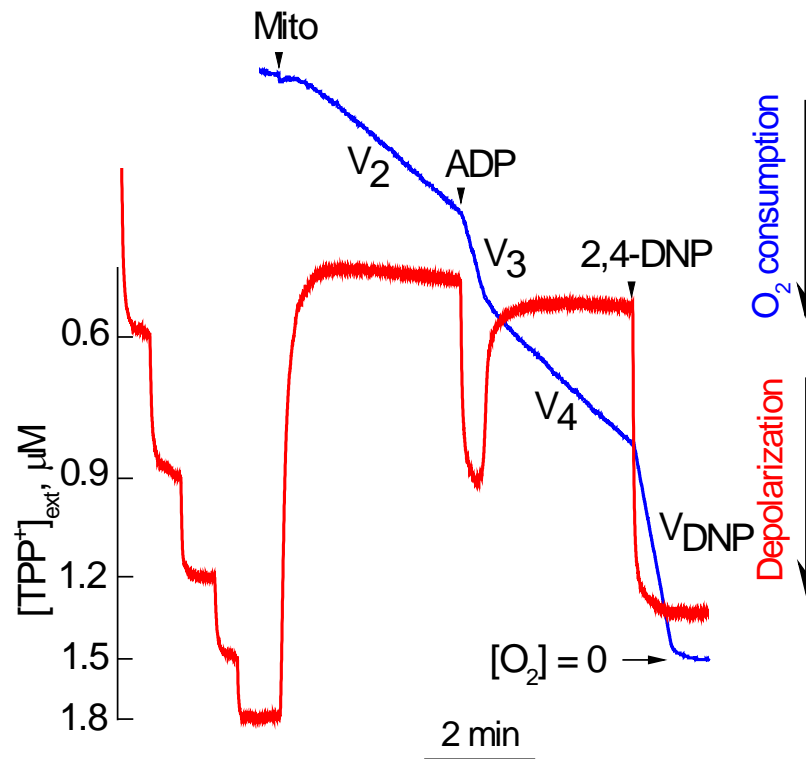


**Figure 2. Representative measurements of respiration (blue trace) and mitochondrial membrane potential (red trace) in isolated synaptic mitochondria.** Where indicated, 50  $\mu\text{g}$  mitochondria (Mito), 300  $\mu\text{M}$  ADP, and 60  $\mu\text{M}$  2,4-dinitrophenol (2,4-DNP) were added to the chamber. Respiration and membrane potential were measured simultaneously. Respiration was measured with a Clark-type oxygen electrode. Membrane potential was monitored by following distribution of tetraphenylphosphonium ( $\text{TPP}^+$ ) across the inner mitochondrial membrane with  $\text{TPP}^+$ -sensitive electrode. Prior to addition of mitochondria, five pulses of 30  $\mu\text{M}$   $\text{TPP}^+$  were added to the chamber to calibrate the system for later membrane potential calculations. The incubation medium contained 125 mM KCl, 3 mM  $\text{KH}_2\text{PO}_4$ , 0.5 mM  $\text{MgCl}_2$ , 3 mM pyruvate, 1 mM malate, 10 mM HEPES, pH 7.4, 10  $\mu\text{M}$  EGTA, 0.1% BSA (free from fatty acids). The measurements were performed under continuous stirring at 37°C in a 0.4 mL chamber. (From: Brustovetsky, N., and Brustovetsky, T. Monitoring of permeability transition pore in isolated individual brain mitochondria. Stefan Strack and Yuriy M. Usachev (eds.), *Techniques to Investigate Mitochondrial Function in Neurons*, Neuromethods, Humana Press, vol. 123, 199-210, 2017)



## **a. Defects in Oxidative Metabolism**

In early papers concerning HD-associated alterations in bioenergetics, even before the discovery of the mutation in Htt, investigators reported some defects in mitochondrial respiratory activity. In postmortem brain tissues from HD patients, decreased respiratory activity of caudate mitochondria was found (Brennan, Jr. *et al.* 1985), and defects in mitochondrial Complexes II, III, and IV were described (Gu *et al.* 1996; Browne *et al.* 1997). However, it was not obvious whether these respiratory defects contributed to HD pathogenesis or if they were a result of the late stage of HD pathology. To resolve this issue, various experimental models of HD have been developed and utilized in search of a mechanistic link between mutation in Htt and HD pathology (Pouladi *et al.* 2013). The effects of mHtt on oxidative metabolism have been examined with polyglutamine–glutathione S-transferase (polyQ-GST) fusion proteins as surrogates for mHtt (Puranam *et al.* 2006; Rockabrand *et al.* 2007), with cell models expressing mHtt (Trettel *et al.* 2000) as well as with numerous HD rodent models that express full-length or fragments of endogenous or human mHtt with different lengths of polyQ stretch (Heng *et al.* 2007; Ramaswamy *et al.* 2007).

### **i. Evidence Supporting Oxidative Metabolism Defects in HD**

The polyQ-GST fusion proteins were generated and tested in experiments with isolated mitochondria from wild-type (WT) animals. In experiments with Q62-GST fusion protein applied to liver mitochondria isolated from WT mice, investigators found a slight inhibition of ADP-stimulated respiration, but no inhibition of respiratory Complexes, ATP synthase, or adenine nucleotide translocase (Puranam *et al.* 2006). Another mHtt substitute, GST-51Q exon 1 fusion protein, resulted in depolarization in isolated rat brain cortical mitochondria accompanied by a significant increase in oxygen consumption by the organelles, suggesting mitochondrial uncoupling but not inhibition of mitochondrial

respiratory Complexes (Rockabrand *et al.* 2007). Interestingly, in this study, GST-20 exon 1 fusion protein with an unexpanded polyQ stretch produced similar effects, arguing against the role of an expanded polyQ stretch in the observed mitochondrial defects and suggesting non-polyQ dependent effects of the GST fusion proteins in this study.

The opportunities to investigate the effects of mHtt on cell physiology and biochemistry were significantly expanded with the advent of conditionally immortalized, mutant STHdh<sup>Q111/Q111</sup> striatal neuronal progenitor cells (Trettel *et al.* 2000). Although Milakovic and Johnson observed reduced respiration and ATP production using these cells, they found no difference in activities of mitochondrial Complex I–IV in mutant STHdh<sup>Q111/Q111</sup> cells compared with STHdh<sup>Q7/Q7</sup> cells (Milakovic and Johnson 2005). The authors concluded that mHtt may impair mitochondrial bioenergetics via different mechanisms that do not directly affect respiratory Complexes. In line with this conclusion, Seong *et al.* found lower cellular ATP in STHdh<sup>Q111/Q111</sup> cells compared with STHdh<sup>Q7/Q7</sup> cells potentially indicating decreased energy production (Seong *et al.* 2005). The authors found inhibition of ADP uptake by mitochondria from mutant cells; however, activity of adenine nucleotide translocase that catalyzes ADP/ATP exchange across the inner membrane remained unchanged. Mitochondrial membrane potential was decreased whereas intracellular Ca<sup>2+</sup> was elevated in mutant cells. The elevated intracellular Ca<sup>2+</sup> was proposed to be responsible for inhibition of ADP transport into mitochondria. Indeed, inhibition of Ca<sup>2+</sup> influx into STHdh<sup>Q111/Q111</sup> cells with EGTA in the bath solution or NMDA receptor antagonist MK-801 significantly increased ATP/ADP ratio in these cells, suggesting improvement in ADP translocation into mitochondria (Seong *et al.* 2005). Recently, in experiments with STHdh<sup>Q111/Q111</sup> cells, Siddiqui *et al.* found slightly reduced maximal respiratory activity without any difference in basal respiration (Siddiqui *et al.* 2012). The authors obtained a similar result with primary

cultures of HD diploid skin fibroblasts. Consistent with these findings, in experiments with heterozygous and homozygous STHdh<sup>Q111/Q7</sup> and STHdh<sup>Q111/Q111</sup> striatal neuronal progenitor cells, Napoli *et al.* found deficient oxidative phosphorylation and decreased Complex I and IV activities as well as a decrease in F<sub>0</sub>F<sub>1</sub>-ATPase activity (Napoli *et al.*, 2013). It has to be noted, however, that immortalized neuronal progenitor cells may differ functionally and morphologically from primary neurons and, therefore, mHtt effects on oxidative metabolism in these cells should be taken cautiously, especially, bearing in mind negative results produced in numerous experiments with primary neurons, brain slices, and whole HD animals.

In addition to experiments with polyQ-GST fusion proteins and immortalized neuronal progenitor cells, experiments with isolated mitochondria and cells in culture derived from HD animal models provided important information about the possible effects of mHtt on oxidative metabolism. Tabrizi *et al.*, using biochemical assays, found a significant decrease in activities of Complex IV and aconitase in the striatum of R6/2 mice (Tabrizi *et al.* 2000). In line with these findings, Bae *et al.*, using the same methodology, reported decreased activity of Complex IV in striatum of N171-82Q transgenic mice (Bae *et al.* 2005). Later, Kim *et al.* found significant reduction in States 3 and 4 respiration of succinate-fueled striatal mitochondria from pre-symptomatic transgenic D9-N171-98Q mice, also known as DE5 mice, compared with their age-matched controls, suggesting Complex II impairment (Kim *et al.* 2011). On the other hand, Complex I and IV activities as well as activity of ATP synthase were not altered in the striatum of young and old DE5 mice compared with WT littermates. Interestingly, succinate-supported respiration in States 3 and 4 as well as maximal carbonylcyanide-p-trifluorometh-oxyphenylhydrazone (FCCP)-stimulated respiration were found to be increased in symptomatic DE5 mice compared with pre-symptomatic animals (Kim *et al.* 2011). Damiano *et al.* also reported defects in respiration of mitochondria isolated from

forebrains of N171-82Q transgenic mice (Damiano *et al.* 2013). With malate/glutamate (Complex I substrates) or succinate (Complex II substrate) supplemented with glutamate, ADP-stimulated respiration of mitochondria from 2–3-month-old N171-82Q transgenic mice was lower compared to respiration of mitochondria from control N171-Q18 mice. Recently, Aidt *et al.* measured respiration of striatum homogenates from 12-week-old R6/2 mice and found a slight but statistically significant decrease in Complex II and Complex IV flux control ratios defined as respiratory rates normalized to the maximal uncoupled respiration (Aidt *et al.* 2013). The authors interpreted these data as an indication of respiratory impairment in striatal mitochondria of R6/2 mice. However, how mHtt, a 350-kDa cytosolic protein that binds to the outer mitochondrial membrane but cannot cross it (Choo *et al.* 2004), impairs the respiratory chain in the inner mitochondrial membrane remains not completely understood. One possibility is that mHtt might decrease expression and/or mitochondrial import of proteins, involved in oxidative metabolism. Indeed, loss of Complex II activity was found in the postmortem striatum of HD patients and associated with a decreased expression of two subunits of Complex II, iron-sulfur subunit Ip (30 kDa) and FAD subunit Fp (70 kDa) (Benchoua *et al.* 2006). Similarly, Damiano *et al.* demonstrated preferential loss of Complex II in mitochondria isolated from forebrains of N171-82Q transgenic mice (Damiano *et al.* 2013). Recently, Yano *et al.* reported mHtt-mediated inhibition of mitochondrial protein import (Yano *et al.* 2014). On the other hand, no decrease in Complex II levels (judged by the levels of 30- and 70-kDa subunits of Complex II) was found in brain mitochondria isolated from Hdh150Q knock-in mice (Orr *et al.* 2008) and in mitochondria of STHdh<sup>Q111/Q111</sup> cells (Milakovic and Johnson 2005). Possible alterations in oxidative metabolism could decrease ATP production in cells expressing mHtt. Indeed, Lim *et al.* reported a significant decrease in ATP level in cortex of R6/1 mice compared with WT control (Lim *et al.* 2014). However, although in HD striatum is considered the most vulnerable region

of the brain (Zuccato *et al.* 2010), a decrease of ATP in striatum was much less pronounced and was not statistically significant suggesting ATP deficiency may not be involved in striatal degeneration (Lim *et al.* 2014).

## **ii. Evidence Against Oxidative Metabolism Defects in HD**

In addition to studies reporting mHtt-induced impairment of oxidative metabolism, there are numerous studies that demonstrate the lack thereof. Trushina *et al.* discovered a reduction in mitochondrial motility due to sequestration of trafficking motor components by mHtt aggregates but did not find signs of mitochondrial dysfunction in striatal neurons derived from YAC72 mice (Trushina *et al.* 2004). Mitochondrial morphology was not altered in these neurons, and the levels of ATP and lactate (an indicator of glycolytic activity) were similar in neurons from WT and YAC72 mice. Olah *et al.* reported that the activities of Complexes I–IV in brain mitochondria from 20-week-old transgenic N171-82Q mice were not decreased compared with mitochondria from WT animals (Olah *et al.* 2008). Interestingly, the authors found that ATP levels in the homogenate of the posterior brain regions of N171-82Q mice were significantly higher than in brains from WT mice. In addition, the authors noticed an increased glycolytic rate in cytosolic extracts from brain tissue of N171-82Q mice (Olah *et al.* 2008). Based on these observations, the authors concluded that expression of the N-terminal fragment of mHtt is not accompanied by decreased activity of the mitochondrial respiratory chain or decline in glycolytic rate. Consistent with this, Guidetti *et al.* did not find any changes in mitochondrial electron transport through Complexes I–IV in the striatum and cerebral cortex of HD48 and HD89 mice, expressing full-length mHtt with either 48 or 89 Qs in polyQ stretches, compared with WT animals (Guidetti *et al.* 2001). Moreover, these investigators failed to find changes in the activity of Complexes I–IV in the neostriatum and cerebral cortex in pre-symptomatic and pathological grade 1 HD cases. Oliveira *et*

*al.* reported that respiration of cultured striatal neurons derived from heterozygous knock-in Hdh<sup>150/+</sup> mice and their WT littermates was similar (Oliveira *et al.* 2007). Later, Gouarne *et al.* measured respiration of cultured striatal neurons from heterozygous transgenic BACHD rats and found no difference compared with WT neurons, when cells were incubated in the presence of 25 mM glucose and 1 mM pyruvate (Gouarne *et al.* 2013). However, when neurons were incubated in a low-glucose (2.5 mM) medium, the authors observed a modest decrease in maximal, FCCP-stimulated respiration of mHtt-expressing cells. Interestingly, this difference between mutant and WT cells was observed only with striatal but not cortical neurons. The authors proposed that mHtt expression results in a dysfunction in glycolysis that might precede defects in mitochondrial respiration (Gouarne *et al.* 2013). Yano *et al.* reported that respiration of synaptic and nonsynaptic mitochondria from forebrains of pre-symptomatic and mid-stage disease R6/2 mice (the authors used two distinct R6/2 strains: 150 CAG R6/2 and 195 CAG R6/2) was not different from that of mitochondria from WT littermates (Yano *et al.* 2014). Consistent with this, in a recent study with neurons and astrocytes from BACHD mice, Boussicault *et al.* found no evidence for direct effect of mHtt with 97 Qs on oxidative metabolism in these cells *in vitro* (Boussicault *et al.* 2014). In this study, mHtt did not affect the glycolytic rate in single cells as measured by FRET and did not decrease mitochondrial membrane potential in neurons assessed with fluorescent dye Rhodamine 123. Taken together, these data obtained with isolated mitochondria and cells in culture argue against mHtt-induced impairment of oxidative metabolism in animal models of HD.

In addition to isolated mitochondria and cells in culture, experiments with animal brain slices and whole animals *in vivo* provided further insights into the possible effect of mHtt on respiratory activity. Weydt *et al.* reported that oxygen consumption measured by indirect calorimetry of the whole animals was slightly increased in transgenic HD N171-

82Q mice at baseline, especially during fasting (Weydt *et al.* 2006). The oxygen consumption rates (OCRs) in brain slices from 11-week-old, pre-symptomatic N171-82Q mice incubated with 20 mM glucose were similar. However, when brain slices were incubated with 5 mM lactate and 1 mM pyruvate, OCRs for HD slices were significantly lower (Weydt *et al.* 2006). Thus, the ability of lactate to be converted to pyruvate and subsequently undergo oxidative metabolism in the citric acid cycle appeared to be impaired in brains of N171-82Q mice. At the same time, respiration of brain slices fueled by succinate was normal, indicating no impairment of Complex II and the rest of respiratory chain. Goodman *et al.* reported that 8-week-old R6/2 mice had oxygen consumption, energy expenditure, and respiratory exchange ratio (RER, defined as CO<sub>2</sub> release rate/O<sub>2</sub> consumption rate) similar to WT animals (Goodman *et al.* 2008). With 14-week-old R6/2 mice, the authors found significantly increased oxygen consumption and energy expenditure, while RER was not significantly different. Van der Burg *et al.* found elevated oxygen consumption in 6- to 12-week-old R6/2 mice compared with WT littermates (van der Burg *et al.* 2008). In elegant *in vivo* experiments with magnetic resonance spectroscopy (<sup>31</sup>PMRS), Tkac *et al.* found no significant change in ATP concentration in the brain of knock-in Q111 mice (Tkac *et al.* 2012). ADP concentration was increased in brain of Q111 mice at 6 weeks but returned to nearly normal level at 13 weeks. In R6/2 mice, however, these parameters remained normal (Tkac *et al.* 2012). The authors proposed that brain energy homeostasis in these HD mouse models is maintained from early ages until the pathological symptoms become apparent. Overall, these data argue against an overt inhibitory effect of mHtt on oxidative energy metabolism.

The experiments with cell and animal models generate important information about HD, but only studies with human tissues and HD patients provide an ultimate test of the hypotheses tested in animal studies. Severe reduction in the activity of

mitochondrial respiratory chain complexes was found in caudate/putamen from human postmortem brain tissue, suggesting that these abnormalities may underlie HD pathology (Brennan, Jr. *et al.* 1985;Gu *et al.* 1996;Browne *et al.* 1997). However, *in vivo* measurements of oxygen consumption and glucose metabolism with positron emission tomography in early-stage HD patients demonstrated that, while glucose consumption was somewhat reduced in striatum, its respiratory capacity was not significantly altered (Powers *et al.* 2007b). Consistent with this, the mid-stage HD patients do not show energy imbalance *in vivo* compared to age-matched healthy individuals as judged by indirect calorimetry in a human respiratory chamber (Gaba *et al.* 2005). Anecdotal evidence indicates that pre-symptomatic individuals who tested positive for the mutation in *HTT* do not experience any energy deficit and are able to, for example, participate in high-level athletic competition, supporting the lack of mHtt-triggered mitochondrial dysfunction. As an example, British rower Sarah Winckless, who carries the mutation in *Htt*, has competed in multiple Olympic games (English 2014). Turner *et al.* studied the respiratory chain function in skeletal muscle biopsies from HD patients and also failed to find a significant difference in the activities of Complexes I–IV compared with age-matched controls (Turner *et al.* 2007). Powers *et al.* investigated platelet mitochondrial citrate synthase and Complex I and I/III activities in HD patients and found no difference compared with healthy controls, whereas striatal volume was already significantly reduced in patients with HD (Powers *et al.* 2007a). Because HD pathology was already manifested by striatal atrophy, the authors concluded that a deficit in energy production due to impairment of mitochondrial respiratory chain is not important for the mechanism of neuronal death in early HD.

Thus, the existing literature supports two different views on the interaction of mHtt with oxidative metabolism system. One group of investigators reports detrimental effects of mHtt on oxidative metabolism, whereas another group does not find evidence



for such effects. This contradiction limits our understanding of HD pathogenesis and impedes the development of new treatment approaches for HD. Consequently, this contradiction has to be resolved in order to provide explicit answers to the questions of whether mHtt results in defects in oxidative metabolism and whether these defects contribute to HD pathogenesis and therefore represent a valid target for the development of effective HD therapies.

#### **b. Defects in Mitochondrial Calcium Handling and Calcium Uptake**

One of the main hypotheses regarding HD pathology postulates that expression of mHtt results in defects in  $\text{Ca}^{2+}$  signaling in neurons (Bezprozvanny and Hayden 2004) most likely due to augmented activity of NMDA subtype of ionotropic glutamate receptors (Zhang *et al.* 2008), abnormalities in IP3 receptor function (Tang *et al.* 2003), and aberrations in mitochondrial  $\text{Ca}^{2+}$  handling (Panov *et al.* 2002). The inner mitochondrial membrane has a  $\text{Ca}^{2+}$  channel (Baughman *et al.* 2011; De *et al.* 2011), historically called “the mitochondrial  $\text{Ca}^{2+}$  uniporter” (MCU) (Bernardi *et al.* 1999), that mediates  $\text{Ca}^{2+}$  influx into the mitochondrial matrix driven by large membrane potential (160-180 mV) negative inside of mitochondria. The magnitude of mitochondrial  $\text{Ca}^{2+}$  uptake capacity is restricted by the sensitivity of mitochondria to the damaging effect of  $\text{Ca}^{2+}$ , manifested in an induction of the permeability transition pore (PTP) (Chalmers and Nicholls 2003). PTP induction leads to mitochondrial depolarization and inhibition of potential-dependent processes such as oxidative phosphorylation and  $\text{Ca}^{2+}$  uptake (Bernardi *et al.* 1999).

#### **i. Evidence Supporting Mitochondrial $\text{Ca}^{2+}$ Handling Defects in HD**

Several studies demonstrated mHtt-induced defects in mitochondrial  $\text{Ca}^{2+}$  uptake (defects in mitochondrial  $\text{Ca}^{2+}$  handling). An early paper by Panov *et al.* reported

bioenergetics abnormalities and a reduction in  $\text{Ca}^{2+}$  uptake capacity by mitochondria isolated from cells and tissues expressing mHtt (Panov *et al.* 2002). Mitochondria from lymphoblasts of patients with HD as well as brain nonsynaptic mitochondria from pathological YAC72 mice, expressing mHtt with a stretch of 72 Qs, had a diminished membrane potential and were depolarized at smaller  $\text{Ca}^{2+}$  loads compared with mitochondria from healthy YAC18 mice, expressing Htt with a stretch of 18 Qs. These defects appeared to be upstream of the onset of pathological or behavioral abnormalities and could be replicated by a fusion protein GST-Q62 containing expanded polyQ repeat. It is known that  $\text{Ca}^{2+}$  uptake capacity could be increased by a combination of ADP and cyclosporin A (CsA), efficient inhibitors of the PTP (Chalmers and Nicholls 2003; Novgorodov *et al.* 1992). However, Panov *et al.* reported that the  $\text{Ca}^{2+}$  handling defect persisted even in the presence of these PTP inhibitors (Panov *et al.* 2002). Thus, the mechanism of the mitochondrial  $\text{Ca}^{2+}$  handling defect was not clarified in this study, but based on the fact that ADP and CsA failed to eliminate the difference between mitochondria from mutant and WT animals, PTP involvement could be excluded. Intriguingly, the effect of mHtt on mitochondrial  $\text{Ca}^{2+}$  uptake capacity appeared to be elusive, and in the next study, Panov *et al.* found that “the defect in  $\text{Ca}^{2+}$  handling in brain mitochondria was consistently observed only if brain mitochondria were isolated without bovine serum albumin (BSA)” (Panov *et al.* 2003). The authors proposed that BSA could displace mHtt from its binding sites on mitochondria, but did not provide experimental evidence supporting this hypothesis.

Soon after that, Choo *et al.* showed that liver mitochondria from homozygous knock-in Hdh<sup>150/150</sup> mice had augmented predisposition to the  $\text{Ca}^{2+}$ -induced PTP (Choo *et al.* 2004). The authors also found that GST-fused N-terminal truncated mHtt (GST-exon1-Q65 or Htt65), containing 65 glutamines, and GST-Q62 fusion protein, containing 62 glutamines, significantly increased mitochondrial susceptibility to  $\text{Ca}^{2+}$ -dependent

PTP induction. Htt65 reduced  $\text{Ca}^{2+}$  threshold for PTP induction and could directly stimulate  $\text{Ca}^{2+}$ -dependent PTP induction in mouse liver mitochondria (Choo *et al.* 2004). Later, Milakovic *et al.* showed that in mitochondria isolated from conditionally immortalized striatal progenitor cells  $\text{STHdh}^{\text{Q111/Q111}}$ , mHtt with 111 glutamines, augmented mitochondrial sensitivity to  $\text{Ca}^{2+}$ -induced decrease in ADP-activated respiration (State 3) and mitochondrial depolarization (Milakovic *et al.* 2006). In addition, mHtt reduced mitochondrial  $\text{Ca}^{2+}$  uptake capacity that could be salvaged by a combination of ADP and CsA, the inhibitors of the PTP (Novgorodov *et al.* 1992), thus linking PTP induction to the mHtt-induced  $\text{Ca}^{2+}$  handling defect. In line with this, Lim *et al.*, using the same cell lines, demonstrated that mitochondria from the cells had reduced  $\text{Ca}^{2+}$  uptake capacity due to increased susceptibility to PTP induction (Lim *et al.* 2008). In support of these findings, Gizatullina *et al.* observed increased propensity of skeletal muscle mitochondria from R6/2 mice to  $\text{Ca}^{2+}$ -induced PTP compared with mitochondria from WT mice (Gizatullina *et al.* 2006). In the following study, Gellerich *et al.* examined brain mitochondria isolated from transgenic HD rats expressing 727 amino acid fragments of mHtt with a 51Q stretch (Gellerich *et al.* 2008). The authors found that the mHtt fragments reduced membrane potential stability in response to  $\text{Ca}^{2+}$ , decreased  $\text{Ca}^{2+}$  uptake capacity, and diminished  $\text{Ca}^{2+}$  threshold for PTP induction.

In addition to isolated mitochondria, neurons in culture have been used to study detrimental effects of mHtt on  $\text{Ca}^{2+}$  signaling and mitochondrial  $\text{Ca}^{2+}$  handling. Fernandes *et al.* reported that  $\text{Ca}^{2+}$  influx into cells mediated by the NMDA subtype of ionotropic glutamate receptors resulted in augmented mitochondrial depolarization in medium spiny neurons from YAC128 mice (Fernandes *et al.* 2007). This effect was paralleled by reduced clearance of elevated cytosolic  $\text{Ca}^{2+}$  following NMDA withdrawal. Suppression of the PTP by CsA or bongkreikic acid resulted in a decrease in cytosolic  $\text{Ca}^{2+}$  and diminished mitochondrial depolarization induced by NMDA in neurons from

YAC128 mice, but not from WT mice. Based on these observations, the authors concluded that mitochondria in medium spiny neurons from YAC128 mice have increased susceptibility to PTP induction by  $\text{Ca}^{2+}$  (Fernandes *et al.* 2007). In support of this view, Quintanilla *et al.* found that rat cortical neurons expressing a fragment of mHtt with 104 glutamines (Q104-GFP) are more susceptible to  $\text{Ca}^{2+}$  stress compared with neurons expressing a fragment of Htt with 25 glutamines (Q25-GFP) (Quintanilla *et al.* 2013). The authors also reported that mitochondrial defects in mutant  $\text{STHdh}^{\text{Q111/Q111}}$  cells and cortical neurons expressing Q104-GFP were attenuated by CsA, suggesting an important role for PTP in mitochondrial injury induced by  $\text{Ca}^{2+}$  stress in cells expressing mHtt. Overall, these data suggest that mHtt impairs mitochondrial  $\text{Ca}^{2+}$  uptake capacity by increasing susceptibility to PTP induction. Similar to studies aimed at elucidating mHtt effects on oxidative metabolism, the major remaining question is how does mHtt, a 350-kDa cytosolic protein that binds to the outer mitochondrial membrane but does not cross it (Choo *et al.* 2004), affect mitochondrial  $\text{Ca}^{2+}$  handling and increase propensity to PTP induction, which are the processes mainly associated with the inner mitochondrial membrane.

## **ii. Evidence Against Mitochondrial $\text{Ca}^{2+}$ Handling Defects in HD**

Despite reported defects in mitochondrial  $\text{Ca}^{2+}$  handling, some investigators did not find evidence for mHtt-induced mitochondrial  $\text{Ca}^{2+}$  handling deficiency and increased propensity to PTP induction in the presence of mHtt. In an early study using striatal nonsynaptic mitochondria from HD mice (Q50, Q92, Q111, and R6/2 mice), there was no increased susceptibility to  $\text{Ca}^{2+}$ -induced PTP induction in mitochondria from HD mice compared with mitochondria from respective WT animals (Brustovetsky *et al.* 2005a). Surprisingly, this study found increased resistance to  $\text{Ca}^{2+}$  in striatal mitochondria isolated from HD mice. In line with these findings, Oliveira *et al.* demonstrated that

nonsynaptic mitochondria from R6/2 and YAC128 mice had augmented  $\text{Ca}^{2+}$  uptake capacity compared with mitochondria from WT mice. Additionally, this study reported that mitochondria from Hdh150/+ and Hdh150/150 mice had similar  $\text{Ca}^{2+}$  uptake capacity compared with mitochondria from WT animals (Oliveira *et al.* 2007). The reason for the increased  $\text{Ca}^{2+}$  uptake capacity is not clear, but it may reflect compensatory adaptation to augmented  $\text{Ca}^{2+}$  influx via activated NMDA receptors and/or increased  $\text{Ca}^{2+}$  release from endoplasmic reticulum via abnormally activated IP3 receptors (Bezprozvanny and Hayden 2004). The lack of mHtt-induced impairment of mitochondrial  $\text{Ca}^{2+}$  handling argues against facilitated PTP induction in the presence of mHtt and, consequently, does not support involvement of the PTP in HD pathogenesis (Brustovetsky *et al.* 2005a;Oliveira *et al.* 2007). Additional evidence for the lack of mitochondrial  $\text{Ca}^{2+}$  handling defects came from experiments by Chang *et al.* who transiently exposed cortical neurons expressing N-terminal fragment of mHtt or full-length mHtt to glutamate and used FCCP-induced mitochondrial depolarization to release  $\text{Ca}^{2+}$  accumulated in the mitochondrial matrix (Chang *et al.* 2006). In these experiments, the authors failed to find a significant effect of mHtt on the ability of neuronal mitochondria to accumulate  $\text{Ca}^{2+}$  following exposure of neurons to excitotoxic glutamate. Recently, Wang *et al.* evoked  $\text{Ca}^{2+}$  mobilization in medium spiny neurons by stimulating group I metabotropic glutamate receptors and eliciting inositol 1,4,5-trisphosphate (InsP3) generation. They found significantly higher  $\text{Ca}^{2+}$  accumulation in mitochondria of neurons from YAC128 mice compared with neurons from WT mice (Wang *et al.* 2013). These data argue against mHtt-induced mitochondrial  $\text{Ca}^{2+}$  handling defects. However, even if these defects exist, their role in HD pathogenesis could be nonessential. Consistent with the dispensable role of mitochondrial  $\text{Ca}^{2+}$  handling defects in HD pathogenesis, Perry *et al.* demonstrated that R6/2 mice crossed with cyclophilin D knockout mice (cyclophilin D (CyD) is an important regulatory component

of the PTP that sensitizes the pore to  $\text{Ca}^{2+}$  (Tanveer *et al.* 1996; Basso *et al.* 2005) had augmented neuronal mitochondrial  $\text{Ca}^{2+}$  uptake capacity without any improvement in either behavioral or neuropathological characteristics (Perry *et al.* 2010). The authors reasoned that increased  $\text{Ca}^{2+}$  capacity of neuronal mitochondria is not advantageous for R6/2 mice. Altogether, these results cast doubt on the ability of mHtt to increase susceptibility to PTP induction and to decrease mitochondrial  $\text{Ca}^{2+}$  uptake capacity. Consequently, these data question the role of mitochondrial  $\text{Ca}^{2+}$  handling defects in HD pathogenesis. Thus, there are two distinct schools of thought, mHtt induces defects in mitochondrial  $\text{Ca}^{2+}$  uptake and increases susceptibility to PTP induction, versus no deleterious alterations in mitochondrial function associated with mHtt. The reason for this discrepancy is not clear, but it could be related to the use of different HD models and variations in methodological approaches.

### **C. Hypothesis and Goals**

The evidence presented in this introduction demonstrates that **the main question of whether mHtt interaction with mitochondria leads to mitochondrial dysfunction** remains unresolved, and a plethora of data exists to support both viewpoints: the presence or the lack of mitochondrial dysfunction induced by mHtt. Significant experience in both mitochondrial and HD studies accumulated over 30 years of research has prepared our lab to address the question whether mHtt causes mitochondrial dysfunction. Defects in bioenergetics and  $\text{Ca}^{2+}$  handling are considered by some investigators to be major contributing factors to neuronal dysfunction in HD (Beal *et al.* 1993). It has been shown that HD patients at early stages of the disease have impaired glucose metabolism (Kuhl *et al.* 1985). In postmortem brain tissue from HD patients, decreased respiratory activity of HD caudate mitochondria (Brennan, Jr. *et al.* 1985) and defects in mitochondrial Complexes II, III and IV were found (Gu *et al.*

1996; Browne *et al.* 1997). Additionally, mitochondria in some HD models have shown alterations in Ca<sup>2+</sup> uptake (Panov *et al.* 2007; Gellerich *et al.* 2008). However, other investigators failed to find definitive evidence for a deleterious effect of mHtt on energy metabolism or Ca<sup>2+</sup> uptake. Guidetti *et al.* (Guidetti *et al.* 2001) and Olah *et al.* (Olah *et al.* 2008), for example, failed to find a difference in activity of mitochondrial Complexes I–IV in brain mitochondria of HD mice compared with mitochondria from wild-type animals. Some groups have found no defect or even increased Ca<sup>2+</sup> uptake capacity in certain HD models (Brustovetsky *et al.* 2005a; Oliveira *et al.* 2007).

The striatum is the brain region that is most susceptible to neurodegeneration in HD (Vonsattel *et al.* 1985). However, although the use of whole brain mitochondria for the study of mHtt-mediated dysfunction may provide evidence of mitochondrial dysfunction, it may also produce confounding results since mitochondria from other brain regions could obscure dysfunction that is present only in striatal mitochondria. For this reason, mitochondria isolated only from the striatal region may be better suited for evaluating the presence of respiratory or Ca<sup>2+</sup> handling deficiencies. Consequently, **I hypothesize that, if mitochondria isolated from the whole brain do not display measurable dysfunction, then such dysfunction may be observable in mitochondria isolated exclusively from striatum.**

It has been shown that mHtt is subject to cleavage by caspases, generating polyQ-containing fragments of the protein (Wellington *et al.* 2000; Wellington *et al.* 2002). Whether HD pathogenesis is mediated by full-length mHtt or fragments of mHtt remains not completely understood. Previous studies suggested that mHtt fragments might be more toxic than full-length mHtt (Kim *et al.* 1999; Li *et al.* 2000) and it was shown that reduction in mHtt fragment generation improved the phenotype of HD mice (Tian *et al.* 2014; Wong *et al.* 2015). Based on the existing literature, **I hypothesize that mHtt (full-length, fragments, or both) impairs mitochondrial respiratory and/or Ca<sup>2+</sup> uptake**

**functions.** If full-length mHtt does not affect mitochondrial functions, then mHtt fragments could be more effective in damaging mitochondria.

We will test our hypotheses by pursuing the following goals:

**Goal 1:** Using the transgenic YAC128 mouse model of HD, determine if full-length human mHtt induces mitochondrial respiratory or Ca<sup>2+</sup> handling deficiencies.

**Goal 2:** Using isolated ***striatal*** mitochondria from YAC128 mice, examine if human mHtt induces mitochondrial respiratory and/or Ca<sup>2+</sup> handling defects.

**Goal 3:** Using the transgenic R6/2 mouse model of HD, determine if fragments of human mHtt induce mitochondrial respiratory or Ca<sup>2+</sup> handling deficiencies.



## **II. Materials and Methods**

### **A. Materials**

Pyruvate, malate, succinate, glutamate, glycine, EGTA, ADP, oligomycin, rotenone, antimycin A, 2,4-dinitrophenol, N-methyl-D-glucamine (NMDG) and carbonylcyanide-p-trifluorometh-oxyphenylhydrazone (FCCP) were purchased from Sigma (St. Louis, MO). Tetraphenylphosphonium chloride was from Fluka (Buchs, Switzerland). Percoll was from GE Healthcare Bio-Sciences (Pittsburgh, PA). Bovine serum albumin (BSA), free from free fatty acids, was from MP Biomedicals (Irvine, CA, USA). Fura-2FF-AM was from Teflabs (Austin, TX). Ionomycin was from LKT Laboratories (St. Paul, MN)

### **B. Animals**

All procedures with animals were performed in accordance with the Institutional Animal Care and Use Committee approved protocol. All efforts were made to minimize animal suffering, to reduce the number of animals used, and to utilize alternatives to *in vivo* techniques, if available. All animal experiments were carried out in accordance with the National Institutes of Health guide for the care and use of Laboratory animals (NIH Publications No. 80-23, revised 1978). YAC128 and R6/2 mice as well as respective wild-type (WT) lines were purchased from Jackson Laboratories (Bar Harbor, ME) and breeding colonies were established in the Laboratory Animal Resource Center at Indiana University School of Medicine, Indianapolis, IN. YAC128 mice express full-length human mHtt containing 128 glutamines in the polyglutamine (polyQ) stretch, including upstream and downstream regulatory elements in addition to WT mouse Htt. Female FVB/NJ mice (background strain) were bred with male YAC128 mice. R6/2 mice express the N-terminal fragment of the human mHtt gene that encodes a pathologically expanded polyglutamine stretch with 144 glutamines (Mangiarini *et al.* 1996). R6/2 mice

and their WT littermates were generated by crossing WT CBAxC57Bl/6 F1 males with CBAxC57Bl/6 females that had ovary transplants from R6/2 mice. Mice were housed under standard conditions with free access to food and water. In our studies, mice of both sexes were used.

For our respiration and membrane potential experiments with YAC128 mice, we used early symptomatic 2-month-old YAC128 mice and their wild-type (WT) littermates (background: FVB/NJ) as well as 10-month-old YAC128 and age-matched WT littermates. To evaluate the expression of nuclear encoded mitochondrial proteins, we used 2- and 10-month-old YAC128 mice and their age-matched WT littermates. Previously, it was reported that YAC128 mice at 2 months of age begin to show behavioral abnormalities and are considered to be early symptomatic (Van Raamsdonk *et al.* 2005a; Van Raamsdonk *et al.* 2005b). A recent study using electron microscopy demonstrated a significant reduction in excitatory synapses of striatal neurons in 12-month-old YAC128 mice (Singaraja *et al.* 2011). At 12 months of age, YAC128 mice show significant striatal loss and are considered to be at an advanced stage of HD pathology (Slow *et al.* 2003). Therefore, we were interested in assessing mitochondrial Ca<sup>2+</sup> handling in mice at both ages. Consequently, in our experiments, we used early symptomatic 2-month-old and mature 12-month-old YAC128 mice, control age-matched YAC18 mice, and their age-matched wild-type FVB/NJ littermates. In experiments with isolated brain mitochondria from R6/2 mice, we used symptomatic 6- to 8-week-old mice and their WT littermates (background: B6CBA).

Every animal used for experiments was genotyped by PCR assay on tail DNA. PCR of tail DNA was carried out according to the protocol furnished by Jackson Laboratories. For YAC128 samples the oligonucleotide primers used were oIMR6533 (GGCTGAGGAAGCTGAGGAG) and TmoIMR1594 (CCGCTCAGGTTCTGCTTTTA) (Invitrogen, Carlsbad, CA). The PCR reaction mixture was prepared with 1  $\mu$ L DNA

template and 24  $\mu\text{L}$  Platinum PCR SuperMix (Invitrogen) containing 0.39  $\mu\text{M}$  of each primer for a total reaction volume of 25  $\mu\text{L}$ . Cycling conditions were 5 min at 95  $^{\circ}\text{C}$ , 35 cycles of 30 s at 95  $^{\circ}\text{C}$ , 30 s at 56  $^{\circ}\text{C}$ , 60 s at 72  $^{\circ}\text{C}$ , 10 min at 72  $^{\circ}\text{C}$ . For R6/2 samples oligonucleotide primers used were oIMR1594 (CCGCTCAGGTTCTGCTTTTA) and oIMR1596 (TTGAAGGACTTGAGGGACTC) obtained from Invitrogen. Oligonucleotide primers oIMR7338 (CTAGGCCACAGAATTGAAAGATCT) and oIMR7339 (GTAGGTGGAAATTCTAGCATCATCC) (all from Invitrogen) were used as internal positive control. For R6/2 samples the PCR reaction mixture consisted of 1  $\mu\text{L}$  DNA template and 23  $\mu\text{L}$  Platinum PCR SuperMix (Invitrogen) supplemented with 0.5  $\mu\text{M}$  of each primer (Invitrogen), total volume 25  $\mu\text{L}$ . Cycling conditions were 2 min at 94 $^{\circ}\text{C}$ , 10 cycles for 20 s at 94 $^{\circ}\text{C}$  followed by 15 s at 65 $^{\circ}\text{C}$  with  $-0.5^{\circ}\text{C}$  per cycle temperature decrease and 10 s at 68 $^{\circ}\text{C}$ . Then, 28 cycles for 15 s at 94  $^{\circ}\text{C}$  followed by 15 s at 60  $^{\circ}\text{C}$  and 10 s at 72  $^{\circ}\text{C}$ , concluded by 1 min at 72 $^{\circ}\text{C}$  (Jackson Laboratories, Bar Harbor, ME). For all samples, PCR reaction products were visualized on a 1.2% agarose gel run at 100 V for 60 min with Tris–acetate–EDTA running buffer containing 1 $\times$  GelRed<sup>TM</sup> Nucleic Acid Gel Stain (Biotium, Hayward, CA).

### **C. Isolation and Purification of Mitochondria**

Mitochondria were isolated in a mannitol-sucrose medium and purified on a discontinuous Percoll gradient as previously described (Brustovetsky et al. 2002). The isolation procedure is schematically depicted in Figure 3. Mitochondria were isolated from either three whole brains, two hearts, or two livers from each mouse line for each experiment. For isolated striatal mitochondria, nine mice were used in each experiment to prepare nonsynaptic striatal mitochondria and 15 mice were used in each experiment to prepare synaptic striatal mitochondria. Organs were removed according to an IACUC-approved protocol, and, if necessary, striata were dissected. The tissue were immersed

into isolation medium containing 225 mM mannitol, 75 mM sucrose, 1 mM EGTA, and 10mM HEPES, pH 7.4 that was chilled to 4°C. The tissue was washed with isolation medium, minced coarsely with scissors, and homogenized. Liver and heart tissue were first homogenized in a 50mL Potter-Elvehjem homogenizer with Teflon-coated pestle attached to an electric homogenizer. Then pre-homogenized heart or liver tissue or freshly dissected brain tissue was homogenized manually in a 15 mL glass Dounce homogenizer (10 strokes with pestle A, then 30 strokes with pestle B) on ice. Homogenate was then diluted with 40 mL of Isolation Buffer 1 (composition described below) and centrifuged for 10 minutes at 2,400 rpm in an Avanti J-26XP centrifuge (Beckman) outfitted with a JA-25.50 rotor (650 x g for 10 minutes) (1<sup>st</sup> centrifugation). Then, supernate was moved to a new tube and centrifuged for 10 minutes at 12,500 rpm (18,850 x g) in a Beckman Centrifuge Avanti J-26XP outfitted with a JA-25.50 rotor (2<sup>nd</sup> centrifugation). Supernate was discarded and pellet was re-suspended in 35 mL of Isolation Buffer 2 (composition described below) and centrifuged for 10 minutes at 12,500 rpm (18,850 x g) in a Beckman Centrifuge Avanti J-26XP outfitted with a JA-25.50 rotor (3<sup>rd</sup> centrifugation). For heart, liver, and unpurified brain mitochondria, the pellet was re-suspended in 0.5 mL of Isolation Buffer 3 (composition described below) and stored on ice. For brain purified brain mitochondria, the pellet was re-suspended in 5 mL of Isolation Buffer 3. The suspension was then layered onto the top of discontinuous Percoll gradients (26%/40%) that were prepared in Beckman Ultra-Clear centrifuge tubes and centrifuged for 28 minutes at 15,500 rpm (41,100 x g) in a Beckman Ultracentrifuge Optima L100K, outfitted with a SW41Ti bucket rotor (4<sup>th</sup> centrifugation). Following this centrifugation, five layers were produced. In Figure 4, the layers are marked numerically and described as follows: 1 – clear (top); 2 – thick white with a yellowish hue, this layer contains synaptosomes; 3 – slightly cloudy thick layer; 4 – thin turbid layer, this layer contains nonsynaptic mitochondria; 5 – clear (bottom). At this

point, layers that contained synaptosomes and nonsynaptic mitochondria were collected into separate tubes. Nonsynaptic mitochondria were re-suspended in Isolation Buffer 3 and momentarily set aside.

Synaptic mitochondria were isolated from synaptosomes by nitrogen cavitation using a nitrogen cell disruption bomb, model 4639 (Parr Instrument Company, Moline, IL), cooled on ice. Synaptosomes were transferred into an ice-cold 10 mL glass beaker and placed into the nitrogen bomb on ice under 1,100 psi for 13 minutes. Then, the ruptured synaptosomes were layered on top of a discontinuous Percoll gradient (24%/40%) and centrifuged for 28 minutes at 15,500 rpm (41,100 x g) in a Beckman Ultracentrifuge Optima L100K, outfitted with a SW41Ti bucket rotor (4' centrifugation). The next two centrifugations (5<sup>th</sup> and 6<sup>th</sup> centrifugations were performed together with nonsynaptic mitochondria. The pellet of synaptic mitochondria was re-suspended in Isolation Buffer 3. Then, together with previously re-suspended nonsynaptic mitochondria, synaptic mitochondria were centrifuged for 20 minutes at 15,500 rpm (41,100 x g) in a Beckman Ultracentrifuge Optima L100K, outfitted with a SW41Ti bucket rotor (5<sup>th</sup> centrifugation). The pellets were re-suspended in Isolation Buffer 3 and centrifuged again for 20 minutes at 15,500 rpm (41,100 x g) in a Beckman Ultracentrifuge Optima L100K, outfitted with a SW41Ti bucket rotor (6<sup>th</sup> centrifugation). The pellets were collected, re-suspended in Isolation Buffer 3 (0.25-0.3 mL for nonsynaptic mitochondria and 0.1 mL for synaptic mitochondria), and stored on ice. These comprised the stock suspensions for nonsynaptic and synaptic mitochondria. All centrifugations, procedures, and solutions were maintained at 4°C throughout the protocol. Isolation Buffer 1: 225 mM mannitol, 75 mM sucrose, 1 mM EGTA, and 10mM HEPES, pH 7.4 adjusted with KOH. Isolation Buffer 2: 225 mM mannitol, 75 mM sucrose, 0.1 mM EGTA, and 10mM HEPES, pH 7.4 adjusted with KOH. Isolation Buffer 3: 395 mM sucrose, 0.1 mM EGTA, and 10mM HEPES, pH 7.4 adjusted with KOH.

Percoll Buffer: 320 mM sucrose, 1 mM EGTA, 10 mM HEPES, pH 7.4 adjusted with KOH. It was previously proposed that BSA may preclude mHtt from binding to the mitochondrial outer membrane (Panov *et al.* 2003), therefore, unless indicated otherwise, BSA was omitted from solutions used in isolation procedures and from incubation medium. Only where indicated, isolation solutions and incubation medium were supplemented with 0.1% BSA (free from fatty acids; MP Biomedicals, cat. # 150421).

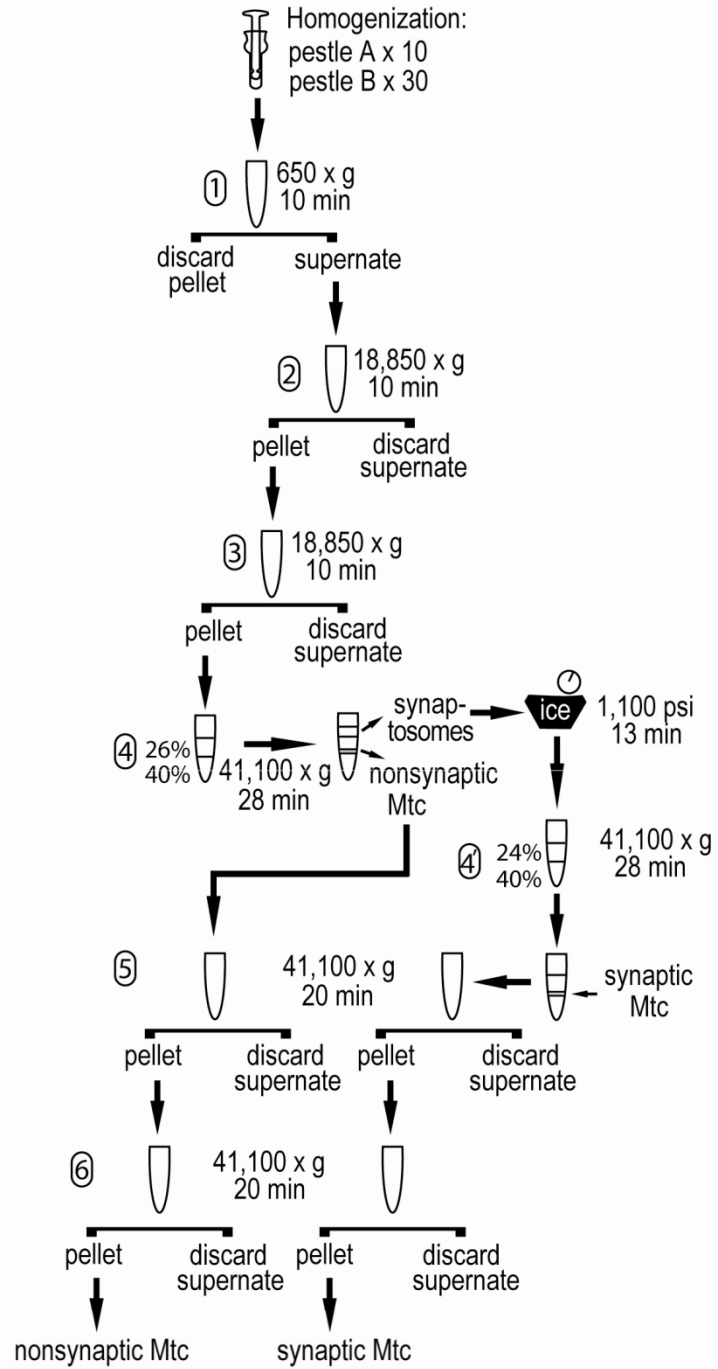


**Figure 3. Isolation and purification of brain nonsynaptic and synaptic mitochondria.**

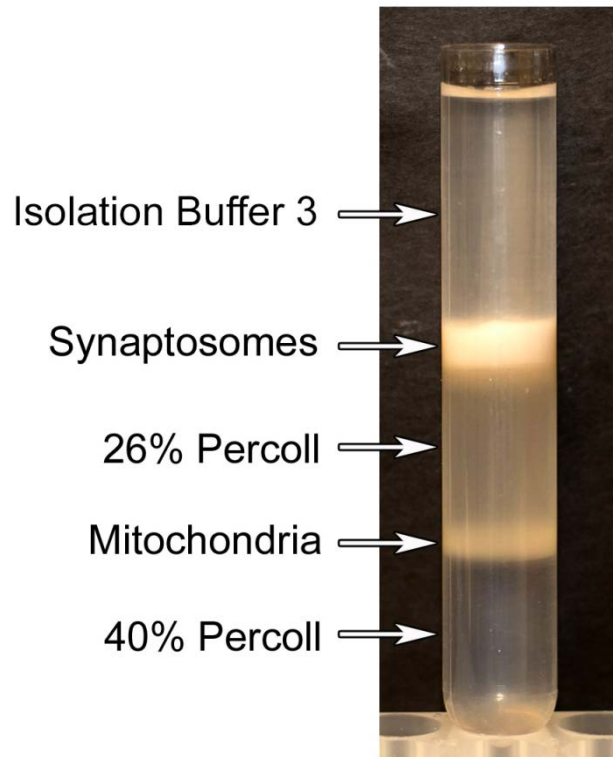


**Figure 4. Separation of nonsynaptic mitochondria and synaptosomes on discontinuous Percoll gradient.** After the fourth centrifugation, five layers are visible. From top: 1 – clear (top), Isolation Buffer 3; 2 – thick white-yellowish, synaptosomes; 3 – slightly cloudy thick layer, 26% Percoll; 4 – thin turbid layer, nonsynaptic mitochondria; 5 – clear (bottom), 40% Percoll.



#### **D. Western Blotting**

Brain homogenates, cytosolic fractions, and isolated mitochondria that were previously treated with Protease Inhibitor Cocktail (Roche, Indianapolis, IN ref# 04693124001) were solubilized by incubation in NuPAGE LDS sample buffer (Invitrogen) plus a reducing agent at 70 °C for 10 min. Either Bis-Tris Mops gels (4–12%, Invitrogen) or Tris-Acetate gels (3–8%, Invitrogen) were used to separate proteins by electrophoresis. Either 10 or 40 µg protein per lane was loaded. Following electrophoresis, proteins were transferred to Hybond-ECL nitrocellulose membrane (Amersham Biosciences, Piscataway, NJ). Blots were incubated for 1 h at room temperature in blocking solution of either 5% milk or 5% BSA dissolved in phosphate-buffered saline, pH 7.2, and 0.15% Triton X-100. Then, where indicated, blots were incubated with one of the following primary antibodies: mouse monoclonal anti-Htt 2166 (mAb 2166, 1:1000, Millipore, Temecula, CA), mouse monoclonal anti-polyQ 1C2 (mAb 1574, 1:3000, Millipore), rabbit polyclonal anti-calnexin (1:1200, Abcam, Cambridge, MA), rabbit monoclonal anti-MEK1/2 (1:2000, Pierce, Rockford, IL), mouse monoclonal anti-Complex I 39 kDa subunit (1:1000, Invitrogen), mouse monoclonal anti-Complex II 30 kDa subunit (1:1000, Invitrogen), mouse monoclonal anti-Complex II 70 kDa subunit (1:1000, Invitrogen), mouse monoclonal anti-aconitase 2 (1:1000, Abcam), rabbit polyclonal anti-manganese superoxide dismutase (MnSOD, 1:2000, Millipore), mouse monoclonal anti-ATP synthase  $\alpha$  subunit (1:1000, Abcam), mouse monoclonal anti-CyD antibody (1:500, Calbiochem, San Diego, CA), mouse monoclonal anti-COX IV (1:2500, Invitrogen), rabbit polyclonal anti-VDAC1 (1:1000, Calbiochem). Blots were incubated with either goat anti-mouse or goat anti-rabbit IgG (1:25000 or 1:20000, respectively) coupled with horseradish peroxidase (Jackson ImmunoResearch Laboratories, West Grove, PA) and developed with Supersignal West Pico chemiluminescent reagents (Pierce). Molecular mass markers See Blue Plus 2 Standards (7 µl) (Invitrogen) and

HiMark Pre-stained High Molecular Weight Protein Standards (7  $\mu$ l) (Invitrogen) were used for molecular mass determination. NIH ImageJ 1.48v software (<http://rsb.info.nih.gov/ij>) was used to quantify band densities.

### **E. Mitochondrial Respiration**

Mitochondrial respiration was measured under continuous stirring in 0.4 ml thermostated chamber at 37°C in the standard incubation medium containing 125 mM KCl, 0.5 mM MgCl<sub>2</sub>, 3 mM KH<sub>2</sub>PO<sub>4</sub>, 10 mM Hepes, pH 7.4, 10  $\mu$ M EGTA supplemented either with 3 mM pyruvate plus 1 mM malate or 3 mM succinate plus 3 mM glutamate. The chamber was equipped with a Clark-type oxygen electrode and a tightly closed lid. The slope of the oxygen electrode trace corresponded to the respiratory rate. Experiments with succinate were supplemented with glutamate to prevent inhibition of succinate dehydrogenase by oxaloacetate (Wojtczak 1969;Brustovetsky and Dubinsky 2000a).

### **F. Mitochondrial Ca<sup>2+</sup> Uptake**

Mitochondrial Ca<sup>2+</sup> uptake was measured with a miniature Ca<sup>2+</sup>-selective electrode in a 0.3 ml chamber at 37°C under continuous stirring. Uptake of Ca<sup>2+</sup> by mitochondria is indicated by a decrease in external Ca<sup>2+</sup> in the chamber. The standard incubation medium contained 125 mM KCl, 0.5 mM MgCl<sub>2</sub>, 3 mM KH<sub>2</sub>PO<sub>4</sub>, 10 mM Hepes, pH 7.4, 10  $\mu$ M EGTA, and was supplemented either with 3 mM pyruvate plus 1 mM malate or 3 mM succinate plus 3 mM glutamate. Succinate was used in combination with glutamate to prevent oxaloacetate inhibition of succinate dehydrogenase (Wojtczak 1969;Brustovetsky and Dubinsky 2000a). Additionally, the incubation medium was supplemented with 0.1 mM ADP and 1  $\mu$ M oligomycin as described previously

(Chalmers and Nicholls 2003).  $\text{Ca}^{2+}$  was delivered to mitochondria as 10  $\mu\text{M}$   $\text{CaCl}_2$  pulses. Data were quantified as  $\text{Ca}^{2+}$  uptake capacity per mg of mitochondrial protein.

### **G. Mitochondrial Membrane Potential and Swelling**

Mitochondrial membrane potential was evaluated in 0.3 ml thermostated chamber at 37°C in the standard incubation medium containing 125 mM KCl, 0.5 mM  $\text{MgCl}_2$ , 3 mM  $\text{KH}_2\text{PO}_4$ , 10 mM HEPES, pH 7.4, 10  $\mu\text{M}$  EGTA supplemented either with 3 mM pyruvate plus 1 mM malate or 3 mM succinate plus 3 mM glutamate. The chamber was outfitted with a tetraphenylphosphonium ( $\text{TPP}^+$ ) electrode that followed  $\text{TPP}^+$  distribution between the incubation medium and mitochondria (Kamo *et al.* 1979). A decrease in external  $\text{TPP}^+$  concentration corresponds to mitochondrial polarization, while an increase of  $\text{TPP}^+$  in the incubation medium corresponds to depolarization. Mitochondrial swelling was evaluated at 37°C and continuous stirring by following changes in light scattering of mitochondrial suspension at 525 nm with an incident light beam at 180° in a 0.3 ml chamber. The incubation medium for light scattering measurements contained 215 mM mannitol, 70 mM sucrose, 0.5 mM  $\text{MgCl}_2$ , 3 mM  $\text{KH}_2\text{PO}_4$ , 10 mM HEPES, pH 7.4, 10  $\mu\text{M}$  EGTA, 3 mM succinate, 3 mM glutamate. A decrease in light scattering of mitochondrial suspension indicated mitochondrial swelling. Maximal mitochondrial swelling was induced by alamethicin (30  $\mu\text{g/ml}$ ). Maximal swelling was taken as 100%.  $\text{Ca}^{2+}$ -induced swelling was calculated as a percentage of maximal swelling (Brustovetsky *et al.* 2005b).

### **H. Transmission Electron Microscopy**

Prior to fixation, mitochondria were incubated for 10 min at 37°C in the standard incubation medium. Then, mitochondria or striatal neurons were fixed in 2.5% glutaraldehyde in either mitochondrial incubation medium or the standard neuron bath

solution at room temperature for 15 min. Samples were then centrifuged at  $15,800 \times g$  for 5 min, and the supernatant was discarded. The pellet was layered with a fresh solution of 2% paraformaldehyde plus 2% glutaraldehyde in 0.1 M phosphate buffer and left overnight at 4 °C. The samples were postfixed in 1% osmium tetroxide for 1 h and dehydrated through a series of graded ethyl alcohols before embedding in the resin Embed® 812 (Electron Microscopy Sciences, Fort Washington, PA). Thick sections were cut on an Ultracut UCT microtome (Leica, Bannockburn, IL), and then thin sections were cut using a diamond knife (Diatome, Electron Microscopy Sciences) at 70–90 nm and stained with uranyl acetate and lead citrate. Digital electron micrographs were taken using a Tecnai G12 BioTwin electron microscope (FEI, Hillsboro, OR) equipped with an AMT 2.6 × 2.6 K digital CCD camera. Mitochondrial morphology was analyzed in a blind manner as described previously. Mitochondrial populations were categorized into three classes: (i) condensed mitochondria with dark, shrunk matrices and distinct vacuolization, (ii) swollen mitochondria with light, expanded matrices and (iii) orthodox mitochondria with evenly spread grey matrices. Mitochondria were counted and morphological distribution was statistically analyzed using one-way analysis of variance followed by Bonferroni's *post hoc* test (GraphPad Prism® 4.0, GraphPad Software Inc., San Diego, CA). This procedure was performed with the help of Caroline Miller at the Electron Microscopy Center, Indiana University School of Medicine.

## **I. ATP and ADP Measurements**

ADP and ATP were determined using a luciferin/luciferase-based ATP bioluminescent somatic cell assay (Sigma) and a GloMax 20/20 luminometer (Promega). Mitochondria were incubated for 10 min at 37°C in the standard incubation medium supplemented with 3 mM succinate plus 3 mM glutamate and then ADP and ATP were measured. Cultured striatal neurons (10 DIV) were lysed on ice with the Releasing

Reagent (Sigma) for 10 minutes. ATP was measured following precipitation of proteins by perchlorate (4%) and subsequent neutralization of extracts by KOH as measured by an esophageal pH electrode. ADP was converted to ATP using pyruvate kinase in the presence of phosphoenolpyruvate (Kimmich *et al.* 1975).

## **J. Blue Native-PAGE and Western Blotting**

Synaptic and nonsynaptic mitochondria from WT and YAC128 mice were solubilized in a sample buffer (Invitrogen) with 1% digitonin and Proteinase Inhibitor Cocktail (Roche) for 15 min on ice and then centrifuged at 100,000g for 30 min. Mitochondrial proteins (15 µg) were separated on NativePAGE™ 3–12% Bis–Tris gel. Following electrophoresis, protein bands were stained with SimplyBlue™ SafeStain. NativeMark™ was used as molecular weight marker. All reagents were from Invitrogen. For western blotting, the proteins were transferred on Immobilon™-FL PVDF membrane (EMD Millipore) and mitochondrial Complex I subunit Ndufa9 was detected using monoclonal antibodies against Ndufa9 (mAb 14713, Abcam).

## **K. Cell Culture**

Primary cultures of striatal and cortical neurons were prepared from individual dissected striata and cortices of postnatal day 1 mouse pups as previously described (Dubinsky 1993), but without pooling cells from different animals together. The striata or cortices were removed, coarsely minced, and incubated for 20 minutes at 37°C in L-15 medium with 3 mg·ml<sup>-1</sup> papain and 3 mg·ml<sup>-1</sup> bovine serum albumin (BSA). After gentle trituration in growth medium, the cell suspension was layered on L-44 with 100 mg·ml<sup>-1</sup> BSA and centrifuged at 500 rpm for 5 minutes. The pellet was then resuspended in growth medium. To inhibit proliferation of non-neuronal cells, 35 mg·ml<sup>-1</sup> uridine plus 15 mg·ml<sup>-1</sup> 5-fluoro-2'-deoxyuridine were added 24 h after plating. Neurons were

maintained in a 5% CO<sub>2</sub> atmosphere at 37 °C in Neurobasal Medium with B27 supplement (Life Technologies), and medium osmolality set to 280 mOsm. We used neuronal-glia co-culture derived from postnatal day 1 mouse pups because it is more physiologically relevant and allows for the study of more mature, better developed cells than pure neuronal culture derived from embryonic animals.

For respirometry experiments, neurons were plated on Seahorse plates that were previously coated with poly-L-lysine and without pre-plated glia. For fluorescence experiments and ATP measurements, neurons were plated onto glass bottom Petri dishes without pre-plated glia as previously described for calcium imaging experiments (Dubinsky 1993).

#### **L. Cell Respirometry**

Oxygen consumption rates (OCRs) of cultured striatal and cortical neurons (9 DIV) were measured using Seahorse XF24 flux analyzer (Seahorse Bioscience, Billerica, MA). Seahorse cell culture plates were coated for 1 hour with 20mg/mL poly-L-Lysine prior to seeding cells. Neuronal cultures were grown in the assay plates at 10<sup>5</sup> cells per well. Before performing measurements, the growth medium was replaced by the standard bath solution supplemented with 10 mM glucose and 15 mM pyruvate or 2.5 mM glucose alone as indicated. The standard bath solution contained 139 mM NaCl, 3 mM KCl, 0.8 mM MgCl<sub>2</sub>, 1.8 mM CaCl<sub>2</sub>, 10 mM HEPES, pH 7.4. In experiments, in which 2.5 mM glucose was used, sucrose was supplemented to maintain osmolality similar to that in the growth medium (300 mosm). Experiments consisted of 12 measurement periods that each consisted of three functions. At the beginning of each measurement period, the medium was re-oxygenated with a three-minute mixing period, followed by a two-minute wait period to allow equal distribution of oxygen, then a three-minute measurement period in which the rate of the decrease in oxygen concentration

was measured. Cellular respiration was measured under four conditions. Initially, three basal measurements were made with cells in the presence of only glucose and pyruvate, then cell respiration was assessed in the presence of the ATP-synthase inhibitor oligomycin (1  $\mu$ M) , followed by evaluation of uncoupled respiration in the presence of 2,4-dinitrophenol (60  $\mu$ M), and finally non-mitochondrial respiration in the presence of mitochondrial respiratory complex inhibitors rotenone (1  $\mu$ M) and antimycin A (1  $\mu$ M). Measurements of extracellular acidification rate (ECAR) and OCR were made simultaneously during each experiment.

### **M. Calcium Imaging**

Cytosolic  $\text{Ca}^{2+}$  was assessed in striatal neurons (10–12 days *in vitro*, DIV) by loading neurons at 37 °C with 2.6  $\mu$ M Fura-2FF-AM (Molecular Probes, Eugene, OR) in the standard bath solution containing 139 mM NaCl, 3 mM KCl, 0.8 mM  $\text{MgCl}_2$ , 1.8 mM  $\text{CaCl}_2$ , 10 mM NaHEPES, pH 7.4 and 5 mM glucose. Osmolarity of the bath solutions was measured with an Osmette II osmometer (Precision Systems Inc., Natick, MA) to ensure that it was similar to the osmolarity of the growth medium (280 mosm). A Nikon Eclipse TE2000-U inverted microscope using a Nikon CFI Plan Fluor 20x 0.45 NA objective and a back-thinned EM-CCD camera, Hamamatsu C9100-12 (Hamamatsu Photonic Systems, Bridgewater, NJ) controlled by Simple PCI software 6.1 (Compix Inc., Sewickley, PA) was used to take fluorescent images. A Lambda-LS system (Sutter Instruments, Novato, CA) was used to deliver excitation light. A Lambda 10-2 optical filter changer (Sutter Instruments, Novato, CA) was used to control excitation filters (340  $\pm$  5 and 380  $\pm$  7 nm). Fluorescence was recorded through a 505 nm dichroic mirror at 535  $\pm$  25 nm. Images were taken every 15 seconds for the duration of the experiment. The exposure time was chosen that provided satisfactory image quality but minimal exposure. The ratio of  $F_{340}/F_{380}$ , calculated following background subtraction in both

channels, was used to monitor changes in cytosolic  $\text{Ca}^{2+}$  concentration ( $[\text{Ca}^{2+}]_c$ ). After 90 seconds of baseline fluorescence recording in standard bath solution, glutamate (25  $\mu\text{M}$ ) plus glycine (10  $\mu\text{M}$ ) was applied to the neuronal culture. At the end of the experiment, the glutamate-containing solution was replaced with a glutamate-,  $\text{Ca}^{2+}$ - and  $\text{Na}^+$ -free solution. The  $\text{Na}^+$  was replaced by equimolar N-methyl-D-glucamine (NMDG). Then 1  $\mu\text{M}$  FCCP was applied to the neurons, causing neuronal mitochondria to depolarize and leading to release of accumulated mitochondrial  $\text{Ca}^{2+}$  into the cytosol. The Grynkiewicz method (Grynkiewicz *et al.* 1985) was used for calculation of  $[\text{Ca}^{2+}]_c$  from Fura-2FF signals, using an assumed  $K_d$  for Fura-2FF of 5.5  $\mu\text{M}$ . Fluorescence background was subtracted in every experiment. As has been suggested previously (Dietz *et al.* 2007; Stanika *et al.* 2009), it should be noted that the  $\text{Ca}^{2+}$  binding and spectroscopic properties of fluorescent dyes can differ depending on the intracellular environment. Therefore calculations of  $[\text{Ca}^{2+}]_c$  should be considered estimates.

#### **N. Neuronal Transfection**

To visualize mitochondria within live cells, cultured striatal neurons were transfected in suspension during plating using an electroporator BTX 630 ECM (Harvard Apparatus, Holliston, MA) with a plasmid encoding mitochondrially-targeted enhanced yellow fluorescent protein (mito-eYFP, generously provided by Dr. Roger Tsien, UCSD) (4  $\mu\text{g}$  plasmid per 100 $\mu\text{L}$  of cell suspension,  $5 \times 10^6$  cells). This procedure usually provided a 10–15% transfection rate in primary neuronal cultures. The transfected neurons were imaged 8–10 days after transfection.



## **O. Live-cell Laser Spinning-disk Confocal Microscopy**

Mitochondrial morphology in live striatal neurons was analyzed by confocal microscopy. Serial images of neuronal mitochondria, visualized with mito-eYFP, were collected using spinning-disk confocal microscopy. A Nikon Eclipse TE2000-U microscope equipped with a Yokogawa spinning-disk confocal unit CSU-10, a back-thinned EM-CCD camera Andor iXon<sup>EM+</sup> DU-897 (Andor Technology, South Windsor, CT), and a motorized stage Prior H-117 (Prior Scientific, Rockland, MA) was employed. This setup was controlled by Andor iQ 1.4 software (Andor Technology, South Windsor, CT). To image mitochondria, neurons were exposed to excitation light at 488 nm using an air-cooled Kr/Ar laser T643-RYB-A02 (Melles Griot, Carlsbad, CA). The laser power was set to the minimum (<5%) to prevent photobleaching while maintaining excellent image quality. Fluorescence was collected through a 505 nm dichroic mirror and a 535 ± 25 nm emission filter using a Nikon CFI Plan Apo 100× 1.4 NA objective. Serial images (z-stacks) were collected using the piezoelectric positioning device PIFOC P-721 (Physik Instrumente, Auburn, MA) with a z-step of 0.1 μm. The spatial resolution of the Andor iXon<sup>EM+</sup> DU-897 camera was increased by installing a 2× extender lens in front of the camera. Three-dimensional blind deconvolution of z-stacks and 3D rendering were performed using AutoDeblur Gold CF 1.4.1 software (MediaCybernetics, Silver Spring, MD). Three-dimensional maximal projection reconstructions of the mitochondrial network in live neurons were performed using Imaris 6.4.0 (Bitplane Inc., St. Paul, MN).

## **P. Calorimetric Analysis**

Calorimetric analysis was performed to determine whole-animal metabolic activity. Oxygen consumption, CO<sub>2</sub> release, energy expenditure, food consumption and motor activity were measured in 10-month-old YAC128 and WT mice with an Animal Monitoring System (LabMaster, TSE Systems, Midland, MI). The system consists of an

eight-cage open-circuit layout equipped with an air pump, a control unit, a sample switch unit to draw air samples from the cages and an air-drying unit. After 72 h acclimation in the calorimetric cages, the mice were recorded for 96 h for the previously mentioned parameters. The system measures O<sub>2</sub> consumed and CO<sub>2</sub> produced. These values were averaged to determine the hourly rate of each parameter. Energy expenditure was calculated by the Weir equation (Weir 1949) as modified by Bruss *et al.* (Bruss *et al.* 2010): Energy expenditure (kcal/h) = [(3.815 + 1.232 × RER) × VO<sub>2</sub>]/1000, where VO<sub>2</sub> is in milliliters/hour.

#### **Q. Mouse Body Composition**

Fat mass and lean body mass of WT and YAC128 mice were estimated by dual-energy x-ray absorptiometry (DEXA) scanning. A PIXImus II mouse densitometer (Lunar Corp., Madison, WI) was used in the Department of Cell Biology and Anatomy, Indiana University School of Medicine. During scanning, the mice were maintained in the anesthetized state by a constant flow of isoflurane gas (2% with oxygen at a rate of 1 l/min) administered by a nose cone. The duration of the scan was 4–5 min.

#### **R. Statistics**

Experimental data are shown as mean ± SEM of indicated number of independent experiments. Statistical analysis of the experimental results consisted of unpaired *t*-test or one-way ANOVA followed by Bonferroni's *post hoc* test (GraphPad Prism® 4.0, GraphPad Software Inc., San Diego, CA). Every experiment was performed using several different preparations of isolated mitochondria or several separate neuronal-glial platings. Power analysis was performed using G\*Force software version 3.1.9.2 (by Franz Faul, Universitat Kiel, Germany) to establish the sample size necessary to detect a 10% and 20% difference between mitochondria from WT and

YAC128 mice. The results of this analysis are shown in Tables 2 and 3. Based on this power analysis, the number of experiments that gives an 80% likelihood (the accepted level in statistical analysis) of detecting 10% difference between two means at the significance level of  $\alpha = 0.05$  is within the range of 6–10 experiments. Five to six experiments give an 80% likelihood of detecting 20% difference between two means at the significance level of  $\alpha = 0.05$ .

**Table 2. Calculation of a sample size using Power Analysis method for YAC128.**

<b>Respiration</b>						
<b>Nonsynaptic Mtc</b>				<b>Synaptic Mtc</b>		
Pyruvate + Malate						
Effect size	10%	20%	30%	10%	20%	30%
V <sub>3</sub>	29.7	59.4	89.1	30.8	61.6	92.4
SD	22.6	22.6	22.6	18.6	18.6	18.6
N=	10	4	3	7	3	3
V <sub>DNP</sub>	21.8	43.6	65.4	20.6	41.2	61.8
SD	14.4	14.4	14.4	13.5	13.5	13.5
N=	8	4	3	8	4	3
<b>Nonsynaptic Mtc</b>				<b>Synaptic Mtc</b>		
Succinate + Glutamate						
Effect size	10%	20%	30%	10%	20%	30%
V <sub>3</sub>	31.8	63.6	95.4	40.7	81.4	122.1
SD	23.5	23.5	23.5	22.8	22.8	22.8
N=	10	4	3	7	3	3
V <sub>DNP</sub>	49.1	98.2	147.3	70.9	141.8	212.7
SD	25.1	25.1	25.1	43.9	43.9	43.9
N=	6	3	3	8	3	3
<b>Membrane potential (<math>\Delta\psi</math>)</b>						
<b>Nonsynaptic Mtc</b>				<b>Synaptic Mtc</b>		
Pyruvate + Malate						
Effect size	10%	20%	30%	10%	20%	30%
$\Delta\psi$	15.2	30.4	45.6	14.6	29.2	43.8
SD	6.8	6.8	6.8	7.9	7.9	7.9
N=	6	3	3	6	3	3
<b>Nonsynaptic Mtc</b>				<b>Synaptic Mtc</b>		
Succinate + Glutamate						
Effect size	10%	20%	30%	10%	20%	30%
$\Delta\psi$	16.6	33.2	49.8	15.7	31.4	47.1
SD	8.0	8.0	8.0	9.2	9.2	9.2
N=	6	3	3	7	3	3

Power analysis was performed using G\*Force software version 3.1.9.2 (by Franz Faul, Universitat Kiel, Germany) to establish the sample size necessary to detect a 10% and 20% difference between mitochondria from WT and YAC128 mice. Based on this power analysis, the number of experiments that gives an 80% likelihood (the accepted level in statistical analysis) of detecting 10% difference between two means at the significance level of  $\alpha=0.05$  is within the range of 6 to 10 experiments. The number of experiments suitable for statistical analysis was assumed to be 3 or higher. V<sub>3</sub>, respiratory rate in the presence of 200  $\mu$ M ADP; V<sub>DNP</sub>, respiratory rate in the presence of 60  $\mu$ M 2,4-DNP;  $\Delta\psi$ , mitochondrial membrane potential; SD, standard deviation. Where indicated, the incubation medium was supplemented either with 3 mM pyruvate plus 1 mM malate or with 3 mM succinate plus 3 mM glutamate.

**Table 3. Calculation of a sample size using Power Analysis method for R6/2.**

Respiration							
Effect size	Nonsynaptic Mtc			Pyruvate + Malate	Synaptic Mtc		
	10%	20%	30%		10%	20%	30%
V <sub>3</sub>	31.6	54.9	91.8		32.7	63.6	89.4
SD	20.7	20.7	20.7		19.4	19.4	19.4
N=	10	4	3		10	4	3
V <sub>DNP</sub>	24.7	41.2	64.6		27.4	43.8	66.9
SD	17.6	17.6	17.6		18.5	18.5	18.5
N=	6	3	3		9	4	3
Effect size	Nonsynaptic Mtc			Succinate + Glutamate	Synaptic Mtc		
	10%	20%	30%		10%	20%	30%
V <sub>3</sub>	29.3	59.7	99.1		46.5	77.2	131.4
SD	15.8	15.8	15.8		18.2	18.2	18.2
N=	10	3	3		6	4	3
V <sub>DNP</sub>	54.7	92.8	143.5		77.7	151.3	222.2
SD	24.9	24.9	24.9		38.2	38.2	38.2
N=	7	3	3		9	4	3

Power analysis was performed using G\*Force software version 3.1.9.2 (by Franz Faul, Universitat Kiel, Germany) to establish the sample size necessary to detect a 10% and 20% difference between mitochondria from WT and R6/2 mice. Based on this power analysis, the number of experiments that gives an 80% likelihood (the accepted level in statistical analysis) of detecting 10% difference between two means at the significance level of  $\alpha=0.05$  is within the range of 6 to 10 experiments. The number of experiments suitable for statistical analysis was assumed to be 3 or higher. V<sub>3</sub>, respiratory rate in the presence of 200  $\mu$ M ADP; V<sub>DNP</sub>, respiratory rate in the presence of 60  $\mu$ M 2,4-DNP;  $\Delta\psi$ , mitochondrial membrane potential; SD, standard deviation. Where indicated, the incubation medium was supplemented either with 3 mM pyruvate plus 1 mM malate or with 3 mM succinate plus 3 mM glutamate.

### **III. Results**

#### **A. Oxidative Metabolism and Ca<sup>2+</sup> Handling in the YAC128 Mouse Model of HD.**

As mentioned previously, several reports have indicated that potential mitochondrial bioenergetic deficiency and mitochondrial Ca<sup>2+</sup> handling defects may be important contributors to neuronal dysfunction in HD (Brennan, Jr. *et al.* 1985;Gu *et al.* 1996;Browne *et al.* 1997). However, other reports have provided data that suggests mitochondrial functions may not be impaired by mHtt (Powers *et al.* 2007b); Powers *et al.* 2007b). The further evaluation of mHtt effects on mitochondrial functions is required to more clearly understand the role of potential mitochondrial dysfunction in HD. Impairment of mitochondrial bioenergetics by mHtt may result in decreased ATP production, potentially leading to neuronal degeneration (Lehninger *et al.* 1993;Wang and Youle 2009). Additionally, alterations to mitochondrial Ca<sup>2+</sup> handling, such as insufficient Ca<sup>2+</sup> uptake capacity or increased susceptibility to induction of the permeability transition pore, may result in excessively high cytosolic Ca<sup>2+</sup> concentration or increased likelihood of mitochondrial damage (Lehninger *et al.* 1993;Wang and Youle 2009). Therefore, if mHtt induces alterations to mitochondrial Ca<sup>2+</sup> handling, it may also lead to neuronal degeneration.

##### **a. Clasping phenotype of YAC128 mice and genotyping.**

In our initial experiments, we used YAC128 mice, which express full-length human mHtt with a 128-glutamine stretch near the N-terminus (Slow *et al.* 2003). At 2 months of age, these mice begin to demonstrate a behavioral abnormality characterized by clasping of fore- and hind-limbs when suspended by the tail (Fig. 5A and B). This behavior is typical for transgenic HD mice (Reddy *et al.* 1999;Milnerwood *et al.* 2006). We regularly observed clasping behavior in 2-month-old YAC128 mice. Overall, out of 288 2-month-old YAC128 mice of both sexes (162 males and 126 females) tested for

clasping behavior, clasping behavior was detected in 158 animals (96 males and 62 females). Clasping behavior was never observed in WT mice. In our study, we used early symptomatic 2-month-old YAC128 mice and their WT littermates as well as 10-month-old YAC128 mice at the later stage of pathology and their age-matched littermates to prepare isolated brain mitochondria. We used animals of both sexes. Every mouse used in our experiments was genotyped (Fig. 5C).

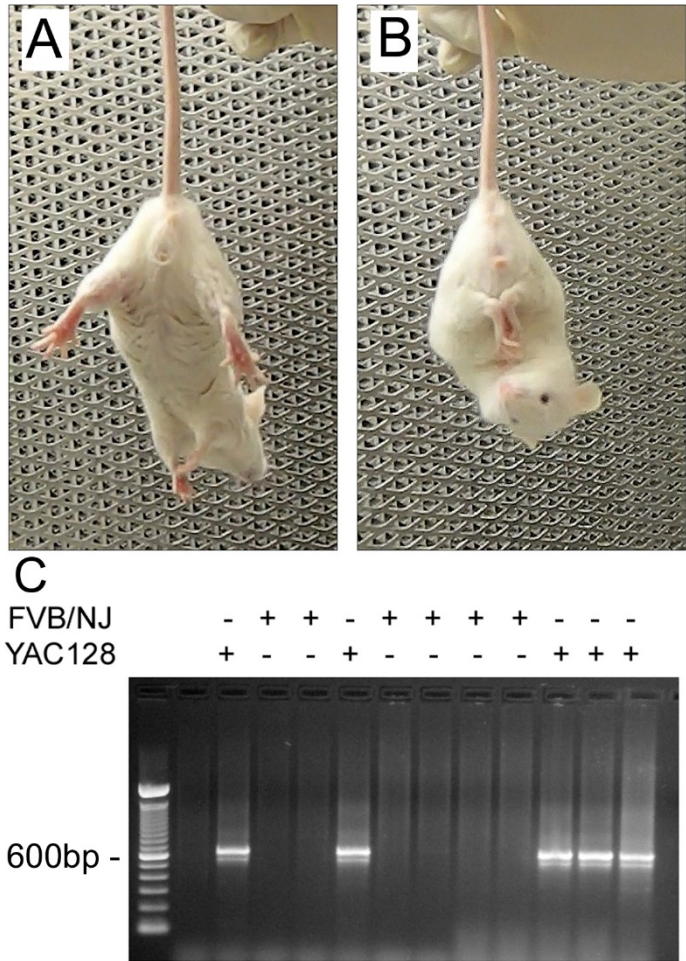


**Figure 5. Behavioral phenotype of 2-month-old YAC128 mice and a representative genotyping.** In **A**, the normal response of a wild-type (WT) FVB/NJ mouse to suspension by the tail with limbs extended out. In **B**, clasp behavior of a YAC128 mouse that was usually observed within 15–45 s of suspension. In **C**, representative genotyping data of tail tissue from WT and YAC128 mice.



## **b. Expression of mHtt and morphological characterization of brain mitochondria isolated from YAC128 mice.**

To confirm the presence of mHtt in isolated mitochondria fraction, western blotting was used. In immunoblotting experiments with brain homogenates, cytosolic fractions, and purified nonsynaptic (neuronal plus glial) and synaptic (neuronal) mitochondrial fractions from WT and YAC128 mice, we used two different antibodies for total Htt and mHtt: monoclonal anti-Htt antibody 2166 (mAb 2166, Millipore), which recognizes both mouse wild-type Htt and human mHtt, and monoclonal anti-polyQ antibody 1C2 (mAb 1574, Millipore), which recognizes mHtt. With mHtt-specific mAb 1C2, a 350 kDa band, representing mHtt, was detected in homogenates, cytosolic and mitochondrial fractions from YAC128 mice, but not in samples from WT animals (Fig. 6A). Probing purified brain synaptic (neuronal) mitochondria with mAb 1C2 produced a distinct band indicating that mHtt is associated with isolated mitochondria. Probing with anti-Htt mAb 2166, we detected a 350 kDa band, corresponding to wild-type Htt, in both WT and YAC128 samples (Fig. 6B). In brain homogenates and cytosolic fractions from YAC128 mice, mAb 2166 detected an additional band with a slightly higher molecular weight that represents mHtt. The level of expression of human mHtt was similar to the expression of endogenous wild-type Htt (Fig. 6B), which is consistent with previously reported data for YAC128 mice (Slow *et al.* 2003; Pouladi *et al.* 2013). Similar results were obtained with nonsynaptic mitochondria isolated from WT and YAC128 mice (data not shown).  $\alpha$ -Tubulin and cytochrome *c* oxidase subunit IV (COX IV) were used as cytosolic and mitochondrial markers, respectively. The weak  $\alpha$ -tubulin bands seen in mitochondrial fractions were most likely due to tubulin binding to voltage-dependent anion channel (VDAC1) in the outer mitochondrial membrane (Carre *et al.* 2002). Interestingly, with mAb 2166, only wild-type Htt was easily detected in purified mitochondria from both WT and YAC128 mice, whereas the mHtt level in YAC128

mitochondria appeared to be much lower (Fig. 6B). This was not because of decreased sensitivity of mAb 2166 to mHtt. In homogenates and cytosolic fractions, mAb 2166 detected both Htt and mHtt with similar sensitivity (Fig. 6B). Only with increased protein loading (50 µg/lane) and extended film exposure, did a mHtt band become evident in mitochondrial fraction (Fig. 6C). The results of densitometry of wild-type mouse Htt and human mHtt bands are shown in Figure 6D. Similar results were obtained with nonsynaptic mitochondria isolated from WT and YAC128 mice (not shown).

In our experiments, we used Percoll gradient-purified synaptic and nonsynaptic brain mitochondria isolated from YAC128 and WT mice. Nonsynaptic mitochondria are derived from neuronal and glial cell bodies and use of these mitochondria will give information about total brain mitochondria. However, neurons are the cell type that is primarily affected in HD and the use of mitochondria from neurons and glia may obscure possible dysfunction that may be present only in neuronal mitochondria. Therefore, in our studies, we assessed the function of both nonsynaptic and synaptic mitochondria, which are derived from synaptic terminals, and thus are mitochondria of only neuronal origin. To characterize the isolated mitochondria, we performed transmission electron microscopy (TEM). The TEM did not reveal overt morphological differences in nonsynaptic (Fig. 7A and B) and synaptic (Fig. 7C and D) mitochondria isolated from 2-month-old YAC128 (Fig. 7A and C) and WT mice (Fig. 7B and D). From these images, mitochondria were categorized into three distinct groups based on morphology (Fig. 7E): orthodox mitochondria with uniform, gray matrices, condensed mitochondria with compacted, dark matrices, and swollen mitochondria with light, vacuolarized matrices. A similar approach was used by our laboratory and others previously (Scorrano *et al.* 2002; Shalbuyeva *et al.* 2006; Brustovetsky *et al.* 2010). In all cases, the majority of mitochondria appeared to be in a condensed state (Fig. 7F), consistent with previously reported morphology of isolated brain mitochondria (Shalbuyeva *et al.* 2006;

Brustovetsky *et al.* 2010). It has to be mentioned that it is very well known that isolated mitochondria do not retain native morphology typical for the organelles inside of the cell. Nevertheless, isolated mitochondria retain biochemical functions such as respiration, membrane potential generation, and ATP synthesis. This makes isolated mitochondria a valuable model to study the effects of different agents, in our case mHtt, under tightly controlled experimental conditions and easy access to the organelles. Thus, the purpose of Figure 7 is to illustrate the lack of overt morphological differences in synaptic and nonsynaptic mitochondria isolated from WT and YAC128 mice. This, however, does not imply the lack of morphological differences *in vivo*.

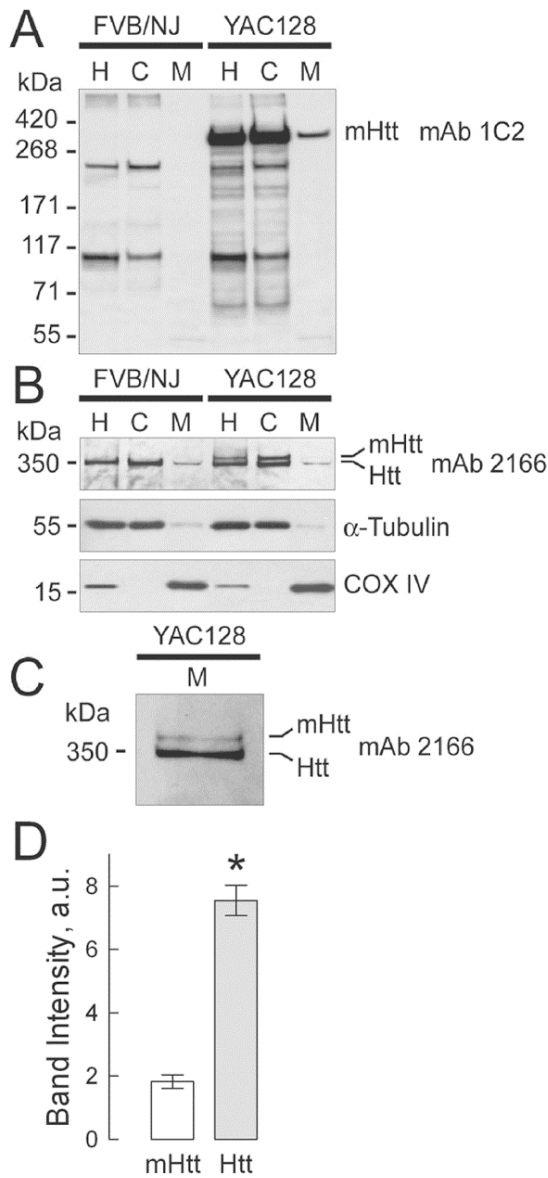


**Figure 6. Detection of wild-type mouse huntingtin (Htt) and mutant human huntingtin (mHtt) in homogenates, and cytosolic and synaptic mitochondrial fractions from 2-month-old YAC128 and WT FVB/NJ mice.** In **A**, mHtt was detected with anti-polyQ 1C2 antibody as a single band exclusively in samples from YAC128 mice. The bands with lower molecular weights (~200 kDa and 100 kDa) are present in both WT and YAC128 samples and most likely represent a result of non-specific cross-reaction with unidentified polyglutamine-containing proteins. In **B**, Htt and mHtt were detected using western blotting with 2166 antibody, which recognizes both Htt and mHtt. In homogenates and cytosolic fractions from WT and YAC128 mice, a 350 kDa band, belonging to wild-type Htt, was detected, whereas two bands, most likely representing both Htt and mHtt, were detected in homogenates and cytosolic fractions from YAC128 mice. Tubulin and COX IV were used as cytosolic and mitochondrial markers, respectively. In mitochondrial fractions from both WT and YAC128 mice, faint bands corresponding to Htt were detected, whereas amounts of mHtt attached to mitochondria were too low to be reliably detected with 2166 antibody. Only after an increase in protein loading (50  $\mu$ g/lane) and in exposure time of the film, did mHtt band become evident

(**C**). In **A–C**: H, homogenate; C, cytosolic fraction; M, mitochondrial fraction. In **D**, the results of densitometry of mHtt and Htt bands obtained with 2166 antibody applied to mitochondrial samples. Data are mean  $\pm$  SEM, N = 7, \* $p$  < 0.01 comparing band intensity for mHtt and wild-type Htt.

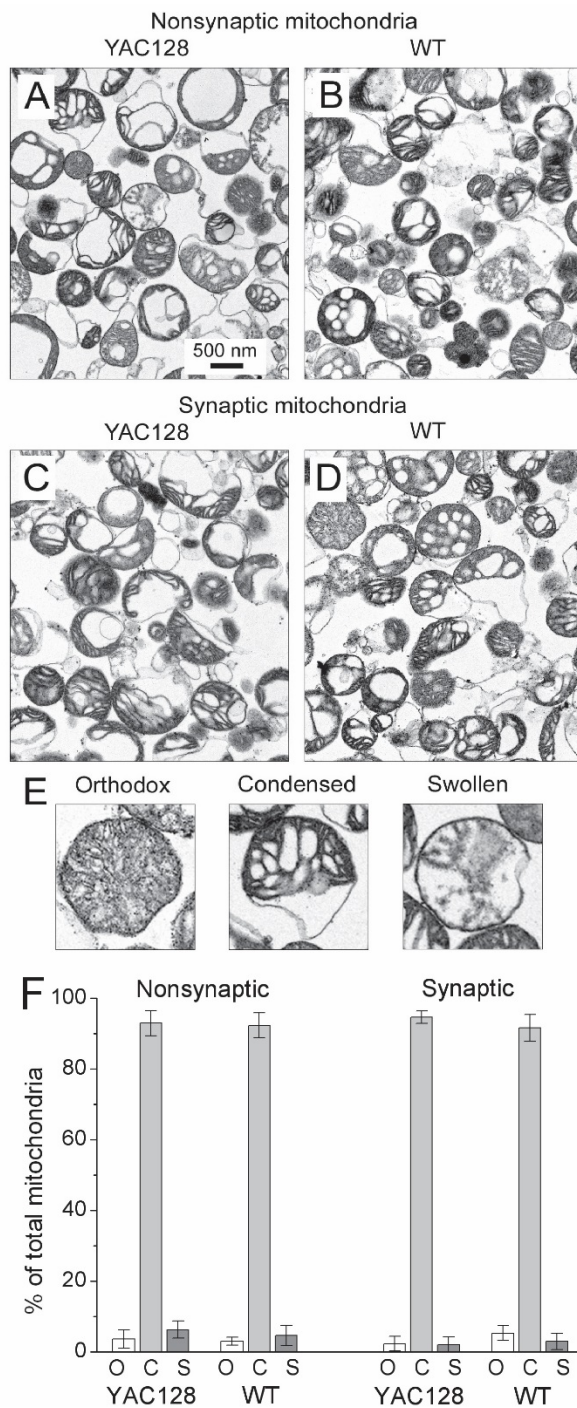


**Figure 7. Representative electron micrographs of nonsynaptic (A, B) and synaptic (C, D) brain mitochondria isolated from YAC128 (A, C) and WT (B, D) mice.** Prior to fixation with 2.5% glutaraldehyde, mitochondria were incubated for 10 min at 37°C in the standard incubation medium. In E, representative images of orthodox, condensed and swollen mitochondria. In F, morphometric analysis of isolated mitochondria: o, orthodox mitochondria; c, condensed mitochondria; s, swollen mitochondria. Data are expressed as a percentage of the total number of analyzed mitochondria. Mitochondria were analyzed in a blind manner as described previously (Shalbuyeva *et al.* 2006; Scorrano *et al.* 2002). The total number of mitochondria analyzed from each type of animal and each type of mitochondria was 450–500.

**c. Respiration of purified brain nonsynaptic and synaptic mitochondria from 2- and 10-month-old YAC128 mice as well as unpurified brain, liver, and heart mitochondria from YAC128 mice.**

Next, we investigated the effect of mHtt expression on respiration of mitochondria isolated from brain (synaptic and nonsynaptic), heart, and liver of WT and YAC128 mice. Previously, it was hypothesized that bovine serum albumin (BSA), usually used to preserve mitochondrial integrity during isolation and purification of brain mitochondria (Lai and Clark 1989), might interfere with mHtt binding to mitochondria and hence could eliminate a functional difference between mitochondria from HD transgenic mice and WT animals (Panov *et al.* 2003). To avoid the possible confounding effect of BSA, we omitted BSA from all isolation and incubation media. We measured mitochondrial respiratory activity with either a combination of Complex I substrates malate (1 mM) and pyruvate (3 mM), or with the Complex II substrate succinate (3 mM). In the latter case, incubation medium was supplemented with 3 mM glutamate to remove oxaloacetate, an endogenous inhibitor of succinate dehydrogenase (Wojtczak 1969; Brustovetsky and Dubinsky 2000a), via a transaminase reaction (Oestreicher *et al.* 1969). We assessed basal respiration with only substrates present in the incubation medium (state 2 or  $V_2$ ), respiration stimulated by ADP (state 3 or  $V_3$ ), respiration after exogenous ADP was consumed by mitochondria (state 4 or  $V_4$ ) and maximal, uncoupled respiration in the presence of 2,4-dinitrophenol (2,4-DNP,  $V_{DNP}$ ). Under each condition, the slope of the line in the respiration trace can be quantified and converted to a respiratory rate. Purified brain nonsynaptic and synaptic mitochondria isolated from 2- (Figs. 8 and 9) or 10-month-old YAC128 mice (Figs. 10 and 11) had similar respiratory rates under all tested conditions compared with mitochondria isolated from age-matched WT animals. KCN (5 mM) completely inhibited respiration, indicating that mitochondria solely contributed to oxygen consumption (Fig. 12). Immunoblotting confirmed the presence of mHtt in

mitochondria isolated from YAC128 mice (Figs. 8E and 9E). Since nonsynaptic and synaptic mitochondria undergo Percoll-gradient purification, it is conceivable that the isolation procedure to obtain purified mitochondria may result in the loss of cellular components that are required for mHtt-induced mitochondrial dysfunction. To test this possibility we also evaluated the respiratory activity of unpurified (mixture of mitochondria and synaptosomes) brain mitochondria. Additionally, although neurons are the most vulnerable cell type in HD, mHtt is a ubiquitously expressed protein that may potentially affect mitochondrial functions in tissues other than the brain. Indeed, at least one study has reported altered mitochondrial structure in cardiomyocytes of a transgenic mouse model of HD (Mihm *et al.* 2007). For this reason we also assessed the respiratory rates of heart and liver mitochondria from YAC128 mice. Unpurified brain, liver, and heart mitochondria isolated from YAC128 and WT mice also had similar respiratory rates (Figs. 13–15). These results suggest that mHtt does not affect respiration of mitochondria isolated from YAC128 mice.

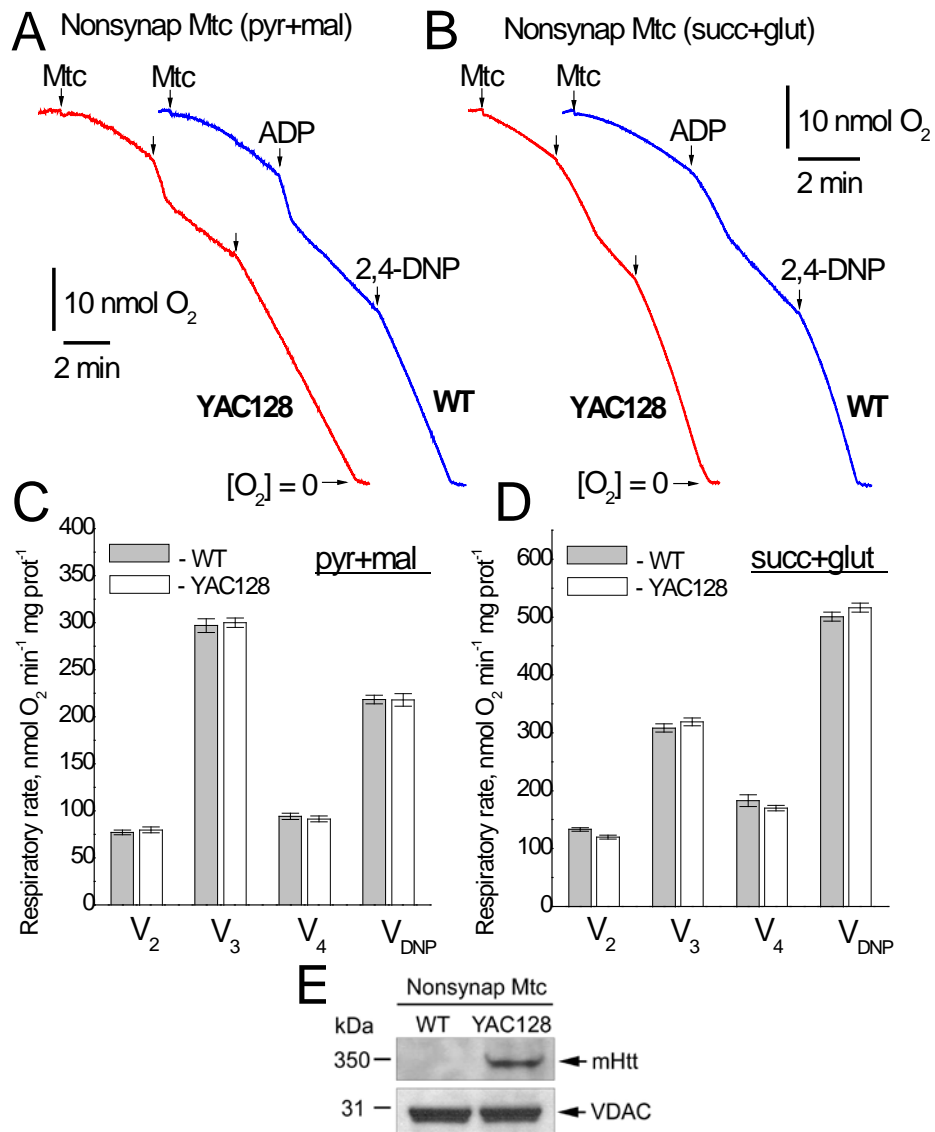


**Figure 8. Respiratory activity of brain nonsynaptic mitochondria isolated from 2-month-old WT (blue traces) and YAC128 (red traces) mice.** In **A** and **B**, representative traces for mitochondrial  $O_2$  consumption. Where indicated, nonsynaptic mitochondria (Mtc), 200  $\mu$ M ADP and 60  $\mu$ M 2,4-dinitrophenol (2,4-DNP) were added. The slope of the line following each addition corresponds to a respiratory rate. In **A**, incubation medium was supplemented with 3 mM pyruvate (pyr) and 1 mM malate (mal). In **B**, incubation medium was with 3 mM succinate (succ) and 3 mM glutamate (glut). In **C** and **D**, statistical analysis of respiratory rates. Data are mean  $\pm$  SEM,  $N = 10$ . In **E**, western blot, indicating the presence of mHtt in nonsynaptic mitochondria from YAC128 mice. VDAC1 was used as a loading control.



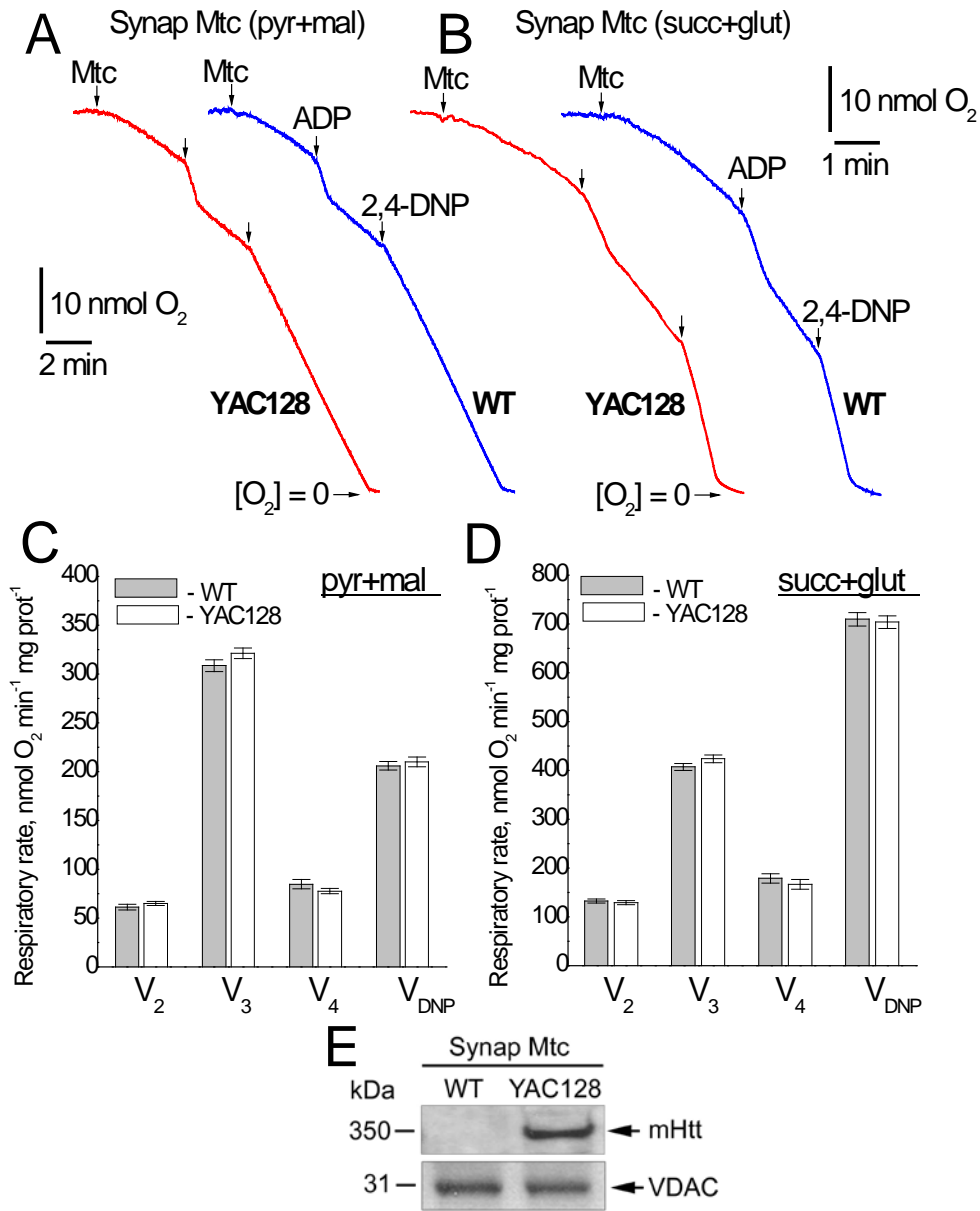


**Figure 9. Respiratory activity of brain synaptic mitochondria isolated from 2-month-old WT (blue traces) and YAC128 (red traces) mice.** In **A** and **B**, representative traces for mitochondrial O<sub>2</sub> consumption. Where indicated, synaptic mitochondria (Mtc), 200 μM ADP and 60 μM 2,4-dinitrophenol (2,4-DNP) were added. In **A**, incubation medium was supplemented with 3 mM pyruvate (pyr) and 1 mM malate (mal). In **B**, incubation medium was supplemented with 3 mM succinate (succ) and 3 mM glutamate (glut). In **C** and **D**, statistical analysis of respiratory rates. Data are mean ± SEM, N = 10. In **E**, western blot, showing the presence of mHtt in synaptic mitochondria from YAC128 mice. VDAC1 was used as a loading control.

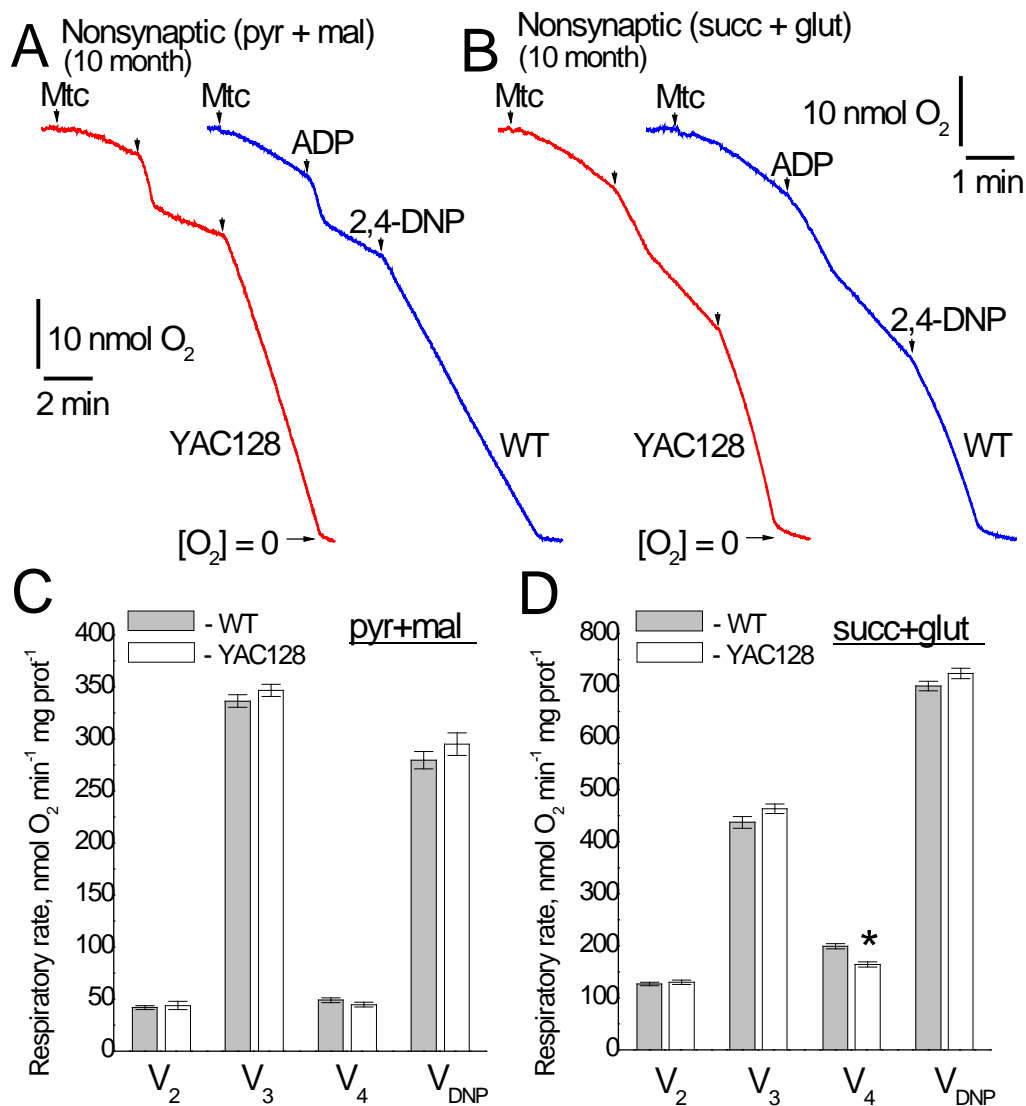


**Figure 10. Respiratory activity of nonsynaptic mitochondria isolated from 10-month-old WT (blue traces) and YAC128 (red traces) mice.** In **A** and **B**, representative traces for mitochondrial O<sub>2</sub> consumption. Where indicated, mitochondria (Mtc), 200  $\mu$ M ADP, and 60  $\mu$ M 2,4-dinitrophenol (2,4-DNP) were added. In **A**, incubation medium was supplemented with 3 mM pyruvate (pyr) and 1 mM malate (mal). In **B**, incubation medium contained 3 mM succinate (succ) and 3 mM glutamate (glut). In **C** and **D**, statistical analysis of respiratory rates. Data are mean  $\pm$  SEM \* $p$  < 0.05 comparing V<sub>4</sub> respiratory rates of mitochondria from WT and YAC128 mice, N = 7.

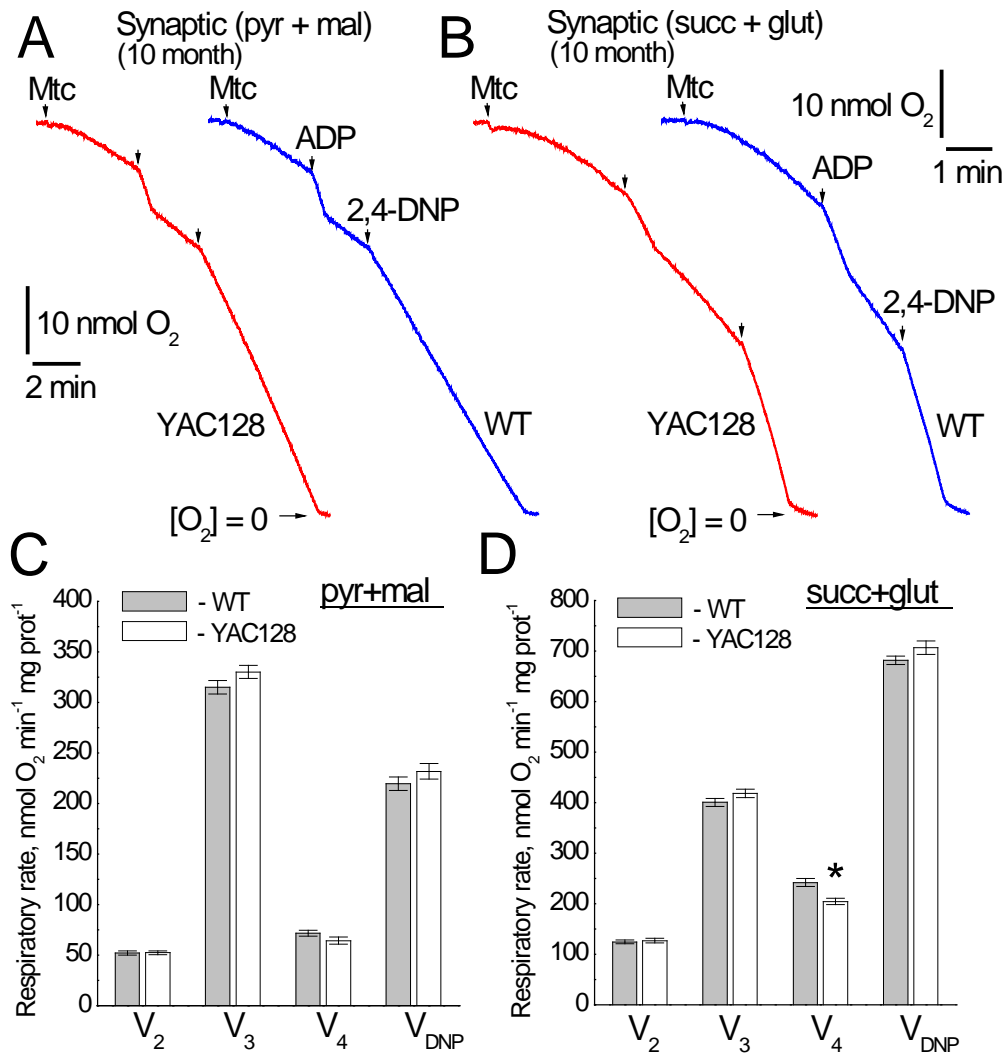


**Figure 11. Respiratory activity of synaptic mitochondria isolated from 10-month-old WT (blue traces) and YAC128 (red traces) mice.** In **A** and **B**, representative traces for mitochondrial O<sub>2</sub> consumption. Where indicated, mitochondria (Mtc), 200 μM ADP, and 60 μM 2,4-dinitrophenol (2,4-DNP) were added. In **A**, incubation medium was supplemented with 3 mM pyruvate (pyr) and 1 mM malate (mal). In **B**, incubation medium contained 3 mM succinate (succ) and 3 mM glutamate (glut). In **C** and **D**, statistical analysis of respiratory rates. Data are mean±SEM. \**p* < 0.05 comparing V<sub>4</sub> respiratory rates of mitochondria from WT and YAC128 mice, N = 7.

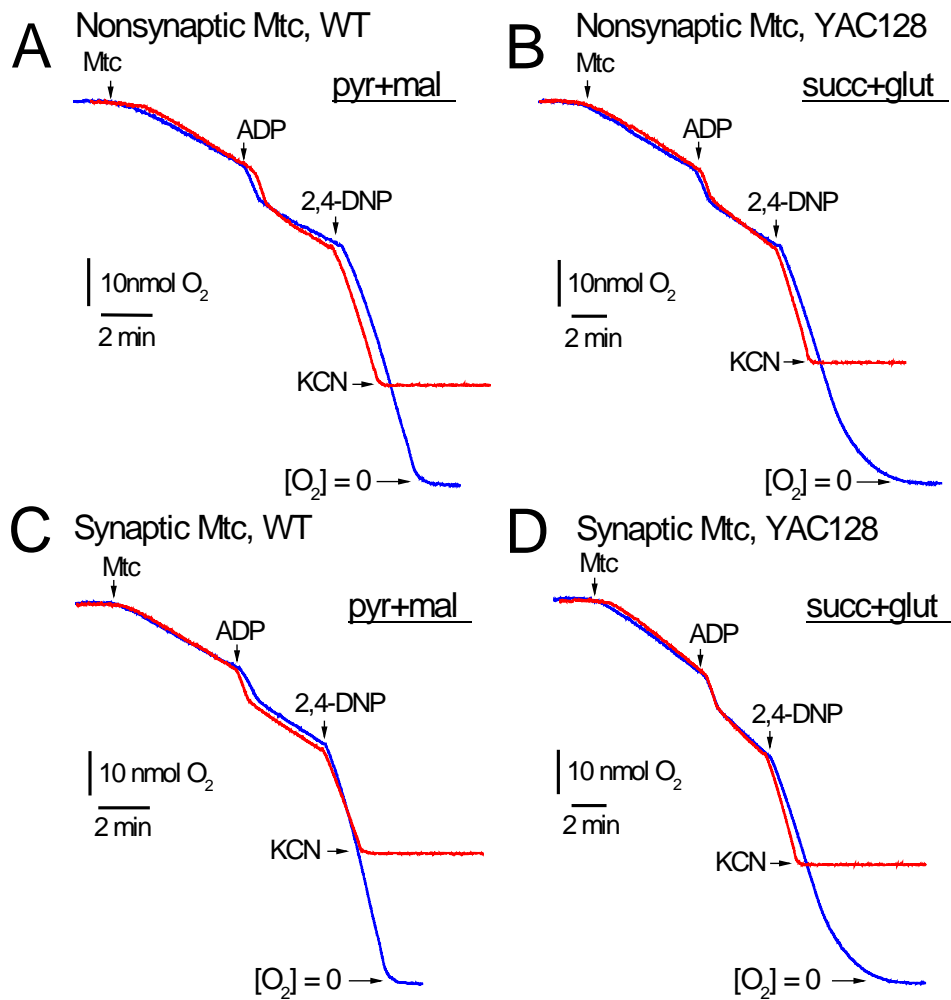


**Figure 12. KCN completely inhibits respiration of isolated brain mitochondria.** In **A** and **B**, representative traces for mitochondrial O<sub>2</sub> consumption by nonsynaptic mitochondria from WT and YAC128 mice. In **C** and **D**, representative traces for mitochondrial O<sub>2</sub> consumption by synaptic mitochondria from WT and YAC128 mice. Where indicated, mitochondria (Mtc), 200  $\mu$ M ADP, 60  $\mu$ M 2,4-dinitrophenol (2,4-DNP), and 5 mM KCN were added. In **A** and **C**, incubation medium was supplemented with 3 mM pyruvate (pyr) and 1 mM malate (mal). In **B** and **D**, incubation medium was supplemented with 3 mM succinate (succ) and 3 mM glutamate (glut).

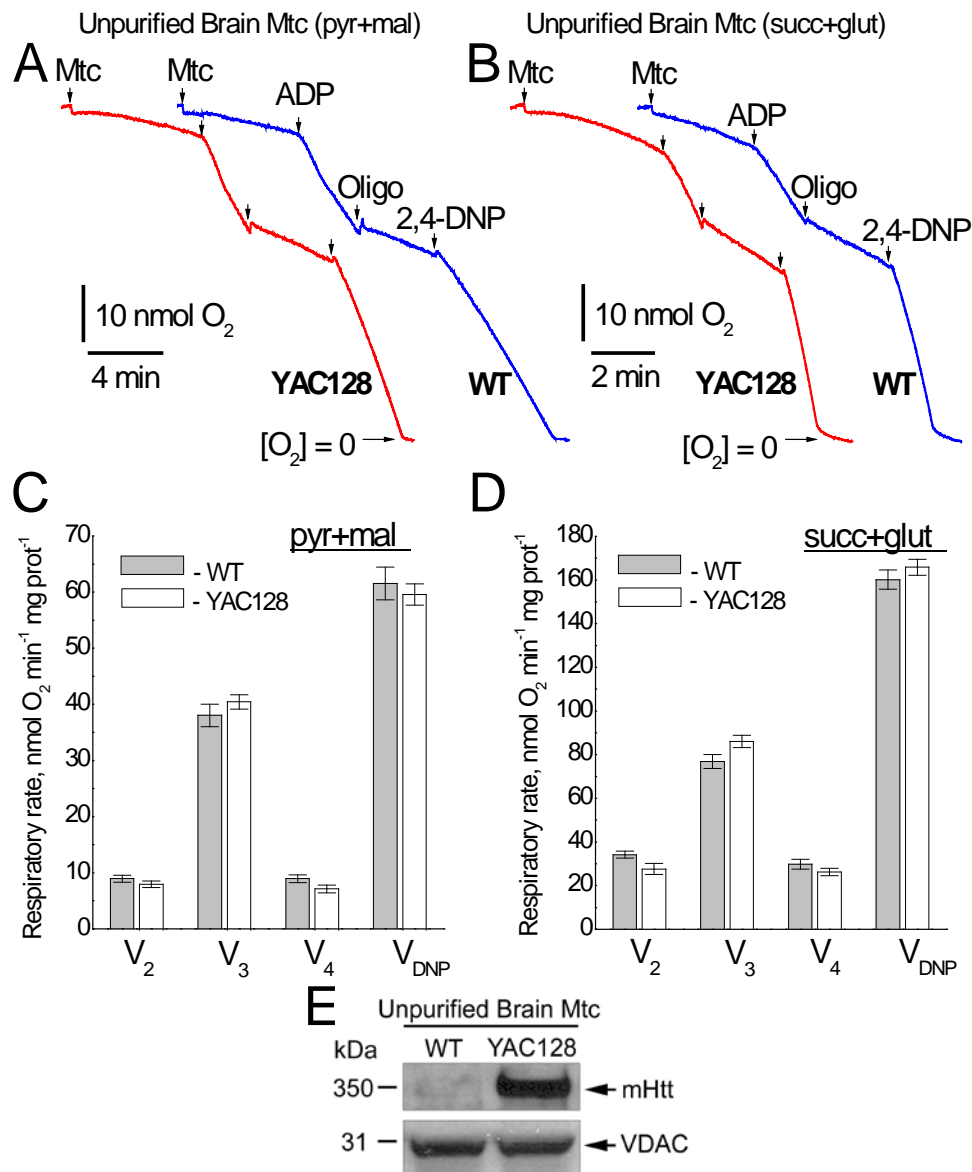


**Figure 13. Respiratory activity of unpurified brain mitochondria isolated from 2-month-old WT (blue traces) and YAC128 (red traces) mice.** In **A** and **B**, representative traces for mitochondrial O<sub>2</sub> consumption. Where indicated, mitochondria (Mtc), 200  $\mu$ M ADP, 1  $\mu$ M oligomycin (to inhibit ATP synthase) and 60  $\mu$ M 2,4-dinitrophenol (2,4-DNP) were added. In **A**, incubation medium was supplemented with 3 mM pyruvate (pyr) and 1 mM malate (mal). In **B**, incubation medium contained 3 mM succinate (succ) and 3 mM glutamate (glut). In **C** and **D**, statistical analysis of respiratory rates. Data are mean  $\pm$  SEM, N = 7. In **E**, western blot, showing the presence of mHtt in unpurified brain mitochondria from YAC128 mice. VDAC1 was used as a loading control.

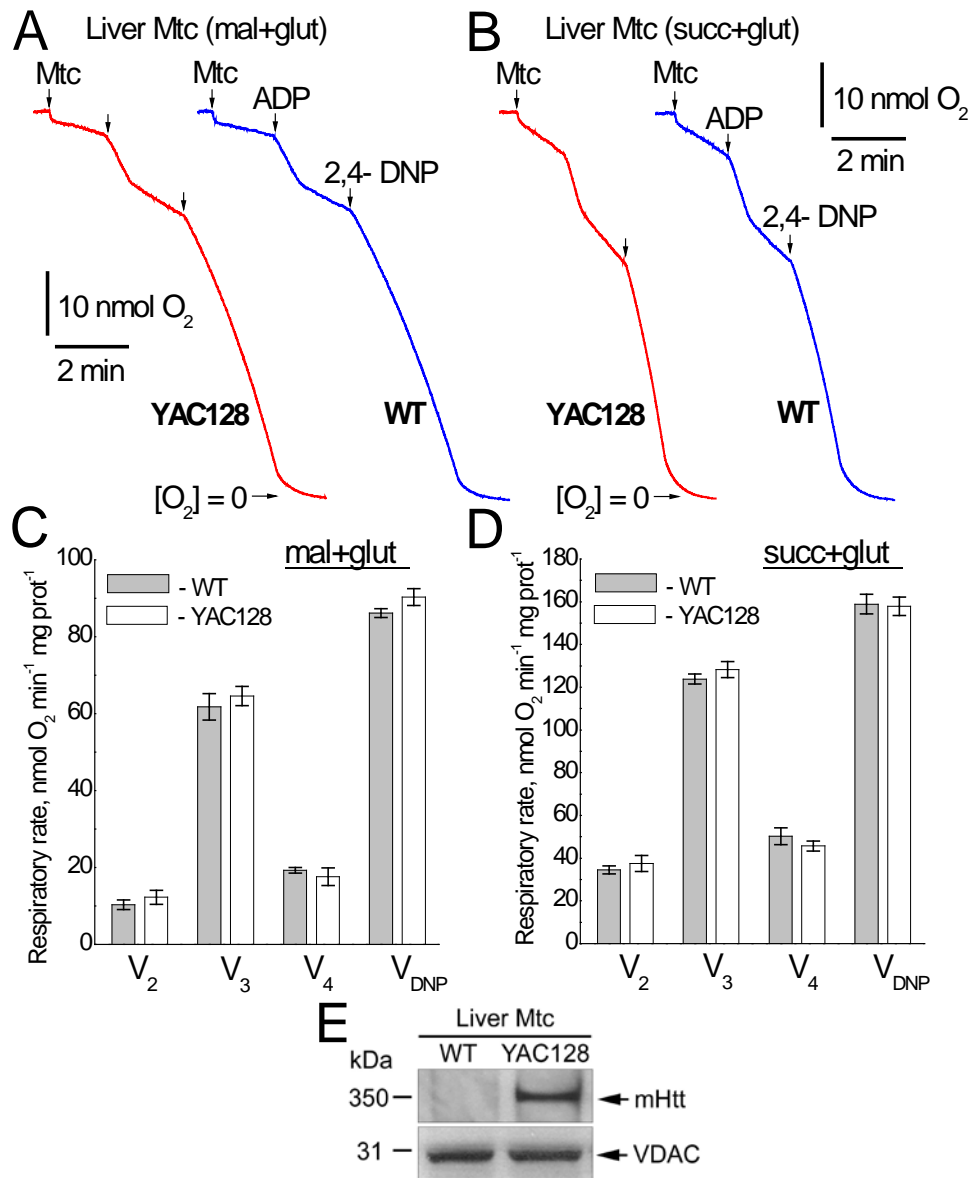


**Figure 14. Respiratory activity of liver mitochondria isolated from 2-month-old WT (blue traces) and YAC128 (red traces) mice.** In **A** and **B**, representative traces for mitochondrial O<sub>2</sub> consumption. Where indicated, mitochondria (Mtc), 200 μM ADP, and 60 μM 2,4-dinitrophenol (2,4-DNP) were added. In **A**, incubation medium was supplemented with 3 mM glutamate (glut) and 1 mM malate (mal). In **B**, incubation medium was with 3 mM succinate (succ) and 3 mM glutamate (glut). In **C** and **D**, statistical analysis of respiratory rates. Data are mean±SEM, N = 6. In **E**, western blot, showing the presence of mHtt in liver mitochondria from YAC128 mice. VDAC1 was used as a loading control.

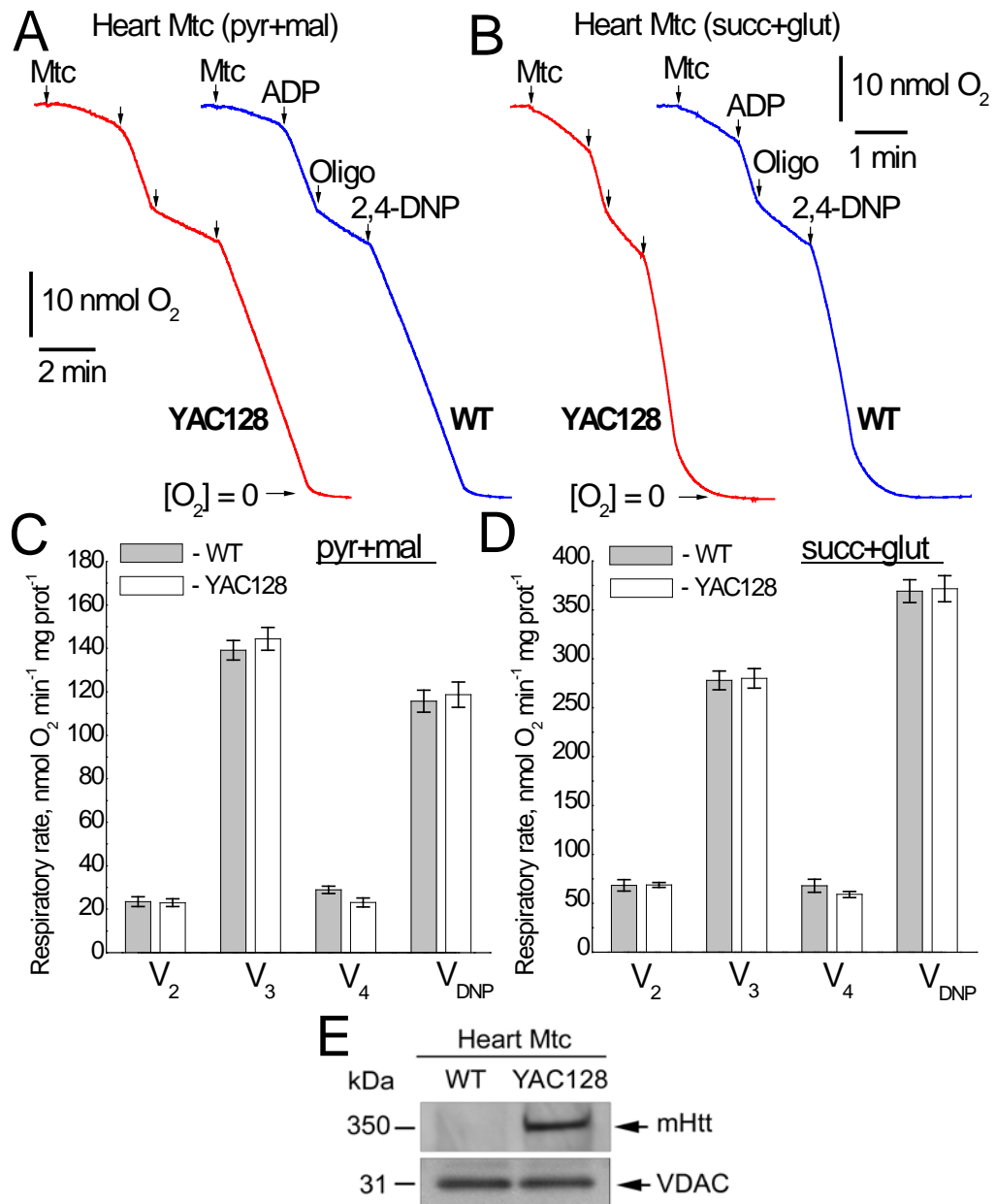


**Figure 15. Respiratory activity of heart mitochondria isolated from 2-month-old WT (blue traces) and YAC128 (red traces) mice.** In **A** and **B**, representative traces for mitochondrial  $O_2$  consumption. Where indicated, mitochondria (Mtc), 200  $\mu$ M ADP, 1  $\mu$ M oligomycin (to inhibit ATP synthase) and 60  $\mu$ M 2,4-dinitrophenol (2,4-DNP) were added. In **A**, incubation medium was supplemented with 3 mM pyruvate (pyr) and 1 mM malate (mal). In **B**, incubation medium was with 3 mM succinate (succ) and 3 mM glutamate (glut). In **C** and **D**, statistical analysis of respiratory rates. Data are mean $\pm$ SEM, N = 6. In **E**, western blot, showing the presence of mHtt in heart mitochondria from YAC128 mice. VDAC1 was used as a loading control.

#### **d. Protein expression in mitochondria from WT and YAC128 mice.**

Consistent with our data, Yano *et al.* (Yano *et al.* 2014) did not find a difference in respiration of synaptic and nonsynaptic mitochondria from R6/2 mice compared with mitochondria from WT animals. However, the authors presented evidence for mHtt-induced inhibition of protein import into mitochondria, and suggested that such an inhibition might affect mitochondrial functions later in the disease progression (Yano *et al.* 2014). According to the authors, this inhibition of mitochondrial protein import should result in a decreased amount of nuclear encoded mitochondrial proteins. However, the authors did not provide immunoblotting data supporting this hypothesis (Yano *et al.* 2014). In an earlier study, Orr *et al.* (Orr *et al.* 2008) demonstrated that expression of nuclear encoded Mn-dependent superoxide dismutase (MnSOD) as well as 30 and 70 kDa subunits of succinate dehydrogenase (Complex II) is similar in brain mitochondria isolated from 3- and 10-month-old heterozygous knock-in 150Q/7Q mice as well as in 3-month-old wild-type 7Q/7Q mice. Milakovic and Johnson (Milakovic and Johnson 2005) also failed to find a difference in expression of 30 and 70 kDa subunits of Complex II in mutant *STHdh*<sup>Q111/Q111</sup> striatal cells compared with wild-type *STHdh*<sup>Q7/Q7</sup> cells. In the present study, we analyzed expression of several nuclear-encoded mitochondrial proteins, including 39 kDa subunit of Complex I, 30 and 70 kDa subunits of Complex II, aconitase 2, subunit IV of cytochrome oxidase (COX IV), MnSOD and  $\alpha$ -subunit of ATP synthase in brain mitochondria isolated from 2- and 10-month-old YAC128 and WT mice. In these immunoblotting experiments, we did not find any evidence for decreased expression of the analyzed proteins in mitochondria of YAC128 compared with mitochondria from WT mice regardless of their age (Fig. 16). Although these experiments indicate that there is no decrease in protein expression, the denaturing process inherent in SDS-PAGE may prevent the observation of more subtle changes to proteins such as alterations in a protein's secondary structure or its native charge



density. Therefore, we performed Blue Native–PAGE followed by western blotting analysis of expression of Ndufa9, a nuclear-encoded subunit of Complex I (Fig. 17). Using this approach, we confirmed no difference in expression of the Complex I subunit in mitochondria isolated from YAC128 and WT mice. These findings argue against mHtt-induced inhibition of the mitochondrial protein import and its potential role in inhibition in mitochondrial respiration.

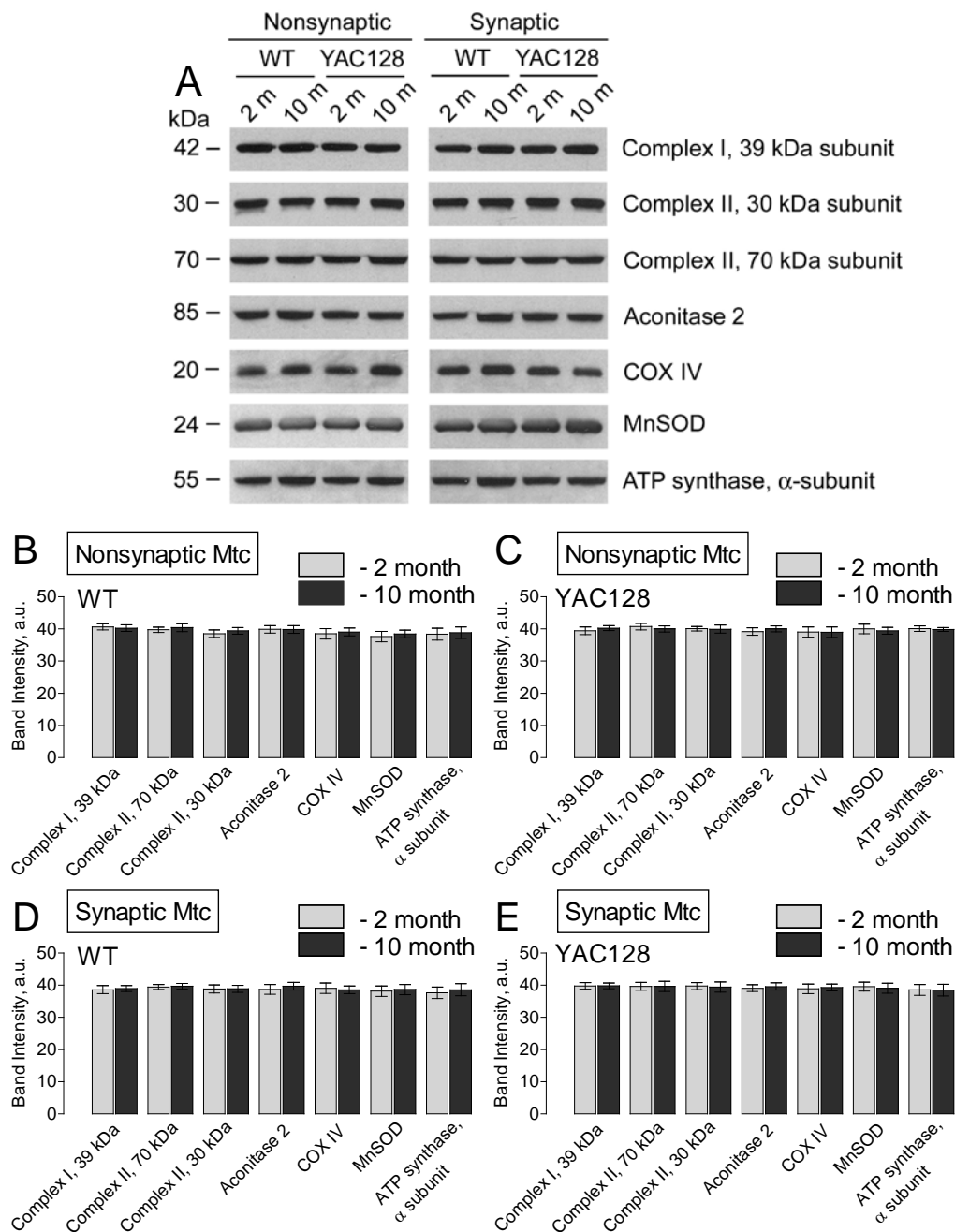


**Figure 16. Expression of nuclear encoded mitochondrial proteins in nonsynaptic and synaptic mitochondria isolated from 2- and 10-month-old WT and YAC128 mice.** In **A**, representative western blots generated with antibodies against nuclear encoded mitochondrial proteins including 39 kDa subunit of Complex I, 30 and 70 kDa subunits of Complex II, aconitase 2, subunit IV of cytochrome oxidase (COX IV), MnSOD and  $\alpha$ -subunit of ATP synthase. In **B–E**, the results of densitometry performed with NIH ImageJ 1.48v software. Data are mean  $\pm$  SEM, N = 7.

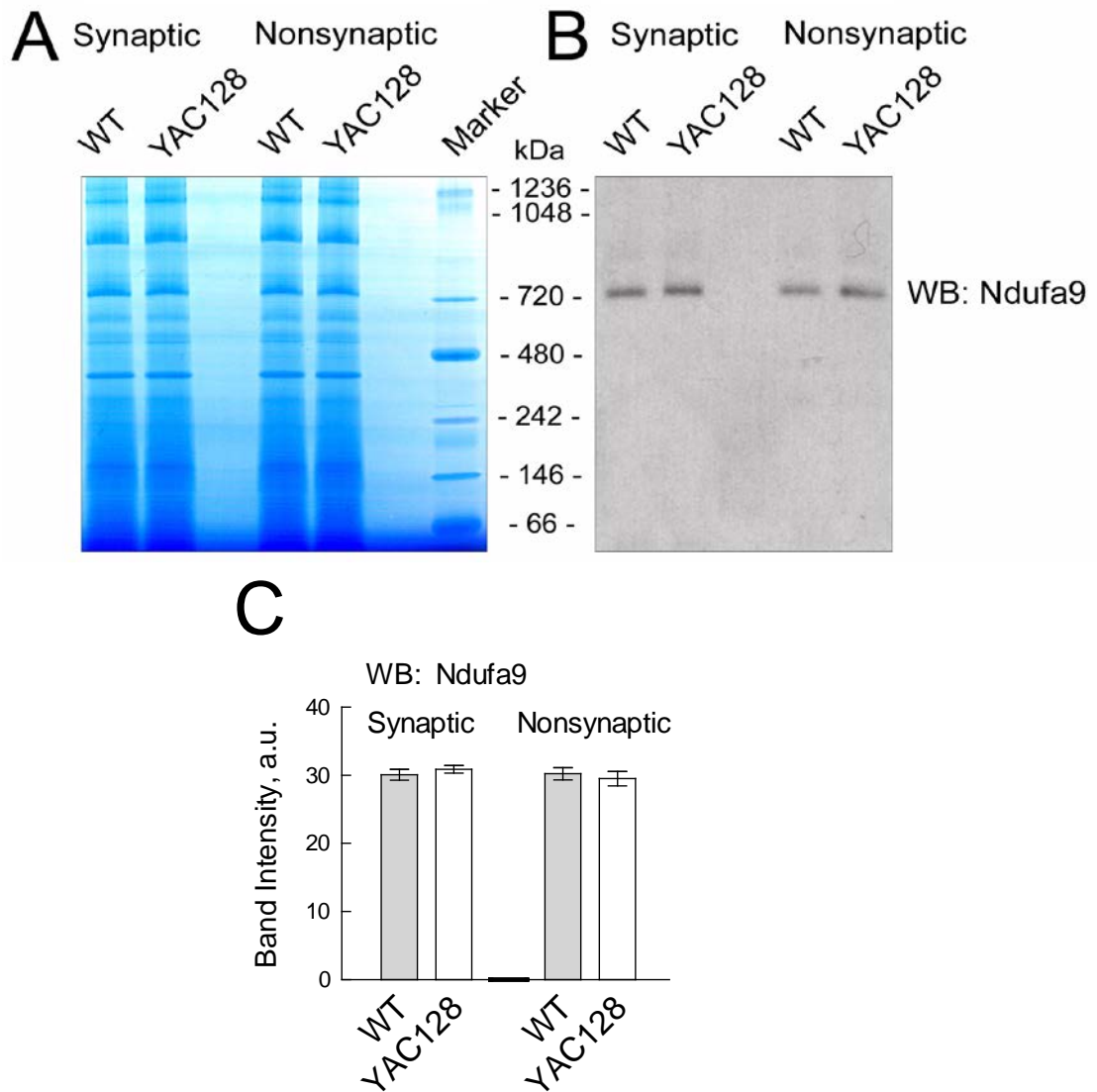


**Figure 17. Blue Native gel electrophoresis and western blotting with brain mitochondria lysates.** Lysates were prepared with brain synaptic and nonsynaptic mitochondria from 10-month-old WT and YAC128 mice as described in Materials and Methods. In **A**, a representative Blue Native gel. In **B**, western blotting with anti-Ndufa9 antibody. Molecular weight of Ndufa9 is 39 kDa. However, after Blue Native-PAGE Ndufa9 is detected in the Complex I with molecular weight above 720 kDa (38). In **C**, the results of densitometry performed with NIH ImageJ 1.48v software. Data are mean  $\pm$  SEM, N = 6.

**e. Membrane potential measurements in nonsynaptic and synaptic mitochondria from YAC128 mice.**

In addition to respiration, we also evaluated mitochondrial membrane potential ( $\Delta\psi$ ) in brain nonsynaptic and synaptic mitochondria by measuring distribution of the lipophilic cation tetraphenylphosphonium (TPP<sup>+</sup>) across the inner mitochondrial membrane (Kamo *et al.* 1979;Brustovetsky *et al.* 2002). TPP<sup>+</sup> accumulates in mitochondria and is distributed across the inner mitochondrial membrane according to membrane potential, therefore measurement of changes in [TPP<sup>+</sup>]<sub>ext</sub> outside of mitochondria provides a means for monitoring mitochondrial membrane potential. The basal mitochondrial membrane potential and responses to ADP were identical in mitochondria from YAC128 and WT mice (Fig. 18). BSA increased membrane potential to the same extent in both YAC128 and WT mitochondria (Fig. 19) most likely due to binding and removal of free fatty acids (Spector *et al.* 1969) thus decreasing free fatty acid-mediated proton permeability of the inner mitochondrial membrane and leading to more polarized mitochondria (Skulachev 1991). Mitochondrial membrane potential appeared to be similar in both nonsynaptic and synaptic mitochondria from YAC128 and WT mice, indicating the lack of dysfunction in mitochondria bound with mHtt.

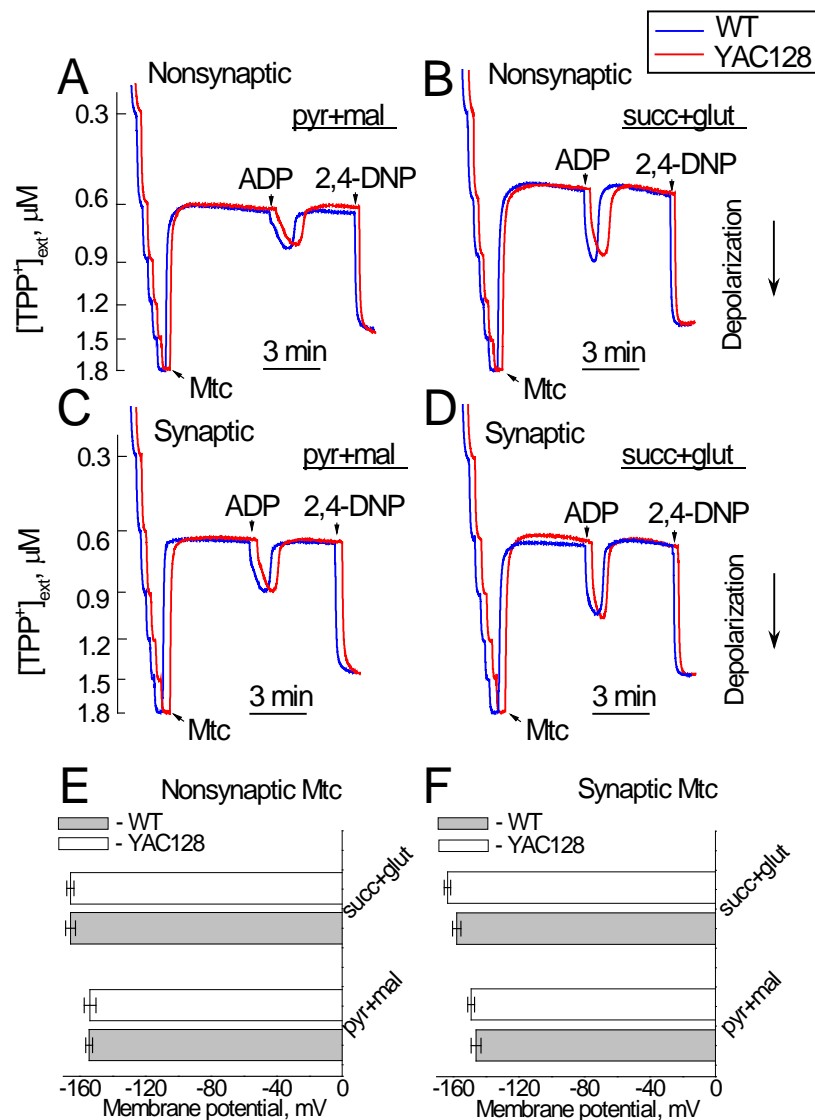


**Figure 18. Mitochondrial membrane potential in nonsynaptic (A, B) and synaptic (C, D) mitochondria isolated from 2-month-old WT (blue traces) and YAC128 (red traces) mice.** In A–D, representative traces for TPP<sup>+</sup> accumulation indicating changes in mitochondrial membrane potential ( $\Delta\psi$ ) in response to 200  $\mu\text{M}$  ADP and 60  $\mu\text{M}$  2,4-dinitrophenol. In A and C, incubation medium was supplemented with 3 mM pyruvate (pyr) and 1 mM malate (mal). In B and D, incubation medium was supplemented with 3 mM succinate (succ) and 3 mM glutamate (glut). The initial part of each trace that resembles a “stair-step” pattern is the calibration which consists of six 0.3  $\mu\text{M}$  TPP<sup>+</sup> pulses and is used to convert [TPP<sup>+</sup>] to mV membrane potential according to Nernst equation (Kamo *et al.* 1979). The upward deflection of the line following addition of mitochondria indicates accumulation of TPP<sup>+</sup> due to mitochondrial membrane potential. Downward deflections of the line indicate the movement of TPP<sup>+</sup> out of mitochondria and is interpreted as depolarization. In E and F, statistical analysis of mitochondrial membrane potential measured 2 min prior to ADP addition. Data are mean  $\pm$  SEM, N = 7.

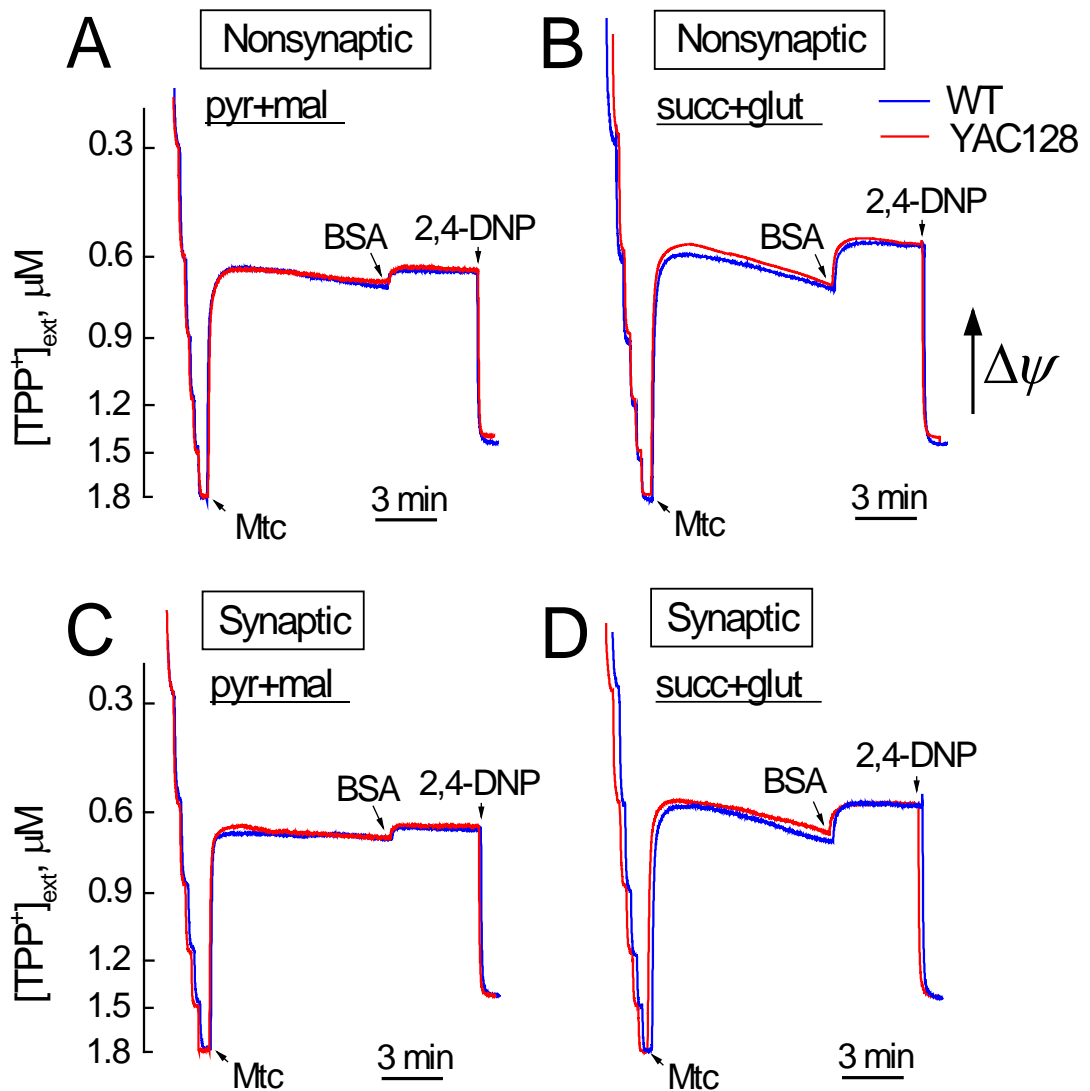


**Figure 19.** The effect of bovine serum albumin (BSA) on mitochondrial membrane potential in nonsynaptic (A, B) and synaptic (C, D) mitochondria isolated from 2-month-old WT (blue traces) and YAC128 (red traces) mice. Representative traces for TPP<sup>+</sup> accumulation indicating changes in mitochondrial membrane potential ( $\Delta\psi$ ) in response to 0.1% BSA (free from fatty acids) and 60  $\mu$ M 2,4-dinitrophenol. In **A** and **C**, incubation medium was supplemented with 3 mM pyruvate (pyr) and 1 mM malate (mal). In **B** and **D**, incubation medium contained 3 mM succinate (succ) and 3 mM glutamate (glut).

**f. Cellular respiration and extracellular acidification of neurons and ATP/ADP measurements in isolated mitochondria and primary neurons from YAC128 mice.**

To further examine a possible effect of mHtt on oxidative metabolism, we evaluated the respiratory activity of striatal and cortical neurons at 9 days *in vitro* (DIV) derived from YAC128 and WT mice (Fig. 20). To measure cell respiration, we used Seahorse XF24 flux analyzer. Cellular respiration was evaluated by measuring oxygen consumption rate (OCR). Simultaneously with respiration, we measured glycolytic activity by following the extracellular acidification rate (ECAR). However, the medium conditions used in this experiment were chosen to accentuate cellular respiration to maximize the possibility that even small differences in respiration could be detected between HD and WT cells, as described previously (Gouarne *et al.* 2013). Moreover, the experimental protocol for measurements of glycolysis differs from the protocol used here for respiration. For these reasons, ECAR data should be considered preliminary and will require further assessment. Nevertheless, we believe that even preliminary ECAR data may provide valuable information. To accentuate mitochondrial respiration, in addition to 10 mM glucose, the bath solution was supplemented with 15 mM pyruvate (Oliveira *et al.* 2007). We measured basal respiratory activity, oligomycin-sensitive respiration coupled to ATP synthesis, and maximal, uncoupled respiration in the presence of 2,4-dinitrophenol (2,4-DNP). At the end of the experiment, cells were treated with a combination of rotenone and antimycin A (both in 1  $\mu$ m), to assess non-mitochondrial respiration. The experiments with striatal and cortical neurons revealed no difference in respiratory rates between cells from YAC128 and WT mice (Fig. 20A and B). Interestingly, maximal respiratory activity of striatal neurons was considerably lower than maximal, uncoupled respiration of cortical neurons (Fig. 20A and B). It is possible that this contributes to increased vulnerability of striatal neurons in HD.

Oligomycin inhibits oxidative phosphorylation and stimulates glycolysis that is manifested in increased ECAR (Wu *et al.* 2007; Ismailoglu *et al.* 2014). However, because 2,4-DNP increases proton permeability of membranes and increases proton extrusion from the cell, ECAR cannot be used as an indicator of glycolytic activity in the presence of protonophore (Gouarne *et al.* 2013). Therefore, similarly to Gouarne *et al.* (Gouarne *et al.* 2013), we did not analyze ECAR data obtained after 2,4-DNP injection. Consequently, Figures 20C and D and 21C and D show bar graphs that illustrate basal and oligomycin-stimulated ECARs in cultured striatal and cortical neurons from YAC128 and WT mice.

In our experiments, basal as well as oligomycin-stimulated ECARs were similar in neurons from YAC128 and WT mice, suggesting similar glycolytic activities in YAC128 and WT cells incubated in 'high glucose medium' (Fig. 20C and D). Recently, Gouarne *et al.* reported that neurons from BACHD rats have lower maximal respiratory rates compared to cells from WT animals, but only if neurons were incubated in the 'low glucose medium' (2.5 mM glucose, no pyruvate) (Gouarne *et al.* 2013). We therefore examined respiratory activities of striatal and cortical neurons from YAC128 and WT mice in the 'low glucose medium' and did not find a significant difference (Fig. 21A and B). However, following oligomycin application, striatal neurons from YAC128 mice demonstrated slight, but statistically significant decrease in oligomycin-stimulated ECAR compared with cells from WT animals, suggesting some decline in glycolytic activity under these conditions (Fig. 21C and D). This is consistent with previously reported data (Gouarne *et al.* 2013). Thus, measurements of respiratory and glycolytic activities with primary striatal and cortical neurons from YAC128 and WT mice revealed the lack of respiratory deficits in cells expressing mHtt and only a marginal decrease in oligomycin-stimulated glycolytic rate when cells were incubated in the 'low glucose medium'.



Consistent with the lack of respiratory defects, we did not find a difference in ATP and ADP levels in isolated nonsynaptic and synaptic brain mitochondria isolated from 2- and 10-month-old animals or in primary striatal neurons (10 DIV) from YAC128 and WT mice (Fig. 22). These results support the lack of bioenergetic deficiency in brain mitochondria and cultured neurons from YAC128 mice.

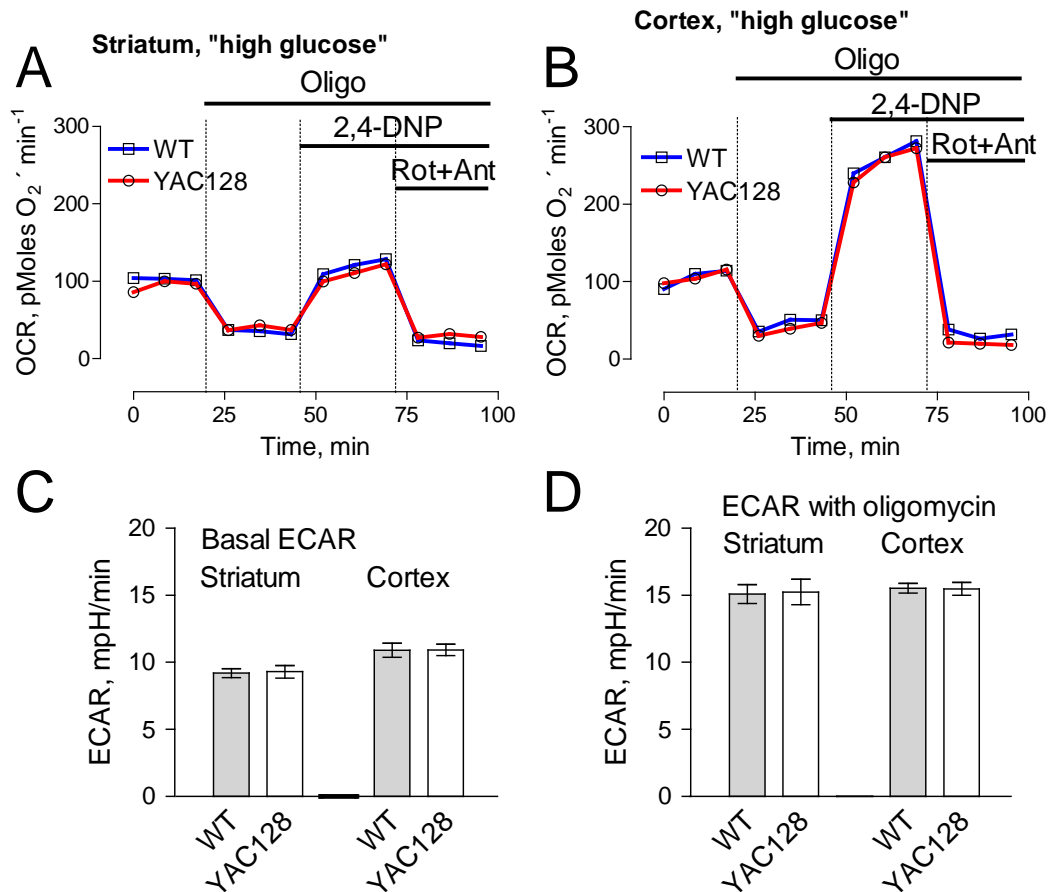


**Figure 20. OCR and ECAR of cultured neurons from YAC128 and WT mice: ‘high glucose conditions’.** In these experiments, we used striatal and cortical neurons derived from postnatal Day 1 YAC128 and WT mice. The cells were grown for 9 days *in vitro* (9 DIV) before measurements. The bath solution contained 10 mM glucose and 15 mM pyruvate to accentuate mitochondrial respiration (Oliveira *et al.* 2007). Where indicated, cells were treated with 1  $\mu$ M oligomycin (Oligo), 60  $\mu$ M 2,4-dinitrophenol (2,4-DNP), 1  $\mu$ M rotenone (Rot) and 1  $\mu$ M antimycin A (Ant). In **A** and **B**, OCR of striatal and cortical neurons, respectively. In **C** and **D**, ECAR of striatal and cortical neurons. The OCR and ECAR were measured with Seahorse XF24 flux analyzer (Seahorse Bioscience, Billerica, MA, USA) at 37°C with 10<sup>5</sup> cells per well. Data are mean  $\pm$  SEM, N = 7.

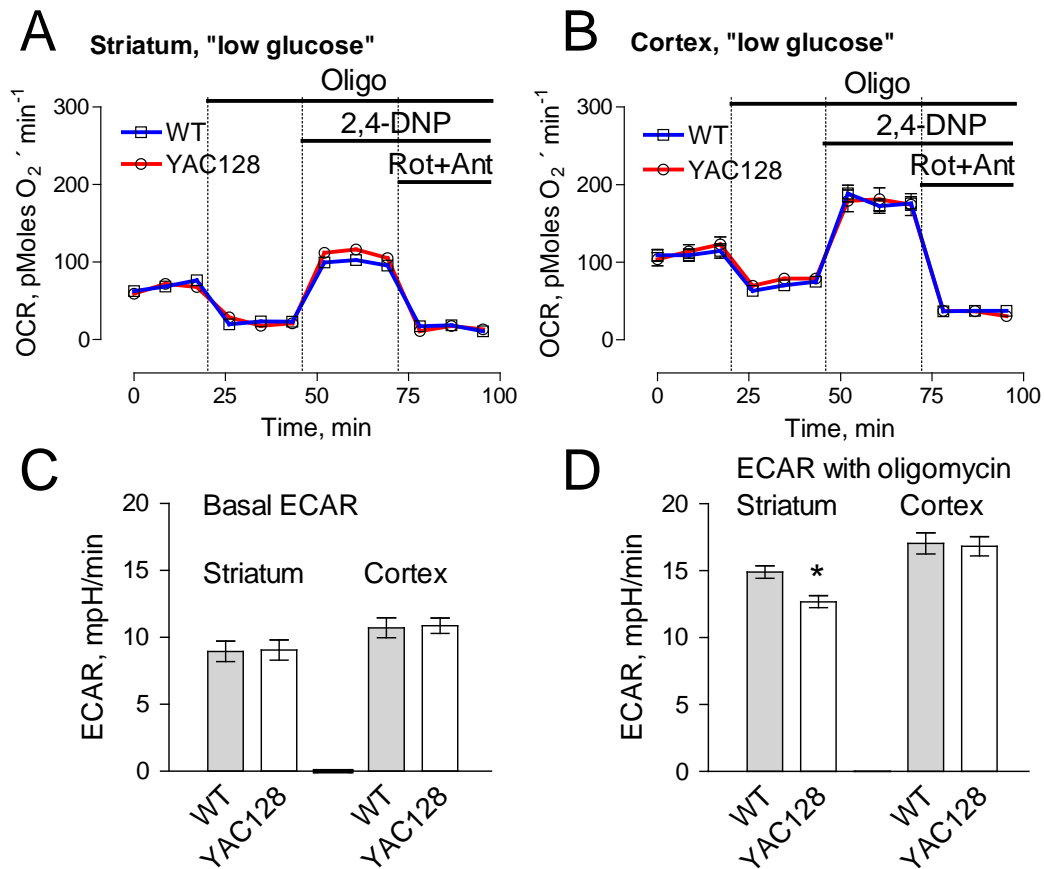


**Figure 21. OCR and ECAR of cultured neurons from YAC128 and WT mice: 'low glucose conditions'.** In these experiments, we used striatal and cortical neurons derived from postnatal Day 1 YAC128 and WT mice. The cells were grown for 9 days *in vitro* (9 DIV) before measurements. The bath solution contained 2.5 mM glucose. Where indicated, cells were treated with 1  $\mu$ M oligomycin (Oligo), 60  $\mu$ M 2,4-dinitrophenol (2,4-DNP), 1  $\mu$ M rotenone (Rot) and 1  $\mu$ M antimycin A (Ant). In **A** and **B**, OCR of striatal and cortical neurons, respectively. In **C** and **D**, ECAR of striatal and cortical neurons. The OCR and ECAR were measured with Seahorse XF24 flux analyzer (Seahorse Bioscience, Billerica, MA, USA) at 37°C with 10<sup>5</sup> cells per well. Data are mean  $\pm$  SEM, N = 7. \* $p$  < 0.05 compared to ECAR produced by WT mitochondria.

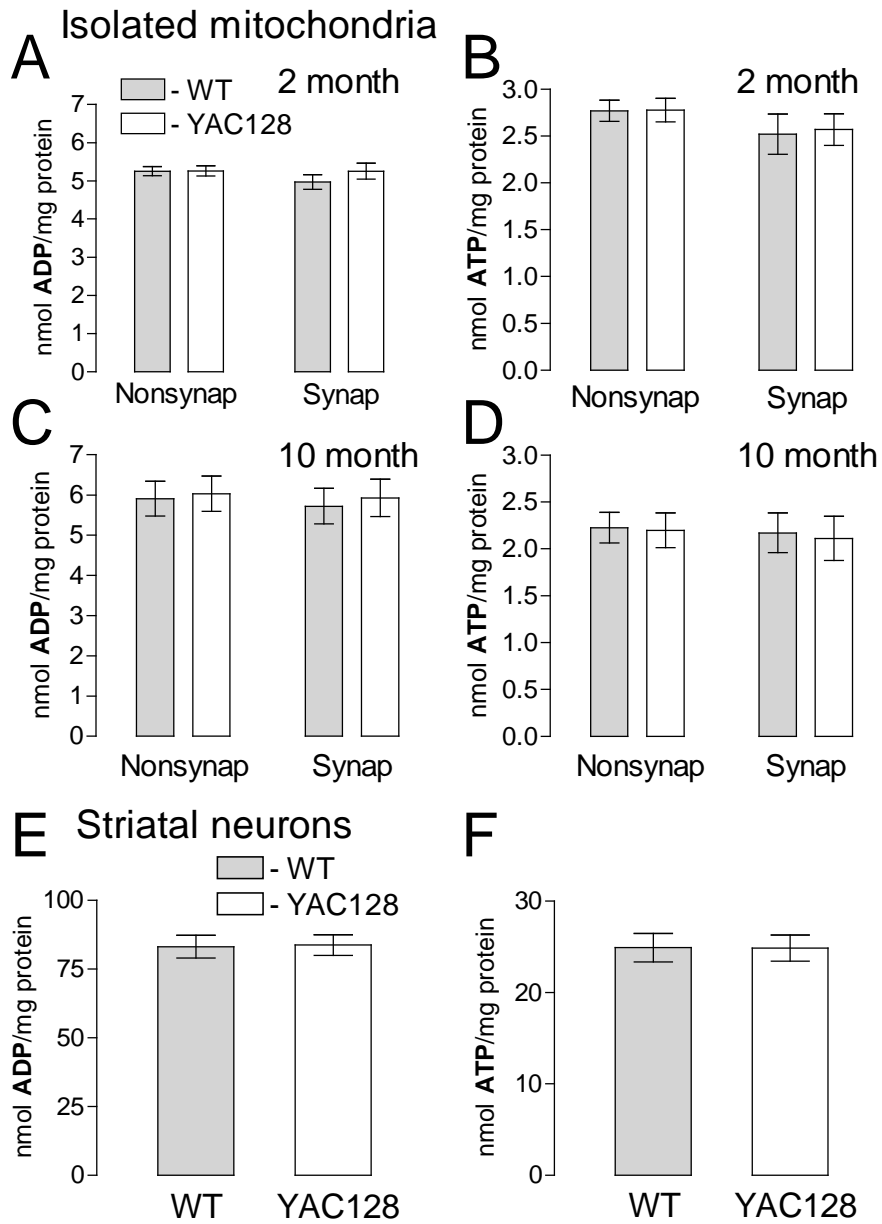


**Figure 22. ADP and ATP content in brain mitochondria (A–D) and cultured striatal neurons (E and F) derived from YAC128 and WT mice.** Synaptic and nonsynaptic mitochondria were isolated from 2- (A and B) or 10-month-old (C and D) mice. Mitochondria (50µg protein) were incubated for 10 min at 37°C in the standard incubation medium supplemented with 3 mM succinate and 3 mM glutamate. In E and F, cultured striatal neurons (10 DIV) were lysed on ice with Releasing Reagent (Sigma). Then, ADP (A, C, E) and ATP (B, D, F) were measured with ATP bioluminescent somatic cell assay kit (Sigma) using Glomax 20/20 luminometer (Promega) as described in Materials and Methods. In A–D, data are mean ± SEM, N = 7. In E and F, data are mean ± SEM, N = 10–11 dishes from five platings.

#### **g. Whole-animal metabolic activity of YAC128 mice.**

Although we did not find any difference in respiration of isolated mitochondria or cultured neurons from YAC128 and WT mice, these results could not exclude an effect of mHtt on mitochondrial respiration *in vivo*. Considering this, we tested oxidative metabolism of YAC128 and WT mice *in vivo*. In these experiments, we chose to use 10-month-old animals, an age that HD mice have previously been found to show evidence of neurodegeneration (striatal atrophy) (Slow *et al.* 2003). Mice were kept in metabolic cages (Animal Monitoring System, Lab Master, TSE Systems, Midland, MI) for 72 h for acclimation and then for the following 96 h, animal OCR, CO<sub>2</sub> release rate and motor activity were monitored. Because adipose tissue does not significantly contribute to overall O<sub>2</sub> consumption, the lean body mass was determined for each mouse by dual-energy X-ray absorptiometry (DEXA) scanning and the OCRs and CO<sub>2</sub> release rates were normalized to animal lean body mass (DePaoli-Roach *et al.* 2012). Our experiments revealed that YAC128 mice and WT littermates have similar motor activity and comparable *in vivo* OCRs and CO<sub>2</sub> release rates (Fig. 23). This finding suggests that there are no significant changes in energy metabolism in YAC128 mice. Additionally, we measured food consumption and fasted blood glucose in YAC128 and WT mice and found no difference in these parameters. However, YAC128 mice were heavier compared with age-matched WT mice and had larger percentage of body fat (Table 4). Thus, whole animal respirometry with YAC128 and WT mice confirmed the lack of respiratory deficiency and supported the conclusion that respiratory activity in YAC128 mice is not affected by mHtt.

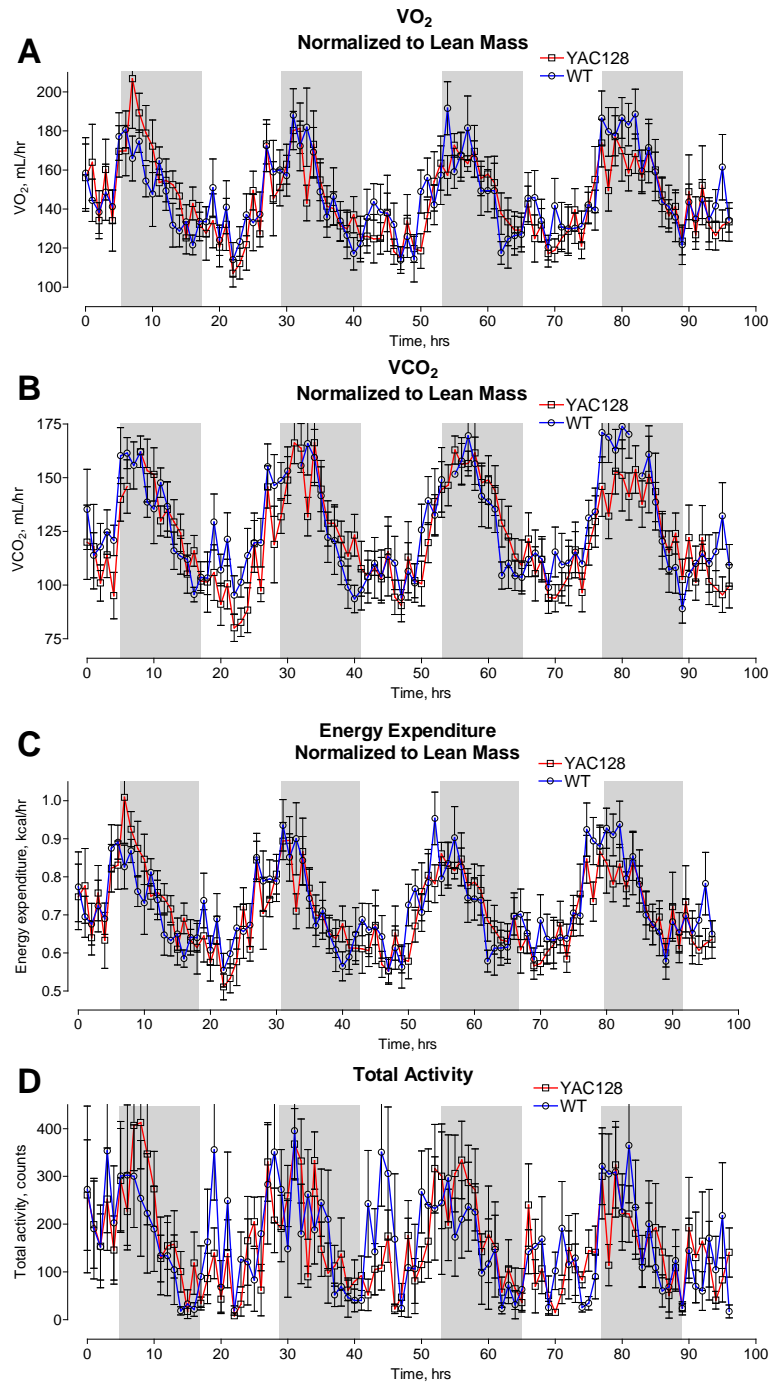


**Figure 23. Oxygen consumption (A), CO<sub>2</sub> release (B), energy expenditure (C), and total physical activity (D) of 10-month-old YAC128 and WT mice.** The animals were analyzed by indirect calorimetry in metabolic cages. Oxygen consumption, CO<sub>2</sub> release, and energy expenditure were normalized to lean mouse body mass determined by DEXA scanning. The shaded areas correspond to the 12-h dark cycles. Data are mean  $\pm$  SEM, N = 8.

**Table 4. Body composition of YAC128 and WT mice.**

	WT	YAC128 (P-value)
Number of mice	8	8
Weight, g	33.1 ± 1.2	39.6 ± 1.3 (0.003)
Food consumption, g/24 h	5.64 ± 0.88	5.12 ± 0.56 (0.13)
Fasted blood glucose, mg/dl	66.3 ± 14.6	70.3 ± 17.7 (0.63)
Fat mass, %	18.9 ± 1.3	22.9 ± 1.4 (0.048)
Lean mass, %	81.1 ± 1.3	77.1 ± 1.4 (0.048)

Data were analyzed using two-tailed unpaired t-test.

#### **h. Ca<sup>2+</sup> uptake capacity of nonsynaptic and synaptic mitochondria from YAC128 mice.**

Mitochondrial Ca<sup>2+</sup> uptake plays an essential role in removal of excessive Ca<sup>2+</sup> from the cytosol (Bernardi *et al.* 1999) and therefore is required for maintenance of Ca<sup>2+</sup> homeostasis in the cell and for cell survival (Bernardi and Rasola 2007). Ca<sup>2+</sup> accumulation in mitochondria is restricted by induction of the mitochondrial PTP that depolarizes mitochondria and thereby limits their ability to accumulate additional Ca<sup>2+</sup> (Bernardi *et al.* 1999). We tested the effect of mHtt on Ca<sup>2+</sup> uptake capacity of mitochondria isolated from YAC128 mice and compared it with Ca<sup>2+</sup> uptake capacity of mitochondria from wild-type FVB/NJ mice. A possible decrease in mitochondrial Ca<sup>2+</sup> uptake capacity could serve as an indicator of mitochondrial impairment in HD such as increased propensity to induction of PTP. Conversely, unchanged or augmented Ca<sup>2+</sup> uptake capacity suggests that there are no defects in mitochondrial Ca<sup>2+</sup> handling. In our hands, Ca<sup>2+</sup> uptake capacity of nonsynaptic mitochondria from 2- and 12-month-old YAC128 mice was slightly, but statistically significantly increased compared with mitochondria from FVB/NJ mice (Fig. 24). This result is consistent with data previously reported by Oliveira *et al.* (2007). The slight increase in Ca<sup>2+</sup> uptake capacity was observed with both Complex I substrates pyruvate/malate and the Complex II substrate succinate used in combination with glutamate to prevent accumulation of oxaloacetate and inhibition of succinate dehydrogenase (Wojtczak 1969; Brustovetsky and Dubinsky 2000a). Synaptic mitochondria from 2-month-old YAC128 mice also had a slight, but statistically significant increase in Ca<sup>2+</sup> uptake capacity compared with mitochondria from age-matched FVB/NJ mice regardless of oxidative substrates (Fig. 25A and D). BSA (Fig. 25B) considerably increased Ca<sup>2+</sup> uptake capacity in synaptic mitochondria from both WT and YAC128 mice. Interestingly, Ca<sup>2+</sup> uptake capacity of synaptic mitochondria



from 12-month-old YAC128 mice was noticeably increased compared with mitochondria from 2-month-old YAC128 mice and age-matched 12-month-old FVB/NJ mice (Fig. 25C).

Earlier, some investigators reported an increased propensity to PTP induction in mitochondria exposed to mHtt (Choo *et al.* 2004;Fernandes *et al.* 2007;Lim *et al.* 2008;Quintanilla *et al.* 2013). However, in a previous study no evidence was found for increased susceptibility to PTP induction in striatal and cortical mitochondria from HD mice compared with mitochondria from wild-type mice (Brustovetsky *et al.* 2005a). In this earlier study, investigators studied PTP induction in nonsynaptic mitochondria. In the present study, we for the first time tested synaptic (neuronal) mitochondria from YAC128 and WT mice (Fig. 26). Mitochondrial swelling and depolarization are the major manifestations of PTP induction (Bernardi *et al.* 1999). Consequently, we investigated an induction of the PTP by simultaneously monitoring a decrease in light scattering of the mitochondrial suspension, indicative of swelling of the organelles, and a release of TPP<sup>+</sup> from mitochondria, indicative of mitochondrial depolarization. Ca<sup>2+</sup>, in a concentration-dependent manner, induced swelling and depolarization of synaptic mitochondria (Fig. 26). To quantify swelling of mitochondria, at the end of the experiment we applied alamethicin (AL), an antibiotic that causes maximal mitochondrial swelling (Brustovetsky and Dubinsky 2000b). Maximal swelling was taken as 100% and mitochondrial swelling following 15 minutes incubation with Ca<sup>2+</sup> was calculated as a percentage of maximal swelling. Both mitochondrial swelling and depolarization in response to Ca<sup>2+</sup> were comparable in mitochondria isolated from YAC128 and wild-type mice. Thus, in our experiments mHtt failed to increase propensity to PTP induction in synaptic (neuronal) mitochondria from YAC128 mice.

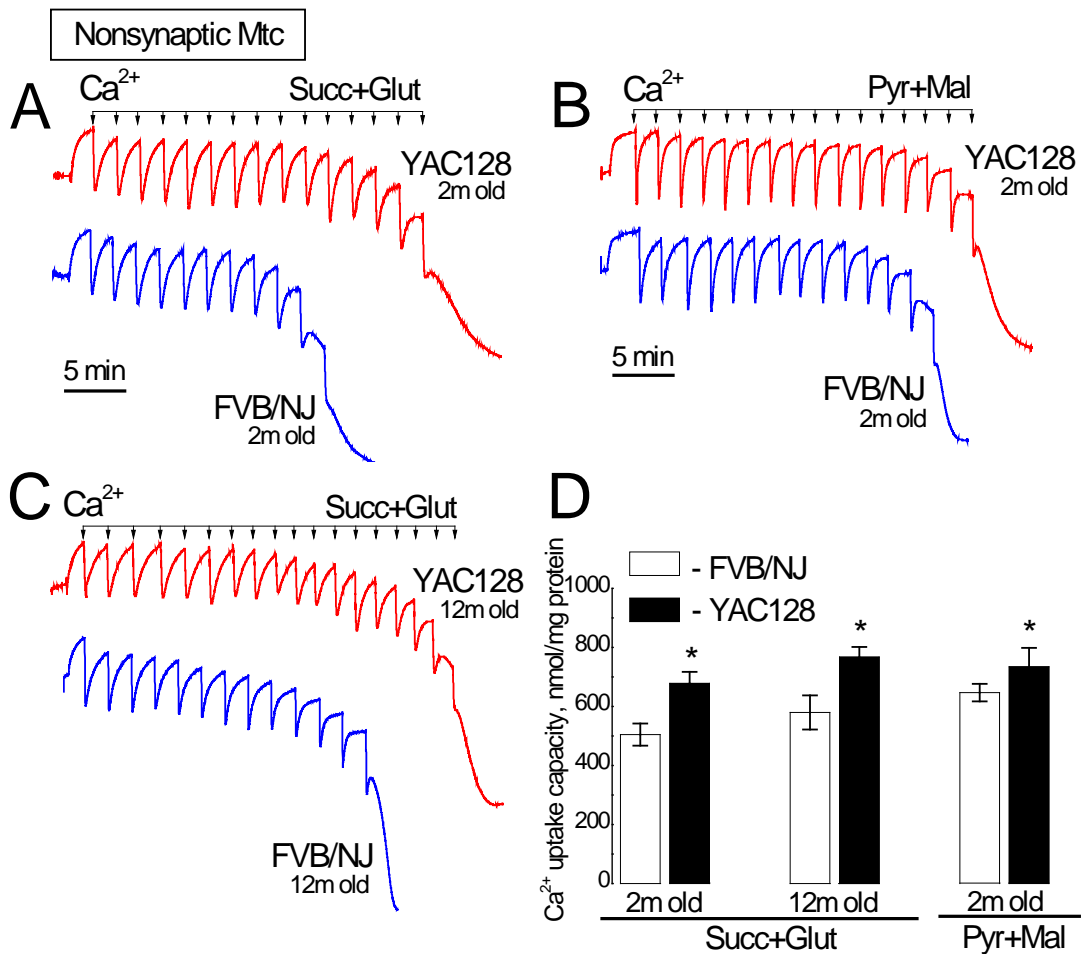


**Figure 24.  $Ca^{2+}$  uptake capacity of brain nonsynaptic mitochondria isolated from YAC128 and wild-type FVB/NJ mice.** Mitochondria were incubated at  $37^{\circ}C$  in the standard incubation medium supplemented either with 3 mM succinate plus 3 mM glutamate or with 3 mM pyruvate plus 1 mM malate as indicated in the Figure. In all  $Ca^{2+}$  uptake experiments, 100  $\mu M$  ADP and 1  $\mu M$  oligomycin were present in the incubation medium. When  $Ca^{2+}$  is added to the chamber, there is a downward deflection of the trace, indicating an increase in the external  $[Ca^{2+}]$ . The trace goes up as  $Ca^{2+}$  is removed from the external medium due to uptake by mitochondria. In **A** and **B**, mitochondria were isolated from 2-month-old mice. In **C**, mitochondria were isolated from 12-month-old mice. In **A–C**, where indicated 10  $\mu M$   $Ca^{2+}$  pulses were applied to mitochondria until mitochondria fail to uptake additional  $Ca^{2+}$ . In **D**, statistical analysis of  $Ca^{2+}$  uptake capacity of mitochondria from YAC128, and wild-type FVB/NJ mice. Data are mean  $\pm$  SEM, \* $p < 0.05$  compared with mitochondria from FVB/NJ, N = 9.

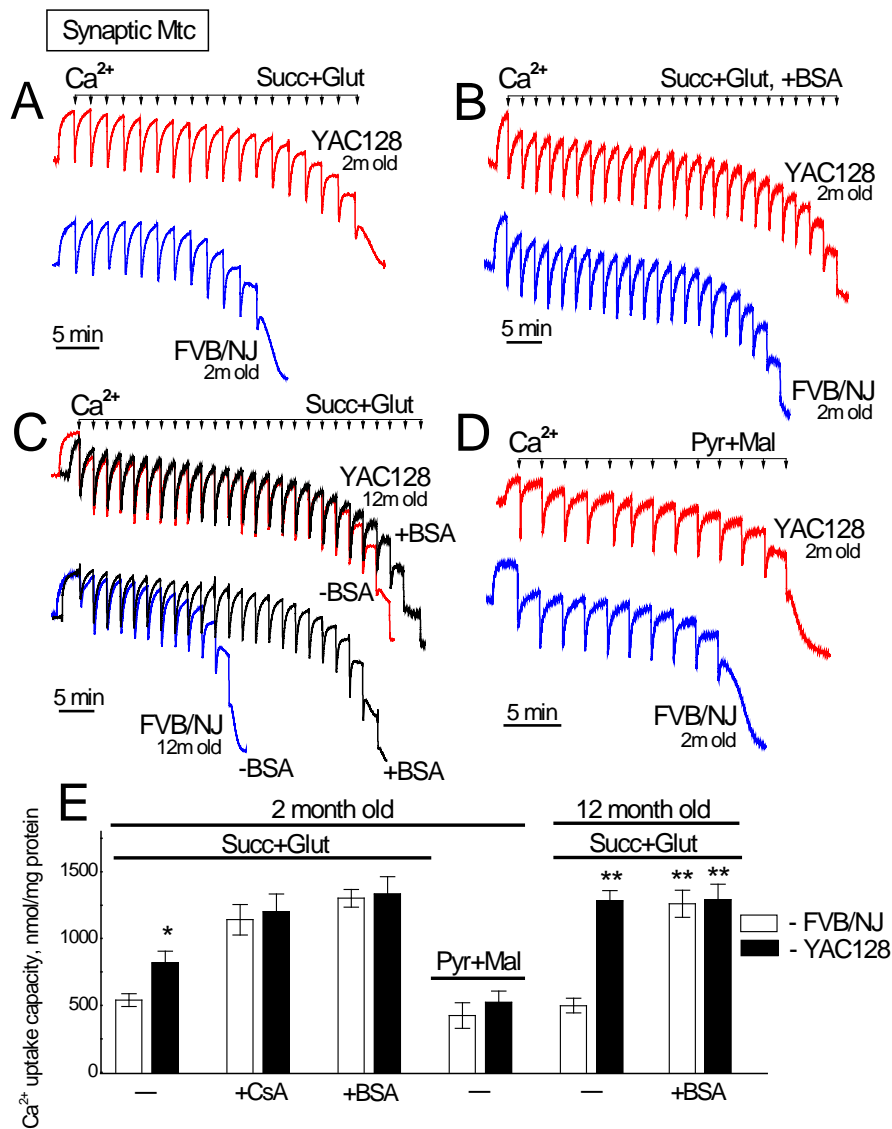


**Figure 25.  $\text{Ca}^{2+}$  uptake capacity of brain synaptic mitochondria isolated from YAC128 and wild-type FVB/NJ mice.** Mitochondria were incubated at  $37^\circ\text{C}$  in the standard incubation medium supplemented either with 3 mM succinate plus 3 mM glutamate or with 3 mM pyruvate plus 1 mM malate as indicated in the Figure. In all  $\text{Ca}^{2+}$  uptake experiments, 100  $\mu\text{M}$  ADP and 1  $\mu\text{M}$  oligomycin were present in the incubation medium. In **B**, incubation medium was additionally supplemented with 0.1% bovine serum albumin (BSA) (free from fatty acids). In **A**, **B**, and **D**, mitochondria were isolated from 2-month-old mice. In **C**, mitochondria were isolated from 12-month-old mice. In **A–D**, where indicated 10  $\mu\text{M}$   $\text{Ca}^{2+}$  pulses were applied to mitochondria until mitochondria fail to uptake additional  $\text{Ca}^{2+}$ . In **E**, statistical analysis of  $\text{Ca}^{2+}$  uptake capacity of mitochondria from YAC128 and wild-type FVB/NJ mice. Data are mean  $\pm$  SEM, \* $p < 0.05$  comparing with FVB/NJ mitochondria; \*\* $p < 0.01$  compared with mitochondria from 12-month-old FVB/NJ mice,  $N = 9$ .

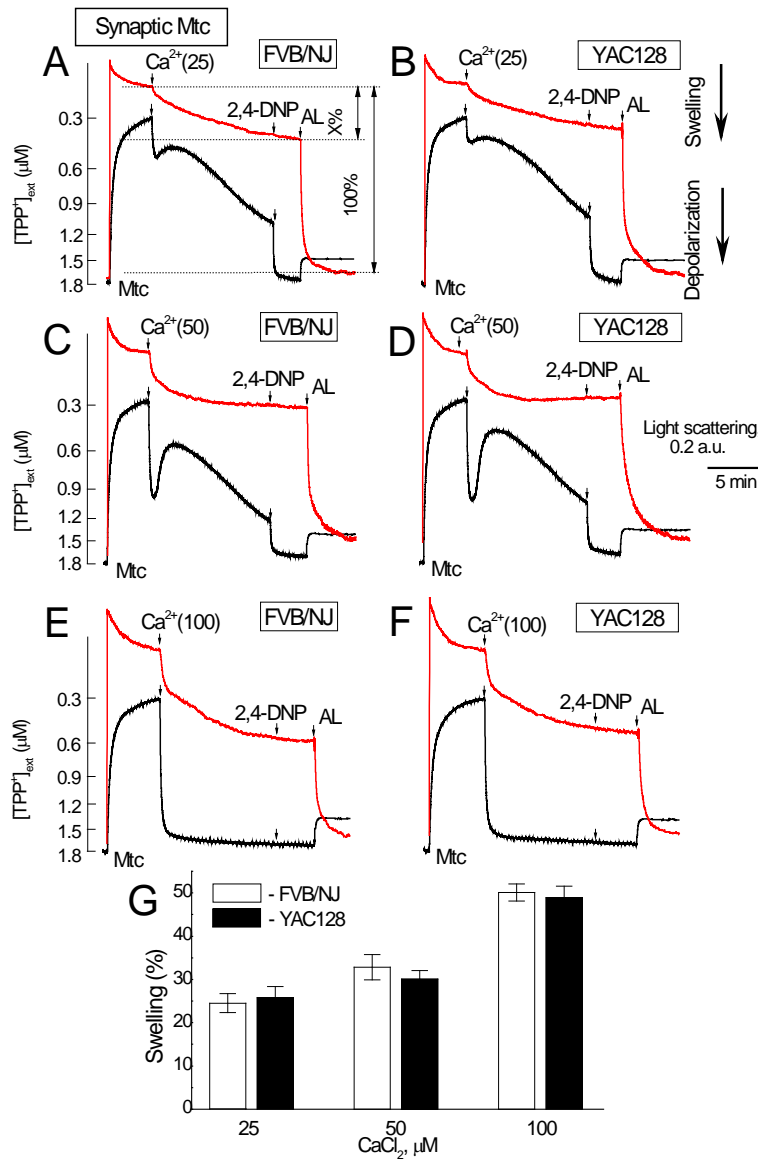


**Figure 26.  $Ca^{2+}$ -induced mitochondrial swelling and depolarization in synaptic mitochondria from WT (A, C, E) and YAC128 (B, D, F) mice.** Mitochondrial swelling was evaluated by following a decline in light scattering of mitochondrial suspension (red traces). A decrease in light scattering indicates mitochondrial swelling. Changes in mitochondrial membrane potential were evaluated by following distribution of tetraphenylphosphonium ( $TPP^+$ ) between incubation medium and mitochondrial matrix (black traces). The decrease in  $TPP^+$  concentration in the incubation medium ( $[TPP^+]_{ext}$ ) indicates  $TPP^+$  accumulation in mitochondria and high membrane potential. The release of  $TPP^+$  from mitochondria indicates a decrease in membrane potential. Mitochondrial swelling and membrane potential were evaluated simultaneously at  $37^\circ C$ . Where indicated 25, 50, or 100  $\mu M$   $Ca^{2+}$  was applied to mitochondria (Mtc). At the end of the experiments, 60  $\mu M$  2,4-dinitrophenol (2,4-DNP) was applied to completely depolarize mitochondria and, then, 30  $\mu g/ml$  alamethicin (AL) was added to induce maximal mitochondrial swelling, taken as 100%. The amount of  $Ca^{2+}$ -induced swelling was determined as percentage of maximal swelling (shown in A as X%). In G, percentage of  $Ca^{2+}$ -induced mitochondrial swelling. Data are mean  $\pm$  SEM, N=8.

## **B. Respiration and Ca<sup>2+</sup> uptake capacity in striatal nonsynaptic and synaptic mitochondria isolated from YAC128 mice.**

Earlier findings suggested abnormalities in mitochondrial respiration and defects in Ca<sup>2+</sup> handling in mitochondria from HD mouse and cell models (Tabrizi *et al.* 2000; Panov *et al.* 2002; Choo *et al.* 2004; Lim *et al.* 2008; Aidt *et al.* 2013; Damiano *et al.* 2013). However, in the previous section, we tested the possible deleterious effects of mHtt on mitochondrial oxidative metabolism and Ca<sup>2+</sup> handling using isolated nonsynaptic and synaptic mitochondria from the **whole brain** of YAC128 mice. However, no evidence was found for mitochondrial dysfunction using mitochondria isolated from the whole brain of YAC128 mice. In HD, different brain regions have different susceptibility to degeneration with striatum being most vulnerable (Vonsattel and DiFiglia 1998). Consequently, it is conceivable that isolation of mitochondria from the whole brain could be a reason for our failure to detect mitochondrial dysfunction in HD mice. In the present section, the respiratory activity and Ca<sup>2+</sup> handling in mitochondria isolated exclusively from the striatal tissues of YAC128 mice were assessed.

### **a. Clasping phenotype of early symptomatic YAC128 mice.**

In this section, the YAC128 mice used ranged in age from 8 to 10 weeks and already showed signs of motor dysfunction manifested as clasping of the fore- and hind-limbs when suspended by the tail (see Fig. 5A and B). Since the mice exhibited this phenotype, it suggests that if altered mitochondrial respiration or Ca<sup>2+</sup> handling contributed to such behavioral aberrations, we should be able to detect such defects in brain mitochondria isolated from these mice. For all experiments, age-matched genetic background FVB/NJ mice were used as control. Before all experiments, every mouse was genotyped by PCR on tail DNA to confirm the presence or absence of the transgene as described in the first section (see Fig. 5C).

**b. Expression of mHtt in striatal mitochondria and purity of mitochondrial preparations.**

Nonsynaptic mitochondria were derived from neuronal somata and glial cells whereas synaptic mitochondria were isolated from neuronal synaptic terminals and, therefore, were of exclusively neuronal origin. Fig. 27A and B shows the absence of MEK1/2, a cytosolic marker, and calnexin, an endoplasmic reticulum (ER) marker, in mitochondrial fractions, suggesting the absence of cytosolic and ER contaminations. On the other hand, mitochondrial fractions contained augmented levels of Complex II, 70 kDa subunit (CII, 70) indicating mitochondrial enrichment in these fractions. Mitochondria from YAC128, but not FVB/NJ mice, contained mHtt detected with mouse monoclonal mHtt-specific antibody 1C2 (1:1000, mAb 1574, Millipore, Temecula, CA) that recognizes the polyglutamine stretch of the protein (Fig. 27C). This is consistent with our previous data (Fig. 6) and with results from others (Choo *et al.* 2004). Huntingtin protein and its mutated form, mHtt, reside in the cytosol (Bates *et al.* 2015) and, therefore, the presence of mHtt in the mitochondrial fraction could be due to cytosolic contamination. However, because mitochondrial fractions did not contain detectable amounts of cytosolic contamination, mHtt present in mitochondrial fractions (Fig. 27C) was unlikely to be the result of cytosolic contamination (Fig. 27A and B). Thus, in our study we used striatal nonsynaptic and synaptic mitochondria which were essentially free from cytosolic and ER contaminations and contained mHtt attached to mitochondria.

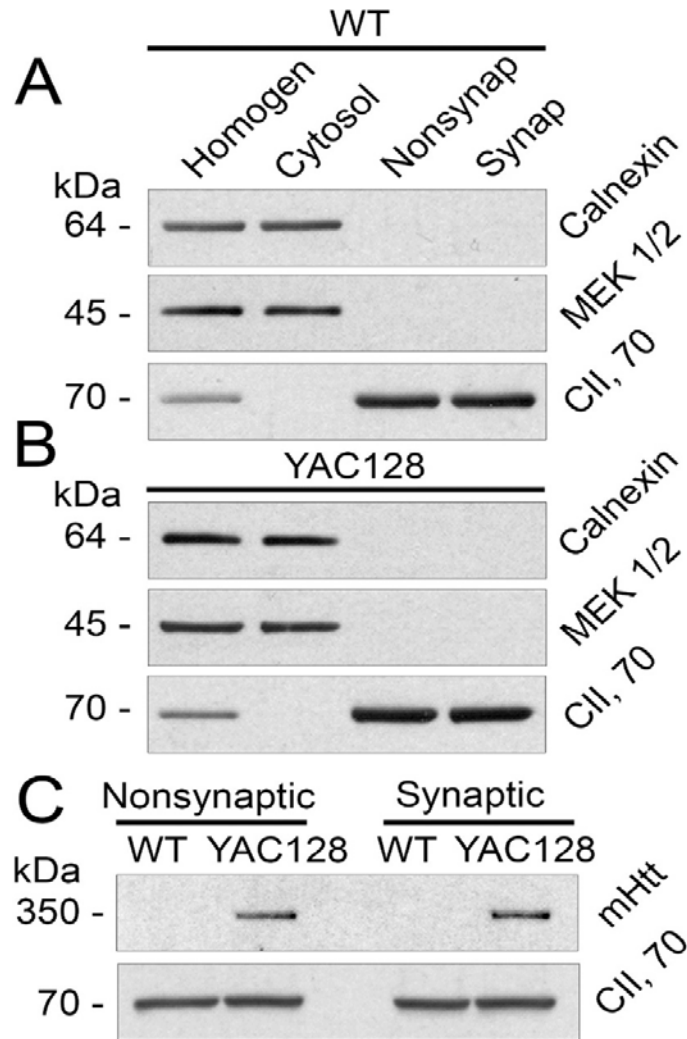


**Figure 27. Purity of striatal nonsynaptic (Nonsynap) and synaptic (Synap) mitochondria isolated from FVB/NJ (A) and YAC128 (B) mice and detection of mHtt in mitochondrial fractions (C).** In **A** and **B**, purity of striatal mitochondrial fraction was assessed by western blotting. Homogenates (Homogen), cytosolic, and mitochondrial fractions were analyzed using antibodies against calnexin (ER marker), MEK1/2 (cytosolic marker), and the 70 kDa subunit of Complex II (mitochondrial marker). In **C**, mHtt was detected as a single band exclusively in samples from YAC128 mice using the mouse monoclonal anti-polyQ antibody 1C2. The 70 kDa subunit of Complex II was used as a mitochondrial marker and a loading control.

### **c. Respiration of nonsynaptic and synaptic striatal mitochondria from YAC128 mice.**

In our experiments, we used striatal nonsynaptic mitochondria fueled with 3 mM pyruvate and 1 mM malate, a combination of Complex I-linked substrates. Mitochondrial respiratory rates were measured under various conditions: basal mitochondrial respiration in the presence of only substrates ( $V_2$ ), ADP-stimulated respiration ( $V_3$ , 300  $\mu$ M ADP), respiration following ADP depletion ( $V_4$ ), and maximal, 2,4-dinitrophenol (2,4-DNP)-stimulated respiration ( $V_{DNP}$ , 60  $\mu$ M 2,4-DNP). Earlier, it was reported that the functional difference between mitochondria from HD and wild-type animals could be reliably detected only in the absence of BSA (Panov *et al.* 2003). In the aforementioned study, BSA eliminated the difference and it was proposed that BSA displaces mHtt from the mitochondrial outer membrane. Consequently, BSA was omitted from all isolation and incubation solutions in our experiments shown in Fig. 28. In these experiments, striatal mitochondria isolated from YAC128 and FVB/NJ mice had similar respiratory rates under every experimental condition.

Previously, it was shown that inhibition of Complex II with 3-nitropropionic acid recapitulated HD pathology in animals (Brouillet *et al.* 1999) and it was demonstrated that activity of Complex II is decreased in striatum of HD patients and in HD mouse striatal neurons (Benchoua *et al.* 2006). Correspondingly, in our experiments, we used 3 mM succinate as a mitochondrial substrate in combination with 3 mM glutamate to remove oxaloacetate via transamination reaction and thus prevent oxaloacetate-mediated inhibition of Complex II (Wojtczak 1969; Brustovetsky and Dubinsky 2000a). In addition, the incubation medium was supplemented with 0.1% BSA (free from fatty acids) to preserve mitochondrial integrity and improve mitochondrial functionality (Lai and Clark 1989). In our previous study, we found that incubation of isolated mitochondria with 0.1% BSA failed to displace mHtt from the organelles (Pellman *et al.* 2015) and,



therefore, we expected to detect mHtt effects on mitochondria despite the presence of BSA. In these experiments, we used nonsynaptic and synaptic mitochondria isolated from striata of YAC128 and FVB/NJ mice. Similar to our previously described experiments (Fig. 28), we did not find any difference in respiratory activity between mitochondria from YAC128 and wild-type FVB/NJ mice (Fig. 29).

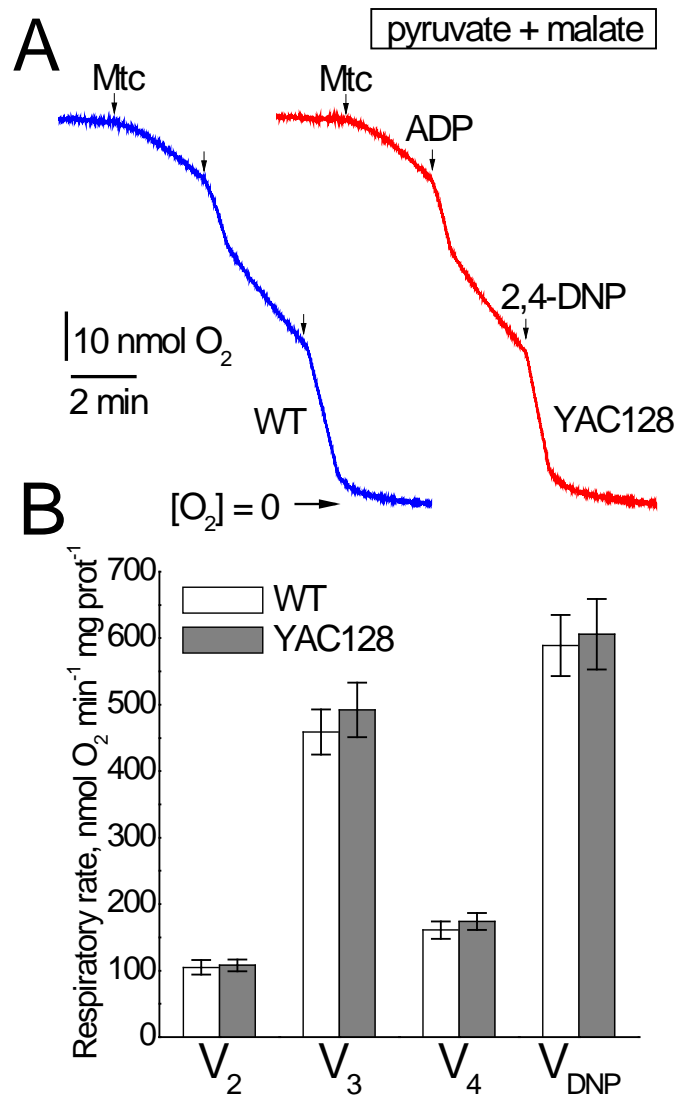


**Figure 28. Respiratory activity of striatal nonsynaptic mitochondria isolated from 2-month-old FVB/NJ (blue trace) and YAC128 (red trace) mice.** In **A**, representative traces of oxygen consumption by striatal nonsynaptic mitochondria. Where indicated, mitochondria (30  $\mu$ g protein), 300  $\mu$ M ADP, or 60  $\mu$ M 2,4-dinitrophenol (2,4-DNP) were added. The incubation medium was supplemented with the Complex I substrates pyruvate (3 mM) plus malate (1 mM). In **B**, the pooled group results demonstrating respiratory rates of striatal nonsynaptic mitochondria. Data are mean  $\pm$  SEM, N = 5.

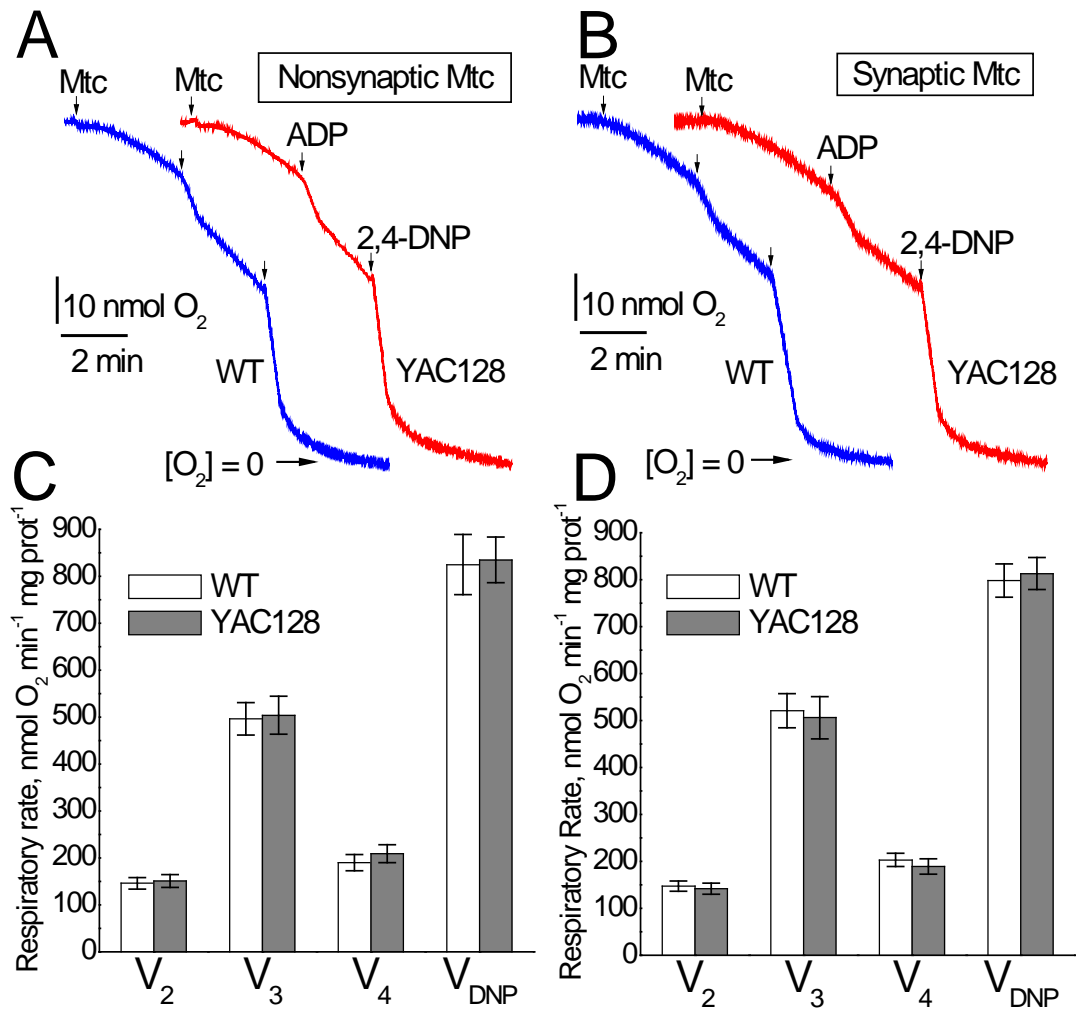


**Figure 29. Respiratory activity of striatal nonsynaptic and synaptic mitochondria isolated from 2-month-old FVB/NJ (blue traces) and YAC128 (red traces) mice.** Representative traces of oxygen consumption by either striatal nonsynaptic (A) or striatal synaptic (B) mitochondria. Where indicated, mitochondria (30  $\mu$ g protein), 200  $\mu$ M ADP, or 60  $\mu$ M 2,4-dinitrophenol (2,4-DNP) were added. The incubation medium was supplemented with the Complex II substrate succinate (3 mM) plus glutamate (3 mM). Additionally, incubation medium was supplemented with 0.1% BSA (free from fatty acids) to maintain mitochondrial integrity (Lai and Clark 1989). The pooled group results demonstrating respiratory rates are shown for striatal nonsynaptic (C) and striatal synaptic (D) mitochondria. Data are mean  $\pm$  SEM, N = 5 (nonsynaptic), N = 4 (synaptic).

**d. Expression of nuclear-encoded proteins in mitochondria from YAC128 and WT mice.**

Recently, inhibition of protein import machinery in mitochondria from HD mice was reported and suggested to be a possible cause of bioenergetic deficit in HD (Yano *et al.* 2014). The decrease in the levels of nuclear-encoded mitochondrial proteins seems to be a logical consequence of inhibition of mitochondrial import into mitochondria. However, this was not tested in the recent study (Yano *et al.* 2014). In the previous section with mitochondria isolated from the whole brain of YAC128 and wild-type FVB/NJ mice no difference was found in expression of nuclear-encoded proteins in mitochondria isolated from the whole brains. In the present section, the levels of protein expression in striatal nonsynaptic and synaptic mitochondria from YAC128 and FVB/NJ mice were evaluated using immunoblotting followed by densitometry (Fig. 30). In these experiments, we did not find a difference in expression of randomly chosen nuclear-encoded proteins located in the inner membrane or matrix of mitochondria from YAC128 and FVB/NJ mice. We also did not find a difference in expression of VDAC1, a protein of the mitochondrial outer membrane.

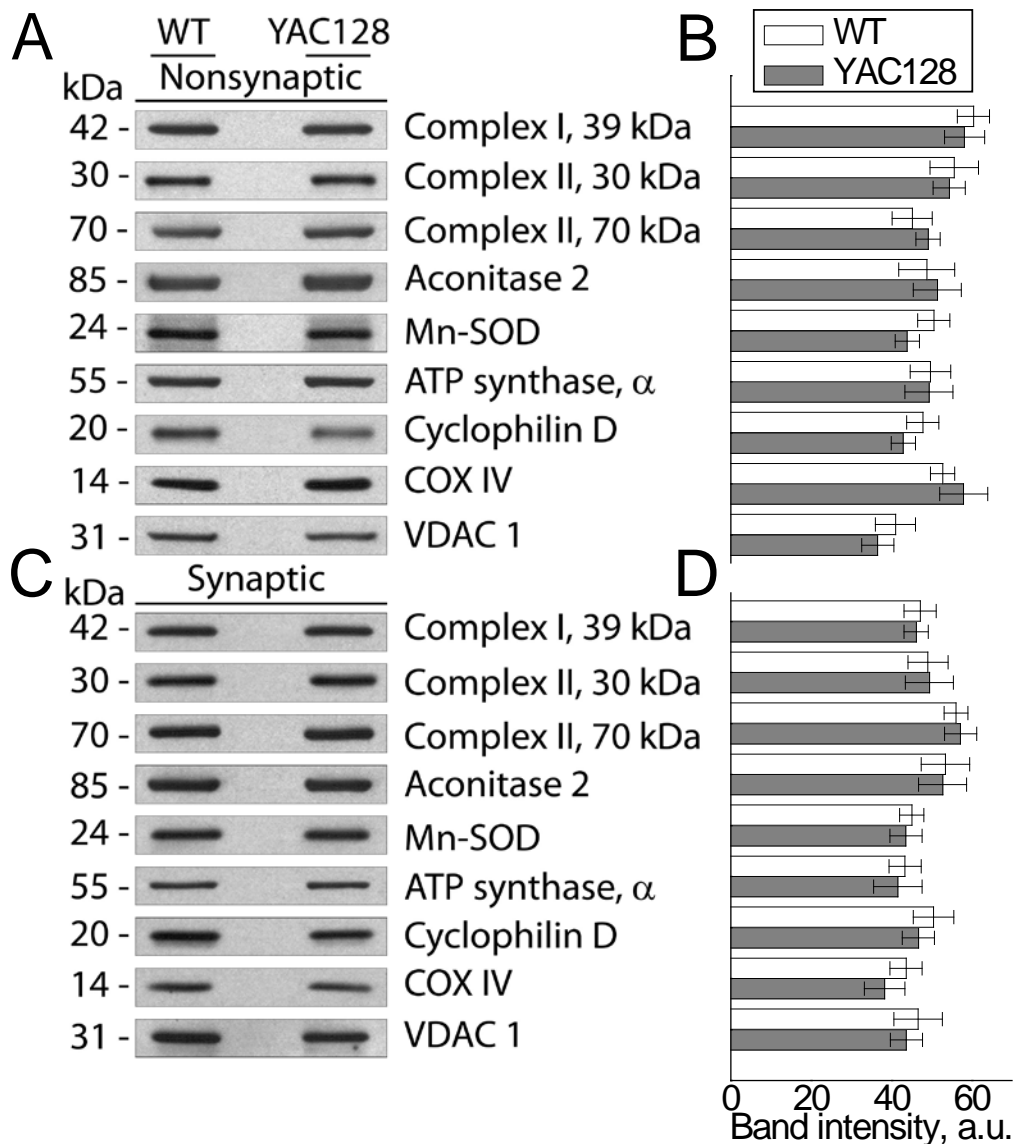


**Figure 30. Expression of nuclear encoded mitochondrial proteins in nonsynaptic and synaptic striatal mitochondria derived from FVB/NJ and YAC128 mice.** In **A** and **C**, are representative western blots of nonsynaptic and synaptic striatal mitochondria isolated from FVB/NJ and YAC128 mice probed with various antibodies against nuclear-encoded mitochondrial proteins including 39 kDa subunit of Complex I, 30 and 70 kDa subunits of Complex II, Aconitase 2, Mn-dependent superoxide dismutase (Mn-SOD), a subunit of ATP synthase, cyclophilin D (CyD), and cytochrome oxidase subunit IV (COX IV). Voltage-dependent anion channel isoform 1 (VDAC1) was used as a loading control. In **B** and **D**, the results of densitometry performed with NIH ImageJ 1.48v software. Data are mean  $\pm$  SEM, N = 6.

**e. Ca<sup>2+</sup> uptake capacity of striatal nonsynaptic and synaptic mitochondria from YAC128 and WT mice.**

Earlier, it was reported that mitochondria from HD mouse and cell models have decreased Ca<sup>2+</sup> uptake capacity compared with mitochondria from wild-type animals and cells (Panov *et al.* 2002;Milakovic *et al.* 2006;Gellerich *et al.* 2008;Lim *et al.* 2008). However, in the previous section, we assessed Ca<sup>2+</sup> uptake capacity in mitochondria isolated from the whole brains of YAC128 and did not find a difference compared to mitochondria from age-matched WT animals. In the present section, Ca<sup>2+</sup> uptake capacity in striatal mitochondria from YAC128 and their genetic background FVB/NJ mice was evaluated. Nonsynaptic mitochondria incubated without BSA and fueled with a combination of 3 mM pyruvate and 1 mM malate or with a combination of 3 mM succinate and 3 mM glutamate (Fig. 31A and B) were used. In both cases, Ca<sup>2+</sup> uptake capacities of mitochondria from YAC128 and FVB/NJ mice were similar. In the latter case, supplementing incubation medium with BSA significantly increased Ca<sup>2+</sup> uptake capacity of mitochondria from both YAC128 and FVB/NJ mice without revealing any difference between mitochondria from these animals (Fig. 31C). Fig. 31D shows statistical analysis of these experiments.

Next, we tested striatal synaptic mitochondria from YAC128 and FVB/NJ mice (Fig. 32). Mitochondria were fueled with a combination of 3 mM succinate and 3 mM glutamate and incubated without BSA. We did not find a difference in Ca<sup>2+</sup> uptake capacity in striatal synaptic mitochondria from YAC128 and FVB/NJ mice (Fig. 32A). Addition of BSA to the incubation medium significantly increased Ca<sup>2+</sup> uptake capacity in mitochondria from both YAC128 and FVB/NJ mice (Fig. 32B). Interestingly, under these conditions striatal synaptic mitochondria from YAC128 mice accumulated even more Ca<sup>2+</sup> than mitochondria from WT animals. Fig. 32C shows statistical analysis of these experiments. Taken together, evaluation of mitochondrial Ca<sup>2+</sup> uptake capacity did not

provide evidence for defects in  $\text{Ca}^{2+}$  handling by striatal mitochondria from YAC128 mice.

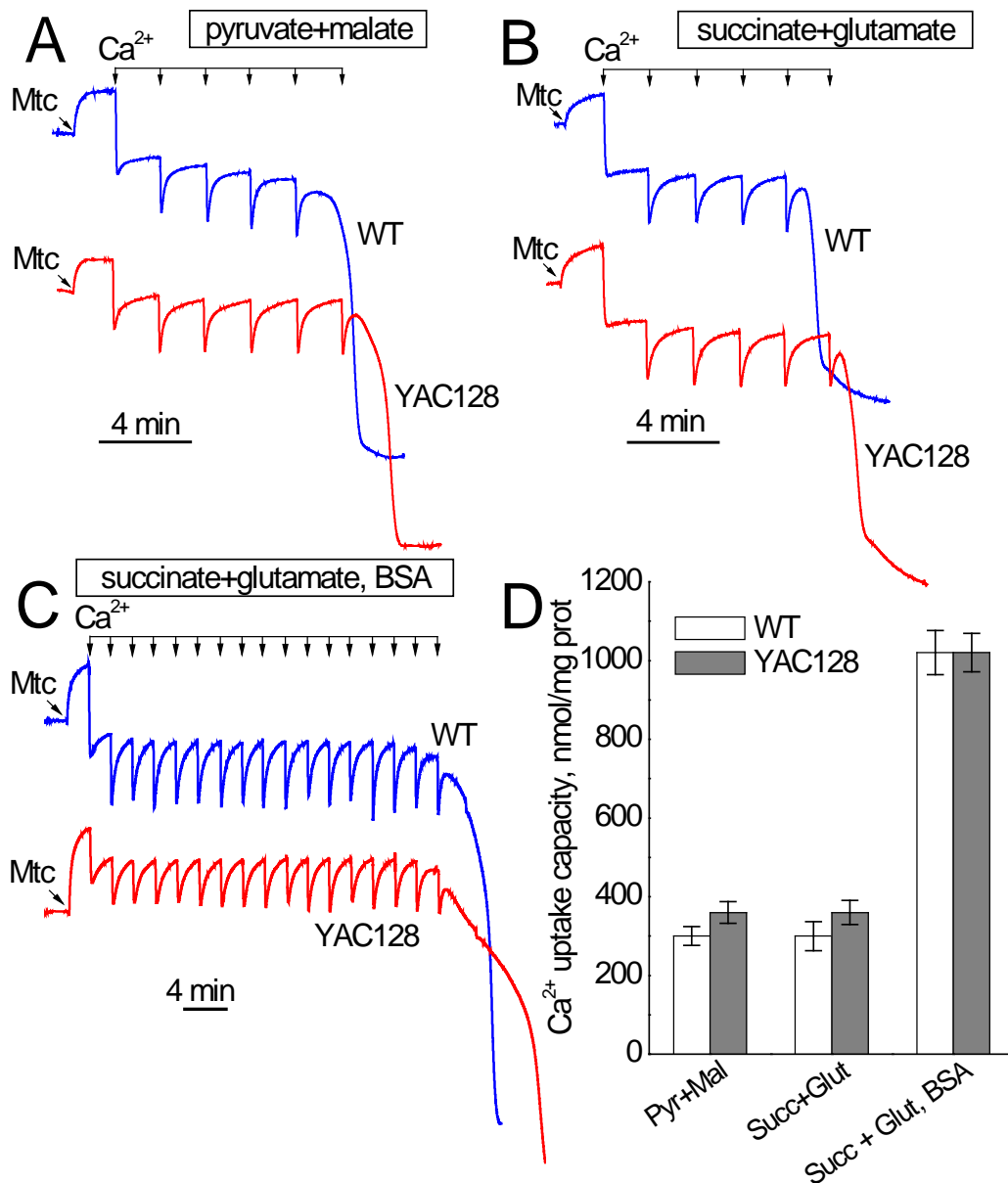


**Figure 31. Ca<sup>2+</sup> uptake capacity of brain nonsynaptic mitochondria isolated from the striatum of FVB/NJ (blue traces) and YAC128 (red traces) mice.** Mitochondrial Ca<sup>2+</sup> uptake capacity was measured in the standard incubation medium supplemented with the Complex I substrates pyruvate (3 mM) and malate (1 mM) (**A**), or the Complex II substrate succinate plus glutamate (both in 3 mM) (**B**). In **C**, in addition to succinate plus glutamate, the incubation medium was supplemented with 0.1% BSA (free from fatty acids). In all experiments, the incubation medium was also supplemented with 100  $\mu$ M ADP and 1  $\mu$ M oligomycin (Chalmers and Nicholls 2003). Where indicated, 10  $\mu$ M Ca<sup>2+</sup> pulses (delivered as CaCl<sub>2</sub>) were applied to mitochondria until mitochondria were unable to accumulate additional Ca<sup>2+</sup> and released previously accumulated Ca<sup>2+</sup>. In **D**, the pooled group results demonstrating Ca<sup>2+</sup> uptake capacity of striatal nonsynaptic mitochondria from FVB/NJ and YAC128 mice. Data are mean  $\pm$  SEM, N = 4.



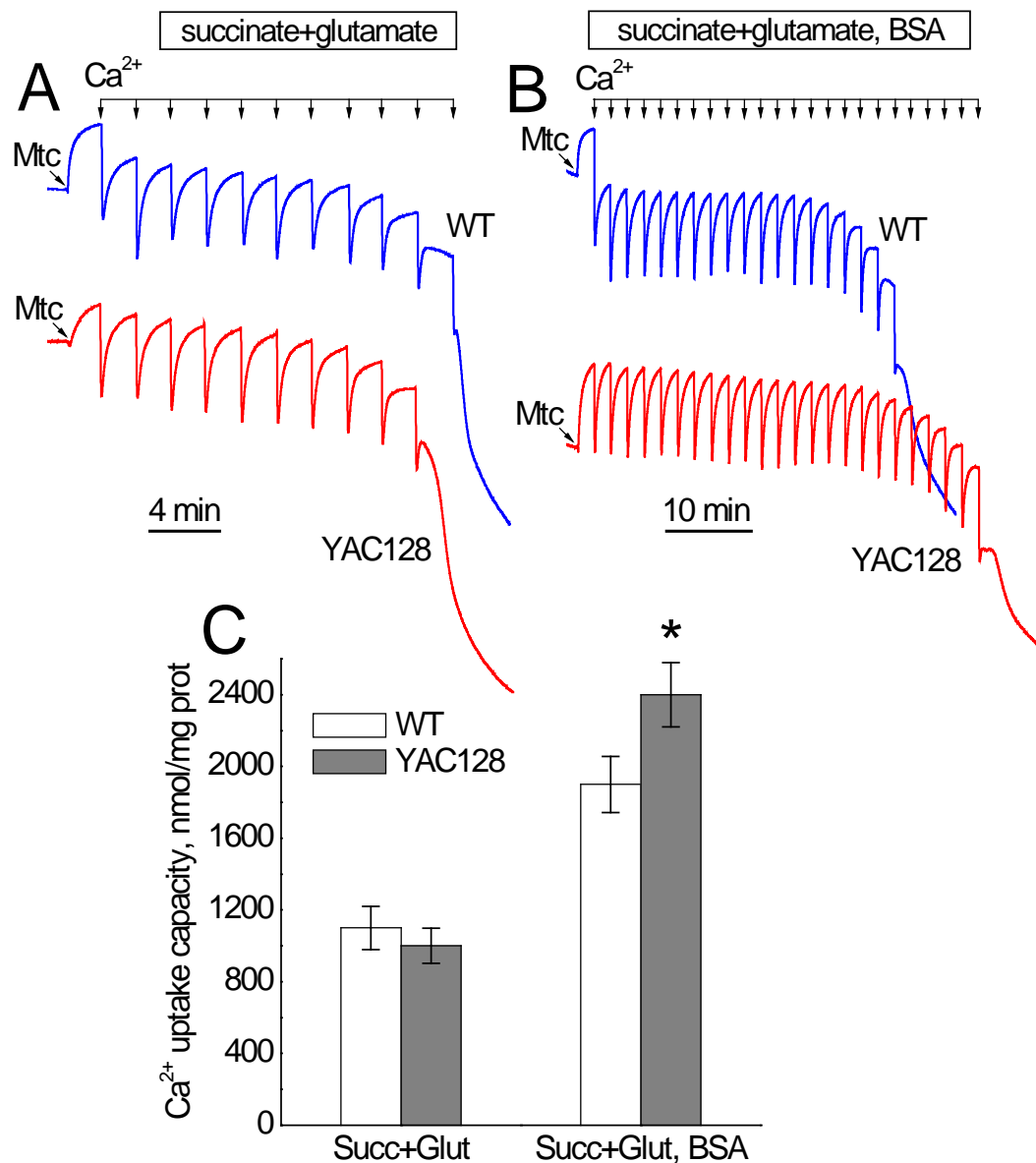


**Figure 32. Ca<sup>2+</sup> uptake capacity of brain synaptic mitochondria isolated from the striatum of FVB/NJ (blue traces) and YAC128 (red traces) mice.** Mitochondrial Ca<sup>2+</sup> uptake capacity was measured in the standard incubation medium supplemented with the Complex II substrate succinate (3 mM) plus glutamate (3 mM) in the absence (A) or presence of 0.1% BSA (B). In all experiments, the incubation medium was also supplemented with 100  $\mu$ M ADP and 1  $\mu$ M oligomycin (Chalmers and Nicholls 2003). Where indicated, 10  $\mu$ M Ca<sup>2+</sup> pulses (delivered as CaCl<sub>2</sub>) were applied to mitochondria until mitochondria were unable to accumulate additional Ca<sup>2+</sup> and released previously accumulated Ca<sup>2+</sup>. In C, the pooled group results showing Ca<sup>2+</sup> uptake capacity of striatal synaptic mitochondria from FVB/NJ and YAC128 mice. Data are mean  $\pm$  SEM, \* $p$  < 0.05 comparing mitochondria from YAC128 and FVB/NJ mice in the presence of 0.1% BSA, N = 5.

### **C. Oxidative metabolism and Ca<sup>2+</sup> handling in the R6/2 mouse model of HD.**

In the previous sections, the effect of human full-length mHtt on respiratory activity and Ca<sup>2+</sup> uptake capacity in brain synaptic and nonsynaptic mitochondria as well as striatal and cortical neurons from transgenic YAC128 mice was investigated. Despite significant effort, no evidence was found for mHtt-induced alterations in respiration and Ca<sup>2+</sup> uptake capacity of mitochondria from wild-type (WT) and YAC128 mice. Whether HD pathogenesis is mediated by full-length mHtt or fragments of mHtt remains not completely understood. Previous studies suggested that mHtt fragments might be more toxic than full-length mHtt (Kim *et al.* 1999; Li *et al.* 2000) and it was shown that reduction in mHtt fragment generation improved the phenotype of HD mice (Wellington *et al.* 2000; Tian *et al.* 2014; Wong *et al.* 2015). Here, **we hypothesized that fragments of human mHtt, contrary to full-length human mHtt, are more deleterious and exert a detrimental effect on mitochondrial respiration and Ca<sup>2+</sup> handling.** Consequently, in the present section, the effect of mHtt fragments on mitochondrial respiratory activity and Ca<sup>2+</sup> handling in synaptic and nonsynaptic brain mitochondria and striatal neurons from the R6/2 mouse model of HD was assessed. In our experiments, we used the R6/2 mouse model of HD because it expresses an exon 1 fragment of human mHtt (Mangiarini *et al.* 1996). These mice exhibit a behavioral phenotype that manifests by 6 weeks of age as limb claspings when suspended by the tail (Mangiarini *et al.* 1996; Stack *et al.* 2005). The presence of this phenotype is consistent with previous reports describing this and other mouse models of HD (Mangiarini *et al.* 1996; Reddy *et al.* 1999).

**a. Clasping phenotype of R6/2 mice and respiration of nonsynaptic and synaptic mitochondria derived from R6/2 and WT mice.**

To assess the effect of mHtt fragments on mitochondrial respiration, we used Percoll gradient-purified brain nonsynaptic (neuronal plus glial) and synaptic (pure neuronal) mitochondria isolated from 6- to 8-week-old R6/2 and background B6CBA (WT) mice. Each R6/2 mouse demonstrated clasping behavior and each animal was genotyped to confirm the presence of the mutation in the *Htt* gene (Fig. 33). Overall, out of 267 6- to 8-week-old R6/2 mice of both sexes (144 males and 123 females) tested for clasping behavior, clasping behavior was detected in 191 animals (106 males and 85 females). WT mice did not display clasping behavior. Previously, it was hypothesized that bovine serum albumin (BSA) may displace mHtt from the outer mitochondrial membrane and hence preclude it from exerting deleterious effects on mitochondrial functions (Panov *et al.* 2003). Therefore, although BSA is commonly used during mitochondrial isolation and purification to maintain integrity of brain mitochondria (Lai and Clark 1989), we omitted BSA from all of our experiments involving isolated mitochondria unless stated otherwise. We assessed mitochondrial respiratory activity in both nonsynaptic (Fig. 34) and synaptic (Fig. 35) mitochondria using either a combination of the Complex I substrates pyruvate (3 mM) and malate (1 mM) or the Complex II substrate succinate (3 mM). In experiments with succinate, the incubation medium was supplemented with glutamate (3 mM) to remove oxaloacetate by transaminase reaction and prevent oxaloacetate-mediated inhibition of succinate dehydrogenase (Wojtczak 1969; Brustovetsky and Dubinsky 2000a). For all experiments, basal respiration of mitochondria was measured in the presence of substrates only ( $V_2$ ), followed by ADP-stimulated respiration ( $V_3$ ), controlled respiration after ADP-depletion ( $V_4$ ), and, finally, maximal, uncoupled respiration stimulated by 2,4-dinitrophenol ( $V_{DNP}$ ). In these experiments, we found that under all tested conditions nonsynaptic and synaptic

mitochondria from R6/2 animals had similar respiratory rates compared with mitochondria from WT animals (Figs. 34 and 35).

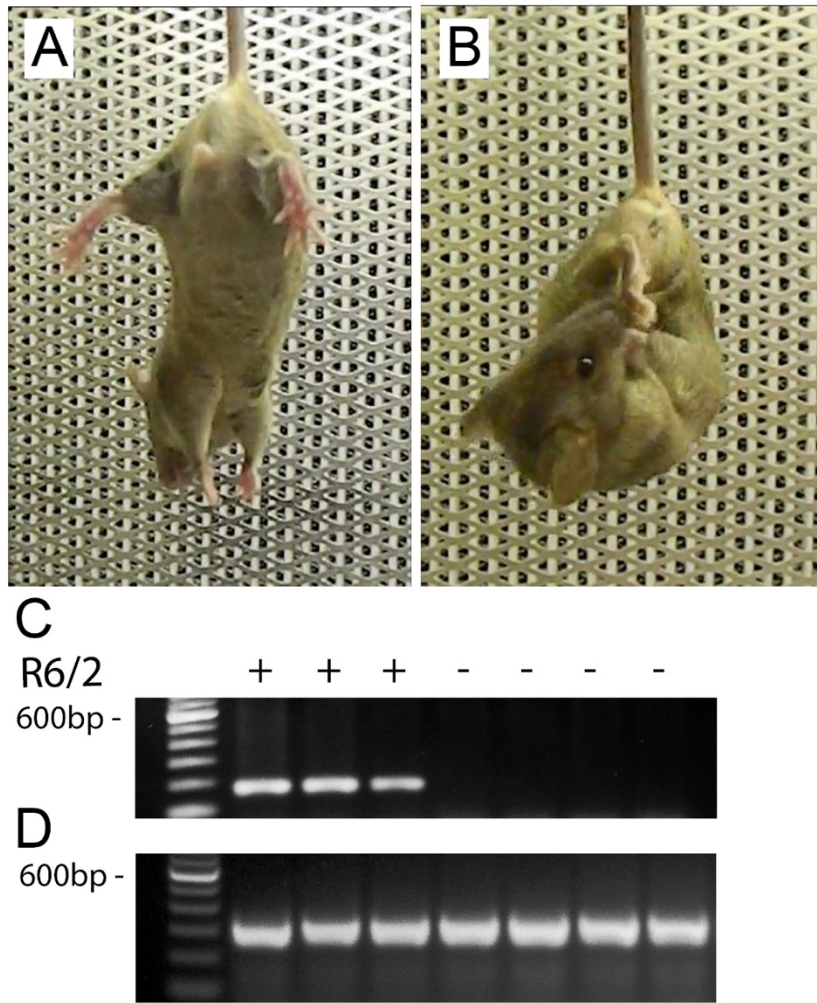


**Figure 33. Comparison of motor phenotype of 6-week-old R6/2 and WT mice and representative genotyping.** In **A**, typical posture of a WT mouse following suspension by the tail with fore- and hind-limbs extended away from the body (**B**) the usual feet-clasping posture adopted by an R6/2 mouse within 10 s of suspension by the tail. In **C**, representative genotyping data of tail tissue from WT and R6/2 mice. In **D**, internal positive control.

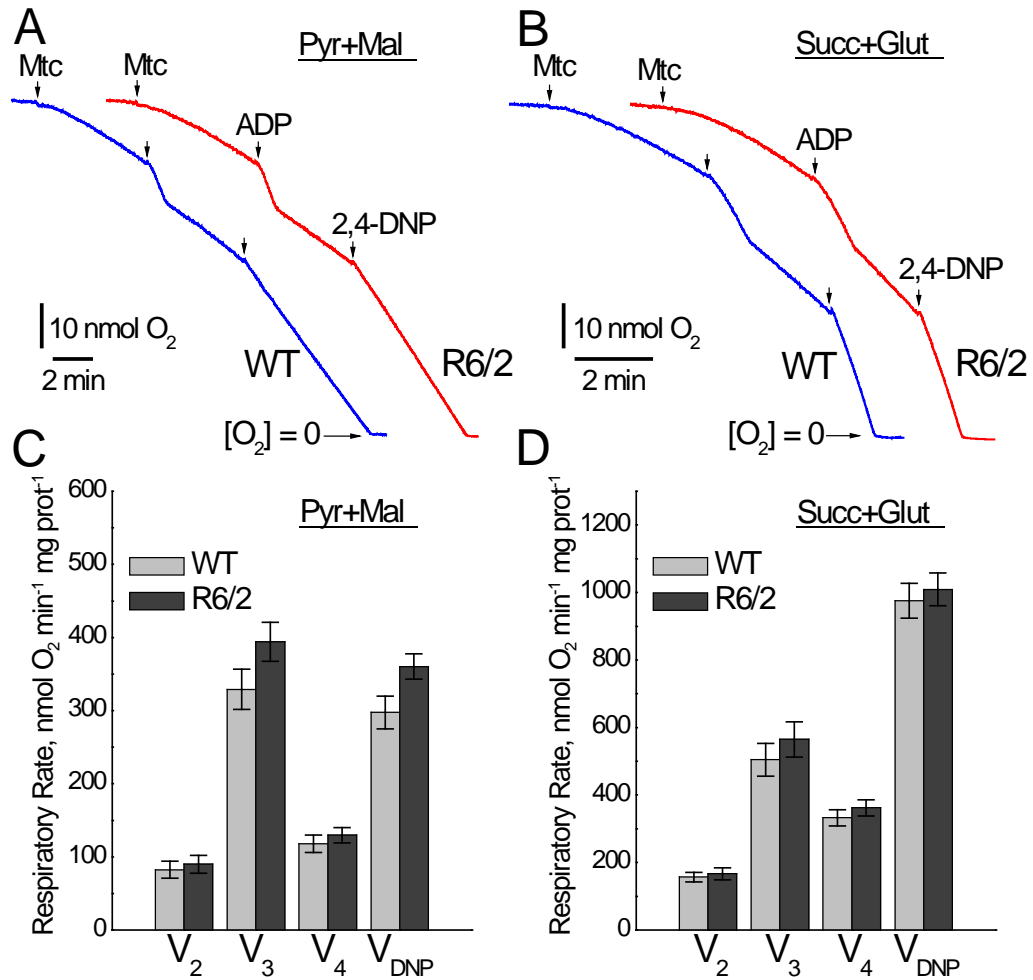


**Figure 34. Respiratory activity of brain nonsynaptic mitochondria isolated from 6- to 8-week-old WT (blue traces) and R6/2 (red traces) mice.** In **A** and **B**, representative traces of mitochondrial O<sub>2</sub> consumption for mitochondria at 37 °C in incubation medium supplemented with pyruvate (3 mM) plus malate (1 mM) or succinate (3 mM) plus glutamate (3 mM), respectively. Arrows indicate the addition of either nonsynaptic mitochondria (Mtc), 200 μM ADP, or 60 μM 2,4-DNP. In **C** and **D**, statistical analyses of respiratory rates. Data are presented as mean ± SEM from 5 separate experiments. Here and in all other experiments with isolated mitochondria, three WT and three transgenic R6/2 mice were used in each experiment.

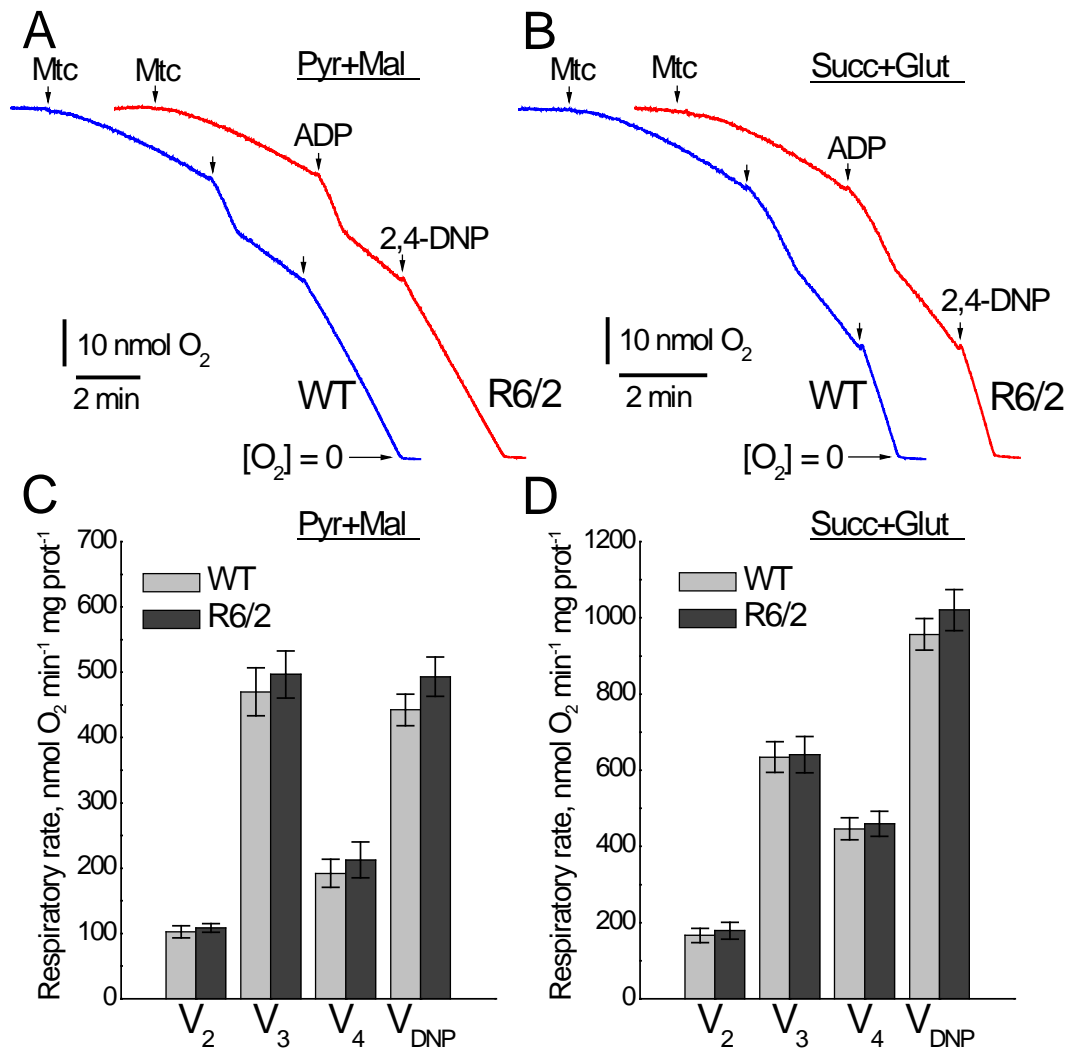


**Figure 35. Respiratory activity of brain synaptic mitochondria isolated from 6- to 8-week-old WT (blue traces) and R6/2 (red traces) mice.** In **A** and **B**, representative traces of mitochondrial O<sub>2</sub> consumption for mitochondria at 37 °C in incubation medium supplemented with pyruvate (3 mM) plus malate (1 mM) or succinate (3 mM) plus glutamate (3 mM), respectively. Arrows indicate the addition of either synaptic mitochondria (Mtc), 200 μM ADP, or 60 μM 2,4-DNP. In **C** and **D**, statistical analyses of respiratory rates. Data are presented as mean ± SEM from five separate experiments.

#### **b. Expression of nuclear-encoded proteins in mitochondria from R6/2 mice.**

In line with our data, Yano *et al.* (Yano *et al.* 2014) did not find a difference in respiratory activity of synaptic and nonsynaptic mitochondria from R6/2 mice compared with mitochondria from WT animals. On the other hand, the authors found evidence for mHtt-induced inhibition of protein import into mitochondria, and proposed that such an inhibition might alter mitochondrial functions at later stages of HD (Yano *et al.* 2014). We analyzed expression of several nuclear-encoded mitochondrial proteins, including a 39 kDa subunit of Complex I, 30 and 70 kDa subunits of Complex II, aconitase 2, Mn-dependent superoxide dismutase (MnSOD), cyclophilin D (CyD) and  $\alpha$ -subunit of ATP synthase in brain nonsynaptic and synaptic mitochondria isolated from 8-week-old R6/2 and WT mice. VDAC1, (voltage-dependent anion channel 1 or mitochondrial porin), a protein in the outer mitochondrial membrane, was used as a loading control. In these experiments, we did not find any evidence for decreased expression of the analyzed proteins in mitochondria from R6/2 compared with mitochondria from WT mice (Fig. 36). These findings argue against mHtt-induced inhibition of mitochondrial protein import and its potential role in inhibition of mitochondrial respiration.



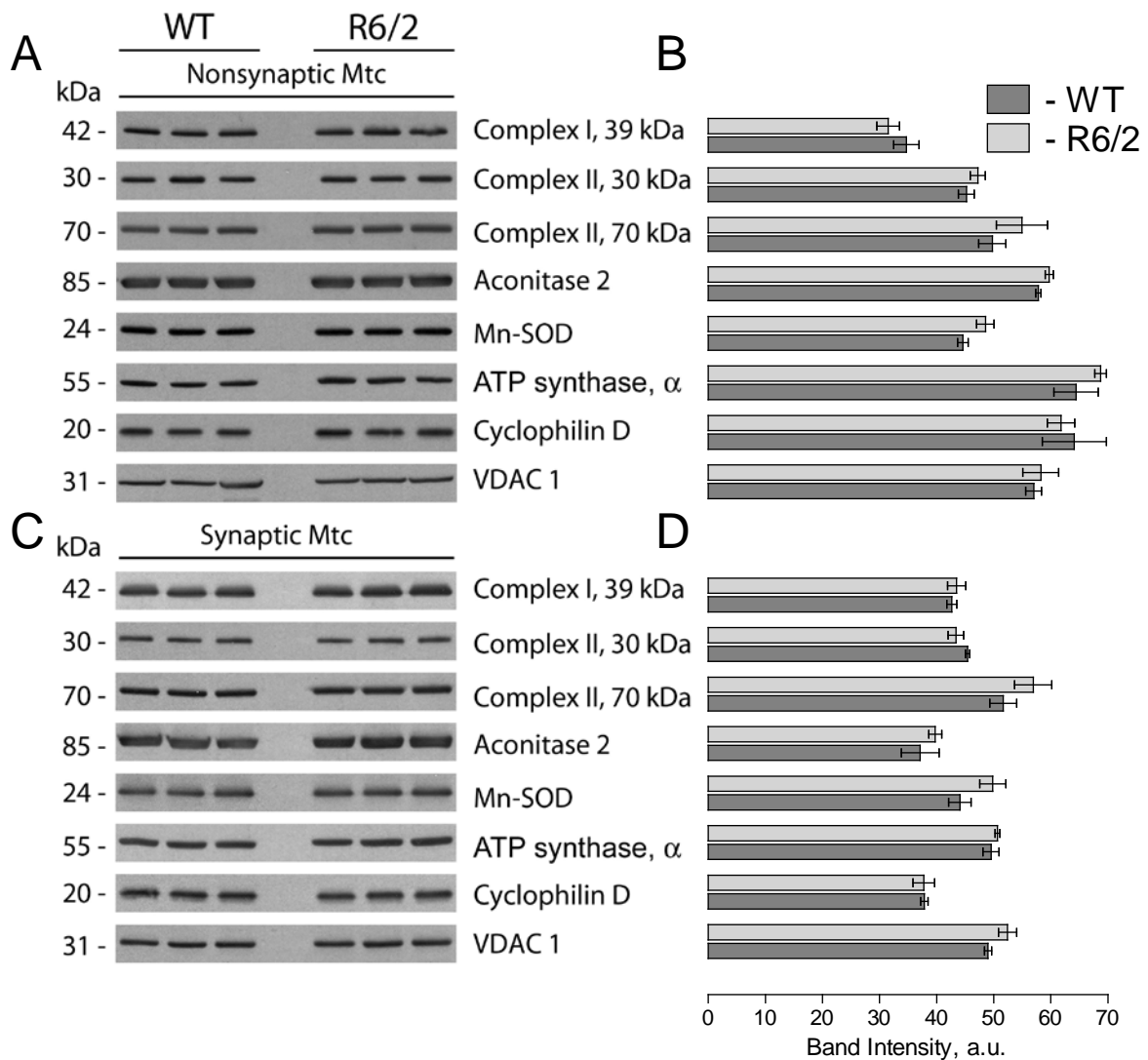


**Figure 36. Expression of nuclear encoded mitochondrial proteins in nonsynaptic and synaptic mitochondria isolated from 8-week-old WT and R6/2 mice.** In **A** and **C**, representative western blots of nonsynaptic (**A**) or synaptic (**C**) mitochondria generated with antibodies against nuclear encoded mitochondrial proteins including 39 kDa subunit of Complex I, 30 and 70 kDa subunits of Complex II, aconitase 2, MnSOD, CyD, and  $\alpha$ -subunit of ATP synthase (ATP synthase,  $\alpha$ ). VDAC1 was used as a loading control. In **B** and **D**, the results of densitometry performed with NIH ImageJ 1.48v software. Data are mean  $\pm$  SEM from six separate experiments.

### **c. Cellular respiration and extracellular acidification of striatal neurons from R6/2 mice.**

Although mitochondria isolated from brains of R6/2 and WT mice had similar respiratory activities, we could not rule out the effect of mHtt fragments on mitochondrial respiration under more physiological conditions. Striatum is the most vulnerable region of the brain in HD (Zuccato *et al.* 2010). Consequently, we examined the respiratory activities of cultured striatal neurons derived from R6/2 and WT mice using the Seahorse XF24 extracellular flux analyzer. Additionally, in these experiments we evaluated glycolytic activities in striatal neurons. OCR was used to evaluate cellular respiration and extracellular acidification rate (ECAR) was used to assess glycolytic activity. Each experiment followed the same protocol with sequential measurements of basal respiratory activity, oligomycin-sensitive respiration coupled to ATP synthesis, and 2,4-DNP-stimulated, maximal respiration. At the end of the experiment, neurons were treated with rotenone and antimycin A to completely inhibit mitochondrial respiration. It was previously suggested that supplementing the bath solution with 15 mM pyruvate in addition to 10 mM glucose would accentuate mitochondrial respiration (Oliveira *et al.* 2007). Under these 'high glucose plus pyruvate' conditions, we did not find any difference in respiration and glycolytic activities of striatal neurons from R6/2 and WT mice (Fig. 37A and C).

Recently, it was proposed that impaired respiratory activity may become apparent in mHtt-expressing neurons when the cells are incubated in a 'low glucose' medium that contained no pyruvate (Gouarne *et al.* 2013). Under these conditions, neurons from BACHD rats had decreased FCCP-stimulated maximal respiratory rates compared with neurons from WT animals. We assessed OCR and ECAR of striatal neurons from R6/2 and WT animals in 'low glucose' medium (2.5 mM glucose, no pyruvate) and did not find any statistically significant difference in respiratory and

glycolytic activities of these cells (Fig. 37B and D). Consistent with the lack of impairment in respiratory and glycolytic activities in striatal neurons, ATP levels in neurons from R6/2 mice ( $17.9 \pm 1.1$  nmol ATP/mg protein, N = 5) were not statistically different compared with ATP levels in neurons from WT mice ( $18.7 \pm 1.0$  nmol ATP/mg protein, N = 5).

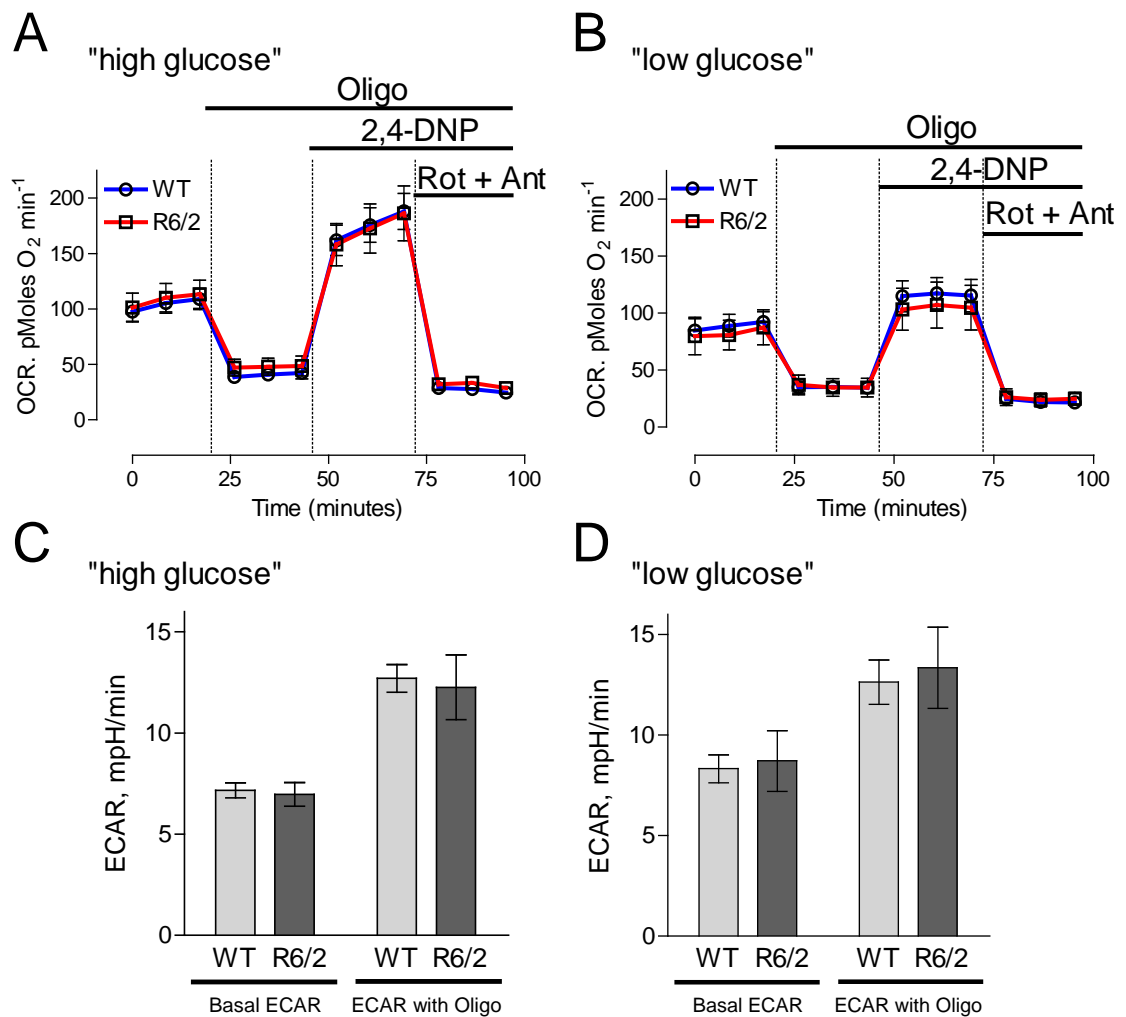


**Figure 37. OCR and ECAR of cultured striatal neurons from WT and R6/2 mice in 'high' and 'low' glucose medium conditions.** Striatal neurons from post-natal day 1 R6/2 and WT mice were grown in culture for 8 DIV before measurements. Where indicated, the bath solution contained either 'high glucose' (10 mM glucose, 15 mM pyruvate) or 'low glucose' (2.5 mM glucose). Where indicated, cells were treated with 1  $\mu$ M oligomycin (Oligo), 60  $\mu$ M 2,4-DNP and 1  $\mu$ M rotenone (Rot) plus 1  $\mu$ M antimycin A (Ant). In **A** and **B**, OCR of striatal neurons in 'high glucose' or 'low glucose' medium conditions, respectively. In **C** and **D**, ECAR of striatal neurons in 'high glucose' or 'low glucose' medium conditions, respectively. A Seahorse XF24 flux analyzer (Seahorse Bioscience, Billerica, MA, USA) was used to measure both OCR and ECAR at 37  $^{\circ}$ C, seeded at  $10^5$  cells per well. Data are mean  $\pm$  SEM from five to nine separate experiments.

**d. Ca<sup>2+</sup> uptake capacity of nonsynaptic and synaptic mitochondria from R6/2 mice.**

Next, we compared the Ca<sup>2+</sup> uptake capacity in synaptic and nonsynaptic mitochondria isolated from 6- to 8-week-old R6/2 and WT mice. Mitochondria were subjected to 10 μM Ca<sup>2+</sup> pulses every 2 min (Figs. 38 and 39). The Ca<sup>2+</sup> uptake capacities in synaptic and nonsynaptic mitochondria from R6/2 and WT mice appeared to be similar. In experiments with synaptic mitochondria, Ca<sup>2+</sup> uptake capacity was lower than in experiments with nonsynaptic mitochondria (Fig. 39). To improve Ca<sup>2+</sup> uptake capacity in synaptic mitochondria, we used BSA, which increases Ca<sup>2+</sup> uptake capacity, as shown in the previous section. In this study, BSA increased Ca<sup>2+</sup> uptake capacity of synaptic mitochondria. Importantly, BSA similarly increased Ca<sup>2+</sup> uptake capacity in synaptic mitochondria from both R6/2 and WT mice (Fig. 39B and C).

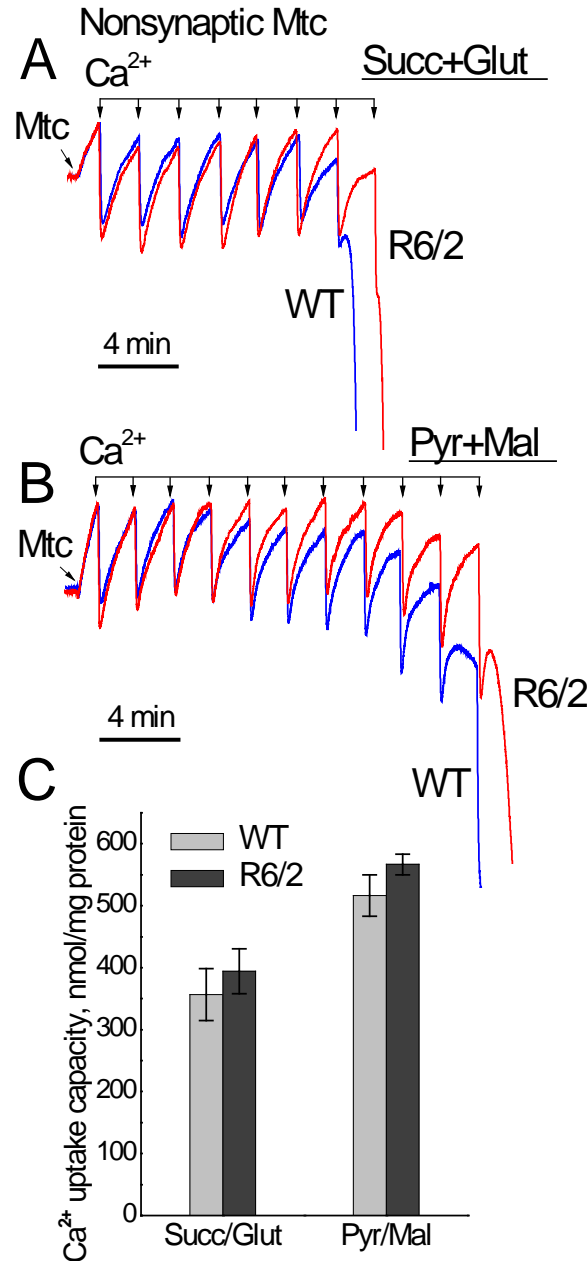


**Figure 38. Ca<sup>2+</sup> uptake capacity of brain nonsynaptic mitochondria isolated from 6- to 8-week-old WT (blue traces) and R6/2 (red traces) mice.** Ca<sup>2+</sup> uptake was assessed in mitochondria incubated at 37 °C in the standard incubation medium supplemented with either 3 mM succinate plus 3 mM glutamate (**A**) or 3 mM pyruvate plus 1 mM malate (**B**). In all Ca<sup>2+</sup> uptake experiments, incubation medium was additionally supplemented with 100 μM ADP and 1 μM oligomycin. In **C**, statistical analysis of Ca<sup>2+</sup> uptake capacity of mitochondria from R6/2 and WT mice. Data are mean ± SEM, N = 5–6 separate experiments.

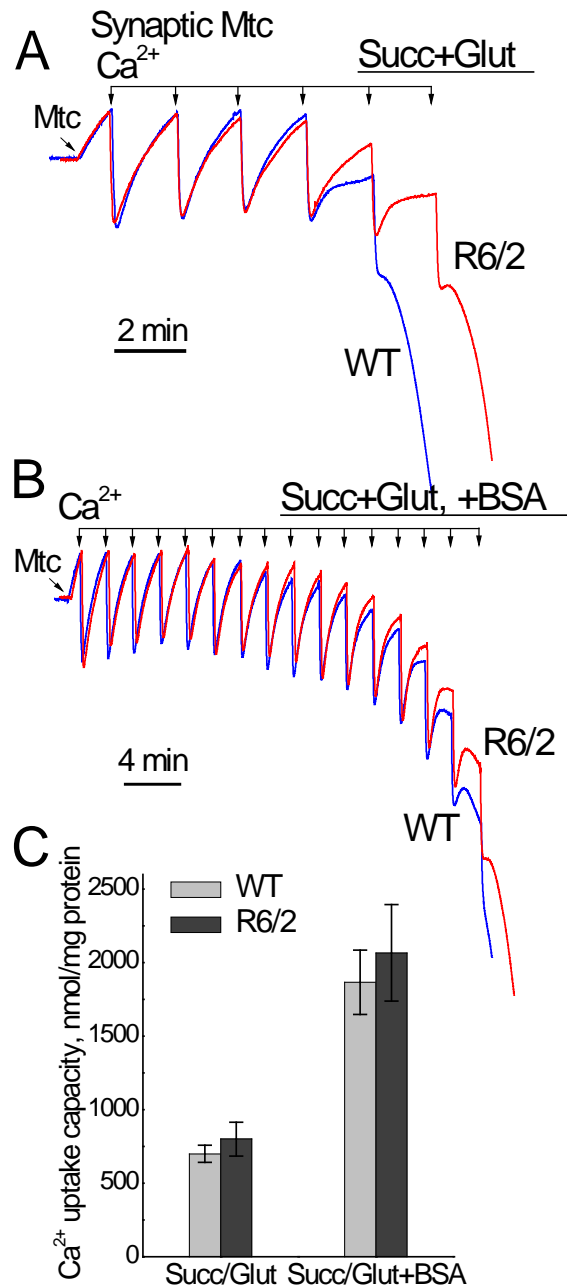


**Figure 39. Ca<sup>2+</sup> uptake capacity of brain synaptic mitochondria isolated from 6- to 8-week-old WT (blue traces) and R6/2 (red traces) mice.** Ca<sup>2+</sup> uptake was assessed in mitochondria incubated at 37 °C in the standard incubation medium supplemented with 3 mM succinate plus 3 mM glutamate either without (**A**) or with (**B**) 0.1% BSA in the incubation medium. In all Ca<sup>2+</sup> uptake experiments, incubation medium was additionally supplemented with 100 μM ADP and 1 μM oligomycin. In **C**, statistical analysis of Ca<sup>2+</sup> uptake capacity of mitochondria from R6/2 and WT mice. Data are mean ± SEM from 5 separate experiments.

#### **e. Mitochondrial Ca<sup>2+</sup> accumulation in striatal neurons from R6/2 mice.**

We also assessed mitochondrial Ca<sup>2+</sup> accumulation in striatal neurons derived from R6/2 and WT mice. For these measurements, we stimulated Ca<sup>2+</sup> influx into neurons and subsequently into mitochondria by briefly exposing cells to glutamate (25 μM glutamate plus 10 μM glycine) (Fig. 40). Changes in cytosolic Ca<sup>2+</sup> were monitored by following fluorescence of Fura-2FF. After glutamate removal and return of cytosolic Ca<sup>2+</sup> to near resting level, the release of mitochondrial Ca<sup>2+</sup> into the cytosol was triggered by mitochondrial depolarization with 1 μM FCCP (Fig. 40). The magnitude of cytosolic Ca<sup>2+</sup> elevation following depolarization was taken as a measure of mitochondrial Ca<sup>2+</sup> accumulation *in situ* as described previously (Chang *et al.* 2006). To avoid Ca<sup>2+</sup> influx into cells from the extracellular medium, Ca<sup>2+</sup> was omitted from the bath solution. To prevent Ca<sup>2+</sup> extrusion from the cell via the Na<sup>+</sup>/Ca<sup>2+</sup> exchanger during FCCP-induced increase in cytosolic Ca<sup>2+</sup>, external Na<sup>+</sup> was replaced with equimolar N-methyl-D-glucamine (NMDG) during FCCP application (Li and Van 1995). NMDG is a bulk organic cation that cannot be transported by the Na<sup>+</sup>/Ca<sup>2+</sup> exchanger and, therefore, precludes the extrusion of Ca<sup>2+</sup> via this mechanism. In these experiments, neurons from R6/2 and WT mice showed comparable transient increases in cytosolic Ca<sup>2+</sup> during glutamate application (Fig. 40C). The increase in cytosolic Ca<sup>2+</sup> triggered by FCCP was also not different between neurons from R6/2 and WT mice (Fig. 40D). This result, similar to the results obtained with Ca<sup>2+</sup> uptake capacity in isolated mitochondria (Figs. 38 and 39), argues against mHtt fragment-mediated alterations in mitochondrial Ca<sup>2+</sup> accumulation in the R6/2 mouse model of HD.



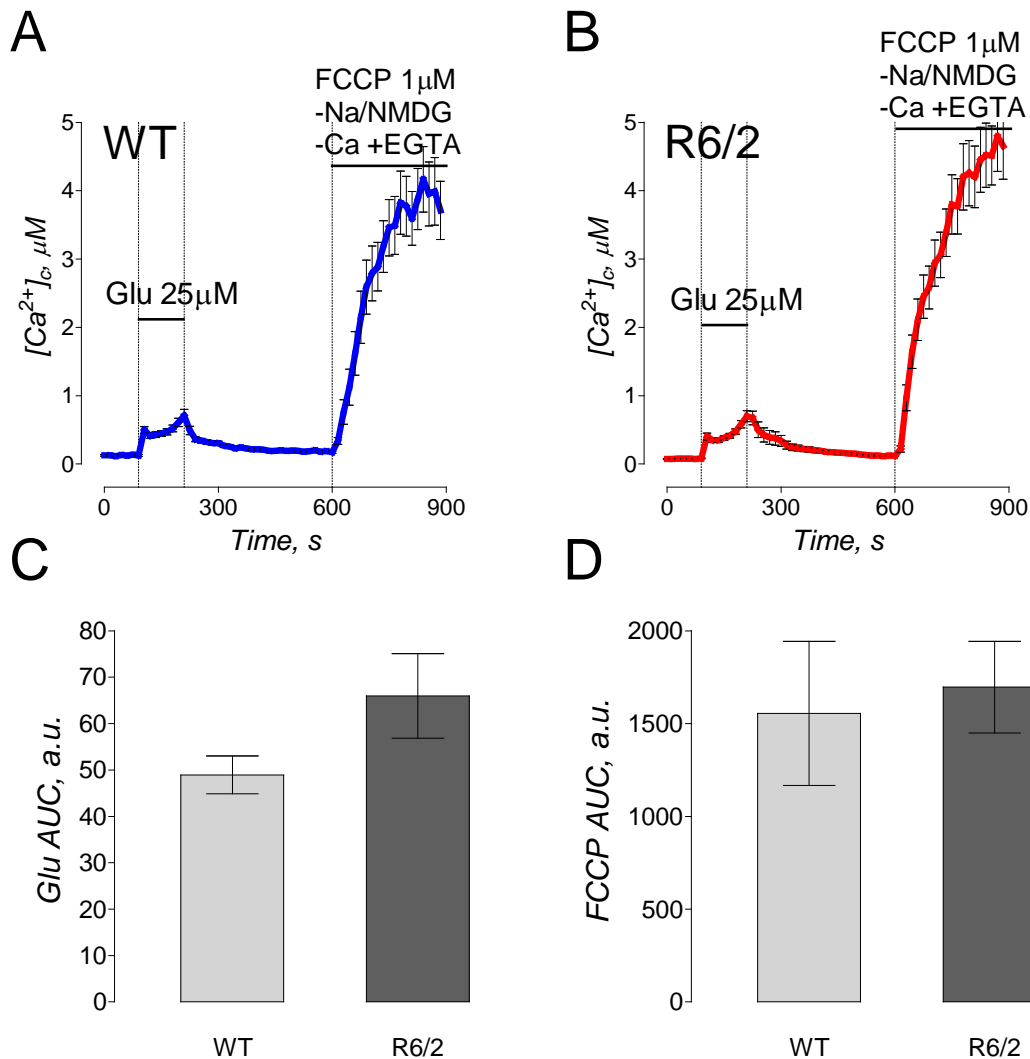


**Figure 40. Mitochondrial  $Ca^{2+}$  accumulation following transient glutamate-induced elevations in cytosolic  $Ca^{2+}$  in striatal neurons derived from WT and R6/2 mice.** In **A** and **B**, the averaged fluorescence signals (mean  $\pm$  SEM) from the representative experiments are shown. Cytosolic  $Ca^{2+}$  was followed by monitoring Fura-2FF  $F_{340}/F_{380}$  fluorescence ratio at 37 °C. In these experiments, striatal neurons (10–13 DIV) were exposed to 25  $\mu$ M glutamate with 10  $\mu$ M glycine for 2 min as indicated. Then, glutamate and glycine were removed to let cytosolic  $Ca^{2+}$  concentration ( $[Ca^{2+}]_c$ ) recover. After  $[Ca^{2+}]_c$  reached near resting level (7 min after glutamate removal) neurons were treated with 1  $\mu$ M FCCP to depolarize mitochondria and release accumulated  $Ca^{2+}$ . To avoid ambiguity concerning possible  $Ca^{2+}$  influx from the outside of the cell, external  $Ca^{2+}$  was removed simultaneously with glutamate and glycine. In addition, to prevent  $Ca^{2+}$  extrusion from the cell by  $Na^+/Ca^{2+}$  exchanger, the external  $Na^+$  was replaced by equimolar NMDG as indicated. In **C** and **D**, the areas under the curve (AUC) for the averaged fluorescence signals are shown. The AUC for glutamate-induced increase in  $[Ca^{2+}]_c$  (Glu AUC) was calculated for the 120-s period beginning with glutamate application. The AUC for FCCP-induced increase in  $[Ca^{2+}]_c$  (FCCP Glu) was calculated for the 300-s period following FCCP application. Data are mean  $\pm$  SEM from five to six separate experiments with 20–25 individual neurons analyzed in each experiment.

## **f. Morphological characterization of mitochondria in striatal neurons from R6/2 mice.**

Despite the lack of respiratory deficiency and mitochondrial  $\text{Ca}^{2+}$  handling defect in mitochondria from R6/2 mice, we cannot rule out possible alterations in mitochondrial morphology in HD. In neurons, altered mitochondrial morphology could lead to, for example, impaired trafficking of mitochondria to distant processes, resulting areas of local energy deficiency within the neuron (Li *et al.* 2010). Previously, morphological imbalance and a shift toward augmented fission was reported in mouse and cell models of HD (Wang *et al.* 2009;Costa *et al.* 2010;Song *et al.* 2011;Shirendeb *et al.* 2012). In addition, a dramatic enlargement of mitochondria in neurons (Tellez-Nagel *et al.* 1974;Bayram-Weston *et al.* 2012a;Bayram-Weston *et al.* 2012b) and peripheral cells (Squitieri *et al.* 2010;Brustovetsky 2016) expressing mHtt was reported. In our experiments, we used live-cell laser spinning-disk confocal microscopy and 3D reconstruction of the mitochondrial network in neurons from WT and R6/2 mice. In parallel experiments, we employed transmission electron microscopy to substantiate data obtained with confocal microscopy. In all analyzed striatal neurons from WT mice (142 neurons), mitochondria had a normal worm-like appearance whereas in about 24% of neurons from R6/2 mice (35 out of 148 analyzed neurons) most of mitochondria were fragmented while some mitochondria were enlarged (Fig. 41). Yet, despite altered mitochondrial morphology in this subpopulation of neurons, the entire neuronal population from R6/2 mice had similar respiratory activities and  $\text{Ca}^{2+}$  handling compared with neurons from WT mice. Whether neurons with abnormal mitochondrial morphology observed in our study have alterations in oxidative metabolism and mitochondrial  $\text{Ca}^{2+}$  handling is not clear yet.

Taken together, our results show no difference in respiratory activities and  $\text{Ca}^{2+}$  handling in isolated brain mitochondria and cultured striatal neurons from R6/2 mice compared with mitochondria and neurons from WT animals.

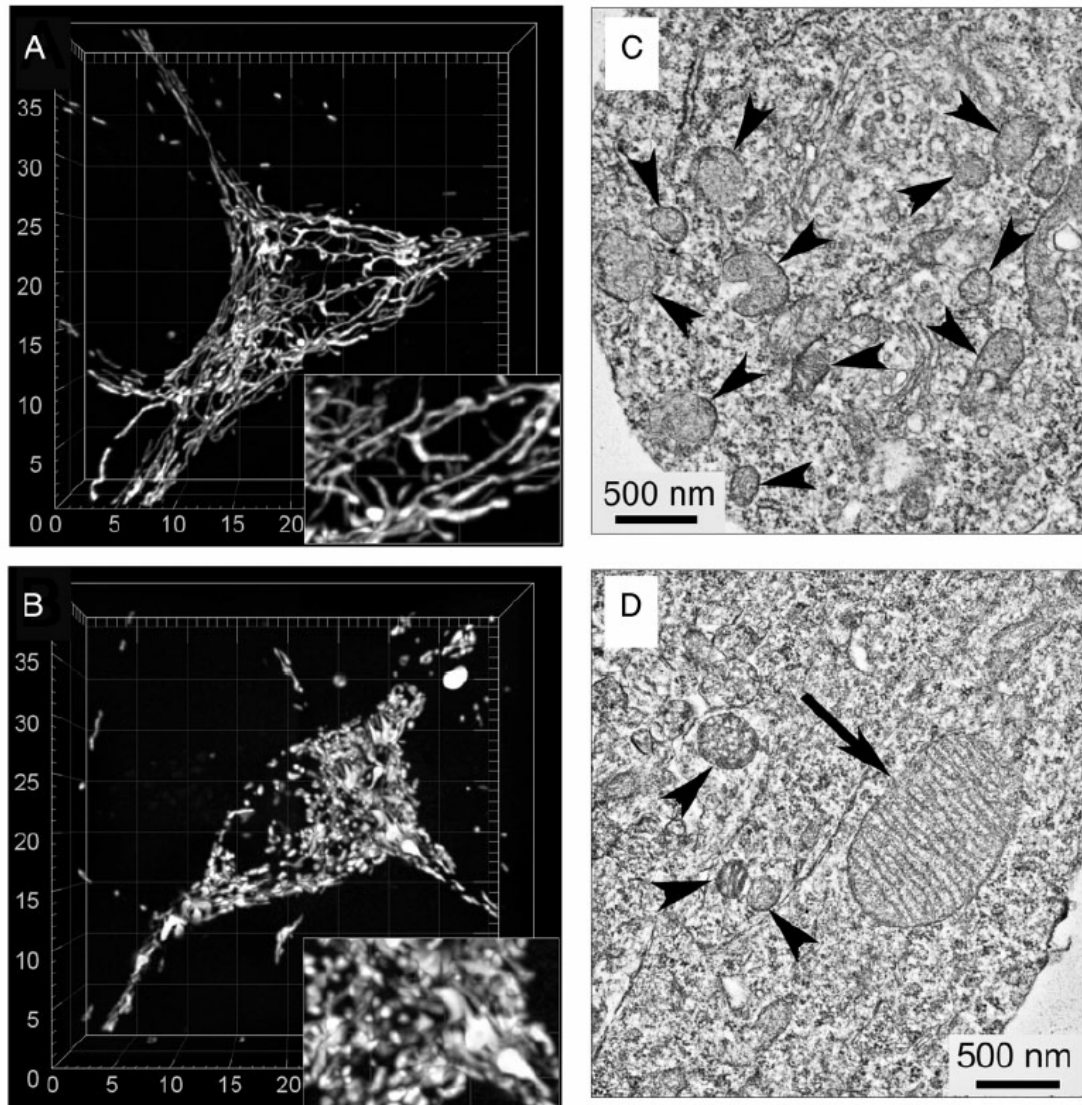


**Figure 41. Representative 3D reconstructions of mitochondrial networks and electron micrographs of cultured striatal neurons from WT (A, C) and R6/2 (B, D) mice.** In **A** and **B**, the representative 3D maximal fluorescence intensity projection images of the mitochondrial network in live cultured striatal neurons (9 DIV) from WT and R6/2 mice, respectively (total number of neurons analyzed in these experiments—142 neurons from WT mice and 148 neurons from R6/2 mice). Cells were analyzed in a blind manner. The scales are in  $\mu\text{m}$ . In **C** and **D**, representative electron micrographs of cultured striatal neurons (9 DIV) from WT and R6/2 mice, respectively. Arrowheads point to small-size, normal-looking mitochondria; the arrow points to enlarged mitochondrion.

## **IV. Discussion and Future Directions**

### **A. Oxidative metabolism and mitochondrial Ca<sup>2+</sup> handling in the YAC128 mouse model.**

In the present work, we, for the first time, evaluated the effect of mHtt on oxidative metabolism of YAC128 mice using a combination of three different experimental models: (i) isolated, whole brain mitochondria, (ii) neurons in culture and (iii) whole YAC128 and WT animals. All three models produced consistent results strongly arguing against a noteworthy deleterious effect of mHtt on mitochondrial oxidative metabolism, mitochondrial Ca<sup>2+</sup> handling, and neuronal glycolysis in YAC128 mice. The lack of respiratory defects suggests that mHtt does not impair mitochondrial oxidative metabolism in YAC128 mice. Consequently, mitochondrial respiratory deficiency most likely does not contribute to HD pathology in YAC128 mice, and if it occurs later in disease progression, it most likely represents a consequence of HD pathology rather than its cause.

In the study with YAC128 mice, we confirmed that mHtt is present in cultured neurons from these mice and that mHtt is associated with mitochondria isolated from transgenic animals. We invariably performed genotyping with every animal and immunoblotting with every sample of isolated mitochondria and cultured neurons to confirm the presence of mHtt in biological materials from YAC128 mice. Consistent with previously reported data (Slow *et al.* 2003; Pouladi *et al.* 2013), in western blotting experiments performed with brain homogenates and cytosolic fractions from YAC128 mice, it was found that human mHtt was expressed at the same level as wild-type mouse Htt. Using mAb 2166, which recognizes both wild-type Htt and mHtt, we detected wild-type Htt associated with mitochondria from both WT and YAC128 mice (Fig. 6B). With mAb 2166, mHtt associated with mitochondria from YAC128 mice was also detected. Surprisingly, the amount of mHtt associated with mitochondria was four times

lower than the amount of mitochondria-bound wild-type Htt. Keeping in mind that similar amounts of mHtt were detected with mAb 2166 in homogenates and cytosolic fractions from YAC128 mice, this suggests that mHtt has lower affinity for mitochondria compared with wild-type Htt. This also suggests that a considerable amount of wild-type Htt is associated with mitochondria, and presumably, wild-type Htt plays some role in regulation of mitochondrial functions. Indeed, a recent study with mouse embryonic stem cells (mESC) revealed that the lack of wild-type Htt in *htt*<sup>-/-</sup> mESCs results in extensive metabolic aberrations (Ismailoglu *et al.* 2014). On the other hand, mESCs expressing mHtt with an expanded poly-Q stretch (Htt-Q140/Q7 mESCs) were bioenergetically indistinguishable from mESCs expressing wild-type Htt (Htt-Q7/Q7 mESCs) (Ismailoglu *et al.* 2014), which is, again, consistent with our results. This study (Ismailoglu *et al.* 2014), as well as our finding regarding the association of wild-type Htt with brain mitochondria, supports a potential role of wild-type Htt in regulation of mitochondrial function since lack of Htt results in mitochondrial functional changes. However, many questions concerning the relationship between wild-type Htt and mitochondria remain to be answered. Is wild-type Htt located on the outer side of the outer mitochondrial membrane, in the intermembrane space, or in the mitochondrial matrix? Is it inserted into the outer membrane or only peripherally attached to the membrane like mHtt? How does wild-type Htt affect mitochondrial respiration, Ca<sup>2+</sup> uptake, and PTP induction? Does mHtt interfere with wild-type Htt-mediated regulation of mitochondrial functions? These and many other questions need to be answered to gain insight into the role of wild-type Htt in the regulation of mitochondrial functions and to better understand possible deleterious effect of mHtt on mitochondria or reasons for the lack of such an effect.

In our experiments, we chose to use both early symptomatic, 2-month-old YAC128 mice as well as 10-month-old YAC128 mice at a more advanced HD stage, expecting to see overt alterations in mitochondrial functions. The 2-month-old YAC128

mice used in our experiments already demonstrated clasping, a clear sign of HD-associated behavioral abnormalities reported previously with other mouse models of HD (Reddy *et al.* 1999; Milnerwood *et al.* 2006). This observation assured us that if mitochondrial respiratory dysfunction plays a role in neuronal alterations leading to behavioral abnormalities, then at this stage of HD progression, we should be able to detect this change in mitochondrial respiratory activity. This would allow for the further investigation of the mechanism of respiratory deficiency induced by mHtt. Even more so, we expected to see mitochondrial dysfunction with 10-month-old YAC128 mice. However, despite all our efforts, we found no indication of mitochondrial dysfunction.

In the present study, we found a minute but statistically significant decline in oligomycin-stimulated ECAR in striatal neurons from YAC128 mice incubated with 2.5 mM glucose. This suggested a decreased glycolytic activity in striatal neurons from YAC128 mice potentially indicating energy deficiency. Previously, oligomycin-stimulated extracellular acidification was interpreted as an indicator of glycolysis activation under conditions of inhibition of oxidative phosphorylation (Wu *et al.* 2007; Ismailoglu *et al.* 2014). However, under these conditions, cellular respiration is significantly suppressed and, consequently, we cannot correlate respiratory rate and glycolytic activity based on the data obtained in the presence of oligomycin.

Since the discovery of a link between the mutation in huntingtin and HD pathogenesis (MacDonald *et al.* 1993), numerous hypotheses concerning the mechanism of detrimental mHtt action have been put forward, and numerous studies have been performed to untangle these mechanisms. The studies regarding possible defects in oxidative metabolism can be divided into two groups: one of which generated experimental data indicating impairment of mitochondrial functions either in animal or cell models of HD (Brennan, Jr. *et al.* 1985; Kuhl *et al.* 1985; Gu *et al.* 1996; Browne *et al.* 1997; Kim *et al.* 2011; Siddiqui *et al.* 2012; Damiano *et al.* 2013; Napoli *et al.* 2013), and

another group that produced data arguing against defects in oxidative metabolism (Higgins *et al.* 1999; Guidetti *et al.* 2001; Milakovic and Johnson 2005; Lee *et al.* 2007; Oliveira *et al.* 2007; Olah *et al.* 2008; Gouarne *et al.* 2013; Boussicault *et al.* 2014). The reasons for these contradictory data are not clear, but it might be related to methodological differences and the use of different experimental models of HD. Interestingly, recent studies with HD patients revealed that oxidative metabolism remains properly operating despite expression of mHtt (Gaba *et al.* 2005; Powers *et al.* 2007b; Turner *et al.* 2007). These observations support the point of view that mHtt does not directly and severely affect mitochondrial functions. This is also in line with the lack of alterations in oxidative metabolism in YAC128 mice examined in the present study.

In earlier studies, a decreased ability of mitochondria to accumulate  $\text{Ca}^{2+}$  has been proposed to contribute to HD pathogenesis (Panov *et al.* 2002; Choo *et al.* 2004; Milakovic *et al.* 2006). On the other hand, in experiments with nonsynaptic mitochondria, we and other investigators failed to find an increase in sensitivity to deleterious  $\text{Ca}^{2+}$  and instead observed an increase in resistance to  $\text{Ca}^{2+}$  that was manifested in augmented  $\text{Ca}^{2+}$  uptake capacity (Brustovetsky *et al.* 2005a). In this study, we did not find evidence of impaired  $\text{Ca}^{2+}$  uptake capacity in either synaptic or nonsynaptic mitochondria from YAC128 mice. On the contrary, both types of mitochondria had increased  $\text{Ca}^{2+}$  capacity, especially, synaptic mitochondria from 12-month-old YAC128 mice. The mechanism underlying augmented  $\text{Ca}^{2+}$  uptake capacity of mitochondria from YAC128 mice remains unknown, and, at the moment, we can only speculate about possible scenarios. The increased  $\text{Ca}^{2+}$  uptake capacity of mitochondria from YAC128 mice may be indicative of compensatory response to augmented  $\text{Ca}^{2+}$  influx via over-activated NMDA receptors and/or increased  $\text{Ca}^{2+}$  release from endoplasmic reticulum normally activated via IP3 receptors, but increased  $\text{Ca}^{2+}$  uptake



capacity is not considered a direct result of intrinsic mitochondrial damage or dysfunction (Bezprozvanny and Hayden 2004).

The lack of deficiencies in oxidative metabolism and mitochondrial  $\text{Ca}^{2+}$  uptake in YAC128 mice suggests that mHtt in these mice does not directly and acutely affect mitochondria. Therefore, mHtt neurotoxicity may likely be mediated by mechanisms unrelated to mitochondria, such as oxidative stress associated with elevated NAD(P)H oxidase activity (Valencia *et al.* 2013) and/or alterations in cholesterol metabolism (Trushina *et al.* 2014). Therefore, mitochondrial bioenergetics or  $\text{Ca}^{2+}$  uptake impairment, if it can be detected, most likely lies downstream of mHtt-induced alterations in other neuronal functions. However, it is also possible that in other cell or animal HD models, full-length or truncated mHtt with different levels of expression and different Htt/mHtt ratio does influence mitochondrial functions. Consequently, further investigations with alternative HD models and cell lines derived from HD patients are necessary to demonstrate and clarify possible deleterious effects of mHtt on oxidative metabolism.

## **B. Oxidative metabolism and $\text{Ca}^{2+}$ handling in striatal mitochondria from YAC128 mice.**

In the previous section (section A), it was shown that nonsynaptic and synaptic mitochondria isolated from whole brains of YAC128 mice have similar respiratory rates and  $\text{Ca}^{2+}$  uptake capacities compared to mitochondria from WT mice. However, the experiments in the previous section (A) utilized mitochondria isolated from the whole brain to assess respiratory rates and  $\text{Ca}^{2+}$  uptake capacity. In HD, the striatum is the most vulnerable brain region whereas hippocampus and cerebellum remain practically intact (Vonsattel and DiFiglia 1998). The use of mitochondria isolated from whole brains was a limitation of the results obtained in the previous section because contribution from

mitochondria from unaffected brain regions may have obscured deficiencies of striatal mitochondria. In this section (section B), we will discuss the results obtained with nonsynaptic and synaptic mitochondria isolated exclusively from striata of 8- to 10-week-old YAC128 and FVB/NJ mice. The results produced with striatal mitochondria are consistent with the data obtained with mitochondria isolated from the whole brain. We did not find evidence for alterations in expression of nuclear-encoded mitochondrial proteins and for impairment of mitochondrial respiration and  $\text{Ca}^{2+}$  uptake capacity in striatal mitochondria from YAC128 mice compared to mitochondria from FVB/NJ mice. These findings argue against mitochondrial bioenergetics and  $\text{Ca}^{2+}$  handling dysfunction as a contributing factor in HD pathogenesis.

In addition to the data obtained with isolated mitochondria, we sought to confirm our findings by using cultured primary neurons. In addition to measuring respiration and  $\text{Ca}^{2+}$  uptake capacity in striatal nonsynaptic and synaptic mitochondria isolated from YAC128 and FVB/NJ mice, we examined oxidative metabolism and mitochondrial  $\text{Ca}^{2+}$  handling in cultured striatal neurons from these animals. Although, two-month-old YAC128 mice already demonstrate clasping behavior, an early symptom associated with mHtt expression (Mangiarini *et al.* 1996; Reddy *et al.* 1999), our data obtained with cultured neurons and isolated mitochondria from YAC128 mice provide no evidence for mitochondrial impairment, suggesting that the motor dysfunction, which most reliably manifests as clasping, may not be associated with mitochondrial alterations.

Mitochondrial respiration generates an electrochemical proton gradient across the mitochondrial inner membrane which is utilized to synthesize ATP in the process of oxidative phosphorylation and to transport  $\text{Ca}^{2+}$  into the mitochondrial matrix. Consequently, impairment of mitochondrial respiration may affect both oxidative phosphorylation and  $\text{Ca}^{2+}$  uptake. In this current study, we did not find a difference in ADP-stimulated respiration and in uncoupled respiration stimulated by 2,4-DNP. This

suggests that the oxidative phosphorylation system and electron transport chain are not affected by mHtt in YAC128 mice. Similar respiratory activities were observed with both malate plus pyruvate, Complex I substrates, and with succinate, a Complex II substrate. This suggests that Complex I and Complex II of the electron transport chain are not impaired by mHtt. These findings are consistent with previously reported data. In early studies, Guidetti *et al.* did not detect alterations in activity of the electron transport chain in the striatum and cerebral cortex of HD48 and HD89 mice, expressing full-length mHtt with 48 or 89 glutamines, respectively, compared to wild-type mice (Guidetti *et al.* 2001). In experiments with cultured striatal neurons from 15- to 17-week-old heterozygous *Hdh*<sup>150</sup> mice, cell respiratory activities were found to be similar (Oliveira *et al.* 2007). Olah *et al.* found that the activities of Complexes I–IV in brain mitochondria from 20-week-old transgenic N171-82Q mice were not diminished compared to mitochondria from wild-type animals (Olah *et al.* 2008). Gouarne *et al.* did not find a difference in respiration of cultured striatal neurons from heterozygous transgenic BACHD rats compared to wild-type neurons, when cells were incubated in the presence of 25 mM glucose and 1 mM pyruvate (Gouarne *et al.* 2013). In experiments with *STHdh*<sup>Q111/Q111</sup> cells, mitochondrial pathways were not significantly altered and the obtained data uniformly refuted a view of direct deleterious mHtt effect on mitochondria (Lee *et al.* 2007). The direct measurements of oxidative metabolism in striatum of HD patients and age-matched controls using positron emission tomography failed to find a difference, which argues against a defect in mitochondrial oxidative phosphorylation and mitochondrial electron transport chain activity (Powers *et al.* 2007b). Finally, Ismailoglu *et al.* studied mouse embryonic stem cells expressing wild-type and 140Q-mHtt and found no difference in cellular bioenergetics of these cell lines (Ismailoglu *et al.* 2014). Collectively, these results suggest no overt respiratory defects in HD mitochondria.

In the previous section (A), we discussed expression of nuclear-encoded proteins in brain mitochondria isolated from whole brains. It had previously been reported that mitochondrial protein import machinery might be impaired by mHtt (Yano *et al.* 2014). Despite finding no alteration in protein expression in whole brain mitochondria, we reasoned that if striatal mitochondria exposed to mHtt had decreased protein expression and other brain regions have no change in expression, such an alteration may not have been detectable in our previous experiments. Although we did not directly assess activity of protein import machinery in striatal mitochondria from YAC128 mice, our data unequivocally demonstrate the lack of respiratory deficits and show the absence of alterations in protein expression in striatal mitochondria from YAC128 mice. Therefore, although we cannot directly confirm that import is not inhibited in mitochondria from these animals using this experiment, having similar mitochondrial protein levels strongly supports the lack of difference seen in functions of mitochondria from WT and HD mice. Taken together, these data suggest that if protein import in mitochondria of HD mice is suppressed, this, nevertheless, does not affect the level of expression of mitochondrial nuclear encoded proteins and, consequently, does not affect mitochondrial respiration.

Mitochondria possess  $\text{Ca}^{2+}$  channels, historically known as “calcium uniporter”, that allows  $\text{Ca}^{2+}$  influx into the mitochondrial matrix driven by high membrane potential, negative inside of the organelle (Bernardi *et al.* 1999). Inside of mitochondria, elevated  $\text{Ca}^{2+}$  can interact with inorganic phosphate and precipitate in the form of hydroxyapatite (Chalmers and Nicholls 2003). This allows for the large  $\text{Ca}^{2+}$  accumulation in mitochondria. The ability of mitochondria to accumulate significant amounts of  $\text{Ca}^{2+}$  is important for maintenance of  $\text{Ca}^{2+}$  homeostasis in the cell (Bernardi and Rasola 2007).  $\text{Ca}^{2+}$  accumulation in mitochondria is limited by induction of the mitochondrial permeability transition pore that depolarizes mitochondria and prevents further  $\text{Ca}^{2+}$  uptake (Bernardi *et al.* 1999). In early studies, decreased  $\text{Ca}^{2+}$  uptake capacity in

mitochondria isolated from HD mouse and cell models was reported, and it was proposed to contribute to HD pathogenesis by affecting  $\text{Ca}^{2+}$  homeostasis in neurons (Panov *et al.* 2002; Milakovic *et al.* 2006; Gellerich *et al.* 2008; Lim *et al.* 2008) However, other investigators failed to find a decrease in mitochondrial  $\text{Ca}^{2+}$  uptake capacity in mitochondria exposed to mHtt with an elongated polyQ stretch (Oliveira *et al.* 2007; De *et al.* 2016). In these studies, the authors either did not find a difference between mitochondria from HD and wild-type animals or they found a paradoxical increase in  $\text{Ca}^{2+}$  accumulation in mitochondria from HD mice. In line with these findings that suggest no impairment of mitochondrial  $\text{Ca}^{2+}$  handling, the results from section A with nonsynaptic and synaptic mitochondria isolated from the whole brain of YAC128 mice and with cultured neurons from these animals substantiate these observations. The results presented in this section (B) demonstrate no deficiency in  $\text{Ca}^{2+}$  handling in nonsynaptic and synaptic mitochondria isolated from striata of YAC128 mice and support previous findings indicating no  $\text{Ca}^{2+}$  accumulation defect in mitochondria from HD mice.

The experiments with isolated mitochondria and cultured neurons provide valuable information about possible effects of mHtt. However, *in vivo* measurements of brain respiratory activity may further enhance our understanding of potential defects in oxidative metabolism in HD. A recent paper by Lou *et al.* described elegant experiments with the use of  $^{17}\text{O}$  magnetic resonance spectroscopy aimed at assessing cerebral mitochondrial respiratory activity in R6/2 mice *in vivo* (Lou *et al.* 2016). In this study, the authors did not find a difference in basal striatal oxygen consumption rate in symptomatic R6/2 mice at rest. Inhibition of oxidative phosphorylation with oligomycin resulted in a similar decrease in respiration, suggesting similar phosphorylation capacity and coupling of oxidative phosphorylation in HD and wild-type mice. Yet, after injection of the uncoupler 2,4-DNP, the authors found a negligible (about 15%), but statistically

significant, decrease in respiratory responses in both striatum and cortex of R6/2 mice compared with respiratory responses of corresponding brain tissues in wild-type animals (Lou *et al.* 2016). The physiological significance of this difference is not evident but it is clear that such conditions (2,4-DNP-induced stimulation) do not take place in a physiological scenario. The ambiguity of the small difference in uncoupled respiration is supported by the fact that natural, sensory stimulation-induced elevation in respiration measured with photoacoustical microscopy (Yao *et al.* 2015) is weaker than 2,4-DNP-induced increase in oxygen consumption. Thus, importance and relevance of small decreases in 2,4-DNP stimulated respiration of mitochondria from HD mice is not obvious. However, such *in vivo* measurements of mitochondrial functions in HD models may provide new insights toward uncovering the role, or lack thereof, of mitochondria in HD pathogenesis

Overall, the data from this section (B) obtained with striatal nonsynaptic and synaptic mitochondria from YAC128 mice and data from previous section (A) with whole-brain mitochondria and cultured striatal and cortical neurons from YAC128 mice do not provide evidence for mitochondrial respiratory deficiency and defects in mitochondrial Ca<sup>2+</sup> handling.

Our data are consistent with anecdotal evidence from individuals who tested positive for the mutation in the *huntingtin* gene, further suggesting a lack of mitochondrial deficits. Although these individuals express mHtt in all tissues beginning from an embryonic stage, they do not begin to show symptoms of the disease until adulthood and instead, during the intervening pre-symptomatic period, they engage in everyday life as cognitively and physically capable individuals. Some individuals with HD even ascend to the highest levels of athletic competition. For example, a British rower, Sarah Winckless, tested positive for the mutation in the *huntingtin* gene in the late 1990s and went on to win two world championships in rowing and to compete in three Olympics,

winning a bronze medal at the Athens Olympic Games in 2004 (English 2014). Since then, she has climbed Mt. Kilimanjaro and biked from London to Paris. Other testimonials abound of patients who capably compete in similarly rigorous sports. Since mitochondria are responsible for the production of energy in the form of ATP, proper mitochondrial function would be essential for individuals to engage in activities that expend large amounts of energy. The observation that pre-symptomatic HD patients can excel in physically strenuous activities raises the question of how mitochondria could support such energy demand if mHtt interferes with the normal mitochondrial functioning. These observations, coupled with our results, support the idea that mHtt per se does not induce mitochondrial dysfunction. This conclusion reinforces the necessity to continue exploring the potential, non-mitochondrial mechanisms of HD pathogenesis.

### **C. Oxidative metabolism and mitochondrial Ca<sup>2+</sup> handling in the R6/2 model.**

In the previous sections (A and B), we discussed the effect of full-length mHtt on mitochondrial functions and did not find evidence for detrimental alterations in mitochondria from YAC128 mice. In this section (C), we will discuss our results obtained with isolated mitochondria and cultured neurons from R6/2 mice expressing mHtt fragments. It remains unclear whether full-length mHtt or mHtt fragments mediate HD pathogenesis. However, some studies suggest that mHtt fragments might be more prone to aggregation and therefore might be more toxic for neurons (Kim *et al.* 1999; Wellington *et al.* 2000). We demonstrated no mitochondrial respiratory or Ca<sup>2+</sup> handling defects in mitochondria and cultured neurons from YAC128 mice, which express human full-length mHtt. Next, we hypothesized that fragments of mHtt might be more harmful to mitochondria than full-length mHtt. If this would be the case, we might expect to detect mitochondrial functional abnormalities induced by mHtt fragments.

In these experiments, two model systems were used: isolated brain mitochondria and primary cultured striatal neurons. It is conceivable that there might be some difference in the results produced with these two model systems. Mitochondria isolated from adult brains may better reflect changes that take place in HD over time. However, isolated mitochondria taken away from their natural intracellular environment may lead to unwanted artifacts (e.g. loss of association with mHtt) and, consequently, to inaccurate interpretations. On the other hand, mitochondria in young, post-natal neurons are immersed within their natural intracellular environment, but they might be too young for developing overt functional defects. The use of both, mitochondria isolated from adult brains and mitochondria in post-natal neurons, complement each other and allows for improved assessment of possible effects of mHtt on the organelles.

Earlier studies reported mitochondrial respiratory dysfunction and a decreased ability of mitochondria to accumulate  $\text{Ca}^{2+}$  in HD mouse models expressing full-length or fragments of mHtt (Panov *et al.* 2002; Lim *et al.* 2008; Kim *et al.* 2011; Damiano *et al.*, 2013). On the other hand, results from this section (C), from sections A and B, and from other investigators (Guidetti *et al.* 2001; Chang *et al.* 2006; Olah *et al.* 2008) suggest that there are no defects in respiration and  $\text{Ca}^{2+}$  uptake in mitochondria isolated from brains of HD mice compared with mitochondria from brains of WT animals. Consistent with these previous findings in other mouse models of HD, the data presented here indicate no defects in respiration and  $\text{Ca}^{2+}$  uptake capacity in brain mitochondria isolated from R6/2 mice compared with brain mitochondria from WT mice. Similarly, experiments with cultured striatal neurons demonstrate no difference in cellular respiratory activity and  $\text{Ca}^{2+}$  handling between neurons from R6/2 and WT mice.

In this study, we used isolated brain mitochondria from symptomatic 6- to 8-week-old R6/2 mice and age-matched WT mice. The R6/2 mice used in these experiments displayed a clasping phenotype typical for HD animals (Mangiarini *et al.*



1996). The presence of clasping behavior assured us that if mitochondrial respiratory abnormalities and aberrant  $\text{Ca}^{2+}$  handling by mitochondria were involved in neuronal dysfunction leading to these behavioral deviations, then it should be possible to detect such changes in respiration,  $\text{Ca}^{2+}$  handling, or both. The lack of difference between mitochondria from WT and R6/2 mice suggests that fragments of mHtt do not impair mitochondrial respiratory and  $\text{Ca}^{2+}$  uptake activities. Accordingly, our data argue against defects of mitochondrial functions as a contributing factor to HD pathogenesis in R6/2 mice.

It was recently reported that inhibition of protein import into mitochondria might result in defects in mitochondrial function and it was suggested that impaired mitochondrial protein import could result in decreased expression of nuclear-encoded mitochondrial proteins (Yano *et al.* 2014). Our data with mitochondria isolated from R6/2 mice indicate no difference in expression of several randomly selected nuclear-encoded mitochondrial proteins, suggesting no defects in mitochondrial protein import. This is consistent with the study by Orr *et al.* that found that expression of nuclear encoded MnSOD as well as 30 and 70 kDa subunits of succinate dehydrogenase (Complex II) is similar in brain mitochondria isolated from 3- and 10-month-old heterozygous knock-in 150Q/7Q mice as well as in 3-month-old WT 7Q/7Q mice (Orr *et al.* 2008). Milakovic and Johnson also failed to demonstrate a difference in expression of 30 and 70 kDa subunits of Complex II in mutant  $\text{STHdh}^{\text{Q111/Q111}}$  striatal cells compared with WT  $\text{STHdh}^{\text{Q7/Q7}}$  cells (Milakovic and Johnson 2005).

Previously, Rosenstock *et al.* reported a significant increase in cytosolic  $\text{Ca}^{2+}$  induced by 1 mM glutamate in cortical and striatal slices of 9 month-old R6/1 transgenic mice. Following glutamate removal, FCCP-mediated mitochondrial depolarization led to  $\text{Ca}^{2+}$  release from mitochondria and resulted in an increase in cytosolic  $\text{Ca}^{2+}$  that was similar in slices from both R6/1 and WT animals. This suggests that there are no defects

in mitochondrial  $\text{Ca}^{2+}$  accumulation in brain slices from R6/1 mice (Rosenstock *et al.* 2010).

The lack of defects in  $\text{Ca}^{2+}$  uptake by nonsynaptic mitochondria isolated from brains of R6/2 mice was also found by David Nicholls' group (Oliveira *et al.* 2007). Contrary to expectations, they found a moderate but statistically significant increase in  $\text{Ca}^{2+}$  uptake capacity of mitochondria isolated from brains of R6/2 mice compared with mitochondria from WT animals. Although we did not find a statistically significant increase in  $\text{Ca}^{2+}$  uptake capacity in isolated brain mitochondria from R6/2 mice, we confirm that  $\text{Ca}^{2+}$  uptake capacity in brain mitochondria from R6/2 mice is not impaired. The authors also found an increase in  $\text{Ca}^{2+}$  uptake capacity in nonsynaptic mitochondria from YAC128 mice, which express full-length mHtt, and found no difference in mitochondria from knock-in Hdh<sup>150/+</sup> mice (Oliveira *et al.* 2007). In addition, the authors did not find a significant difference in respiratory activity of striatal neurons from Hdh<sup>150/+</sup> and WT mice.

The reason for the increased  $\text{Ca}^{2+}$  uptake capacity in mitochondria from HD mice is not clear but might be related to compensatory changes in mitochondria and alterations in susceptibility to induction of the permeability transition pore (PTP), which determines mitochondrial  $\text{Ca}^{2+}$  uptake capacity (Chalmers and Nicholls 2003). Interestingly, Choo *et al.* reported a significantly increased level of glutathione in cortical and striatal mitochondria from R6/2 mice (Choo *et al.* 2005). The authors interpreted this finding as an indication of compensatory reaction (i.e. preconditioning) to protect cells against an increase in mitochondrial oxidative stress. An increase in mitochondrial glutathione may also suggest increased resistance to  $\text{Ca}^{2+}$ -induced damage that manifests as induction of the PTP. Indeed, glutathione was found to be protective against  $\text{Ca}^{2+}$ -induced PTP in liver, heart, and brain mitochondria (Chernyak and Bernardi 1996; Heales and Bolanos 2002; Aon *et al.* 2007). Consequently, the same mechanism

might contribute to the lack of difference in Ca<sup>2+</sup> uptake capacity in this study of mitochondria from R6/2 and WT mice.

Mitochondrial CyD is a component of the mitochondrial PTP that sensitizes it to Ca<sup>2+</sup> (Rasola and Bernardi 2007). Genetic ablation of CyD inhibits PTP induction and significantly increases Ca<sup>2+</sup> uptake capacity in brain mitochondria (Baines *et al.* 2005; Li *et al.* 2009). Considering this, it was logical to propose that if mitochondria from HD mice have increased propensity to PTP induction and, concomitant decrease in Ca<sup>2+</sup> uptake capacity and if this defect in Ca<sup>2+</sup> handling plays an important role in HD pathology, then CyD deletion should protect mitochondria, increase Ca<sup>2+</sup> uptake capacity, and rescue behavioral deficits in R6/2 mice. Perry *et al.* reported elegant experiments in which the authors crossed R6/2 with CyD-knockout mice (CyD<sup>-/-</sup>) and evaluated mitochondrial Ca<sup>2+</sup> uptake capacity in mitochondria from cerebral cortex of crosses of CyD<sup>-/-</sup> and R6/2 mice (Perry *et al.* 2010). The authors found a significant increase in Ca<sup>2+</sup> uptake capacity in mitochondria from R6/2: CyD<sup>-/-</sup> mice but no indication of behavioral improvement or alleviation of HD neuropathological features. From these results, the authors concluded that increasing neuronal mitochondrial Ca<sup>2+</sup> uptake capacity is not beneficial in the R6/2 model of HD. Unfortunately, in this study the authors failed to compare Ca<sup>2+</sup> uptake capacity of brain mitochondria from R6/2 and WT mice. Based on our data and results from David Nicholls' group, Ca<sup>2+</sup> uptake capacities of isolated brain mitochondria and mitochondria in cultured neurons from R6/2 mice are not decreased compared with Ca<sup>2+</sup> capacity of mitochondria from WT animals (Oliveira *et al.* 2007). Consequently, alterations in Ca<sup>2+</sup> uptake capacity most likely do not play a role in HD pathogenesis and one should not expect significant improvement in HD pathology due to an increase in mitochondrial Ca<sup>2+</sup> uptake capacity.

Overall, the full body of data presented here and studies from other investigators (Guidetti *et al.* 2001; Chang *et al.* 2006; Olah *et al.* 2008) show no significant differences

in respiratory activity and Ca<sup>2+</sup> handling in mitochondria exposed to human full-length or truncated mHtt. Consequently, based on our results and data from other groups, the dearth of defects in bioenergetics and Ca<sup>2+</sup> handling makes their contribution to HD pathology unlikely. However, this does not rule out the potential contribution of mitochondria to HD pathogenesis. One caveat of the results with isolated mitochondria used in this and the previous section (sections A and C) is that these data were obtained with mitochondria derived from the whole brain of mice. Since the striatum, the most severely affected brain region in HD, comprises a relatively small fraction of total brain volume, it may be possible that use of whole brain mitochondria could mask mitochondrial deficiencies present in only mitochondria from the striatum. Alternatively, the neurotoxic effect of mHtt or its fragments may be due to mechanisms that are not directly related to mitochondrial bioenergetics or Ca<sup>2+</sup> transport but may indirectly affect these functions. In addition, numerous reports indicate alterations in mitochondrial morphology and trafficking in cell and mouse models of HD (Trushina *et al.* 2004; Shirendeb *et al.* 2011; Song *et al.* 2011). Our observations of alterations in mitochondrial morphology in neurons from R6/2 mice made with spinning-disk confocal and electron microscopy are consistent with previously reported mitochondrial morphological abnormalities found in cells expressing mHtt (Tellez-Nagel *et al.* 1974; Squitieri *et al.* 2006; Wang *et al.* 2009; Costa *et al.* 2010; Squitieri *et al.* 2010; Song *et al.* 2011; Bayram-Weston *et al.* 2012b; Shirendeb *et al.* 2012). It is conceivable that these alterations in mitochondrial morphology as well as in non-mitochondrial mechanisms may play a significant role in neuronal dysfunction and over time may lead to the neuronal loss and behavioral deficits seen in HD.

Although the causes and significance of alterations in mitochondrial morphology are not entirely clear, impairment of trafficking and deficits in the mitochondrial fission/fusion cycle have been reported to accompany morphological changes (Li *et al.*

2010). It is still unclear whether trafficking and fission/fusion impairment are causes or consequences of mitochondrial morphological changes. In our experiments, the observation of both fragmented and enlarged mitochondria in cultured striatal neurons from R6/2 mice indicated a potential impairment of proper fusion and fission, resulting in a non-uniform mitochondrial population. Fragmentation of mitochondria in HD neurons could be the result of direct interaction of mHtt with proteins involved in fission/fusion dynamics, as has been previously suggested (Li *et al.* 2010). Alternatively, increased mitochondrial fragmentation could be the result of an attempt to sequester and remove portions of mitochondria that have been somehow damaged by mHtt (Chen and Chan 2009). Although the mechanism leading to increased fragmentation in mHtt-expressing cells remains unclear, a recent study has indicated that inhibition of mitochondrial fragmentation may attenuate neuronal degeneration (Guo *et al.* 2013a).

Alterations to mitochondrial morphology may also be associated with aberrant mitochondrial trafficking (Chen and Chan 2009). Increased fragmentation of mitochondria has been shown to decrease mitochondrial motility (Li and Conforti 2013). On the other hand, changes to the shape of mitochondria as they become fragmented may impede their entry into neuronal processes, thus precluding mitochondria from efficiently moving to locations of high energy demand, such as synaptic terminals (Li *et al.* 2010). It has been reported that mitochondria in cells expressing mHtt move at a slower rate and stop more frequently (Trushina *et al.* 2004; Shirendeb *et al.* 2011; Song *et al.* 2011), which could partially explain the neuronal degeneration seen in HD if mitochondria are not present in sufficient numbers at neuronal terminals to support local energy demand. Though the mechanism of mHtt-induced mitochondrial motility impediment is not entirely resolved, some evidence suggests that a potential interaction of mHtt with tubulin could block the passage of motor proteins loaded with mitochondria (Smith *et al.* 2009). Thus, the interplay among altered mitochondrial morphology,

impaired trafficking, and aberrant mitochondrial fission/fusion may play an important role in neuronal dysfunction and ultimately the neuronal loss seen in HD.

#### **D. Future Directions**

Despite an immense and ongoing effort, the mechanisms responsible for HD pathology remain not completely understood nearly 25 years after the discovery of the mutation linked to HD. Animal models have enabled researchers to gain some understanding regarding the aberrant function of neurons in the presence of mHtt, but the fundamental underlying processes that mediate striatal neuron loss have not been identified. Additionally, it is unclear whether mHtt may affect mitochondrial functions differently in human neurons compared to neurons derived from animal models of HD. Due to the genetic manipulations that are required to generate HD animal models, there could be unintended functional consequences that may obscure an understanding of the mechanisms by which mHtt leads to neuronal degeneration in humans (Mattis *et al.* 2012). Models expressing multiple copies of the mutated allele, transgenes that become randomly inserted into the genome or lack of human mHtt may all complicate interpretation of experimental results with animals (Ramaswamy *et al.* 2007; Pouladi *et al.* 2013). Symptom manifestation and disease progression in animals may also be incongruent with disease development in humans. Moreover, expression levels of Htt and mHtt and the ratio of expression between the two proteins can differ from one animal model to another and, importantly, can differ from the expression of both proteins in humans (Pouladi *et al.* 2013). Since mHtt and Htt are believed to be implicated in regulation of transcription, differing expression of these proteins may result in larger scale alterations in gene expression. Indeed, Buck *et al.* recently reported that expression of sirtuins, proteins involved in the regulation of mitochondrial functions, was different between HD patients and transgenic mouse models of HD (Buck *et al.* 2017).

Although animal models have helped to improve our understanding of the mechanisms of HD, they are imperfect and different models may yield conflicting data.

However, new technologies have allowed for the study of neurons from human HD patients. The development of a process for somatic cell reprogramming into pluripotent stem cells and the generation of differentiation protocols now permits researchers to investigate disease processes in cell types that had been previously unattainable from living humans. Although HD iPSC lines were first established by Park *et al* in 2008, then subsequently by other groups, it was not until after the HD iPSC Consortium generated and characterized 14 additional iPSC lines from HD patients and controls that reprogrammed neurons from human HD patients began to be studied more intensely (Park *et al.* 2008;Zhang *et al.* 2010;Camnasio *et al.* 2012;Mattis *et al.* 2012). Studies with human iPSCs from HD patients have suggested alterations in the lysosomal pathway, alterations in protein expression, and the presence of mHtt aggregates (Castiglioni *et al.* 2012;Chae *et al.* 2012;Nekrasov *et al.* 2016). GABAergic neurons derived from iPSCs of HD patients display increased mitochondrial fragmentation and increased expression of the mitochondrial fission protein dynamin-related protein (DRP1) compared to neurons from control iPSCs (Guo *et al.* 2013b). Mattis *et al.* showed that, following prolonged exposure to glutamate, iPSC-derived neurons from HD patients demonstrated increased propensity to Ca<sup>2+</sup> dysregulation compared to control neurons (Mattis *et al.* 2012). Additionally, neural stem cells derived from human HD iPSCs displayed lower basal and FCCP-induced maximal respiration compared to control iPSCs (An *et al.* 2012). However, in these latter two studies, experiments were performed with cells that were not completely differentiated to DARPP-32 expressing striatal-like neurons, leaving unaddressed the extent of potential mitochondrial alterations in striatal-like neurons derived from HD iPSCs. For these reasons, we have endeavored to establish and characterize HD iPSCs in our lab with the intent of

differentiating these cells into putative striatal neurons and assessing neuronal and mitochondrial functions.

Cultures of undifferentiated human iPSCs derived from fibroblasts of HD and control patients were established at Harvard University by Dr. George Daley. Initially one HD and one control line was established from previously reprogrammed cells that were obtained from the Harvard Stem Cell Institute. Each line was characterized by morphology and the presence of specific markers throughout the differentiation process. Undifferentiated cells from HD and control lines were organized into tightly packed colonies with clearly demarcated edges and each colony displayed a uniform thickness (Fig. 42A). The presence of characteristic gene expression of the undifferentiated state were first demonstrated using reverse transcription PCR followed by cDNA amplification. The pluripotency genes OCT4, NANOG, and SOX2 were expressed. However, BRACHURY (BRACH),  $\alpha$ -Fetoprotein (AFP), and PAX6, markers of the mesoderm, endoderm, and ectoderm, respectively were not yet being expressed (Fig. 42B). Immunocytochemistry of the pluripotency markers NANOG, SOX2, and OCT4 further indicated their expression in both control and HD undifferentiated colonies. Furthermore, immunocytochemical analysis demonstrated the expression of Tra1-60, Tra1-81, and SSEA4 which are indicative of human pluripotent stem cells (Fig. 42C).

Induction of human PSCs to a primitive anterior neuroepithelial fate commences with the detachment of undifferentiated colonies and the maintenance of embryoid bodies in suspension during the first stage of differentiation. After seven days in suspension, embryoid bodies are re-plated. Following reintroduction to attached culture, nascent progenitor colonies display a rounded, thicker center and a more flat periphery characterized by less tightly packed cells and less sharply defined edges (Fig. 43A). RT-PCR analysis demonstrates the expression of the neural markers PAX6 and SOX1. The anterior neural fate is further indicated by expression of OTX2, RAX, and LHX2. The



expression of these neural-associated genes is present in colonies from control and HD colonies (Fig. 43B). Immunocytochemistry demonstrates that PAX6 and OTX2 are widely expressed in control and HD colonies (Fig. 43C).

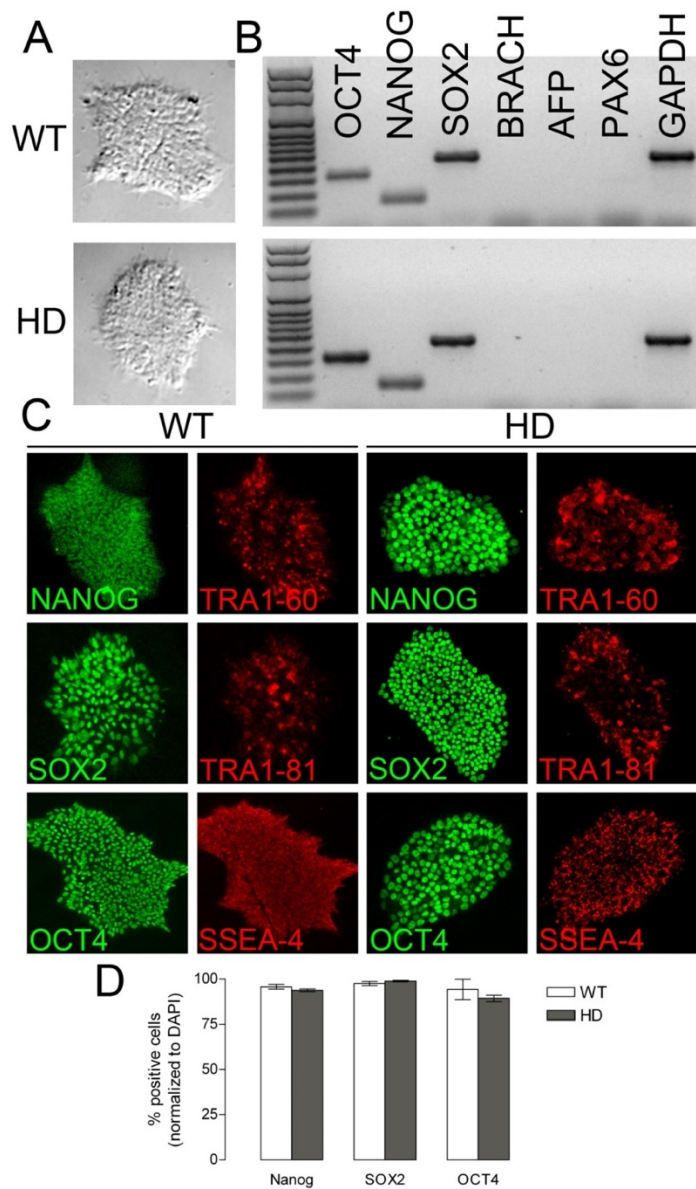


**Figure 42. Characterization of undifferentiated WT and HD hiPSCs.** In **A**, phase contrast images of undifferentiated WT or HD colonies displaying typical round, tightly-packed colonies with sharply defined edges. In **B**, DNA gels using cDNA generated by RT-PCR from WT or HD undifferentiated colonies show the expression of the pluripotency markers OCT4, NANOG, and SOX2. The lack of Brachyury (mesoderm marker) and PAX6 (ectoderm marker) expression indicate colonies have yet to establish germ layers. GAPDH is a constitutively expressed control. In **C**, immunocytochemistry demonstrates the expression of cell surface markers (green) and pluripotency-associated transcription factors (red). In **D**, proportion of WT and HD cells that stained positive for Nanog, SOX2, and OCT4 (normalized to DAPI). Data are mean  $\pm$  SEM.

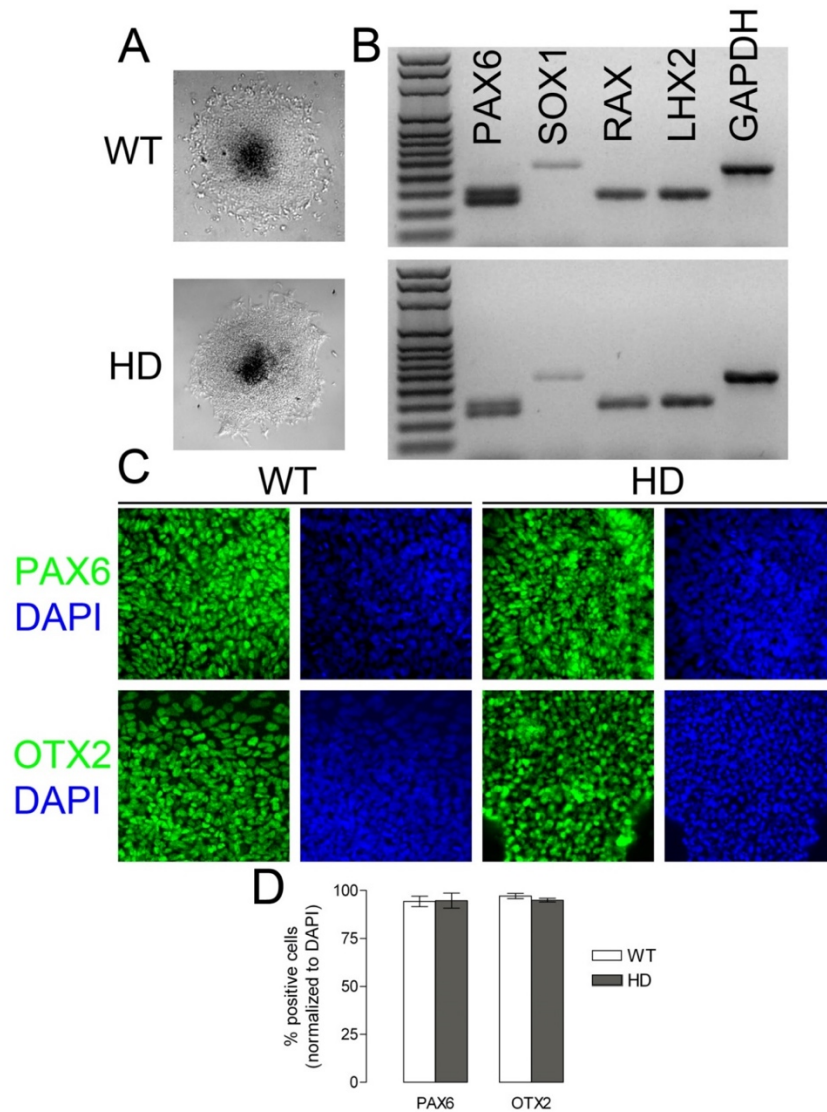


**Figure 43. Characterization of hiPSCs induced to a neural progenitor fate.** In **A**, Phase contrast images of WT and HD hPSC colonies after 10 days of differentiation show a thicker, 3-dimensional center and less defined, flatter periphery. In **B**, DNA gels using cDNA generated by RT-PCR from WT or HD colonies display the expression of neural markers PAX6 and SOX1. RAX and LHX2 expression indicate differentiation to the anterior neural fate. GAPDH is a constitutively expressed control. In **C**, Immunocytochemistry further demonstrates the expression of neural-associated transcription factors. In **D**, Proportion of WT and HD cells that stained positive for Nanog, SOX2, and OCT4 (normalized to DAPI). Data are mean  $\pm$  SEM.

Once the primitive anterior neural fate has been established, colonies are detached from the culture surface and maintained in suspension. Floating colonies will adopt either a neural lineage or a retinal fate that are morphologically distinguishable from each other. The culture is manually enriched for colonies of the neural fate by removing all retinal-fated colonies. Neurospheres fated for neuronal differentiation are characterized by a dark and rounded appearance (Figure 44A). The neural-associated transcription factors PAX6, NEUROD1, and FABP7 are expressed in neurospheres from control and HD lines. Expression of forebrain-associated transcription factors SOX1, DLX1, and EMX1 further indicate the refinement of the neurospheres to the neural lineage and the divergence of cells from the retinal fate. Importantly, cells from the enriched neurosphere population do not express RAX, a marker of the retinal fate (Fig. 44B). Immunocytochemistry indicates the expression of forebrain-associated markers OTX2, SOX1, and DLX5. Nascent neurons are indicated by expression of MAP2 (Fig. 44C).

After being maintained in suspension for 15-20 days, the neurospheres are carefully dissociated by brief incubation in accutase followed by gentle trituration yielding aggregates that are 200-400  $\mu\text{m}$  in diameter. Aggregates are re-plated in the presence of growth factors and maintained for an additional 14 days to generate cortical neurons. Human PSC-derived cortical neurons display typical neuronal morphology, including axonal outgrowth and branching, and stain for the neuronal markers MAP2 and Neurofilament. Supplementation of the culture medium with purlmorphamine induces the differentiation of lateral ganglion eminence progenitors, resulting in expression of gamma-aminobutyric acid (GABA)-ergic neurons (Fig. 45).

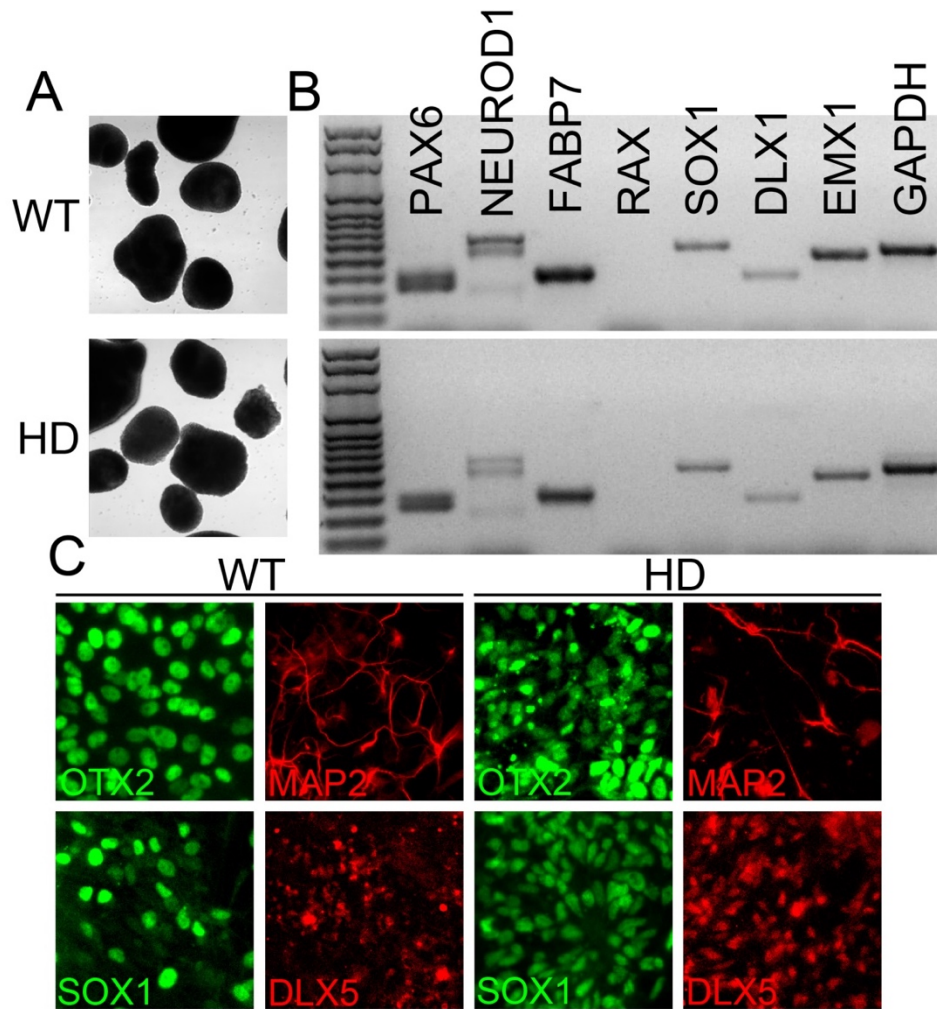


**Figure 44. Characterization of cortical progenitors derived from WT and HD hiPSCs.** In **A**, phase contrast images of neural-fated WT and HD neurospheres in suspension after 40 days of differentiation appear as uniformly round and dark spheres. In **B**, DNA gels using cDNA generated by RT-PCR from WT or HD cortical progenitors display expression of neural-associated transcription factors PAX6, NeuroD1, and FABP7. SOX1, DLX1, and EMX1 more specifically indicate differentiation toward the forebrain fate. Lack of RAX expression indicates a divergence from the retinal lineage. In **C**, immunocytochemistry demonstrates expression of the neural marker SOX1 and markers of the emerging forebrain neurons, OTX2, DLX5, and MAP2.

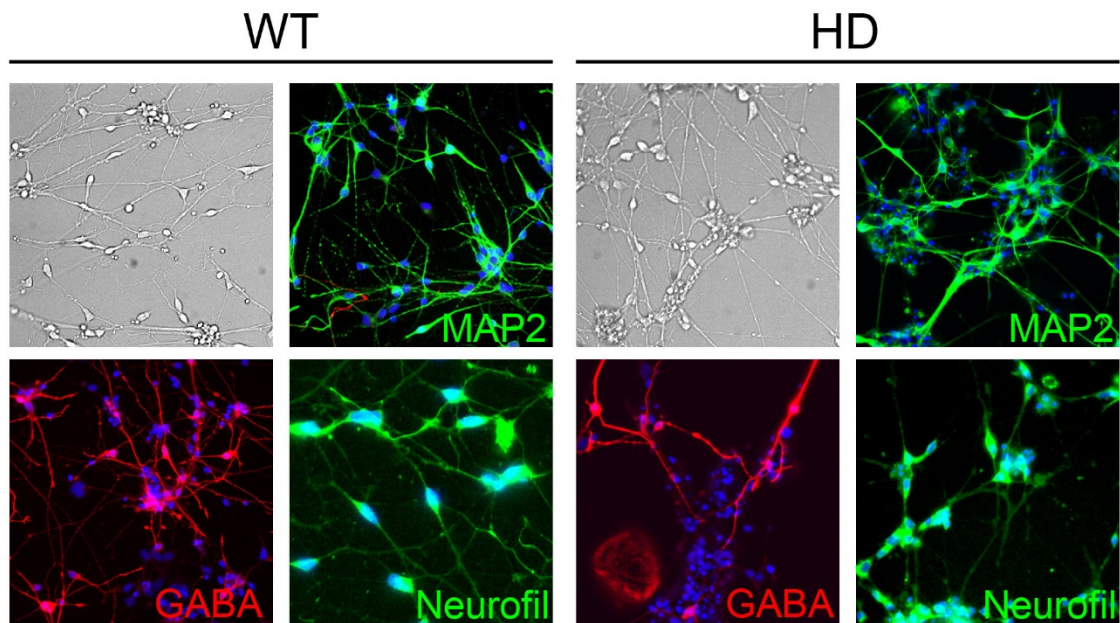


**Figure 45. Characterization of neurons derived from cortical progenitors from WT and HD hiPSCs.** Following 14 days of directed neuronal differentiation, cells display typical neuronal morphologies under phase contrast microscopy and express the neuronal markers MAP2 and Neurofilament-L (Neurofil). Supplementation of the culture medium with purlmorphamine, drives the expression of GABAergic neurons.

The method for generation of striatal-like neuron progenitors diverges from that of cortical progenitors following the establishment of the primitive anterior neural fate. In order to guide cells toward the striatal lineage, previously plated embryoid bodies are maintained in medium supplemented with FGF-8, Shh, valpromide, purmorphamine, and DKK1 until neural rosettes, which are the *in vitro* analog to the neural tube, are formed. Neural rosettes are then selectively removed and re-plated for further growth to generate an enriched culture. Rosettes grow into tightly packed clusters and express neural associated transcription factors as well as forebrain-associated transcription factors (Fig. 46A,B). Immunocytochemistry indicates that nearly all cells express the neural markers OTX2 and SOX1 (Fig. 46C,D). Additionally, these cells express Nestin a marker of neural progenitor cells and Ki-67 a marker indicating that these progenitors are proliferative (Fig. 46C).

After 19 total days in culture, the rosettes are detached from the culture surface and gently dissociated with accutase. Dissociated striatal-like rosettes are re-plated in the presence of BDNF and GDNF as well as purmorphamine, valpromide, and FGF-8 to drive differentiation toward the striatal neuronal fate. The cells are maintained in culture for an additional 14 days to generate MSN-like neurons (Fig. 47). After 14 days, the cells express neuronal markers (MAP2 and Neurofilament) and are GABA-ergic. Moreover, the neurons express the MSN-specific marker DARPP-32 (Fig. 47).

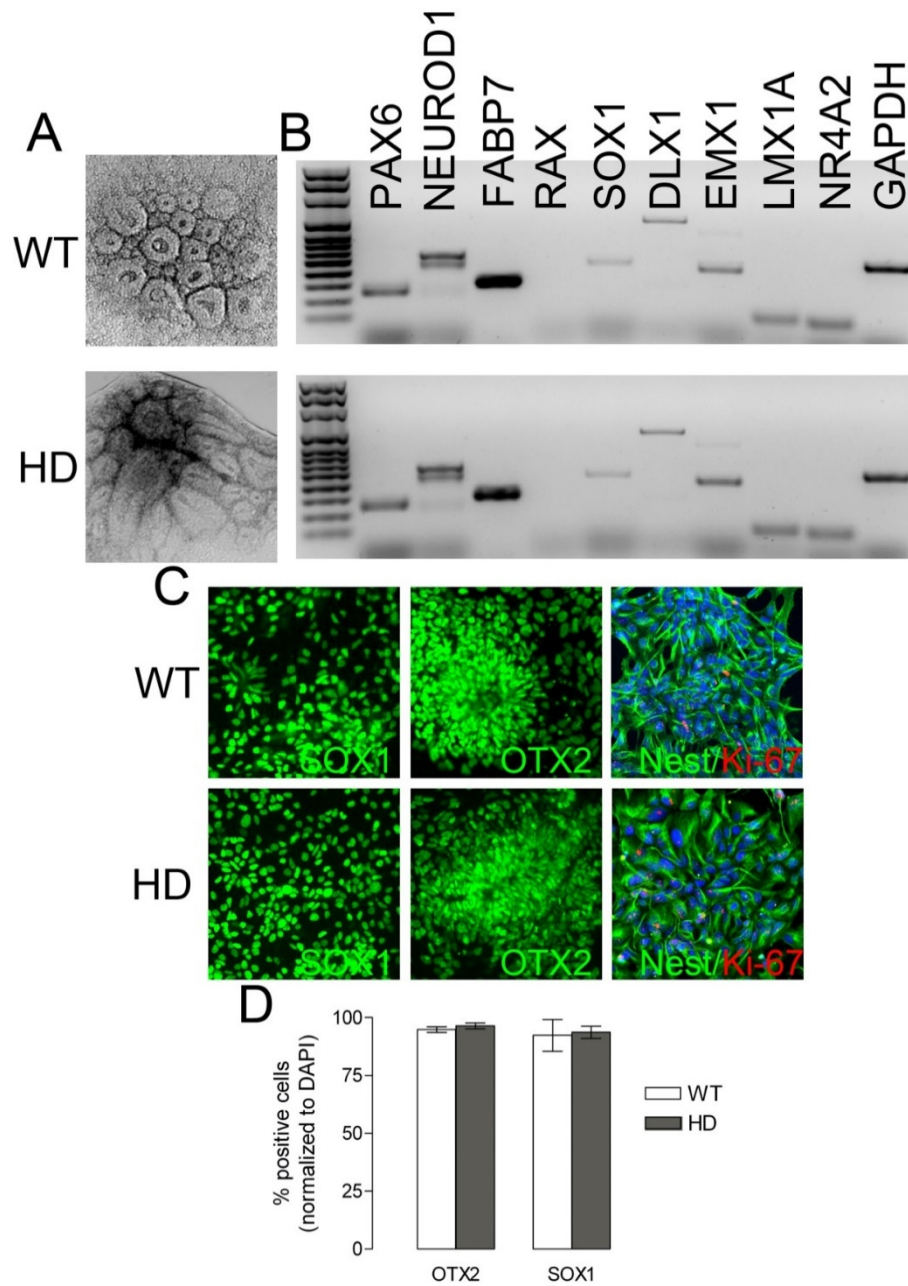


**Figure 46. Characterization of striatal-like progenitors derived from WT and HD hiPSCs.** In **A**, phase contrast images of neural rosette clusters from WT and HD striatal progenitors after 18 days of differentiation. In **B**, DNA gels using cDNA generated by RT-PCR from WT or HD striatal progenitors indicate expression of neural-associated transcription factors (PAX6, NeuroD1, and FABP7) and transcription factors associated with the forebrain lineage (SOX1, DLX1, EMX1). Lack of RAX expression indicates divergence from the retinal fate. Expression of LMX1A and NR4A2 (Nurr1) indicate the potential for these progenitors to differentiate into dopaminergic neurons. In **C**, immunocytochemistry of striatal progenitors demonstrates the expression of neural-associated markers SOX1 and OTX2 as well as Nestin, a marker of progenitor cells, and Ki-67, a proliferation marker. In **D**, proportion of WT and HD cells that stained positive for OTX2 and SOX1 (normalized to DAPI). Data are mean  $\pm$  SEM.



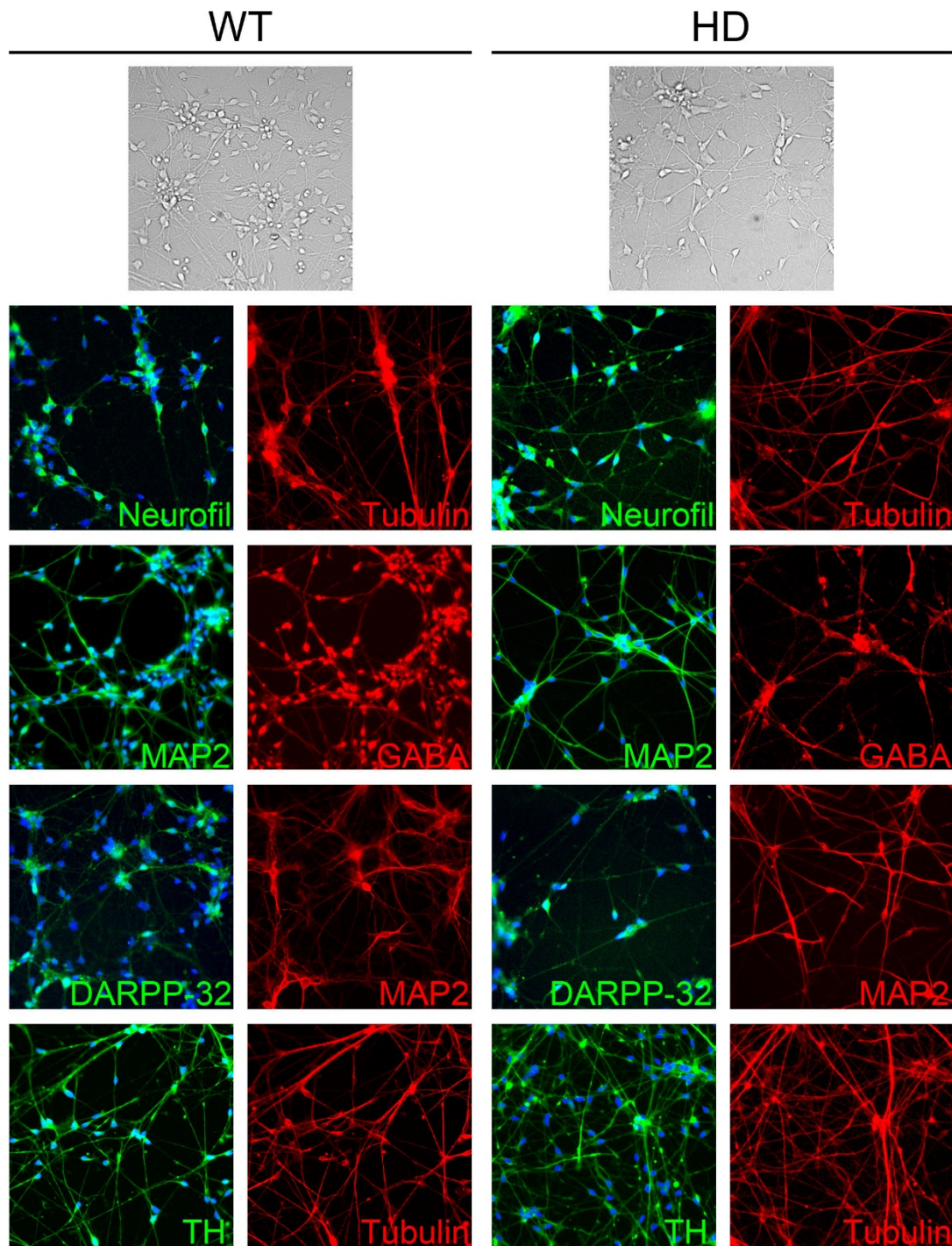


**Figure 47. Characterization of neurons derived from striatal-like progenitors from WT and HD hiPSCs.** Following 14 days of directed neuronal differentiation, cells display typical neuronal morphologies under phase contrast microscopy and express the neuronal markers MAP2 and Neurofilament-L (Neurofil). Supplementation of the culture medium with pumorphamine, valpromide, and FGF-8 results in neurons that are GABA-ergic, DARPP-32-positive and tyrosine hydroxylase (TH)-positive.

To verify the presence of the expanded CAG repeat sequence in cells from the iPSCs from human patients, we performed PCR to amplify the CAG repeat tract (Fig. 48A). Progenitors derived from iPSCs from HD patients possessed one mutated allele with an expansion of 72 CAG repeats, as described previously (Park *et al.* 2008;Zhang *et al.* 2010;An *et al.* 2012). Since the patient from whom these cells were originally taken possessed a CAG expansion with 72 repeats in the mutated allele, this finding indicates that the CAG expansion has not spontaneously contracted or expanded, which has been previously suggested to occur (Duyao *et al.* 1993). To confirm the presence of mHtt in progenitor cell lysates derived from human HD iPSCs, we performed immunoblotting experiments using two different antibodies for total Htt and mHtt: monoclonal anti-Htt antibody 2166 (mAb 2166, Millipore), which recognizes both WT Htt and mHtt, and monoclonal anti-polyQ antibody 1C2 (mAb 1574, Millipore), which recognizes mHtt (Fig. 48B). With mHtt-specific mAb 1C2, a 350 kDa band, representing mHtt, was detected in cell lysates from HD patient-derived cells, but not in cells from controls. Probing with anti-Htt mAb 2166, we detected a 350 kDa band, corresponding to WT Htt, in both WT and HD samples. In cell lysate from HD iPSCs, mAb 2166 detected an additional band with a slightly higher molecular weight that represents mHtt. In HD samples, the level of expression of Htt and mHtt was similar.

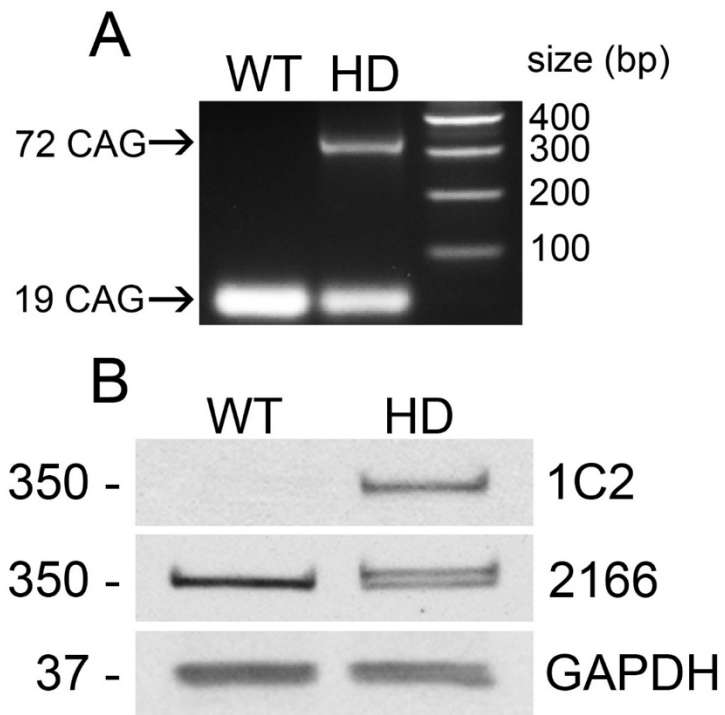


**Figure 48. Genotypic analysis of CAG repeat expansion and expression of mHtt in progenitors derived from human HD iPSCs.** In **A**, DNA gel displaying PCR amplification of the CAG trinucleotide repeat tract from WT and HD samples showing one allele with an expanded CAG stretch in DNA of progenitor cells derived from human HD iPSCs. In **B**, expression of mHtt was detected with anti-polyQ 1C2 antibody as a single band exclusively in samples from HD patients. Htt and mHtt were detected using western blotting with 2166 antibody, which recognizes both Htt and mHtt. In cell lysates from WT and HD progenitors, a 350 kDa band, belonging to WT Htt, was detected, whereas an additional, slightly heavier band representing mHtt was detected in progenitors differentiated from HD patient-derived iPSCs.

Previous studies have indicated  $\text{Ca}^{2+}$  handling defects by mitochondria in cultured neurons from transgenic mouse models of HD. Fernandes *et al.* reported that  $\text{Ca}^{2+}$  influx into cells mediated by NMDA-subtype of ionotropic glutamate receptors resulted in augmented mitochondrial depolarization in MSNs from YAC128 mice and that withdrawal of NMDA resulted in reduced clearance of cytosolic  $\text{Ca}^{2+}$  (Fernandes *et al.* 2007) . We assessed the vulnerability of human iPSC-derived striatal-like neurons from HD patient to excitotoxic insult by monitoring NMDA-induced changes in cytosolic  $\text{Ca}^{2+}$  concentration ( $[\text{Ca}^{2+}]_c$ ) (Fig. 49). Cultured human neurons were loaded with the  $\text{Ca}^{2+}$ -sensitive dye, Fura-2FF-AM, and then recorded for 40 minutes in the presence of 100  $\mu\text{M}$  NMDA (plus 10  $\mu\text{M}$  glycine). In human WT neurons, application of NMDA resulted in a brief spike in  $[\text{Ca}^{2+}]_c$  that returned to nearly baseline level within 3 minutes and remained stable for the duration of the experiment (Fig. 49A). Human HD neurons exposed to NMDA showed an initial increase in  $[\text{Ca}^{2+}]_c$ , but there was no return of  $[\text{Ca}^{2+}]_c$  to a basal level. After 20 minutes, human HD neurons underwent delayed  $\text{Ca}^{2+}$  dysregulation, indicated by sustained increase in  $[\text{Ca}^{2+}]_c$  (Fig. 49B).

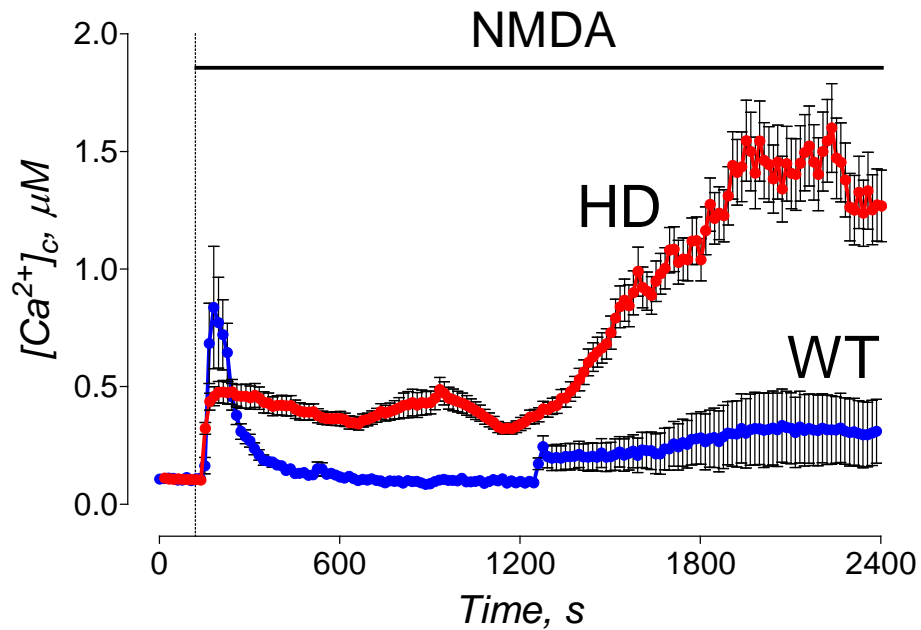


**Figure 49.  $Ca^{2+}$  dynamics in response to NMDA in striatal neurons derived from WT (blue trace) and HD (red trace) human iPSCs.** Striatal neurons (14 DIV) were loaded with  $Ca^{2+}$ -sensitive dye Fura-2FF-AM to monitor changes in cytosolic  $Ca^{2+}$  concentration ( $[Ca^{2+}]_c$ ). Blue and red traces represent average  $[Ca^{2+}]_c \pm SEM$  from experiments with neurons derived from iPSCs from a healthy individual and HD patient, respectively (N = 20-25 neurons per experiment). Where indicated, 100  $\mu M$  NMDA plus 10  $\mu M$  glycine was applied to neurons.

These results demonstrate our ability to direct the differentiation of human iPSCs derived from HD patients into both cortical and striatal neurons. Functional studies indicate that these striatal neurons are responsive to NMDA and that there may be some difference in  $\text{Ca}^{2+}$  signaling between human WT and HD neurons. In future studies, human striatal neurons will be used to assess the effect of mHtt on their functions. Initially, mitochondrial functions of neurons from HD patients will be evaluated by analyzing their respiratory activity, glycolytic activity, and further evaluating mitochondrial  $\text{Ca}^{2+}$  handling functions. If, in experiments with cultured human neurons, we will find signs of mitochondrial dysfunction, then we will use mitochondria isolated from these cells to more stringently evaluate the mechanisms underlying mitochondrial dysfunction. Through the study of iPSC lines from HD patients, we may yet begin to answer the vexing questions that still pervade the field and potentially provide insights about mechanisms of pathology that could ultimately lead to the development of new therapeutics for HD that address underlying causes of the disease.

## V. Reference List

- Aidt F. H., Nielsen S. M., Kanters J., Pesta D., Nielsen T. T., Norremolle A., Hasholt L., Christiansen M. and Hagen C. M. (2013) Dysfunctional mitochondrial respiration in the striatum of the Huntington's disease transgenic R6/2 mouse model. *PLoS. Curr.* **5**.
- An M. C., Zhang N., Scott G., Montoro D., Wittkop T., Mooney S., Melov S. and Ellerby L. M. (2012) Genetic correction of Huntington's disease phenotypes in induced pluripotent stem cells. *Cell Stem Cell* **11**, 253-263.
- Aon M. A., Cortassa S., Maack C. and O'Rourke B. (2007) Sequential opening of mitochondrial ion channels as a function of glutathione redox thiol status. *J. Biol. Chem.* **282**, 21889-21900.
- Arrasate M., Mitra S., Schweitzer E. S., Segal M. R. and Finkbeiner S. (2004) Inclusion body formation reduces levels of mutant huntingtin and the risk of neuronal death. *Nature* **431**, 805-810.
- Ashizawa T., Wong L. J., Richards C. S., Caskey C. T. and Jankovic J. (1994) CAG repeat size and clinical presentation in Huntington's disease. *Neurology* **44**, 1137-1143.
- Aylward E. H., Harrington D. L., Mills J. A., Nopoulos P. C., Ross C. A., Long J. D., Liu D., Westervelt H. K. and Paulsen J. S. (2013) Regional atrophy associated with cognitive and motor function in prodromal Huntington disease. *J. Huntingtons. Dis.* **2**, 477-489.
- Bae B. I., Xu H., Igarashi S., Fujimuro M., Agrawal N., Taya Y., Hayward S. D., Moran T. H., Montell C., Ross C. A., Snyder S. H. and Sawa A. (2005) p53 mediates cellular dysfunction and behavioral abnormalities in Huntington's disease. *Neuron* **47**, 29-41.
- Baines C. P., Kaiser R. A., Purcell N. H., Blair N. S., Osinska H., Hambleton M. A., Brunskill E. W., Sayen M. R., Gottlieb R. A., Dorn G. W., Robbins J. and Molkentin J. D. (2005) Loss of cyclophilin D reveals a critical role for mitochondrial permeability transition in cell death. *Nature* **434**, 658-662.
- Baquet Z. C., Gorski J. A. and Jones K. R. (2004) Early striatal dendrite deficits followed by neuron loss with advanced age in the absence of anterograde cortical brain-derived neurotrophic factor. *J. Neurosci.* **24**, 4250-4258.
- Basso E., Fante L., Fowlkes J., Petronilli V., Forte M. A. and Bernardi P. (2005) Properties of the permeability transition pore in mitochondria devoid of Cyclophilin D. *J. Biol. Chem.* **280**, 18558-18561.
- Bates G. P., Dorsey R., Gusella J. F., Hayden M. R., Kay C., Leavitt B. R., Nance M., Ross C. A., Scahill R. I., Wetzel R., Wild E. J. and Tabrizi S. J. (2015) Huntington disease. *Nat. Rev. Dis. Primers.* **1**, 15005.
- Bates G. P., Harper P. S. and Jones L. (2002) Huntington's Disease, Oxford University Press.
- Baughman J. M., Perocchi F., Girgis H. S., Plovanich M., Belcher-Timme C. A., Sancak Y., Bao X. R., Strittmatter L., Goldberger O., Bogorad R. L., Kotliansky V. and Mootha

- V. K. (2011) Integrative genomics identifies MCU as an essential component of the mitochondrial calcium uniporter. *Nature* **476**, 341-345.
- Bayram-Weston Z., Jones L., Dunnett S. B. and Brooks S. P. (2012a) Light and electron microscopic characterization of the evolution of cellular pathology in HdhQ92 Huntington's disease knock-in mice. *Brain Res. Bull.* **88**, 171-181.
- Bayram-Weston Z., Jones L., Dunnett S. B. and Brooks S. P. (2012b) Light and electron microscopic characterization of the evolution of cellular pathology in the R6/1 Huntington's disease transgenic mice. *Brain Res. Bull.* **88**, 104-112.
- Beal M. F., Hyman B. T. and Koroshetz W. (1993) Do defects in mitochondrial energy metabolism underlie the pathology of neurodegenerative diseases? *Trends Neurosci.* **16**, 125-131.
- Beal M. F., Kowall N. W., Ellison D. W., Mazurek M. F., Swartz K. J. and Martin J. B. (1986) Replication of the neurochemical characteristics of Huntington's disease by quinolinic acid. *Nature* **321**, 168-171.
- Benchoua A., Trioulier Y., Zala D., Gaillard M. C., Lefort N., Dufour N., Saudou F., Elalouf J. M., Hirsch E., Hantraye P., Deglon N. and Brouillet E. (2006) Involvement of mitochondrial complex II defects in neuronal death produced by N-terminus fragment of mutated huntingtin. *Mol. Biol. Cell* **17**, 1652-1663.
- Bernardi P. and Rasola A. (2007) Calcium and cell death: the mitochondrial connection. *Subcell. Biochem.* **45**, 481-506.
- Bernardi P., Scorrano L., Colonna R., Petronilli V. and Di Lisa F. (1999) Mitochondria and cell death. Mechanistic aspects and methodological issues. *Eur. J. Biochem.* **264**, 687-701.
- Bezprozvanny I. and Hayden M. R. (2004) Deranged neuronal calcium signaling and Huntington disease. *Biochem. Biophys. Res. Commun.* **322**, 1310-1317.
- Biglan K. M. (2010) Tapping in Huntington disease: a path forward to preventive therapies? *Neurology* **75**, 2142-2143.
- Biglan K. M., Ross C. A., Langbehn D. R., Aylward E. H., Stout J. C., Queller S., Carlozzi N. E., Duff K., Beglinger L. J. and Paulsen J. S. (2009) Motor abnormalities in premanifest persons with Huntington's disease: the PREDICT-HD study. *Mov Disord.* **24**, 1763-1772.
- Bird T. D., Hewitt J., Conneally P. M. and Hayden M. R. (1986) Linkage of the G8 marker on chromosome 4 to Huntington's disease in a large American black family. *N. Engl. J. Med.* **315**, 1165-1166.
- Borlongan C. V., Koutouzis T. K., Freeman T. B., Cahill D. W. and Sanberg P. R. (1995) Behavioral pathology induced by repeated systemic injections of 3-nitropropionic acid mimics the motoric symptoms of Huntington's disease. *Brain Res.* **697**, 254-257.



- Boussicault L., Herard A. S., Calingasan N., Petit F., Malgorn C., Merienne N., Jan C., Gaillard M. C., Lerchundi R., Barros L. F., Escartin C., Delzescaux T., Mariani J., Hantraye P., Flint B. M., Brouillet E., Vega C. and Bonvento G. (2014) Impaired brain energy metabolism in the BACHD mouse model of Huntington's disease: critical role of astrocyte-neuron interactions. *J. Cereb. Blood Flow Metab* **34**, 1500-1510.
- Brand M. D. and Nicholls D. G. (2011) Assessing mitochondrial dysfunction in cells. *Biochem. J.* **435**, 297-312.
- Brandstaetter H., Kruppa A. J. and Buss F. (2014) Huntingtin is required for ER-to-Golgi transport and for secretory vesicle fusion at the plasma membrane. *Dis. Model. Mech.* **7**, 1335-1340.
- Brennan W. A., Jr., Bird E. D. and Aprille J. R. (1985) Regional mitochondrial respiratory activity in Huntington's disease brain. *J. Neurochem.* **44**, 1948-1950.
- Brouillet E., Conde F., Beal M. F. and Hantraye P. (1999) Replicating Huntington's disease phenotype in experimental animals. *Prog. Neurobiol.* **59**, 427-468.
- Browne S. E., Bowling A. C., MacGarvey U., Baik M. J., Berger S. C., Muqit M. M., Bird E. D. and Beal M. F. (1997) Oxidative damage and metabolic dysfunction in Huntington's disease: selective vulnerability of the basal ganglia. *Ann. Neurol.* **41**, 646-653.
- Bruss M. D., Khambatta C. F., Ruby M. A., Aggarwal I. and Hellerstein M. K. (2010) Calorie restriction increases fatty acid synthesis and whole body fat oxidation rates. *Am. J. Physiol. Endocrinol. Metab* **298**, E108-E116.
- Brustovetsky N. (2016) Mutant Huntingtin and Elusive Defects in Oxidative Metabolism and Mitochondrial Calcium Handling. *Mol. Neurobiol.* **53**, 2944-2953.
- Brustovetsky N. and Dubinsky J. M. (2000a) Dual responses of CNS mitochondria to elevated calcium. *J. Neurosci.* **20**, 103-113.
- Brustovetsky N. and Dubinsky J. M. (2000b) Limitations of cyclosporin A inhibition of the permeability transition in CNS mitochondria. *J. Neurosci.* **20**, 8229-8237.
- Brustovetsky N., Jemmerson R. and Dubinsky J. M. (2002) Calcium-induced Cytochrome c release from rat brain mitochondria is altered by digitonin. *Neurosci. Lett.* **332**, 91-94.
- Brustovetsky N., LaFrance R., Purl K. J., Brustovetsky T., Keene C. D., Low W. C. and Dubinsky J. M. (2005a) Age-dependent changes in the calcium sensitivity of striatal mitochondria in mouse models of Huntington's Disease. *J. Neurochem.* **93**, 1361-1370.
- Brustovetsky T. and Brustovetsky N. (2017) Monitoring of permeability transition pore in isolated individual brain mitochondria, in *Techniques to Investigate Mitochondrial Function in Neurons*, (Strack S. and Usachev Y., eds), Humana Press.
- Brustovetsky T., Li T., Yang Y., Zhang J. T., Antonsson B. and Brustovetsky N. (2010) BAX insertion, oligomerization, and outer membrane permeabilization in brain

mitochondria: role of permeability transition and SH-redox regulation. *Biochim. Biophys. Acta* **1797**, 1795-1806.

Brustovetsky T., Shalbuyeva N. and Brustovetsky N. (2005b) Lack of manifestations of diazoxide/5-hydroxydecanoate-sensitive KATP channel in rat brain nonsynaptosomal mitochondria. *J. Physiol* **568**, 47-59.

Buck E., Bayer H., Lindenberg K. S., Hanselmann J., Pasquarelli N., Ludolph A. C., Weydt P., and Witting A. (2017) Comparison of sirtuin 3 levels in ALS and Huntington's disease-differential effects in human tissue samples vs. transgenic mouse models. *Front. Mol. Neurosci.* **10**, 156-171

Camnasio S., Delli C. A., Lombardo A., Grad I., Mariotti C., Castucci A., Rozell B., Lo R. P., Castiglioni V., Zuccato C., Rochon C., Takashima Y., Diaferia G., Biunno I., Gellera C., Jaconi M., Smith A., Hovatta O., Naldini L., Di D. S., Feki A. and Cattaneo E. (2012) The first reported generation of several induced pluripotent stem cell lines from homozygous and heterozygous Huntington's disease patients demonstrates mutation related enhanced lysosomal activity. *Neurobiol. Dis.* **46**, 41-51.

Carre M., Andre N., Carles G., Borghi H., Brichese L., Briand C. and Braguer D. (2002) Tubulin is an inherent component of mitochondrial membranes that interacts with the voltage-dependent anion channel. *J. Biol. Chem.* **277**, 33664-33669.

Castiglioni V., Onorati M., Rochon C. and Cattaneo E. (2012) Induced pluripotent stem cell lines from Huntington's disease mice undergo neuronal differentiation while showing alterations in the lysosomal pathway. *Neurobiol. Dis.* **46**, 30-40.

Cha J. H. (2007) Transcriptional signatures in Huntington's disease. *Prog. Neurobiol.* **83**, 228-248.

Chae J. I., Kim D. W., Lee N., Jeon Y. J., Jeon I., Kwon J., Kim J., Soh Y., Lee D. S., Seo K. S., Choi N. J., Park B. C., Kang S. H., Ryu J., Oh S. H., Shin D. A., Lee D. R., Do J. T., Park I. H., Daley G. Q. and Song J. (2012) Quantitative proteomic analysis of induced pluripotent stem cells derived from a human Huntington's disease patient. *Biochem. J.* **446**, 359-371.

Chalmers S. and Nicholls D. G. (2003) The relationship between free and total calcium concentrations in the matrix of liver and brain mitochondria. *J. Biol. Chem.* **278**, 19062-19070.

Chang D. T., Rintoul G. L., Pandipati S. and Reynolds I. J. (2006) Mutant huntingtin aggregates impair mitochondrial movement and trafficking in cortical neurons. *Neurobiol. Dis.* **22**, 388-400.

Chen H. and Chan D. C. (2009) Mitochondrial dynamics--fusion, fission, movement, and mitophagy--in neurodegenerative diseases. *Hum. Mol. Genet.* **18**, R169-R176.

Chen J. J., Ondo W. G., Dashtipour K. and Swope D. M. (2012) Tetrabenazine for the treatment of hyperkinetic movement disorders: a review of the literature. *Clin. Ther.* **34**, 1487-1504.

- Chen M., Ona V. O., Li M., Ferrante R. J., Fink K. B., Zhu S., Bian J., Guo L., Farrell L. A., Hersch S. M., Hobbs W., Vonsattel J. P., Cha J. H. and Friedlander R. M. (2000) Minocycline inhibits caspase-1 and caspase-3 expression and delays mortality in a transgenic mouse model of Huntington disease. *Nat. Med.* **6**, 797-801.
- Chen S., Bertheliev V., Hamilton J. B., O'Nuallain B. and Wetzel R. (2002) Amyloid-like features of polyglutamine aggregates and their assembly kinetics. *Biochemistry* **41**, 7391-7399.
- Chernyak B. V. and Bernardi P. (1996) The mitochondrial permeability transition pore is modulated by oxidative agents through both pyridine nucleotides and glutathione at two separate sites. *Eur. J. Biochem.* **238**, 623-630.
- Choo Y. S., Johnson G. V., MacDonald M., Detloff P. J. and Lesort M. (2004) Mutant huntingtin directly increases susceptibility of mitochondria to the calcium-induced permeability transition and cytochrome c release. *Hum. Mol. Genet.* **13**, 1407-1420.
- Choo Y. S., Mao Z., Johnson G. V. and Lesort M. (2005) Increased glutathione levels in cortical and striatal mitochondria of the R6/2 Huntington's disease mouse model. *Neurosci. Lett.* **386**, 63-68.
- Cooper J. K., Schilling G., Peters M. F., Herring W. J., Sharp A. H., Kaminsky Z., Masone J., Khan F. A., Delanoy M., Borchelt D. R., Dawson V. L., Dawson T. M. and Ross C. A. (1998) Truncated N-terminal fragments of huntingtin with expanded glutamine repeats form nuclear and cytoplasmic aggregates in cell culture. *Hum. Mol. Genet.* **7**, 783-790.
- Costa V., Giacomello M., Hudec R., Lopreiato R., Ermak G., Lim D., Malorni W., Davies K. J., Carafoli E. and Scorrano L. (2010) Mitochondrial fission and cristae disruption increase the response of cell models of Huntington's disease to apoptotic stimuli. *EMBO Mol. Med.* **2**, 490-503.
- Cui L., Jeong H., Borovecki F., Parkhurst C. N., Tanese N. and Krainc D. (2006) Transcriptional repression of PGC-1alpha by mutant huntingtin leads to mitochondrial dysfunction and neurodegeneration. *Cell* **127**, 59-69.
- Damiano M., Diguët E., Malgorn C., D'Aurelio M., Galvan L., Petit F., Benhaim L., Guillermier M., Houitte D., Dufour N., Hantraye P., Canals J. M., Alberch J., Delzescaux T., Deglon N., Beal M. F. and Brouillet E. (2013) A role of mitochondrial complex II defects in genetic models of Huntington's disease expressing N-terminal fragments of mutant huntingtin. *Hum. Mol. Genet.* **22**, 3869-3882.
- Davies S. W., Turmaine M., Cozens B. A., DiFiglia M., Sharp A. H., Ross C. A., Scherzinger E., Wanker E. E., Mangiarini L. and Bates G. P. (1997) Formation of neuronal intranuclear inclusions underlies the neurological dysfunction in mice transgenic for the HD mutation. *Cell* **90**, 537-548.
- De M. A., Scarlatti C., Costiniti V., Primerano S., Lopreiato R., Cali T., Brini M., Giacomello M. and Carafoli E. (2016) Calcium handling by endoplasmic reticulum and mitochondria in a cell model of Huntington's disease. *PLoS. Curr.* **8**.

- De S. D., Raffaello A., Teardo E., Szabo I. and Rizzuto R. (2011) A forty-kilodalton protein of the inner membrane is the mitochondrial calcium uniporter. *Nature* **476**, 336-340.
- DePaoli-Roach A. A., Segvich D. M., Meyer C. M., Rahimi Y., Worby C. A., Gentry M. S. and Roach P. J. (2012) Laforin and malin knockout mice have normal glucose disposal and insulin sensitivity. *Hum. Mol. Genet.* **21**, 1604-1610.
- Dietz R. M., Kiedrowski L. and Shuttleworth C. W. (2007) Contribution of Na(+)/Ca(2+) exchange to excessive Ca(2+) loading in dendrites and somata of CA1 neurons in acute slice. *Hippocampus* **17**, 1049-1059.
- DiFiglia M., Sapp E., Chase K., Schwarz C., Meloni A., Young C., Martin E., Vonsattel J. P., Carraway R., Reeves S. A. and . (1995) Huntingtin is a cytoplasmic protein associated with vesicles in human and rat brain neurons. *Neuron* **14**, 1075-1081.
- DiFiglia M., Sapp E., Chase K. O., Davies S. W., Bates G. P., Vonsattel J. P. and Aronin N. (1997) Aggregation of huntingtin in neuronal intranuclear inclusions and dystrophic neurites in brain. *Science* **277**, 1990-1993.
- Dragatsis I., Levine M. S. and Zeitlin S. (2000) Inactivation of Hdh in the brain and testis results in progressive neurodegeneration and sterility in mice. *Nat. Genet.* **26**, 300-306.
- Dubinsky J. M. (1993) Intracellular calcium levels during the period of delayed excitotoxicity. *J. Neurosci.* **13**, 623-631.
- Dunah A. W., Jeong H., Griffin A., Kim Y. M., Standaert D. G., Hersch S. M., Mouradian M. M., Young A. B., Tanese N. and Krainc D. (2002) Sp1 and TAFII130 transcriptional activity disrupted in early Huntington's disease. *Science* **296**, 2238-2243.
- Duyao M., Ambrose C., Myers R., Novelletto A., Persichetti F., Frontali M., Folstein S., Ross C., Franz M., Abbott M. and . (1993) Trinucleotide repeat length instability and age of onset in Huntington's disease. *Nat. Genet.* **4**, 387-392.
- Ehrlich M. E. (2012) Huntington's disease and the striatal medium spiny neuron: cell-autonomous and non-cell-autonomous mechanisms of disease. *Neurotherapeutics.* **9**, 270-284.
- English T. (2014) Katherine Grainger: 'It's not fair, it's not how life should be'.
- Fan M. M. and Raymond L. A. (2007) N-methyl-D-aspartate (NMDA) receptor function and excitotoxicity in Huntington's disease. *Prog. Neurobiol.* **81**, 272-293.
- Fasano A. and Bentivoglio A. R. (2009) Tetrabenazine. *Expert. Opin. Pharmacother.* **10**, 2883-2896.
- Fernandes H. B., Baimbridge K. G., Church J., Hayden M. R. and Raymond L. A. (2007) Mitochondrial sensitivity and altered calcium handling underlie enhanced NMDA-induced apoptosis in YAC128 model of Huntington's disease. *J. Neurosci.* **27**, 13614-13623.

- Fusco F. R., Chen Q., Lamoreaux W. J., Figueredo-Cardenas G., Jiao Y., Coffman J. A., Surmeier D. J., Honig M. G., Carlock L. R. and Reiner A. (1999) Cellular localization of huntingtin in striatal and cortical neurons in rats: lack of correlation with neuronal vulnerability in Huntington's disease. *J. Neurosci.* **19**, 1189-1202.
- Gaba A. M., Zhang K., Marder K., Moskowitz C. B., Werner P. and Boozer C. N. (2005) Energy balance in early-stage Huntington disease. *Am. J. Clin. Nutr.* **81**, 1335-1341.
- Gauthier L. R., Charrin B. C., Borrell-Pages M., Dompierre J. P., Rangone H., Cordelieres F. P., De M. J., MacDonald M. E., Lessmann V., Humbert S. and Saudou F. (2004) Huntingtin controls neurotrophic support and survival of neurons by enhancing BDNF vesicular transport along microtubules. *Cell* **118**, 127-138.
- Gellerich F. N., Gizatullina Z. Z., Nguyen H. P., Trumbeckaite S., Vielhaber S., Seppet E., Zierz S., Landwehrmeyer B., Ries O., von Hoersten S. and Striggow F. (2008) Impaired regulation of brain mitochondria by extramitochondrial Ca<sup>2+</sup> in transgenic Huntington disease rats. *J. Biol. Chem.* **283**, 30715-30724.
- Gines S., Ivanova E., Seong I. S., Saura C. A. and MacDonald M. E. (2003) Enhanced Akt signaling is an early pro-survival response that reflects N-methyl-D-aspartate receptor activation in Huntington's disease knock-in striatal cells. *J. Biol. Chem.* **278**, 50514-50522.
- Gizatullina Z. Z., Lindenberg K. S., Harjes P., Chen Y., Kosinski C. M., Landwehrmeyer B. G., Ludolph A. C., Striggow F., Zierz S. and Gellerich F. N. (2006) Low stability of Huntington muscle mitochondria against Ca<sup>2+</sup> in R6/2 mice. *Ann. Neurol.* **59**, 407-411.
- Goldberg Y. P., Nicholson D. W., Rasper D. M., Kalchman M. A., Koide H. B., Graham R. K., Bromm M., Kazemi-Esfarjani P., Thornberry N. A., Vaillancourt J. P. and Hayden M. R. (1996) Cleavage of huntingtin by apopain, a proapoptotic cysteine protease, is modulated by the polyglutamine tract. *Nat. Genet.* **13**, 442-449.
- Goodman A. O., Murgatroyd P. R., Medina-Gomez G., Wood N. I., Finer N., Vidal-Puig A. J., Morton A. J. and Barker R. A. (2008) The metabolic profile of early Huntington's disease--a combined human and transgenic mouse study. *Exp. Neurol.* **210**, 691-698.
- Gouarne C., Tardif G., Tracz J., Latyszenok V., Michaud M., Clemens L. E., Yu-Taeger L., Nguyen H. P., Bordet T. and Pruss R. M. (2013) Early deficits in glycolysis are specific to striatal neurons from a rat model of huntington disease. *PLoS. ONE.* **8**, e81528.
- Govert F. and Schneider S. A. (2013) Huntington's disease and Huntington's disease-like syndromes: an overview. *Curr. Opin. Neurol.* **26**, 420-427.
- Graham R. K., Deng Y., Slow E. J., Haigh B., Bissada N., Lu G., Pearson J., Shehadeh J., Bertram L., Murphy Z., Warby S. C., Doty C. N., Roy S., Wellington C. L., Leavitt B. R., Raymond L. A., Nicholson D. W. and Hayden M. R. (2006) Cleavage at the caspase-6 site is required for neuronal dysfunction and degeneration due to mutant huntingtin. *Cell* **125**, 1179-1191.

- Grynkiewicz G., Poenie M. and Tsien R. Y. (1985) A new generation of Ca<sup>2+</sup> indicators with greatly improved fluorescence properties. *J. Biol. Chem.* **260**, 3440-3450.
- Gu M., Gash M. T., Mann V. M., Javoy-Agid F., Cooper J. M. and Schapira A. H. (1996) Mitochondrial defect in Huntington's disease caudate nucleus. *Ann. Neurol.* **39**, 385-389.
- Guidetti P., Charles V., Chen E. Y., Reddy P. H., Kordower J. H., Whetsell W. O., Jr., Schwarcz R. and Tagle D. A. (2001) Early degenerative changes in transgenic mice expressing mutant huntingtin involve dendritic abnormalities but no impairment of mitochondrial energy production. *Exp. Neurol.* **169**, 340-350.
- Guo X., Disatnik M. H., Monbureau M., Shamloo M., Mochly-Rosen D. and Qi X. (2013a) Inhibition of mitochondrial fragmentation diminishes Huntington's disease-associated neurodegeneration. *J. Clin. Invest* **123**, 5371-5388.
- Guo X., Disatnik M. H., Monbureau M., Shamloo M., Mochly-Rosen D. and Qi X. (2013b) Inhibition of mitochondrial fragmentation diminishes Huntington's disease-associated neurodegeneration. *J. Clin. Invest* **123**, 5371-5388.
- Haines J. L. and Conneally P. M. (1986) Causes of death in Huntington disease as reported on death certificates. *Genet. Epidemiol.* **3**, 417-423.
- Han I., You Y., Kordower J. H., Brady S. T. and Morfini G. A. (2010) Differential vulnerability of neurons in Huntington's disease: The role of cell type-specific features. *J. Neurochem.* **113**, 1073-1091.
- Harjes P. and Wanker E. E. (2003) The hunt for huntingtin function: interaction partners tell many different stories. *Trends Biochem. Sci.* **28**, 425-433.
- Heales S. J. and Bolanos J. P. (2002) Impairment of brain mitochondrial function by reactive nitrogen species: the role of glutathione in dictating susceptibility. *Neurochem. Int.* **40**, 469-474.
- Heemskerk A. W. and Roos R. A. (2012) Aspiration pneumonia and death in Huntington's disease. *PLoS. Curr.* **4**, RRN1293.
- Heng M. Y., Tallaksen-Greene S. J., Detloff P. J. and Albin R. L. (2007) Longitudinal evaluation of the Hdh(CAG)150 knock-in murine model of Huntington's disease. *J. Neurosci.* **27**, 8989-8998.
- Higgins D. S., Hoyt K. R., Baic C., Vensel J. and Sulka M. (1999) Metabolic and glutamatergic disturbances in the Huntington's disease transgenic mouse. *Ann. N. Y. Acad. Sci.* **893**, 298-300.
- Hodgson J. G., Agopyan N., Gutekunst C. A., Leavitt B. R., LePiane F., Singaraja R., Smith D. J., Bissada N., McCutcheon K., Nasir J., Jamot L., Li X. J., Stevens M. E., Rosemond E., Roder J. C., Phillips A. G., Rubin E. M., Hersch S. M. and Hayden M. R. (1999) A YAC mouse model for Huntington's disease with full-length mutant huntingtin, cytoplasmic toxicity, and selective striatal neurodegeneration. *Neuron* **23**, 181-192.

- Houten S. M. and Auwerx J. (2004) PGC-1alpha: turbocharging mitochondria. *Cell* **119**, 5-7.
- Huntington G. (1872) On Chorea. *The Medical and Surgical Reporter: A Weekly Journal* **26**, 317-321.
- Ismailoglu I., Chen Q., Popowski M., Yang L., Gross S. S. and Brivanlou A. H. (2014) Huntingtin protein is essential for mitochondrial metabolism, bioenergetics and structure in murine embryonic stem cells. *Dev. Biol.* **391**, 230-240.
- Jacobsen J. C., Bawden C. S., Rudiger S. R., McLaughlan C. J., Reid S. J., Waldvogel H. J., MacDonald M. E., Gusella J. F., Walker S. K., Kelly J. M., Webb G. C., Faull R. L., Rees M. I. and Snell R. G. (2010) An ovine transgenic Huntington's disease model. *Hum. Mol. Genet.*
- Jia K., Hart A. C. and Levine B. (2007) Autophagy genes protect against disease caused by polyglutamine expansion proteins in *Caenorhabditis elegans*. *Autophagy*. **3**, 21-25.
- Kamo N., Muratsugu M., Hongoh R. and Kobatake Y. (1979) Membrane potential of mitochondria measured with an electrode sensitive to tetraphenyl phosphonium and relationship between proton electrochemical potential and phosphorylation potential in steady state. *J. Membr. Biol.* **49**, 105-121.
- Kaur N., Kumar P., Jamwal S., Deshmukh R. and Gauttam V. (2016) Tetrabenazine: Spotlight on Drug Review. *Ann. Neurosci.* **23**, 176-185.
- Kegel K. B., Meloni A. R., Yi Y., Kim Y. J., Doyle E., Cuiffo B. G., Sapp E., Wang Y., Qin Z. H., Chen J. D., Nevins J. R., Aronin N. and DiFiglia M. (2002) Huntingtin is present in the nucleus, interacts with the transcriptional corepressor C-terminal binding protein, and represses transcription. *J. Biol. Chem.* **277**, 7466-7476.
- Kells A. P., Fong D. M., Dragunow M., During M. J., Young D. and Connor B. (2004) AAV-mediated gene delivery of BDNF or GDNF is neuroprotective in a model of Huntington disease. *Mol. Ther.* **9**, 682-688.
- Kim M., Lee H. S., LaForet G., McIntyre C., Martin E. J., Chang P., Kim T. W., Williams M., Reddy P. H., Tagle D., Boyce F. M., Won L., Heller A., Aronin N. and DiFiglia M. (1999) Mutant huntingtin expression in clonal striatal cells: dissociation of inclusion formation and neuronal survival by caspase inhibition. *J. Neurosci.* **19**, 964-973.
- Kim S. H., Thomas C. A., Andre V. M., Cummings D. M., Cepeda C., Levine M. S. and Ehrlich M. E. (2011) Forebrain striatal-specific expression of mutant huntingtin protein in vivo induces cell-autonomous age-dependent alterations in sensitivity to excitotoxicity and mitochondrial function. *ASN. Neuro.* **3**, e00060.
- Kimmich G. A., Randles J. and Brand J. S. (1975) Assay of picomole amounts of ATP, ADP, and AMP using the luciferase enzyme system. *Anal. Biochem.* **69**, 187-206.
- Kuhl D. E., Markham C. H., Metter E. J., Riege W. H., Phelps M. E. and Mazziotta J. C. (1985) Local cerebral glucose utilization in symptomatic and presymptomatic Huntington's disease. *Res. Publ. Assoc. Res. Nerv. Ment. Dis.* **63**, 199-209.

- Lai J. C. K. and Clark J. B. (1989) Isolation and characterization of synaptic and nonsynaptic mitochondria from mammalian brain., in *Neuromethods*, (A.A.Boulton, G.B.Baker and R.F.Butterworth, eds), pp. 43-98. Humana Press, Clifton, NJ.
- Leavitt B. R., Guttman J. A., Hodgson J. G., Kimel G. H., Singaraja R., Vogl A. W. and Hayden M. R. (2001) Wild-type huntingtin reduces the cellular toxicity of mutant huntingtin in vivo. *Am. J. Hum. Genet.* **68**, 313-324.
- Lee J. M., Ivanova E. V., Seong I. S., Cashorali T., Kohane I., Gusella J. F. and MacDonald M. E. (2007) Unbiased gene expression analysis implicates the huntingtin polyglutamine tract in extra-mitochondrial energy metabolism. *PLoS. Genet.* **3**, e135.
- Lehninger A. L., Nelson D. L. and Cox M. M. (1993) *Principles of Biochemistry*. Worth Publishers, New York.
- Li H., Li S. H., Johnston H., Shelbourne P. F. and Li X. J. (2000) Amino-terminal fragments of mutant huntingtin show selective accumulation in striatal neurons and synaptic toxicity. *Nat. Genet.* **25**, 385-389.
- Li J. Y. and Conforti L. (2013) Axonopathy in Huntington's disease. *Exp. Neurol.* **246**, 62-71.
- Li L. and Van B. C. (1995) Na(+)-Ca2+ exchange in intact endothelium of rabbit cardiac valve. *Circ. Res.* **76**, 396-404.
- Li S. H. and Li X. J. (2004) Huntingtin-protein interactions and the pathogenesis of Huntington's disease. *Trends Genet.* **20**, 146-154.
- Li V., Brustovetsky T. and Brustovetsky N. (2009) Role of cyclophilin D-dependent mitochondrial permeability transition in glutamate-induced calcium deregulation and excitotoxic neuronal death. *Exp. Neurol.* **218**, 171-182.
- Li X. J., Orr A. L. and Li S. (2010) Impaired mitochondrial trafficking in Huntington's disease. *Biochim. Biophys. Acta* **1802**, 62-65.
- Lim D., Fedrizzi L., Tartari M., Zuccato C., Cattaneo E., Brini M. and Carafoli E. (2008) Calcium homeostasis and mitochondrial dysfunction in striatal neurons of Huntington disease. *J. Biol. Chem.* **283**, 5780-5789.
- Lim N. K., Hung L. W., Pang T. Y., Mclean C. A., Liddell J. R., Hilton J. B., Li Q. X., White A. R., Hannan A. J. and Crouch P. J. (2014) Localized changes to glycogen synthase kinase-3 and collapsin response mediator protein-2 in the Huntington's disease affected brain. *Hum. Mol. Genet.* **23**, 4051-4063.
- Lou S., Lepak V. C., Eberly L. E., Roth B., Cui W., Zhu X. H., Oz G. and Dubinsky J. M. (2016) Oxygen consumption deficit in Huntington disease mouse brain under metabolic stress. *Hum. Mol. Genet.*
- MacDonald M. E., Ambrose C. M., Duyao M. P., Myers R. H., Lin C., Srinidhi L., Barnes G., Taylor S. A., James M., Groot N., MacFarlane H., Jenkins B., Anderson M. A., Wexler N. S., Gusella J. F., Bates G. P., Baxendale S., Hummerich H., Kirby S., North



M., Youngman S., Mott R., Zehetner G., Sedlacek Z., Poustka A., Frischauf A. M., Lehrach H., Buckler A. J., Church D., Doucette-Stamm L., O'Donovan M. C., Riba-Ramirez L., Shah M., Stanton V. P., Strobel S. A., Draths K. M., Wales J. L., Dervan P., Housman D. E., Altherr M., Shiang R., Thompson L., Fielder T., Wasmuth J. J., Tagle D., Valdes J., Elmer L., Allard M., Castilla L., Swaroop M., Blanchard K., Collins F. S., Snell R., Holloway T., Gillespie K., Datson N., Shaw D. and Harper P. S. (1993) A novel gene containing a trinucleotide repeat that is expanded and unstable on Huntington's disease chromosomes. *Cell* **72**, 971-983.

Mangiarini L., Sathasivam K., Seller M., Cozens B., Harper A., Hetherington C., Lawton M., Trotter Y., Lehrach H., Davies S. W. and Bates G. P. (1996) Exon 1 of the HD gene with an expanded CAG repeat is sufficient to cause a progressive neurological phenotype in transgenic mice. *Cell* **87**, 493-506.

Martinez-Vicente M., Tallozy Z., Wong E., Tang G., Koga H., Kaushik S., de V. R., Arias E., Harris S., Sulzer D. and Cuervo A. M. (2010) Cargo recognition failure is responsible for inefficient autophagy in Huntington's disease. *Nat. Neurosci.* **13**, 567-576.

Mattis V. B., Svendsen S. P., Ebert A., Svendsen C. N., King A. R., Casale M., Winokur S. T., Castiglioni V., Cattaneo E. and Arjomand J. (2012) Induced pluripotent stem cells from patients with Huntington's disease show CAG-repeat-expansion-associated phenotypes. *Cell Stem Cell* **11**, 264-278.

McGeer E. G. and McGeer P. L. (1976) Duplication of biochemical changes of Huntington's chorea by intrastriatal injections of glutamic and kainic acids. *Nature* **263**, 517-519.

Menalled L. B. (2005) Knock-in mouse models of Huntington's disease. *NeuroRx*. **2**, 465-470.

Menzies F. M., Fleming A., Caricasole A., Bento C. F., Andrews S. P., Ashkenazi A., Fullgrabe J., Jackson A., Jimenez S. M., Karabiyik C., Licitra F., Lopez R. A., Pavel M., Puri C., Renna M., Ricketts T., Schlotawa L., Vicinanza M., Won H., Zhu Y., Skidmore J. and Rubinsztein D. C. (2017) Autophagy and Neurodegeneration: Pathogenic Mechanisms and Therapeutic Opportunities. *Neuron* **93**, 1015-1034.

Mihm M. J., Amann D. M., Schanbacher B. L., Altschuld R. A., Bauer J. A. and Hoyt K. R. (2007) Cardiac dysfunction in the R6/2 mouse model of Huntington's disease. *Neurobiol. Dis.* **25**, 297-308.

Milakovic T. and Johnson G. V. (2005) Mitochondrial respiration and ATP production are significantly impaired in striatal cells expressing mutant huntingtin. *J. Biol. Chem.* **280**, 30773-30782.

Milakovic T., Quintanilla R. A. and Johnson G. V. (2006) Mutant huntingtin expression induces mitochondrial calcium handling defects in clonal striatal cells: functional consequences. *J. Biol. Chem.* **281**, 34785-34795.

- Milnerwood A. J., Cummings D. M., Dallerac G. M., Brown J. Y., Vatsavayai S. C., Hirst M. C., Rezaie P. and Murphy K. P. (2006) Early development of aberrant synaptic plasticity in a mouse model of Huntington's disease. *Hum. Mol. Genet.* **15**, 1690-1703.
- Mitchell P. (1961) Coupling of phosphorylation to electron and hydrogen transfer by a chemi-osmotic type of mechanism. *Nature* **191**, 144-148.
- Myers R. H. (2004) Huntington's disease genetics. *NeuroRx*. **1**, 255-262.
- Nance M. A. and Myers R. H. (2001) Juvenile onset Huntington's disease--clinical and research perspectives. *Ment. Retard. Dev. Disabil. Res. Rev.* **7**, 153-157.
- Napoli E., Wong S., Hung C., Ross-Inta C., Bomdica P. and Giulivi C. (2013) Defective mitochondrial disulfide relay system, altered mitochondrial morphology and function in Huntington's disease. *Hum. Mol. Genet.* **22**, 989-1004.
- Nekrasov E. D., Vigont V. A., Klyushnikov S. A., Lebedeva O. S., Vassina E. M., Bogomazova A. N., Chestkov I. V., Semashko T. A., Kiseleva E., Suldina L. A., Bobrovsky P. A., Zimina O. A., Ryazantseva M. A., Skopin A. Y., Illarioshkin S. N., Kaznacheyeva E. V., Lagarkova M. A. and Kiselev S. L. (2016) Manifestation of Huntington's disease pathology in human induced pluripotent stem cell-derived neurons. *Mol. Neurodegener.* **11**, 27.
- Neuwald A. F. and Hirano T. (2000) HEAT repeats associated with condensins, cohesins, and other complexes involved in chromosome-related functions. *Genome Res.* **10**, 1445-1452.
- Nishino H., Hida H., Kumazaki M., Shimano Y., Nakajima K., Shimizu H., Ooiwa T. and Baba H. (2000) The striatum is the most vulnerable region in the brain to mitochondrial energy compromise: a hypothesis to explain its specific vulnerability. *J. Neurotrauma* **17**, 251-260.
- Novgorodov S. A., Gudz T. I., Milgrom Y. M. and Brierley G. P. (1992) The permeability transition in heart mitochondria is regulated synergistically by ADP and cyclosporin A. *J. Biol. Chem.* **267**, 16274-16282.
- Oestreicher A. B., van den Bergh S. G. and Slater E. C. (1969) The inhibition by 2,4-dinitrophenol of the removal of oxaloacetate formed by the oxidation of succinate by rat-liver and -heart mitochondria. *Biochim. Biophys. Acta* **180**, 45-55.
- Olah J., Klivenyi P., Gardian G., Vecsei L., Orosz F., Kovacs G. G., Westerhoff H. V. and Ovadi J. (2008) Increased glucose metabolism and ATP level in brain tissue of Huntington's disease transgenic mice. *FEBS J.* **275**, 4740-4755.
- Oliveira J. M. (2010a) Mitochondrial bioenergetics and dynamics in Huntington's disease: tripartite synapses and selective striatal degeneration. *J. Bioenerg. Biomembr.*
- Oliveira J. M. (2010b) Nature and cause of mitochondrial dysfunction in Huntington's disease: focusing on huntingtin and the striatum. *J. Neurochem.*

- Oliveira J. M., Jekabsons M. B., Chen S., Lin A., Rego A. C., Goncalves J., Ellerby L. M. and Nicholls D. G. (2007) Mitochondrial dysfunction in Huntington's disease: the bioenergetics of isolated and in situ mitochondria from transgenic mice. *J. Neurochem.* **101**, 241-249.
- Orr A. L., Li S., Wang C. E., Li H., Wang J., Rong J., Xu X., Mastroberardino P. G., Greenamyre J. T. and Li X. J. (2008) N-terminal mutant huntingtin associates with mitochondria and impairs mitochondrial trafficking. *J. Neurosci.* **28**, 2783-2792.
- Pan X., Liu J., Nguyen T., Liu C., Sun J., Teng Y., Fergusson M. M., Rovira I. I., Allen M., Springer D. A., Aponte A. M., Gucek M., Balaban R. S., Murphy E. and Finkel T. (2013) The physiological role of mitochondrial calcium revealed by mice lacking the mitochondrial calcium uniporter. *Nat. Cell Biol.* **15**, 1464-1472.
- Panov A., Dikalov S., Shalbuyeva N., Hemendinger R., Greenamyre J. T. and Rosenfeld J. (2007) Species- and tissue-specific relationships between mitochondrial permeability transition and generation of ROS in brain and liver mitochondria of rats and mice. *Am. J. Physiol Cell Physiol* **292**, C708-C718.
- Panov A. V., Burke J. R., Strittmatter W. J. and Greenamyre J. T. (2003) In vitro effects of polyglutamine tracts on Ca<sup>2+</sup>-dependent depolarization of rat and human mitochondria: relevance to Huntington's disease. *Arch. Biochem. Biophys.* **410**, 1-6.
- Panov A. V., Gutekunst C. A., Leavitt B. R., Hayden M. R., Burke J. R., Strittmatter W. J. and Greenamyre J. T. (2002) Early mitochondrial calcium defects in Huntington's disease are a direct effect of polyglutamines. *Nat. Neurosci.* **5**, 731-736.
- Park I. H., Arora N., Huo H., Maherali N., Ahfeldt T., Shimamura A., Lensch M. W., Cowan C., Hochedlinger K. and Daley G. Q. (2008) Disease-specific induced pluripotent stem cells. *Cell* **134**, 877-886.
- Paulson H. L. and Albin R. L. (2011) Huntington's Disease: Clinical Features and Routes to Therapy.
- Pellman J. J., Hamilton J., Brustovetsky T. and Brustovetsky N. (2015) Ca<sup>2+</sup> handling in isolated brain mitochondria and cultured neurons derived from the YAC128 mouse model of Huntington's disease. *J. Neurochem.* **134**, 652-667.
- Perry G. M., Tallaksen-Greene S., Kumar A., Heng M. Y., Kneynsberg A., van G. T., Detloff P. J., Albin R. L. and Lesort M. (2010) Mitochondrial calcium uptake capacity as a therapeutic target in the R6/2 mouse model of Huntington's disease. *Hum. Mol. Genet.* **19**, 3354-3371.
- Petersen A., Hansson O. and Brundin P. (2001) [Huntington disease--yet another mad protein?]. *Lakartidningen* **98**, 5756-8, 5761.
- Pouladi M. A., Morton A. J. and Hayden M. R. (2013) Choosing an animal model for the study of Huntington's disease. *Nat. Rev. Neurosci.* **14**, 708-721.

- Powers W. J., Haas R. H., Le T., Videen T. O., Hershey T., McGee-Minnich L. and Perlmutter J. S. (2007a) Normal platelet mitochondrial complex I activity in Huntington's disease. *Neurobiol. Dis.* **27**, 99-101.
- Powers W. J., Videen T. O., Markham J., McGee-Minnich L., Antenor-Dorsey J. V., Hershey T. and Perlmutter J. S. (2007b) Selective defect of in vivo glycolysis in early Huntington's disease striatum. *Proc. Natl. Acad. Sci. U. S. A* **104**, 2945-2949.
- Pringsheim T., Wiltshire K., Day L., Dykeman J., Steeves T. and Jette N. (2012) The incidence and prevalence of Huntington's disease: a systematic review and meta-analysis. *Mov Disord.* **27**, 1083-1091.
- Puranam K. L., Wu G., Strittmatter W. J. and Burke J. R. (2006) Polyglutamine expansion inhibits respiration by increasing reactive oxygen species in isolated mitochondria. *Biochem. Biophys. Res. Commun.* **341**, 607-613.
- Qin Z. H., Wang Y., Kegel K. B., Kazantsev A., Apostol B. L., Thompson L. M., Yoder J., Aronin N. and DiFiglia M. (2003) Autophagy regulates the processing of amino terminal huntingtin fragments. *Hum. Mol. Genet.* **12**, 3231-3244.
- Quintanilla R. A., Jin Y. N., von B. R. and Johnson G. V. (2013) Mitochondrial permeability transition pore induces mitochondria injury in Huntington disease. *Mol. Neurodegener.* **8**, 45.
- Ramaswamy S., McBride J. L. and Kordower J. H. (2007) Animal models of Huntington's disease. *ILAR Journal* **48**, 356-373.
- Rasola A. and Bernardi P. (2007) The mitochondrial permeability transition pore and its involvement in cell death and in disease pathogenesis. *Apoptosis.* **12**, 815-833.
- Ravikumar B., Duden R. and Rubinsztein D. C. (2002) Aggregate-prone proteins with polyglutamine and polyalanine expansions are degraded by autophagy. *Hum. Mol. Genet.* **11**, 1107-1117.
- Ravikumar B., Vacher C., Berger Z., Davies J. E., Luo S., Oroz L. G., Scaravilli F., Easton D. F., Duden R., O'Kane C. J. and Rubinsztein D. C. (2004) Inhibition of mTOR induces autophagy and reduces toxicity of polyglutamine expansions in fly and mouse models of Huntington disease. *Nat. Genet.* **36**, 585-595.
- Reddy P. H., Charles V., Williams M., Miller G., Whetsell W. O., Jr. and Tagle D. A. (1999) Transgenic mice expressing mutated full-length HD cDNA: a paradigm for locomotor changes and selective neuronal loss in Huntington's disease. *Philos. Trans. R. Soc. Lond B Biol. Sci.* **354**, 1035-1045.
- Reilmann R., Leavitt B. R. and Ross C. A. (2014) Diagnostic criteria for Huntington's disease based on natural history. *Mov Disord.* **29**, 1335-1341.
- Reiner A., Albin R. L., Anderson K. D., D'Amato C. J., Penney J. B. and Young A. B. (1988) Differential loss of striatal projection neurons in Huntington disease. *Proc. Natl. Acad. Sci. U. S. A* **85**, 5733-5737.

- Ridley R. M., Frith C. D., Crow T. J. and Conneally P. M. (1988) Anticipation in Huntington's disease is inherited through the male line but may originate in the female. *J. Med. Genet.* **25**, 589-595.
- Rigamonti D., Bauer J. H., De-Fraja C., Conti L., Sipione S., Sciorati C., Clementi E., Hackam A., Hayden M. R., Li Y., Cooper J. K., Ross C. A., Govoni S., Vincenz C. and Cattaneo E. (2000) Wild-type huntingtin protects from apoptosis upstream of caspase-3. *J. Neurosci.* **20**, 3705-3713.
- Rockabrand E., Slepko N., Pantalone A., Nukala V. N., Kazantsev A., Marsh J. L., Sullivan P. G., Steffan J. S., Sensi S. L. and Thompson L. M. (2007) The first 17 amino acids of Huntingtin modulate its sub-cellular localization, aggregation and effects on calcium homeostasis. *Hum. Mol. Genet.* **16**, 61-77.
- Roos R. A. (2010) Huntington's disease: a clinical review. *Orphanet. J. Rare. Dis.* **5**, 40.
- Rosas H. D., Koroshetz W. J., Chen Y. I., Skeuse C., Vangel M., Cudkowicz M. E., Caplan K., Marek K., Seidman L. J., Makris N., Jenkins B. G. and Goldstein J. M. (2003) Evidence for more widespread cerebral pathology in early HD: an MRI-based morphometric analysis. *Neurology* **60**, 1615-1620.
- Rosen G. D. and Williams R. W. (2001) Complex trait analysis of the mouse striatum: independent QTLs modulate volume and neuron number. *BMC. Neurosci.* **2**, 5.
- Rosenstock T. R., Bertoncini C. R., Teles A. V., Hirata H., Fernandes M. J. and Smaili S. S. (2010) Glutamate-induced alterations in Ca<sup>2+</sup> signaling are modulated by mitochondrial Ca<sup>2+</sup> handling capacity in brain slices of R6/1 transgenic mice. *Eur. J. Neurosci.* **32**, 60-70.
- Roze E., Bonnet C., Betuing S. and Caboche J. (2010) Huntington's disease. *Adv. Exp. Med. Biol.* **685**, 45-63.
- Sathasivam K., Lane A., Legleiter J., Warley A., Woodman B., Finkbeiner S., Paganetti P., Muchowski P. J., Wilson S. and Bates G. P. (2010) Identical oligomeric and fibrillar structures captured from the brains of R6/2 and knock-in mouse models of Huntington's disease. *Hum. Mol. Genet.* **19**, 65-78.
- Schilling G., Sharp A. H., Loev S. J., Wagster M. V., Li S. H., Stine O. C. and Ross C. A. (1995) Expression of the Huntington's disease (IT15) protein product in HD patients. *Hum. Mol. Genet.* **4**, 1365-1371.
- Scorrano L., Ashiya M., Buttle K., Weiler S., Oakes S. A., Mannella C. A. and Korsmeyer S. J. (2002) A distinct pathway remodels mitochondrial cristae and mobilizes cytochrome c during apoptosis. *Dev. Cell* **2**, 55-67.
- Seong I. S., Ivanova E., Lee J. M., Choo Y. S., Fossale E., Anderson M., Gusella J. F., Laramie J. M., Myers R. H., Lesort M. and MacDonald M. E. (2005) HD CAG repeat implicates a dominant property of huntingtin in mitochondrial energy metabolism. *Hum. Mol. Genet.* **14**, 2871-2880.

- Shalbuyeva N., Brustovetsky T., Bolshakov A. and Brustovetsky N. (2006) Calcium-dependent spontaneously reversible remodeling of brain mitochondria. *J. Biol. Chem.* **281**, 37547-37558.
- Sharp A. H., Loev S. J., Schilling G., Li S. H., Li X. J., Bao J., Wagster M. V., Kotzuk J. A., Steiner J. P., Lo A. and . (1995) Widespread expression of Huntington's disease gene (IT15) protein product. *Neuron* **14**, 1065-1074.
- Shimohata M., Shimohata T., Igarashi S., Naruse S. and Tsuji S. (2005) Interference of CREB-dependent transcriptional activation by expanded polyglutamine stretches--augmentation of transcriptional activation as a potential therapeutic strategy for polyglutamine diseases. *J. Neurochem.* **93**, 654-663.
- Shirasaki D. I., Greiner E. R., Al-Ramahi I., Gray M., Boontheung P., Geschwind D. H., Botas J., Coppola G., Horvath S., Loo J. A. and Yang X. W. (2012) Network organization of the huntingtin proteomic interactome in mammalian brain. *Neuron* **75**, 41-57.
- Shirendeb U., Reddy A. P., Manczak M., Calkins M. J., Mao P., Tagle D. A. and Reddy P. H. (2011) Abnormal mitochondrial dynamics, mitochondrial loss and mutant huntingtin oligomers in Huntington's disease: implications for selective neuronal damage. *Hum. Mol. Genet.* **20**, 1438-1455.
- Shirendeb U. P., Calkins M. J., Manczak M., Anekonda V., Dufour B., McBride J. L., Mao P. and Reddy P. H. (2012) Mutant huntingtin's interaction with mitochondrial protein Drp1 impairs mitochondrial biogenesis and causes defective axonal transport and synaptic degeneration in Huntington's disease. *Hum. Mol. Genet.* **21**, 406-420.
- Shoulson I. and Young A. B. (2011) Milestones in huntington disease. *Mov Disord.* **26**, 1127-1133.
- Siddiqui A., Rivera-Sanchez S., Castro M. R., Acevedo-Torres K., Rane A., Torres-Ramos C. A., Nicholls D. G., Andersen J. K. and Ayala-Torres S. (2012) Mitochondrial DNA damage is associated with reduced mitochondrial bioenergetics in Huntington's disease. *Free Radic. Biol. Med.* **53**, 1478-1488.
- Singaraja R. R., Huang K., Sanders S. S., Milnerwood A. J., Hines R., Lerch J. P., Franciosi S., Drisdell R. C., Vaid K., Young F. B., Doty C., Wan J., Bissada N., Henkelman R. M., Green W. N., Davis N. G., Raymond L. A. and Hayden M. R. (2011) Altered palmitoylation and neuropathological deficits in mice lacking HIP14. *Hum. Mol. Genet.* **20**, 3899-3909.
- Skulachev V. P. (1991) Fatty acid circuit as a physiological mechanism of uncoupling of oxidative phosphorylation. *FEBS Lett.* **294**, 158-162.
- Slow E. J., van R. J., Rogers D., Coleman S. H., Graham R. K., Deng Y., Oh R., Bissada N., Hossain S. M., Yang Y. Z., Li X. J., Simpson E. M., Gutekunst C. A., Leavitt B. R. and Hayden M. R. (2003) Selective striatal neuronal loss in a YAC128 mouse model of Huntington disease. *Hum. Mol. Genet.* **12**, 1555-1567.
- Smith R., Bacos K., Fedele V., Soulet D., Walz H. A., Obermuller S., Lindqvist A., Bjorkqvist M., Klein P., Onnerfjord P., Brundin P., Mulder H. and Li J. Y. (2009) Mutant

huntingtin interacts with {beta}-tubulin and disrupts vesicular transport and insulin secretion. *Hum. Mol. Genet.* **18**, 3942-3954.

Song W., Chen J., Petrilli A., Liot G., Klinglmayr E., Zhou Y., Poquiz P., Tjong J., Pouladi M. A., Hayden M. R., Masliah E., Ellisman M., Rouiller I., Schwarzenbacher R., Bossy B., Perkins G. and Bossy-Wetzel E. (2011) Mutant huntingtin binds the mitochondrial fission GTPase dynamin-related protein-1 and increases its enzymatic activity. *Nat. Med.* **17**, 377-382.

Spector A. A., John K. and Fletcher J. E. (1969) Binding of long-chain fatty acids to bovine serum albumin. *J. Lipid Res.* **10**, 56-67.

Squitieri F., Cannella M., Sgarbi G., Maglione V., Falleni A., Lenzi P., Baracca A., Cislighi G., Saft C., Ragona G., Russo M. A., Thompson L. M., Solaini G. and Fornai F. (2006) Severe ultrastructural mitochondrial changes in lymphoblasts homozygous for Huntington disease mutation. *Mech. Ageing Dev.* **127**, 217-220.

Squitieri F., Falleni A., Cannella M., Orobello S., Fulceri F., Lenzi P. and Fornai F. (2010) Abnormal morphology of peripheral cell tissues from patients with Huntington disease. *J. Neural Transm.* **117**, 77-83.

Stack E. C., Kubilus J. K., Smith K., Cormier K., Del Signore S. J., Guelin E., Ryu H., Hersch S. M. and Ferrante R. J. (2005) Chronology of behavioral symptoms and neuropathological sequela in R6/2 Huntington's disease transgenic mice. *J. Comp Neurol.* **490**, 354-370.

Stanika R. I., Pivovarova N. B., Brantner C. A., Watts C. A., Winters C. A. and Andrews S. B. (2009) Coupling diverse routes of calcium entry to mitochondrial dysfunction and glutamate excitotoxicity. *Proc. Natl. Acad. Sci. U. S. A* **106**, 9854-9859.

Steffan J. S., Kazantsev A., Spasic-Boskovic O., Greenwald M., Zhu Y. Z., Gohler H., Wanker E. E., Bates G. P., Housman D. E. and Thompson L. M. (2000) The Huntington's disease protein interacts with p53 and CREB-binding protein and represses transcription. *Proc. Natl. Acad. Sci. U. S. A* **97**, 6763-6768.

Sugars K. L. and Rubinsztein D. C. (2003) Transcriptional abnormalities in Huntington disease. *Trends Genet.* **19**, 233-238.

Tabrizi S. J., Workman J., Hart P. E., Mangiarini L., Mahal A., Bates G., Cooper J. M. and Schapira A. H. (2000) Mitochondrial dysfunction and free radical damage in the Huntington R6/2 transgenic mouse. *Ann. Neurol.* **47**, 80-86.

Tang T. S., Tu H., Chan E. Y., Maximov A., Wang Z., Wellington C. L., Hayden M. R. and Bezprozvanny I. (2003) Huntingtin and huntingtin-associated protein 1 influence neuronal calcium signaling mediated by inositol-(1,4,5) triphosphate receptor type 1. *Neuron* **39**, 227-239.

Tanveer A., Virji S., Andreeva L., Totty N. F., Hsuan J. J., Ward J. M. and Crompton M. (1996) Involvement of cyclophilin D in the activation of a mitochondrial pore by Ca<sup>2+</sup> and oxidant stress. *Eur. J. Biochem.* **238**, 166-172.

- Tellez-Nagel I., Johnson A. B. and Terry R. D. (1974) Studies on brain biopsies of patients with Huntington's chorea. *J. Neuropathol. Exp. Neurol.* **33**, 308-332.
- Tian J., Yan Y. P., Zhou R., Lou H. F., Rong Y. and Zhang B. R. (2014) Soluble N-terminal fragment of mutant Huntingtin protein impairs mitochondrial axonal transport in cultured hippocampal neurons. *Neurosci. Bull.* **30**, 74-80.
- Tkac I., Henry P. G., Zacharoff L., Wedel M., Gong W., Deelchand D. K., Li T. and Dubinsky J. M. (2012) Homeostatic adaptations in brain energy metabolism in mouse models of Huntington disease. *J. Cereb. Blood Flow Metab* **32**, 1977-1988.
- Trettel F., Rigamonti D., Hilditch-Maguire P., Wheeler V. C., Sharp A. H., Persichetti F., Cattaneo E. and MacDonald M. E. (2000) Dominant phenotypes produced by the HD mutation in STHdh(Q111) striatal cells. *Hum. Mol. Genet.* **9**, 2799-2809.
- Trottier Y., Devys D., Imbert G., Saudou F., An I., Lutz Y., Weber C., Agid Y., Hirsch E. C. and Mandel J. L. (1995) Cellular localization of the Huntington's disease protein and discrimination of the normal and mutated form. *Nat. Genet.* **10**, 104-110.
- Trushina E., Canaria C. A., Lee D. Y. and McMurray C. T. (2014) Loss of caveolin-1 expression in knock-in mouse model of Huntington's disease suppresses pathophysiology in vivo. *Hum. Mol. Genet.* **23**, 129-144.
- Trushina E., Dyer R. B., Badger J. D., Ure D., Eide L., Tran D. D., Vrieze B. T., Legendre-Guillemin V., McPherson P. S., Mandavilli B. S., Van H. B., Zeitlin S., McNiven M., Aebersold R., Hayden M., Parisi J. E., Seeberg E., Dragatsis I., Doyle K., Bender A., Chacko C. and McMurray C. T. (2004) Mutant huntingtin impairs axonal trafficking in mammalian neurons in vivo and in vitro. *Mol. Cell Biol.* **24**, 8195-8209.
- Turner C., Cooper J. M. and Schapira A. H. (2007) Clinical correlates of mitochondrial function in Huntington's disease muscle. *Mov Disord.* **22**, 1715-1721.
- Tydlacka S., Wang C. E., Wang X., Li S. and Li X. J. (2008) Differential activities of the ubiquitin-proteasome system in neurons versus glia may account for the preferential accumulation of misfolded proteins in neurons. *J. Neurosci.* **28**, 13285-13295.
- Valencia A., Sapp E., Kimm J. S., McClory H., Reeves P. B., Alexander J., Ansong K. A., Masso N., Frosch M. P., Kegel K. B., Li X. and DiFiglia M. (2013) Elevated NADPH oxidase activity contributes to oxidative stress and cell death in Huntington's disease. *Hum. Mol. Genet.* **22**, 1112-1131.
- van der Burg J. M., Bacos K., Wood N. I., Lindqvist A., Wierup N., Woodman B., Wamsteeker J. I., Smith R., Deierborg T., Kuhar M. J., Bates G. P., Mulder H., Erlanson-Albertsson C., Morton A. J., Brundin P., Petersen A. and Bjorkqvist M. (2008) Increased metabolism in the R6/2 mouse model of Huntington's disease. *Neurobiol. Dis.* **29**, 41-51.
- Van Raamsdonk J. M., Murphy Z., Slow E. J., Leavitt B. R. and Hayden M. R. (2005a) Selective degeneration and nuclear localization of mutant huntingtin in the YAC128 mouse model of Huntington disease. *Hum. Mol. Genet.* **14**, 3823-3835.



- Van Raamsdonk J. M., Pearson J., Murphy Z., Hayden M. R. and Leavitt B. R. (2006) Wild-type huntingtin ameliorates striatal neuronal atrophy but does not prevent other abnormalities in the YAC128 mouse model of Huntington disease. *BMC. Neurosci.* **7**, 80.
- Van Raamsdonk J. M., Pearson J., Slow E. J., Hossain S. M., Leavitt B. R. and Hayden M. R. (2005b) Cognitive dysfunction precedes neuropathology and motor abnormalities in the YAC128 mouse model of Huntington's disease. *J. Neurosci.* **25**, 4169-4180.
- Velier J., Kim M., Schwarz C., Kim T. W., Sapp E., Chase K., Aronin N. and DiFiglia M. (1998) Wild-type and mutant huntingtins function in vesicle trafficking in the secretory and endocytic pathways. *Exp. Neurol.* **152**, 34-40.
- Ventruiti A. and Cuervo A. M. (2007) Autophagy and neurodegeneration. *Curr. Neurol. Neurosci. Rep.* **7**, 443-451.
- Vonsattel J. P. and DiFiglia M. (1998) Huntington disease. *J. Neuropathol. Exp. Neurol.* **57**, 369-384.
- Vonsattel J. P., Myers R. H., Stevens T. J., Ferrante R. J., Bird E. D. and Richardson E. P., Jr. (1985) Neuropathological classification of Huntington's disease. *J. Neuropathol. Exp. Neurol.* **44**, 559-577.
- Walker F. O. and Raymond L. A. (2004) Targeting energy metabolism in Huntington's disease. *Lancet* **364**, 312-313.
- Wang C. and Youle R. J. (2009) The role of mitochondria in apoptosis\*. *Annu. Rev. Genet.* **43**, 95-118.
- Wang H., Lim P. J., Karbowski M. and Monteiro M. J. (2009) Effects of overexpression of huntingtin proteins on mitochondrial integrity. *Hum. Mol. Genet.* **18**, 737-752.
- Wang J. Q., Chen Q., Wang X., Wang Q. C., Wang Y., Cheng H. P., Guo C., Sun Q., Chen Q. and Tang T. S. (2013) Dysregulation of mitochondrial calcium signaling and superoxide flashes cause mitochondrial genomic DNA damage in Huntington disease. *J. Biol. Chem.* **288**, 3070-3084.
- Warby S. C., Doty C. N., Graham R. K., Carroll J. B., Yang Y. Z., Singaraja R. R., Overall C. M. and Hayden M. R. (2008) Activated caspase-6 and caspase-6-cleaved fragments of huntingtin specifically colocalize in the nucleus. *Hum. Mol. Genet.* **17**, 2390-2404.
- Weir J. B. (1949) New methods for calculating metabolic rate with special reference to protein metabolism. *J. Physiol* **109**, 1-9.
- Wellington C. L., Ellerby L. M., Gutekunst C. A., Rogers D., Warby S., Graham R. K., Loubser O., van Raamsdonk J., Singaraja R., Yang Y. Z., Gafni J., Bredesen D., Hersch S. M., Leavitt B. R., Roy S., Nicholson D. W. and Hayden M. R. (2002) Caspase cleavage of mutant huntingtin precedes neurodegeneration in Huntington's disease. *J. Neurosci.* **22**, 7862-7872.

- Wellington C. L., Singaraja R., Ellerby L., Savill J., Roy S., Leavitt B., Cattaneo E., Hackam A., Sharp A., Thornberry N., Nicholson D. W., Bredesen D. E. and Hayden M. R. (2000) Inhibiting caspase cleavage of huntingtin reduces toxicity and aggregate formation in neuronal and nonneuronal cells. *J. Biol. Chem.* **275**, 19831-19838.
- Weydt P., Pineda V. V., Torrence A. E., Libby R. T., Satterfield T. F., Lazarowski E. R., Gilbert M. L., Morton G. J., Bammler T. K., Strand A. D., Cui L., Beyer R. P., Easley C. N., Smith A. C., Krainc D., Luquet S., Sweet I. R., Schwartz M. W. and La Spada A. R. (2006) Thermoregulatory and metabolic defects in Huntington's disease transgenic mice implicate PGC-1alpha in Huntington's disease neurodegeneration. *Cell Metab* **4**, 349-362.
- Wheeler V. C., Auerbach W., White J. K., Srinidhi J., Auerbach A., Ryan A., Duyao M. P., Vrbanc V., Weaver M., Gusella J. F., Joyner A. L. and MacDonald M. E. (1999) Length-dependent gametic CAG repeat instability in the Huntington's disease knock-in mouse. *Hum. Mol. Genet.* **8**, 115-122.
- Wheeler V. C., Persichetti F., McNeil S. M., Mysore J. S., Mysore S. S., MacDonald M. E., Myers R. H., Gusella J. F. and Wexler N. S. (2007) Factors associated with HD CAG repeat instability in Huntington disease. *J. Med. Genet.* **44**, 695-701.
- Wheeler V. C., White J. K., Gutekunst C. A., Vrbanc V., Weaver M., Li X. J., Li S. H., Yi H., Vonsattel J. P., Gusella J. F., Hersch S., Auerbach W., Joyner A. L. and MacDonald M. E. (2000) Long glutamine tracts cause nuclear localization of a novel form of huntingtin in medium spiny striatal neurons in HdhQ92 and HdhQ111 knock-in mice. *Hum. Mol. Genet.* **9**, 503-513.
- Woda J. M., Calzonetti T., Hilditch-Maguire P., Duyao M. P., Conlon R. A. and MacDonald M. E. (2005) Inactivation of the Huntington's disease gene (Hdh) impairs anterior streak formation and early patterning of the mouse embryo. *BMC. Dev. Biol.* **5**, 17.
- Wojtczak A. B. (1969) Inhibitory action of oxaloacetate on succinate oxidation in rat-liver mitochondria and the mechanism of its reversal. *Biochim. Biophys. Acta* **172**, 52-65.
- Wong B. K., Ehrnhoefer D. E., Graham R. K., Martin D. D., Ladha S., Uribe V., Stanek L. M., Franciosi S., Qiu X., Deng Y., Kovalik V., Zhang W., Pouladi M. A., Shihabuddin L. S. and Hayden M. R. (2015) Partial rescue of some features of Huntington Disease in the genetic absence of caspase-6 in YAC128 mice. *Neurobiol. Dis.* **76**, 24-36.
- Wu M., Neilson A., Swift A. L., Moran R., Tamagnine J., Parslow D., Armistead S., Lemire K., Orrell J., Teich J., Chomicz S. and Ferrick D. A. (2007) Multiparameter metabolic analysis reveals a close link between attenuated mitochondrial bioenergetic function and enhanced glycolysis dependency in human tumor cells. *Am. J. Physiol Cell Physiol* **292**, C125-C136.
- Yang D., Wang C. E., Zhao B., Li W., Ouyang Z., Liu Z., Yang H., Fan P., O'Neill A., Gu W., Yi H., Li S., Lai L. and Li X. J. (2010) Expression of Huntington's disease protein results in apoptotic neurons in the brains of cloned transgenic pigs. *Hum. Mol. Genet.* **19**, 3983-3994.

- Yang S. H., Cheng P. H., Banta H., Piotrowska-Nitsche K., Yang J. J., Cheng E. C., Snyder B., Larkin K., Liu J., Orkin J., Fang Z. H., Smith Y., Bachevalier J., Zola S. M., Li S. H., Li X. J. and Chan A. W. (2008) Towards a transgenic model of Huntington's disease in a non-human primate. *Nature* **453**, 921-924.
- Yano H., Baranov S. V., Baranova O. V., Kim J., Pan Y., Yablonska S., Carlisle D. L., Ferrante R. J., Kim A. H. and Friedlander R. M. (2014) Inhibition of mitochondrial protein import by mutant huntingtin. *Nat. Neurosci.* **17**, 822-831.
- Yao J., Wang L., Yang J. M., Maslov K. I., Wong T. T., Li L., Huang C. H., Zou J. and Wang L. V. (2015) High-speed label-free functional photoacoustic microscopy of mouse brain in action. *Nat. Methods* **12**, 407-410.
- Yu-Taeger L., Petrasch-Parwez E., Osmand A. P., Redensek A., Metzger S., Clemens L. E., Park L., Howland D., Calaminus C., Gu X., Pichler B., Yang X. W., Riess O. and Nguyen H. P. (2012) A novel BACHD transgenic rat exhibits characteristic neuropathological features of Huntington disease. *J. Neurosci.* **32**, 15426-15438.
- Zhang H., Li Q., Graham R. K., Slow E., Hayden M. R. and Bezprozvanny I. (2008) Full length mutant huntingtin is required for altered Ca<sup>2+</sup> signaling and apoptosis of striatal neurons in the YAC mouse model of Huntington's disease. *Neurobiol. Dis.* **31**, 80-88.
- Zhang N., An M. C., Montoro D. and Ellerby L. M. (2010) Characterization of Human Huntington's Disease Cell Model from Induced Pluripotent Stem Cells. *PLoS. Curr.* **2**, RRN1193.
- Zheng G., Dwoskin L. P. and Crooks P. A. (2006) Vesicular monoamine transporter 2: role as a novel target for drug development. *AAPS. J.* **8**, E682-E692.
- Zuccato C., Belyaev N., Conforti P., Ooi L., Tartari M., Papadimou E., MacDonald M., Fossale E., Zeitlin S., Buckley N. and Cattaneo E. (2007) Widespread disruption of repressor element-1 silencing transcription factor/neuron-restrictive silencer factor occupancy at its target genes in Huntington's disease. *J. Neurosci.* **27**, 6972-6983.
- Zuccato C. and Cattaneo E. (2007) Role of brain-derived neurotrophic factor in Huntington's disease. *Prog. Neurobiol.* **81**, 294-330.
- Zuccato C. and Cattaneo E. (2009) Brain-derived neurotrophic factor in neurodegenerative diseases. *Nat. Rev. Neurol.* **5**, 311-322.
- Zuccato C., Ciammola A., Rigamonti D., Leavitt B. R., Goffredo D., Conti L., MacDonald M. E., Friedlander R. M., Silani V., Hayden M. R., Timmusk T., Sipione S. and Cattaneo E. (2001) Loss of huntingtin-mediated BDNF gene transcription in Huntington's disease. *Science* **293**, 493-498.
- Zuccato C., Marullo M., Conforti P., MacDonald M. E., Tartari M. and Cattaneo E. (2008) Systematic assessment of BDNF and its receptor levels in human cortices affected by Huntington's disease. *Brain Pathol.* **18**, 225-238.

Zuccato C., Tartari M., Crotti A., Goffredo D., Valenza M., Conti L., Cataudella T., Leavitt B. R., Hayden M. R., Timmusk T., Rigamonti D. and Cattaneo E. (2003) Huntingtin interacts with REST/NRSF to modulate the transcription of NRSE-controlled neuronal genes. *Nat. Genet.* **35**, 76-83.

Zuccato C., Valenza M. and Cattaneo E. (2010) Molecular mechanisms and potential therapeutical targets in Huntington's disease. *Physiol Rev.* **90**, 905-981.

## CURRICULUM VITAE

James M. Hamilton

### Education

Ph.D. in Pharmacology Department of Pharmacology and Toxicology Indiana University, Indianapolis, IN	Aug 2012 – Nov 2017 GPA: 3.98 / 4.00
B.S. in Biology <i>with Highest Distinction</i> Major: Cell, Molecular, and Developmental Biology Minor: History Purdue University, West Lafayette, IN	Aug 2008 – May 2012 GPA: 3.94 / 4.00

### Research Experience

*May 2013 – Present*

**Graduate Research** with Dr. Nickolay Brustovetsky  
Assessing respiration, calcium uptake, and membrane potential in isolated mitochondria expressing mutant huntingtin; measuring oxygen consumption in primary neuronal culture from mice expressing mutant huntingtin; evaluating mitochondrial function in induced pluripotent stem cells from Huntington's disease patients  
Department of Pharmacology and Toxicology, Indiana University School of Medicine Indianapolis, IN

*March 2013 – May 2013*

**Laboratory Rotation** with Dr. Tao Lu  
Investigating post-translational control of NFkB signaling using techniques including western blotting and focus-forming assays  
Department of Pharmacology and Toxicology, Indiana University School of Medicine Indianapolis, IN

*October 2012 – December 2012*

**Laboratory Rotation** with Dr. Eri Hashino  
Studying the regulation of developmental signals during inner ear development using 3D culture  
Department of Pharmacology and Toxicology, Indiana University School of Medicine Indianapolis, IN

*March 2009 – May 2012*

**Undergraduate Research Assistant** with Dr. Daniel Suter  
Evaluating the role of ROS as signaling molecules in growth cone guidance and motility in *Aplysia* using live cell imaging and fluorescence microscopy  
Department of Biology, Purdue University, West Lafayette, IN

*September 2008 – January 2009*

**Undergraduate Research Assistant** with Dr. Michael G. Rossmann  
Analyzing X-ray crystallography data to determine virus structure  
Department of Biology, Purdue University, West Lafayette, IN

## Publications

**Hamilton J**, Brustovetsky T, Brustovetsky N. (2017) Oxidative metabolism and  $\text{Ca}^{2+}$  handling in striatal mitochondria from YAC128 mice, a model of Huntington's disease. *Neurochemistry International*, [Epub ahead of print].

Lakhter AJ, **Hamilton J**, Konger R, Brustovetsky N, Broxmeyer H, Naidu S. (2016) Glucose-independent acetate metabolism promotes melanoma cell survival and tumor cell growth. *Journal of Biological Chemistry*, 291(42): 21869-21879.

**Hamilton J**, Pellman JJ, Brustovetsky T, Harris RA, Brustovetsky N. (2016) Oxidative metabolism and  $\text{Ca}^{2+}$  handling in isolated brain mitochondria and striatal neurons from R6/2 mice, a model of Huntington's disease. *Human Molecular Genetics*, 25(13): 2762-2775.

**Hamilton J**, Pellman JJ, Brustovetsky T, Harris RA, Brustovetsky N. (2015) Oxidative metabolism in YAC128 mouse model of Huntington's disease. *Human Molecular Genetics*, 24(17): 4862-4878.

Pellman JJ, **Hamilton J**, Brustovetsky T, and Brustovetsky N. (2015)  $\text{Ca}^{2+}$  handling in isolated brain mitochondria and cultured neurons derived from YAC128 mouse model of Huntington's disease. *J Neurochemistry*, 134(4): 653-667.

Lakhter AJ, **Hamilton J**, Dagher PC, Mukkamala S, Hato T, Dong XC, Mayo LD, Harris RA, Shekhar A, Ivan M, Brustovetsky N, Naidu SR. (2014) Ferroptosis: a cell death from modulation of oxidative phosphorylation and PKM2-dependent glycolysis in melanoma. *Oncotarget*, 5(24): 12694-12703.

## Presentations and Abstracts

**Hamilton J**, Brustovetsky T, Brustovetsky N. Respiration and  $\text{Ca}^{2+}$  handling by striatal mitochondria purified from the brains of YAC128 mice, a model of Huntington's disease. Poster Presentation. Indianapolis Chapter of the Society for Neuroscience 2017 Annual Meeting, Indianapolis, IN, 2017.

**Hamilton J**, Brustovetsky T, Brustovetsky N. Respiration and  $\text{Ca}^{2+}$  handling by striatal mitochondria purified from the brains of YAC128 mice, a model of Huntington's disease. Poster Presentation. 46<sup>th</sup> Annual Society for Neuroscience Meeting, San Diego, CA, 2016.

**Hamilton J**, Brustovetsky T, Brustovetsky N. Respiration and  $\text{Ca}^{2+}$  handling by striatal mitochondria purified from the brains of YAC128 mice, a model of Huntington's disease. Poster Presentation. Gill Symposium, Bloomington, IN, 2016.

**Hamilton J**, Brustovetsky T, Brustovetsky N. Respiratory activity and  $\text{Ca}^{2+}$  uptake in brain mitochondria from R6/2 mice, a model of Huntington's disease. Poster Presentation. Pharmacology/Toxicology Department Recruitment Event, Indianapolis, IN, 2016.

**Hamilton J**, Brustovetsky T, Brustovetsky N. Respiratory activity and  $\text{Ca}^{2+}$

uptake in brain mitochondria from R6/2 mice, a model of Huntington's disease. Poster Presentation. Indianapolis Chapter of the Society for Neuroscience 2016 Annual Meeting, Indianapolis, IN, 2016.

**Hamilton J.** Oxidative metabolism and  $Ca^{2+}$  handling in the R6/2 mouse model of HD. Oral Presentation. Department of Pharmacology Student Seminar Series, Indianapolis, IN, 2015.

**Hamilton J**, Brustovetsky T, Brustovetsky N. Respiratory activity and  $Ca^{2+}$  uptake in brain mitochondria from R6/2 mice, a model of Huntington's disease. Poster Presentation. 45<sup>th</sup> Annual Society for Neuroscience Meeting, Chicago, IL, 2015.

**Hamilton J**, Brustovetsky T, Brustovetsky N. Respiratory activity and  $Ca^{2+}$  uptake in brain mitochondria from R6/2 mice, a model of Huntington's disease. Poster Presentation. Gill Symposium, Bloomington, IN, 2015.

**Hamilton J.** Oxidative metabolism in the YAC128 mouse model of HD. Oral Presentation. Department of Pharmacology Student Seminar Series, Indianapolis, IN, 2015.

**Hamilton J**, Brustovetsky T, Brustovetsky N. Respiratory activity of isolated mitochondria, cultured neurons, and whole YAC128 mice, a model of Huntington's disease. Poster Presentation. 44<sup>th</sup> Annual Society for Neuroscience Meeting, Washington, D. C., 2014.

**Hamilton J**, Brustovetsky T, Brustovetsky N. Respiratory activity of isolated mitochondria, cultured neurons, and whole YAC128 mice, a model of Huntington's disease. Poster Presentation. Gill Symposium, Bloomington, IN, 2014.

**Hamilton J**, Brustovetsky T, Brustovetsky N. Respiratory activity of isolated mitochondria, cultured neurons, and whole YAC128 mice, a model of Huntington's disease. Poster Presentation. Indianapolis Chapter for the Society of Neuroscience 2014 Annual Meeting, Indianapolis, IN, 2014.

**Hamilton J**, Brustovetsky T, Brustovetsky N. Respiratory activity of isolated mitochondria, cultured neurons, and whole YAC128 mice, a model of Huntington's disease. Poster Presentation. Pharmacology/Toxicology Department Recruitment Event, Indianapolis, IN, 2014.

**Hamilton J**, Brustovetsky T, Brustovetsky N. The lack of effect of mutant huntingtin on bioenergetics of isolated brain mitochondria and neuronal/astroglial cultures. Poster Presentation. Indianapolis Chapter of the Society for Neuroscience 2013 Annual Meeting, Indianapolis, IN, 2013.

**Hamilton J**, Brustovetsky T, Brustovetsky N. The lack of effect of mutant huntingtin on bioenergetics of isolated brain mitochondria and neuronal/astroglial cultures. Poster Presentation. Gill Symposium, Bloomington, IN, 2013.

## **Awards and Honors**

K.K. Chen Fellowship, Department of Pharmacology and Toxicology  
Indiana University School of Medicine, 2017  
Graduate and Professional Educational Grant, Graduate Division  
Indiana University School of Medicine, 2016  
Graduate Student Travel Grant  
Indiana University School of Medicine, 2016  
R. R. Paradise Travel Award, Department of Pharmacology and Toxicology  
Indiana University School of Medicine, 2016  
R. R. Paradise Travel Award, Department of Pharmacology and Toxicology  
Indiana University School of Medicine, 2014  
University Fellowship  
Indiana University, 2012

## **Professional and Academic Organizations**

Society for Neuroscience  
Student Member, 2014-Present  
Phi Beta Kappa  
Member, 2010-Present  
Beta Beta Beta National Biological Honor Society  
Member 2010-Present  
Vice-President, Xi Pi Chapter, 2011-2012

## **Leadership and Service**

Big Brothers Big Sisters of Central Indiana (BBBSCI)  
Mentor, 2015-Present  
Circle of Friends Self-advocacy Organization  
Executive Board Member, 2016-Present  
Member, 2015-Present  
Central Indiana Science Outreach (CINSO)  
Event volunteer, 2015-Present  
Trained one M.S. student  
Indiana University School of Medicine, spring 2014  
IBMG Graduate Program Recruitment  
Student ambassador, 2014-Present